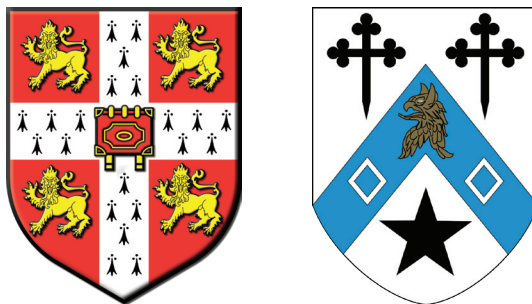


Structural and biochemical studies of the yeast linker histone, Hho1p

Lara May Osmotherly

Newnham College

Department of Biochemistry, University of Cambridge



This dissertation is submitted for the degree of
Doctor of Philosophy

September 2010

Contents

Contents	i
List of Figures	vii
List of Tables	x
Declaration	xi
Statement of length	xii
Summary	xiii
Acknowledgements	xiv
Abbreviations	xv
Definitions	xvi
1 General Introduction	2
1.1 Chromatin	2
1.1.1 The nucleosome	2
1.1.2 Higher-order chromatin structure	5
1.2 Epigenetics	10
1.2.1 Core histone post-translational chemical-modifications . .	11
1.2.2 Core histone subtypes	14
1.2.3 DNA methylation	15
1.3 Linker histones	16
1.3.1 The role of linker histones in transcriptional regulation and epigenetics	17
1.3.1.1 Linker histone variants	17
1.3.1.2 Post-translational modifications of linker histones	19
1.3.1.3 Linker histones and core histone post- translational modification	23
1.3.1.4 Gene-specific effects of linker histones	23
1.3.2 The role of linker histones in chromatin structure	25
1.3.2.1 The structure of linker histones	25
1.3.2.2 Linker histone binding in the nucleosome	25
1.3.2.3 Linker histone binding to DNA in chromatin . . .	28
1.3.2.4 Linker histones and higher-order chromatin structure	31

1.4	Yeast chromatin	32
1.5	The yeast linker histone	34
1.5.1	Structural studies of Hho1p	37
1.5.2	Location of Hho1p in yeast chromatin	38
1.5.3	Effect of Hho1p on chromatin structure	39
1.5.4	Effect of Hho1p on transcription	40
1.5.5	Bi-functionality of Hho1p?	43
1.5.6	Roles of Hho1p in yeast	46
1.6	Introduction to work presented in this Thesis	47
2	Structural investigation of GII, the second “globular” domain of Hho1p	50
2.1	Introduction	50
2.2	Materials and methods	53
2.2.1	Bacteria	53
2.2.1.1	Bacterial growth media	53
2.2.1.2	Bacterial strains	53
2.2.2	Plasmids	53
2.2.3	Expression and purification of Hho1p and the GII domain	55
2.2.3.1	Expression of ¹⁵ N-Hho1p	55
2.2.3.2	Purification of Hho1p	55
2.2.3.3	Expression of ¹⁵ N-GII and ¹³ C, ¹⁵ N-GII	57
2.2.3.4	Purification of the GII domain	57
2.2.4	Protein characterisation	57
2.2.4.1	SDS/polyacrylamide gel-electrophoresis	57
2.2.4.2	Amino acid analysis	58
2.2.4.3	Mass spectrometry	58
2.2.5	NMR spectroscopy	58
2.2.5.1	NMR sample conditions	58
2.2.5.2	Chemical shift deviations from random coil	59
2.2.5.3	Heteronuclear NOE measurements	59
2.2.5.4	Chemical-shift difference measurements	60
2.2.5.5	ATSL-labelling of the GII domain	60
2.3	Results	61
2.3.1	The GII domain of Hho1p exists as a folded and an “un- folded” species in the context of the full-length protein	61
2.3.2	Sequence-based disorder prediction indicates that the he- lices of the GII domain of Hho1p are less ordered than those in the GI domain	64
2.3.3	NMR assignments of the “unfolded” GII domain of Hho1p	64
2.3.4	The GII domain of Hho1p contains regions of residual structure	69
2.3.5	Urea reduces, but does not abolish, residual structure in the GII domain of Hho1p	70
2.3.6	Contacts between helices I and III may be important in the packing of the GII domain of Hho1p	73

2.4	Discussion	75
2.4.1	The GII domain exists as a folded and an “unfolded” species, both as an isolated domain and in the context of full-length Hho1p	75
2.4.2	The “unfolded” form of the GII domain of Hho1p contains regions of residual structure and may fold through interactions between these regions	77
2.5	Summary	79
3	Hho1p acts within chromatin in a similar manner to canonical linker histones	81
3.1	Introduction	81
3.2	Materials and methods	84
3.2.1	Yeast	84
3.2.1.1	Yeast growth medium	84
3.2.1.2	Yeast strains	84
3.2.2	Plasmids	84
3.2.3	Proteins	85
3.2.3.1	Expression and purification of the yeast core histone H4, Hhf2p	85
3.2.3.2	Expression and purification of Hho1p and NGIL proteins	87
3.2.4	Extraction of chromatin and linker histones from chicken erythrocytes	87
3.2.4.1	Isolation of chicken erythrocyte nuclei	87
3.2.4.2	Preparation of medium-length chromatin by micrococcal nuclease digestion	88
3.2.4.3	Size-fractionation of chromatin through sucrose gradients	88
3.2.4.4	Salt-stripping of linker histones from chicken erythrocyte chromatin	89
3.2.4.5	Preparation of core histone octamers from linker histone-depleted chicken erythrocyte chromatin	89
3.2.4.6	Isolation of linker histones H1 and H5 from chicken erythrocytes	90
3.2.4.7	Isolation of 147 base pair competitor DNA from linker histone-depleted chicken erythrocyte chromatin	90
3.2.5	Isolation of yeast nuclei	91
3.2.6	DNA characterisation	92
3.2.6.1	Agarose gel-electrophoresis	92
3.2.6.2	Native PAGE	93
3.2.7	Western blotting	93
3.2.7.1	Antibodies	93
3.2.7.2	Protein transfer and immunodetection	93
3.2.7.3	Nitrocellulose membrane stripping	94

3.2.8	Chemical cross-linking	94
3.2.9	Reconstitution of nucleosome arrays	95
3.2.9.1	Purification of DNA arrays	95
3.2.9.2	Reconstitution of nucleosome arrays by continuous salt dialysis	96
3.2.9.3	Fixing reconstituted nucleosome arrays with glutaraldehyde	96
3.2.9.4	Folding of nucleosome arrays	97
3.2.9.5	<i>Ava I</i> digestion of nucleosome arrays	97
3.2.9.6	Analytical ultra-centrifugation	97
3.3	Results	98
3.3.1	Hho1p is less abundant than metazoan linker histones	98
3.3.2	Comparison of cross-linked products of chromatin containing Hho1p or canonical linker histones	100
3.3.3	Hho1p-containing nucleosome arrays are structurally similar to those containing canonical linker histones	103
3.4	Discussion	115
3.4.1	Hho1p is present at about 1 molecule per 5–10 nucleosomes and may form dimers upon cross-linking of yeast chromatin	115
3.4.2	Hho1p increases the compaction of reconstituted nucleosome arrays; the second globular domain does not seem to be required	116
3.5	Summary	118
4	Hho1p interactions with chromatin proteins	120
4.1	Introduction	120
4.2	Materials and methods	124
4.2.1	Plasmids	124
4.2.2	Proteins	125
4.2.2.1	HMGB1	125
4.2.2.2	Hmo1p	125
4.2.2.3	Expression and purification of Nhp6ap	125
4.2.2.4	Expression and purification of Htz1p	126
4.2.2.5	Expression and purification of Sir2p	127
4.2.3	Chemical cross-linking	128
4.2.4	Western blotting	128
4.2.4.1	Antibodies	128
4.2.5	Analytical gel filtration	128
4.2.6	Co-immunoprecipitation	129
4.2.6.1	Anti-Hho1 immunoprecipitation	129
4.2.6.2	HTZ1-TAP immunoprecipitation	130
4.2.7	Chromatin immunoprecipitation assay	130
4.2.7.1	Culture growth, cross-linking and whole-cell extract	130
4.2.7.2	TAP-tag precipitation	131
4.2.7.3	Purification of DNA	132

4.2.7.4	PCR analysis	132
4.3	Results	133
4.3.1	Searching for Hho1p-interacting partners	133
4.3.2	Investigation of Hho1p interaction with HMG box proteins, Hmo1p and Nhp6ap	134
4.3.3	Investigation of Hho1p interaction with Htz1p	140
4.3.4	Investigation of Hho1p interaction with Sir2p	145
4.4	Discussion	147
4.4.1	General searches for Hho1p-interacting partners	147
4.4.2	Hho1p does not appreciably interact with Hmo1p, Nhp6ap or Htz1p, but does cross-link with Sir2p in solution	150
4.5	Summary	153
5	Investigation of phosphorylation of Hho1p — biochemistry and linker domain structure	155
5.1	Introduction	155
5.2	Materials and methods	157
5.2.1	Plasmids	157
5.2.1.1	Cloning of pET17b-HHO1-linker	158
5.2.2	Proteins	159
5.2.2.1	Expression and purification of Hho1p and Hho1p-truncation proteins	159
5.2.2.2	Expression and purification of ¹³ C, ¹⁵ N-linker domain of Hho1p	159
5.2.3	Phosphorylation of Hho1p and Hho1p-truncation proteins	160
5.2.4	HEPES/Histidine gel-electrophoresis	161
5.2.5	DNA cellulose assay	161
5.2.6	Four-way junction DNA gel-shift assay	162
5.2.6.1	Synthesis of four-way junction DNA	162
5.2.6.2	Gel-shift assays with four-way junction DNA	163
5.2.7	Sucrose gradient assay for binding of Hho1p and Hho1p-truncation proteins to chromatin	163
5.2.8	NMR studies of the ¹³ C, ¹⁵ N-labelled linker domain of Hho1p	163
5.2.9	DNA sequencing	164
5.3	Results	165
5.3.1	Phosphorylation of Hho1p and Hho1p-truncation proteins by CDK2/Cyclin A	165
5.3.2	Effect of phosphorylation on the interaction of Hho1p and domain deletion mutants with DNA and chromatin	168
5.3.3	Structural effects of phosphorylation on the linker domain of Hho1p	173
5.3.3.1	Predicted structural character of the linker domain of Hho1p	173
5.3.3.2	Production of the linker domain of Hho1p	173
5.3.3.3	NMR studies of the linker domain of Hho1p	177

5.3.3.4	The linker domain of Hho1p is phosphorylated at Ser4, Ser14 and Thr27 by CDK2/Cyclin A	182
5.3.3.5	Effect of phosphorylation on the structure of the linker domain of Hho1p	190
5.4	Discussion	193
5.4.1	Phosphorylation of Hho1p by CDK2/Cyclin A occurs mainly in the linker domain	193
5.4.2	Phosphorylation affects the biochemistry of Hho1p and Hho1p-truncation proteins	195
5.4.3	The linker domain of Hho1p is mainly unstructured, but may have some helical character around residues 24–38 . .	196
5.4.4	Phosphorylation of the linker domain by CDK2/Cyclin A occurs at three sites	197
5.4.5	Phosphorylation of the linker domain by CDK2/Cyclin A changes the helical character of residues 24–38	199
5.4.6	Comparison of the effect of phosphorylation on the linker domain of Hho1p and the C-terminal tail of histone H1 . .	200
5.5	Summary	202
6	Concluding Remarks	204
A	NMR resonances of the “unfolded” species of the GII domain of Hho1p	210
B	NMR resonances of the linker region of Hho1p	213
C	NMR resonances of the phosphorylated linker region of Hho1p	215
	Bibliography	218

List of Figures

1.1	Structure of the nucleosome	3
1.2	Higher-order chromatin structure	6
1.3	Chromatin higher-order chromatin structure is determined by nucleosome repeat length and linker histone content	9
1.4	Post-translational modifications of human core histones	12
1.5	Post-translational modifications of human linker histones	20
1.6	Structure of the globular domains of chicken linker histones H1 and H5	26
1.7	Conservation of the DNA binding sites of linker histones	27
1.8	Binding of linker histone to the chromatosome	29
1.9	The yeast linker histone, Hho1p	35
2.1	The effect of sodium phosphate concentration on the GI and GII domains of Hho1p	51
2.2	¹ H- ¹⁵ N HSQC spectrum of ¹⁵ N-labelled Hho1p	62
2.3	The GII domain of Hho1p exists as a folded and an “unfolded” species in the context of the full-length protein	63
2.4	Structure and disorder predictions for the GI and GII domains of Hho1p	65
2.5	NMR spectroscopy of the GII domain of Hho1p in conditions where peaks from the “unfolded” species dominate	66
2.6	Magnetisation transfers of NMR experiments used in this Thesis	68
2.7	Comparison of the folded and “unfolded” forms of GII in 10 mM sodium phosphate	71
2.8	Urea titration into the GII domain of Hho1p	72
2.9	Heteronuclear NOE measurements for the GII domain of Hho1p in buffers containing various concentrations of urea	74
2.10	Attaching ATSL to the GII domain at cysteine 61 causes the equilibrium to shift to the “unfolded” species in 10 mM sodium phosphate buffer	76
3.1	Determining the ratio of Hho1p to nucleosomes in yeast whole-cell extract through semi-quantitative Western blots	99

3.2	Cross-linking of linker histone-depleted chicken erythrocyte chromatin bound with linker histones	101
3.3	Cross-linking of <i>S. cerevisiae</i> nuclei shows a ladder of Hho1p-containing products	102
3.4	Nucleosome array reconstitution components	104
3.5	Nucleosome array reconstitution	105
3.6	Titration of linker histones into nucleosome arrays	106
3.7	Compaction of nucleosome arrays upon addition of linker histone . .	108
3.8	Folding of nucleosome arrays upon addition of linker histone	109
3.9	Analysis of folded nucleosome arrays by analytical ultracentrifugation	111
3.10	Hho1p may protect nucleosome arrays from digestion by <i>Ava I</i>	113
3.11	Digestion of DNA and nucleosome arrays with <i>Ava I</i> does not indicate bridging by Hho1p	114
4.1	Cartoons indicating the domain structure of proteins used in this Chapter	122
4.2	The acidic tail of HMGB1 is required for cross-linking to both histone H1 and Hho1p	135
4.3	Hmo1p does not cross-link to histone H1 or Hho1p in solution	136
4.4	Nhp6ap and Hho1p cross-link in solution with DMS but not with EDC	138
4.5	Gel-filtration of Hho1p and Nhp6ap	139
4.6	Hho1p and Htz1p immunoprecipitation from <i>S. cerevisiae</i> whole-cell extract	141
4.7	Chemical cross-linking of recombinant Hho1p and Htz1p	142
4.8	PCR analysis of Hho1p and Htz1p association with regions of the ADH2 and PHO5 genes in <i>S. cerevisiae</i>	144
4.9	Chemical cross-linking of Hho1p and Sir2p in solution	146
4.10	Gel-filtration of Hho1p and Sir2p	148
5.1	Hho1p and Hho1p-truncation proteins used in this Chapter	166
5.2	Phosphorylation of Hho1p and Hho1p-truncation proteins using CDK2/Cyclin A	167
5.3	Effect of phosphorylation on the dissociation of Hho1p and Hho1p-truncation proteins from DNA-cellulose with increasing concentration of NaCl	169
5.4	Effect of phosphorylation on Hho1p and Hho1p-truncation proteins binding to four-way junction DNA	171
5.5	Phosphorylation has no effect on affinity of Hho1p and Hho1p-truncation proteins for chromatin in sucrose gradient assays	172
5.6	Disorder and secondary structure prediction of the linker domain of Hho1p	174
5.7	Expression of the linker domain of Hho1p	175

5.8	Purification of the linker domain of Hho1p	176
5.9	NMR spectroscopy of the linker domain of Hho1p	178
5.10	Shift deviations from random coil for the linker domain of Hho1p . .	180
5.11	Analysis of the dynamics of the linker domain of Hho1p	181
5.12	Phosphorylation of the linker domain of Hho1p	183
5.13	NMR peak shifts upon phosphorylation of the linker domain of Hho1p	184
5.14	Using C^β resonances to report on phosphorylation of residues in the linker domain of Hho1p	187
5.15	^1H - ^{15}N HSQC peak loss upon phosphorylation of the linker domain of Hho1p	189
5.16	Shift deviations from random coil for the unphosphorylated and phosphorylated linker domain of Hho1p	191
5.17	Analysis of the dynamics of the unphosphorylated and phosphory- lated linker domain of Hho1p	192

List of Tables

2.1	Bacterial growth media	54
2.2	Bacterial strains	54
3.1	Yeast growth medium	84
3.2	Yeast strains	84
3.3	Ratio of core nucleosome to Hho1p in yeast cells	98
4.1	Primers used for PCR analyses of Hho1p and Htz1p localisation	132
5.1	Primers used to clone the linker domain of Hho1p	158
5.2	Four-way junction DNA oligonucleotides	162

Declaration

This dissertation is the result of my own work that was carried out during my time at the Department of Biochemistry, University of Cambridge between October 2006 and August 2010. This dissertation has not been submitted, in whole or in part, to any other university and includes nothing which is the outcome of work done in collaboration except where specifically indicated in the text.

Lara May Osmotherly

Newnham College, Cambridge
September 2010

Statement of length

This Thesis does not exceed 60,000 words excluding figures, photographs, tables, appendices and bibliography.

Lara May Osmotherly

Newnham College, Cambridge
September 2010

Summary

The basic unit of eukaryotic chromatin is the nucleosome core, which contains 147 base pairs of DNA wrapped around an octamer of core histone proteins. Linker histones bind through their globular domain at the nucleosome dyad and to internucleosomal DNA through their C-terminal basic tail. The *Saccharomyces cerevisiae* linker histone homologue, Hho1p, contains two domains, GI and GII, that have sequence similarity to the globular domain of the canonical linker histone H1.

The individual domains of Hho1p differ in their structural and functional properties, for example in 10 mM sodium phosphate GI is folded while GII exists as two species: folded and “unfolded”. In **Chapter 2** the structure of the second globular domain of Hho1p, GII, is further investigated. NMR studies indicate residual structure in the “unfolded” form of GII, especially at the start of helices I and III.

Chapter 3 considers the structural roles of Hho1p within chromatin. Semi-quantitative Western blotting is used to measure the abundance of Hho1p relative to nucleosomes in yeast. Analysis of reconstituted nucleosome arrays containing NGIL (Hho1p with the second globular domain removed) are indistinguishable from those containing full-length Hho1p, in gel-based assays and by analytical ultracentrifugation, suggesting the GII domain may not have a major role in chromatin compaction.

Chapter 4 focuses on the interaction of Hho1p with chromatin proteins. Chemical cross-linking and gel filtration indicate that Hho1p does not interact significantly with the putative HMGB1 homologues Hmo1p and Nhp6ap *in vitro*. Hho1p and Htz1p, the yeast histone H2A.Z subtype, do not appear to interact directly in co-immunoprecipitation and chemical cross-linking assays, while chromatin immunoprecipitation studies show no evidence of colocalisation across the ADH2 and PHO5 genes. Hho1p and Sir2p cross-link in solution, but purification difficulties precluded further investigation.

The effect of phosphorylation on the interaction of Hho1p and related truncation proteins with DNA and chromatin are investigated in **Chapter 5**. Phosphorylation reduces their affinity for linear DNA, but has different effects on the binding to four-way junction DNA for Hho1p and NGIL, compared with LGII (the linker region and GII domain of Hho1p). Phosphorylation has no obvious effect on the affinity of these proteins for chromatin in sucrose gradient centrifugation assays. NMR spectroscopy studies show that the linker region is mostly unstructured, with a short region showing some α -helical character. Phosphorylation of the linker domain changes its structural character.

Acknowledgements

Firstly, I would like to thank Professor Dame Jean Thomas for her advice and guidance throughout my studies. I am grateful for the rigorous training received and for her support of my ambitions to teach. I thank Dr Katherine Stott for her NMR expertise and for demystifying the technique. It has been a pleasure to migrate from her student, striving with undergraduate chemistry, to colleague and office-mate and I am continually inspired by her success in blending a scientific career with a young family. I also thank Dr Mat Watson for his encyclopedic knowledge and his enthusiasm for problem-solving experiments with me, which *almost* make up for the continual “borrowing” of my pipettes and icebox.

My time in the lab would have been much poorer without the friendship and support of the other “JOTties”. It’s been lovely to work alongside Alex, sharing our lab experiences and enjoying good chats, and Laura, with her bubbly personality and caring spirit. I miss the “buzz” in the bays from Jen, John, Becky, Sarion, Tatyana and Varsha, and fondly remember coffee breaks at Martin’s and trips to Lawyers’ and Snug.

I thank Fred for his “rescues” when things were broken or missing, as well as his humour and conversation. I thank members of Protein and Nucleic Acid Facility, DNA Sequencing and Photographic Unit in the Department for technical assistance. I am grateful for Dr Andrew Travers and Dr Daniela Rhodes allowing me to collaborate with their lab members and I thank Mark, Edwige and Andrew for their technical skills and kindness in helping me navigate in unfamiliar labs. I gratefully acknowledge the BBSRC, the Board of Graduate Studies Hardship Award Scheme and the Access to Learning Fund for financial aid.

Warmest thanks must go to my family and friends who have supported me throughout this endeavour. I thank my parents for quietly encouraging me to aim for whatever *I* want to achieve and I am so grateful for my family’s unconditional love. I am thankful for my friends, who have been a continual source of diversion and entertainment in often stressful times, including through the magic of lindy hop. Finally, I thank Nick for his love and support over the years, for encouraging my self-belief and for how he can’t fail to improve my day with his warmth and sense of fun.

Thank you, everyone!

Abbreviations

In addition to the accepted abbreviations (<http://www.biochemj.org/bj/bji2a.htm#table1>), the following have been used in this Thesis.

$\{^1\text{H}\}^{15}\text{N}$ NOE	heteronuclear nuclear Overhauser effect
A_{260}	absorbance measured at 260 nm
ATSL	(1-acetoxy-2,2,5,5-tetramethyl- δ -3-pyrroline-3-methyl) methanethiosulfonate
C-terminal	carboxy-terminal
CDK	cyclin-dependent kinase
CE	chicken erythrocyte
ChIP	chromatin immunoprecipitation
ChIP-chip	chromatin immunoprecipitation analysed on microarray chips
DMS	dimethyl sulfoxide
DSS	disuccinimidyl suberate
DTT	dithiothreitol ((2S,3S)-1,4-Bis-sulfanylbutane-2,3-diol)
EDC	1-ethyl-3-[3-dimethylaminopropyl]carbodiimide
ESI-TOF	electrospray ionisation time-of-flight
FRAP	fluorescence recovery after photobleaching
GFP	green fluorescent protein
GST	glutathione S-transferase
HA	human influenza hemagglutinin
HRP	horseradish peroxidase
HSQC	heteronuclear single quantum coherence
IPTG	isopropyl β -D-thiogalactopyranoside
kDa	kilo Dalton
N-terminal	amino-terminal
NP-40	tergitol-type NP-40 (nonyl phenoxy polyethoxy ethanol)
OD_{600}	optical density measured at 600 nm
PCA	perchloric acid
qPCR	quantitative polymerase chain reaction
rDNA	ribosomal DNA
RNAP	RNA polymerase
rpm	revolutions per minute
SAXS	small-angle X-ray scattering
SGA	synthetic gene analysis
TBE	tris-boric acid-EDTA
TBS	tris-buffered saline
TBS-T	tris-buffered saline, plus Tween
TCA	trichloroacetic acid

Definitions

1 absorbance unit: the quantity of material that, in 1 ml solution, has an absorbance of 1 at a given wavelength when measured in a 1 cm pathlength cuvette.

1 unit (U) of micrococcal nuclease: the amount of micrococcal nuclease that releases 1 A_{260} unit of oligonucleotide per minute at 37 °C at pH 8.0.

1 unit (U) of restriction endonuclease: the amount of enzyme required to digest 1 μg of λ DNA in 1 hour at 37 °C in a total reaction volume of 50 μl .

1 unit (U) of thrombin: the amount of enzyme required to cleave > 90% of 100 μg of a test GST fusion protein when incubated in 1x PBS at 22 °C for 16 h.

Chapter 1

General Introduction

1 General Introduction

1.1 Chromatin

Chromatin contains approximately equal masses of DNA and small, highly conserved, basic histone proteins that bind the DNA. Packaging the DNA in chromatin allows the genetic material to be condensed from a length of about 2.2 m into a nucleus with a diameter of 10 μm . Different regions of the genome have various compaction levels that can be dynamic. Actively transcribed regions have a more open chromatin structure, euchromatin, while transcriptionally silent regions contain more compacted heterochromatin. As well as genetic information contained within the DNA sequence, chromatin also carries epigenetic information contained in DNA methylation, chemical modification of the histone proteins and inclusion of different histone subtypes.

1.1.1 The nucleosome

Digestion of chromatin by a DNA endonuclease, such as micrococcal nuclease, occurs in stages (Figure 1.1a) (Thomas, 1984). First nucleosomes are produced, containing about 200 base pairs (bp) of DNA, a linker histone (Section 1.3) and an octamer of core histone proteins. Further digestion of the DNA produces chromatosomes that contain 166 bp DNA (Simpson, 1978), and digestion may pause at this point in what is known as a “chromatosome stop”. Yet more digestion releases the linker histone and removes another 20 bp of DNA, producing

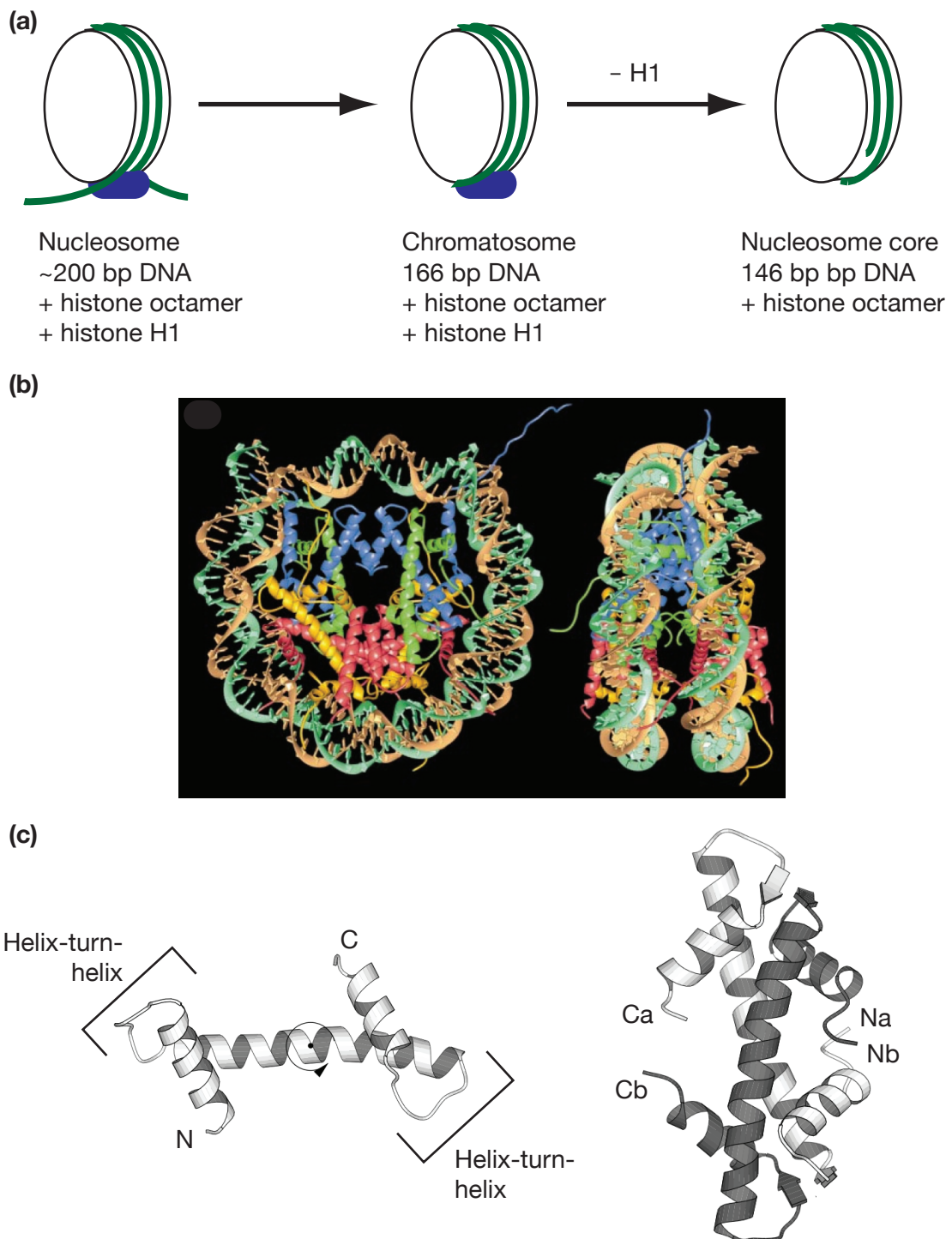


Figure 1.1 Structure of the nucleosome. (a) Schematic of the stages of micrococcal nuclease digestion of chromatin. The histone tails are not shown and the histone octamer is represented as a disc. Adapted from Thomas (1984). (b) Two views of the crystal structure of the nucleosome core at 2.8 Å resolution. 146 bp of DNA is wrapped 1.65 times around an octamer of histone proteins (H2A:yellow; H2B: red; H3: blue; H4:green). From Luger et al. (1997). (c) A histone fold domain, with a helix-turn-helix motif at each end (left), and a dimer of two histones in a “handshake” motif (right). Adapted from Ramakrishnan (1997).

the nucleosome core particle.

The nucleosome is the fundamental unit of chromatin. It contains an octamer of core histone proteins surrounded by 146 bp of DNA, wrapped 1.65 times around the octamer (Figure 1.1b) (Thomas and Kornberg, 1975; Finch et al., 1977; Luger et al., 1997). The octamer is formed from an $(H3)_2(H4)_2$ tetramer flanked by two H2A.H2B dimers. The tetramer is stabilised through a four-helix bundle between the two histone H3s, and the octamer is stabilised through four-helix bundles between histones H2B and H4 (Luger et al., 1997). The histone molecules themselves contain domains with helix-turn-helix histone folds and interact with other histone molecules in a “handshake” motif (Figure 1.1c) (Arents et al., 1991; Ramakrishnan, 1997). The wrapping of the DNA around the histone octamer is stabilised through contacts with the unstructured tails of the core histones (Ausio et al., 1989). The amino-terminal (N-terminal) tails of histones H3 and H4 become structured upon binding to DNA (Baneres et al., 1997).

To wrap around the nucleosome core, the DNA is intensively twisted and curved (Luger et al., 1997; Richmond and Davey, 2003). There is some degree of sequence preference for octamer binding, as short runs of d(A T) at 10 bp intervals promote bending in the DNA minor groove where it faces towards the nucleosome core (Satchwell et al., 1986; Travers, 1987). Due to the structural requirements of the nucleosomal DNA, the affinity of the octamer for various DNA sequences can differ by up to 1000-fold. This was determined by the exchange of nucleosomes onto DNA sequences from linker histone-depleted chromatin, and the relative amounts of nucleosome formed on DNA sequences compared with competitor DNA in reconstitution reactions (Thastrom et al., 1999). Nucleosome affinity is dependent on the stacking energy and flexibility of the local DNA (Virstedt et al., 2004), leading to the suggestion of a “nucle-

osome positioning code” that could facilitate processes such as transcription factor binding, transcription initiation, and chromatin remodelling (Segal et al., 2006).

The most basic level of chromatin is referred to as “beads on a string” or the 10 nm filament. It consists of nucleosomes separated by linker DNA, which varies in length with tissue-type and species (van Holde, 1989). The 10 nm filament compacts the DNA by approximately six-fold in length.

1.1.2 Higher-order chromatin structure

Further compaction involves chromatin folding into higher-order structures. Euchromatic regions of the genome are relatively loosely compacted, allowing proteins to bind and act on the DNA, whereas heterochromatic regions are condensed to a greater extent and are mainly inaccessible to DNA binding proteins.

Formation of higher-order chromatin structures involves internucleosomal interactions. Important contacts occur between the histone H4 N-terminal tail and the H2A/H2B acidic patch, observed in the nucleosome core particle crystal structure (Luger et al., 1997) and shown to exist in chromatin (Dorigo et al., 2003). Acetylation of the histone H4 tail at lysine 16 can disrupt this contact and inhibit compaction of chromatin, but not to such a great extent as the removal of linker histone (Robinson et al., 2008).

The first level of higher-order chromatin structure is the “30 nm fibre”, a transcriptionally inactive superstructure of nucleosomes (Thoma et al., 1979). The structure of this fibre is debated, with various models proposed (Figure 1.2a). The models vary in the relative orientation of, and connections between, the nucleosomes, the path of the linker DNA, the location of linker histone, the number of nucleosomes per turn of the fibre and the dimension of the

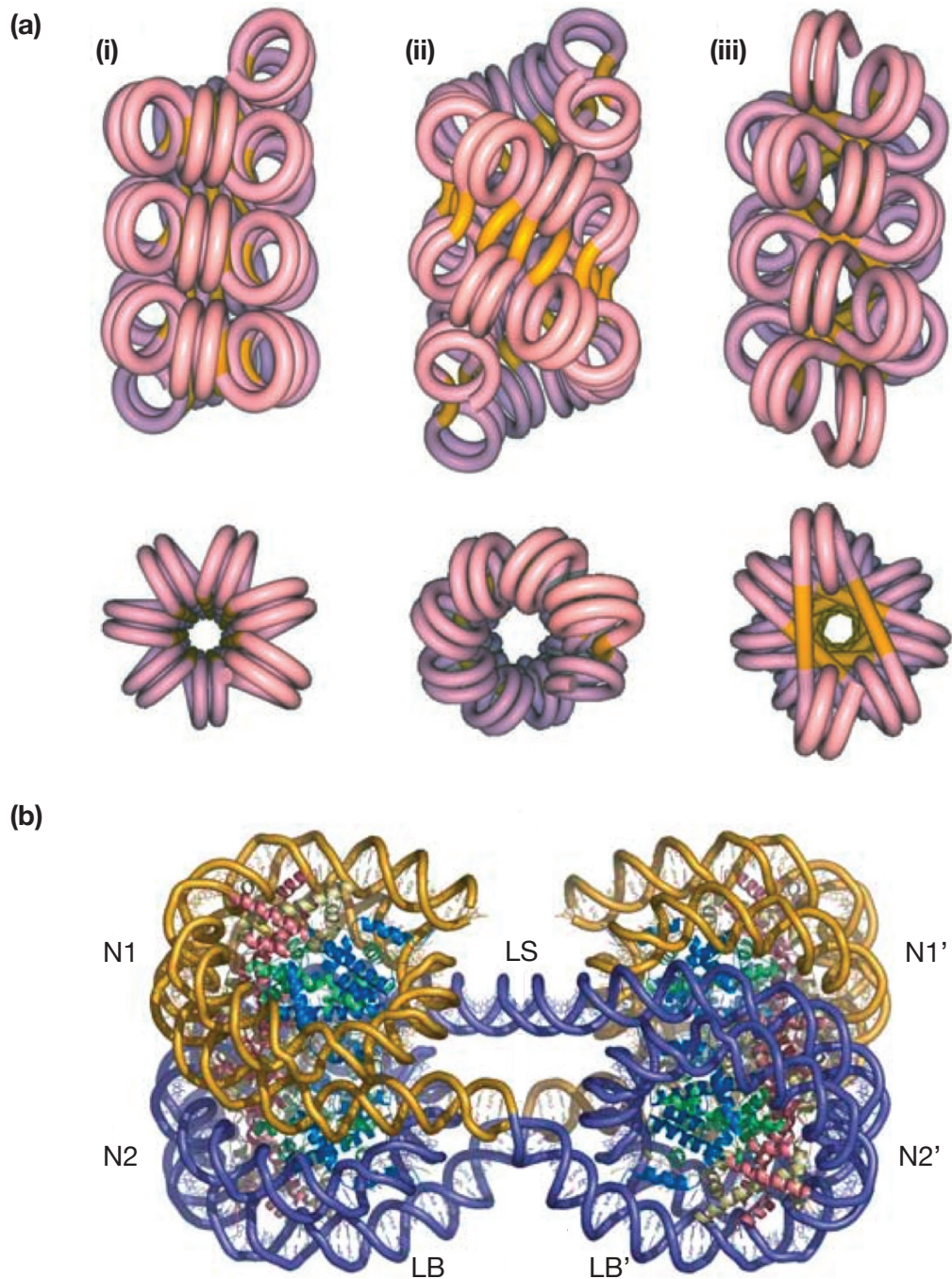


Figure 1.2 Higher-order chromatin structure. (a) Two views of models for the packing of nucleosomes in "30 nm fibres". The linker DNA is indicated in yellow. The models are as follows (i) Solenoid model: a one-start helix of nucleosomes, connected by bent linker DNA (ii) Two-start supercoiled model: a helix of two adjacent stacks of nucleosome with straight linker DNA (iii) Two-start twisted model: a structure containing the linker DNA and histone H1 at the centre of the fibre. From Dorigo et al. (2004). (b) The crystal structure of the tetranucleosome. The two stacks of nucleosomes (N1, N2 and N1', N2') are rotated with respect to each other. Linker DNA connecting N1 to N2', and N2 to N1' is bent (LB, LB'), but that connecting N2' to N2 is straight (LS). From Schalch et al. (2005).

fibre produced (reviewed by Staynov, 2008).

Initial electron microscopy studies of extracted chromatin showed condensation to fibres with approximately 30 nm diameter, upon increasing the ionic strength, and led to a solenoid model being proposed (Finch and Klug, 1976). The solenoid model describes one strand of nucleosomes that coil into a helix with about six nucleosomes per turn. The adjacent nucleosomes are connected through bent linker DNA and linker histone is required to stabilise the fibre structure. In contrast, other groups have proposed two-start models in which there is a zig-zag arrangement of the nucleosomes and straight linker DNA. These two-start models are further divided into helical-ribbon models, where the two strands coil (Worcel et al., 1981; Woodcock et al., 1984), and crossed-linker models, where the two strands twist causing the linker DNA to be at the centre of the fibre (Bednar et al., 1998).

Evidence for two-start “30 nm fibre” comes from *in vitro* chromatin reconstitution assays. Nucleosome arrays, both with and without linker histone, were reconstituted using core histones with site-specific mutations to cysteine (H4-V21C/H2A-E64C). This allowed cross-linking of the chromatin structure, and was followed by digestion with an endonuclease (Dorigo et al., 2004). The number of nucleosomes joined through cross-linking was shown to correspond with theoretical values for two-start, rather than one-start fibres, and full digestion of the arrays was confirmed by reducing the cross-links with DTT. The crystal structure of a tetranucleosome is also consistent with a two-start model, although it does not contain linker histone (Figure 1.2b) (Schalch et al., 2005). One caveat to these experiments is that they both use a 167 bp nucleosome repeat length. These short nucleosome repeat lengths are rare, having only been shown for *Saccharomyces cerevisiae* (*S. cerevisiae*) and cerebral cortex neurons (Thomas and Furber, 1976; Thomas and Thompson, 1977). Other tissues and

species have longer nucleosome repeat lengths.

Electron microscopy data from reconstituted chromatin, containing chicken histone H5 and various nucleosome repeat lengths, indicate a solenoid structure for the “30 nm fibre” (Robinson et al., 2006). Chromatin with 177–207 bp nucleosome repeat lengths form fibres with about 33 nm diameter and 11 nucleosomes per helical turn, whereas longer repeat lengths produce 44 nm fibres and 15 nucleosomes per helical turn. The number of nucleosomes observed in a given length of solenoid fibre is much larger than that suggested in the original solenoid model (6 or 7 nucleosomes per helical turn; Finch and Klug, 1976) leading to a solenoid model containing interdigitated nucleosomes. Nucleosome arrays with 197 bp repeat lengths appear as “puddles” in the absence of linker histone (Figure 1.3a; Routh et al., 2008). The presence of magnesium ions in the buffer promotes disordered nucleosome interactions. As histone H5 is added the fibres become more compact and regular, forming 34 nm fibres with an interdigitated solenoid structure. Co-operativity in the compaction of these nucleosome arrays indicates that folding requires the presence of linker histones in contiguous regions.

Nucleosome arrays with 167 bp nucleosome repeat length, on the other hand, have a different topology (Figure 1.3b; Routh et al., 2008). These arrays can bind up to one histone H5 for approximately every two nucleosome cores before precipitation occurs, as determined by densitometry of nucleosome arrays containing radio-labelled H5 (one phosphorylation reaction per 1500 linker histones). Nucleosome arrays with 167 bp repeat lengths show two-start “ladders” in the absence of linker histone. Upon addition of histone H5 the “ladders” twist, resulting in a 21 nm fibre. There is no co-operativity in the compaction of these nucleosome arrays upon addition of linker histone. This suggests compaction is primarily driven by inter-nucleosomal contacts, rather

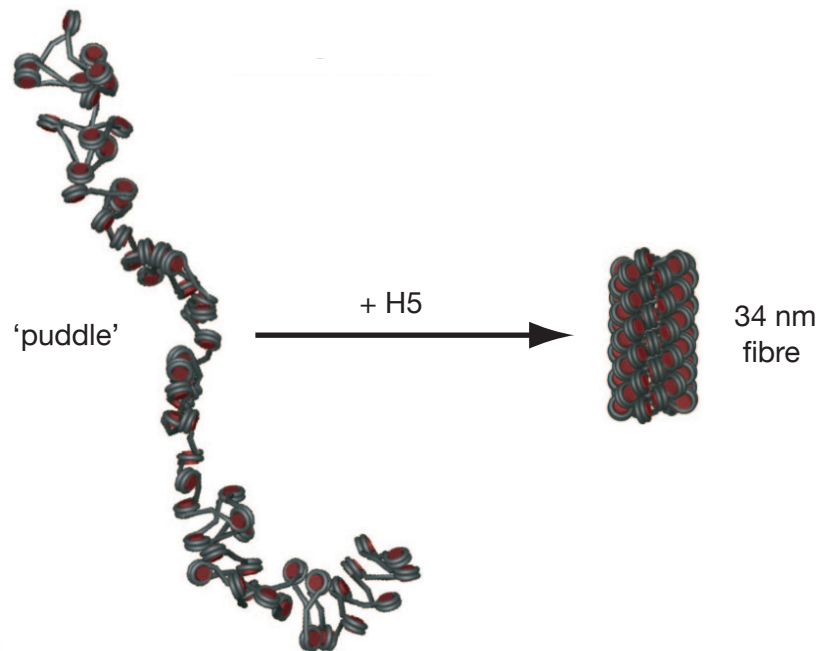
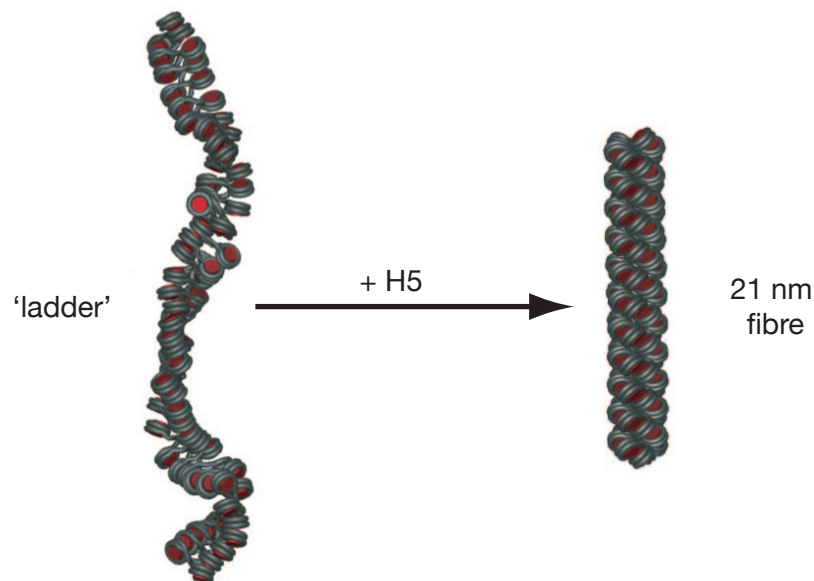
(a) 197 bp repeat length**(b) 167 bp repeat length**

Figure 1.3 Chromatin higher-order structure is determined by nucleosome repeat length and linker histone content. Schematics of the folding of nucleosome arrays upon addition of linker histone H5, based on electron micrograph images. **(a)** The unfolded 197 bp arrays show a disordered 'puddle' arrangement. Addition of linker histone causes formation of a 34 nm fibre, consistent with an interdigitated solenoid structure. **(b)** The unfolded 167 bp repeat arrays show a two-start 'ladder' structure similar to that seen in the crystal structure of the tetranucleosome (Figure 1.2). Addition of linker histone causes formation of a 'thin' 21 nm coiled fibre. Adapted from Routh et al. (2008).

than by the linker histone, probably due to the constraints of having such short linker DNA. The role of linker histones in higher-order chromatin compaction is discussed further in Section 1.3.2.4.

In nature, nucleosome repeat lengths along a filament are less regular than within these reconstituted systems (within the overall average nucleosome repeat length); the chromatin is also dynamic. This raises the possibility that a variety of “30 nm fibre” structures could occur within chromatin, with the local structure depending on linker histone variants and content, and nucleosome repeat lengths, as well as chromatin remodelling complexes (Wu et al., 2007). Two-start chromatin fibres may occur in regions of linker histone depletion, which has been shown to reduce nucleosome repeat lengths in chromatin (Fan et al., 2005). However, nucleosome repeat lengths are more commonly too long to support two-start chromatin fibres and an interdigitated solenoid fibre may form.

Higher levels of organisation than the “30 nm fibre” also occur, with the most compacted form of chromatin occurring in metaphase chromosomes. The progression from “30 nm fibre” to metaphase chromosome occurs through looping of the fibre on to chromosome “scaffolds” of non-histone proteins, via scaffold-associated region DNA sequences (Laemmli et al., 1992; Ottaviani et al., 2008). This chromatin scaffold is coiled into a helix, and the helix further packed to form the highly condensed chromatin structure of metaphase chromosomes (Boy de la Tour and Laemmli, 1988).

1.2 Epigenetics

Epigenetics has been defined as “nuclear inheritance which is not based on differences in DNA sequence” (Holliday, 1994). This may include the post-

translational chemical-modifications of core and linker histones, DNA methylation and inclusion of different histone subtypes. The effects of such chromatin modifications are discussed below.

1.2.1 Core histone post-translational chemical-modifications

Chemical modification of histone proteins has been known for many years (Murray, 1964). Since then a wide variety of post-translational modifications of core histones have been identified including: acetylation, ADP-ribosylation, methylation, phosphorylation, sumoylation and ubiquitination (reviewed by Kouzarides, 2007), as well as biotinylation, carbonylation and glycosylation (Hymes et al., 1995; Wondrak et al., 2000; Liebich et al., 1993). The chemical modifications mostly occur on the N-terminal tails of the core histones, although the carboxy-terminal (C-terminal) tails of histones H2A and H2B have ubiquitination sites at lysines 119 and 120 respectively (Goldknopf and Busch, 1977; Thorne et al., 1987). More recently modifications in the histone fold domains have been reported, at histone H3 on lysines 56 and 79 (Ng et al., 2002; van Leeuwen et al., 2002). Figure 1.4 summarises the known core histone chemical modifications identified in human (adapted from Ray-Gallet et al., 2005), and the most studied modifications are discussed below.

Acetylation is regulated by histone acetyl transferases and histone deacetylases, and occurs on lysine residues, decreasing the positive charge and altering the electrostatic interactions of the histone tails. This, in turn, modifies the inter-nucleosomal contacts and loosens higher-order structure, promoting transcriptional activity (Tse et al., 1998). As such, acetylated core histones are generally associated with transcriptionally active chromatin regions and they are enriched at the 5' end of coding regions (Liu et al., 2005; Schneider et al., 2006). An exception is acetylation of lysine 12 of histone H4, which is associ-

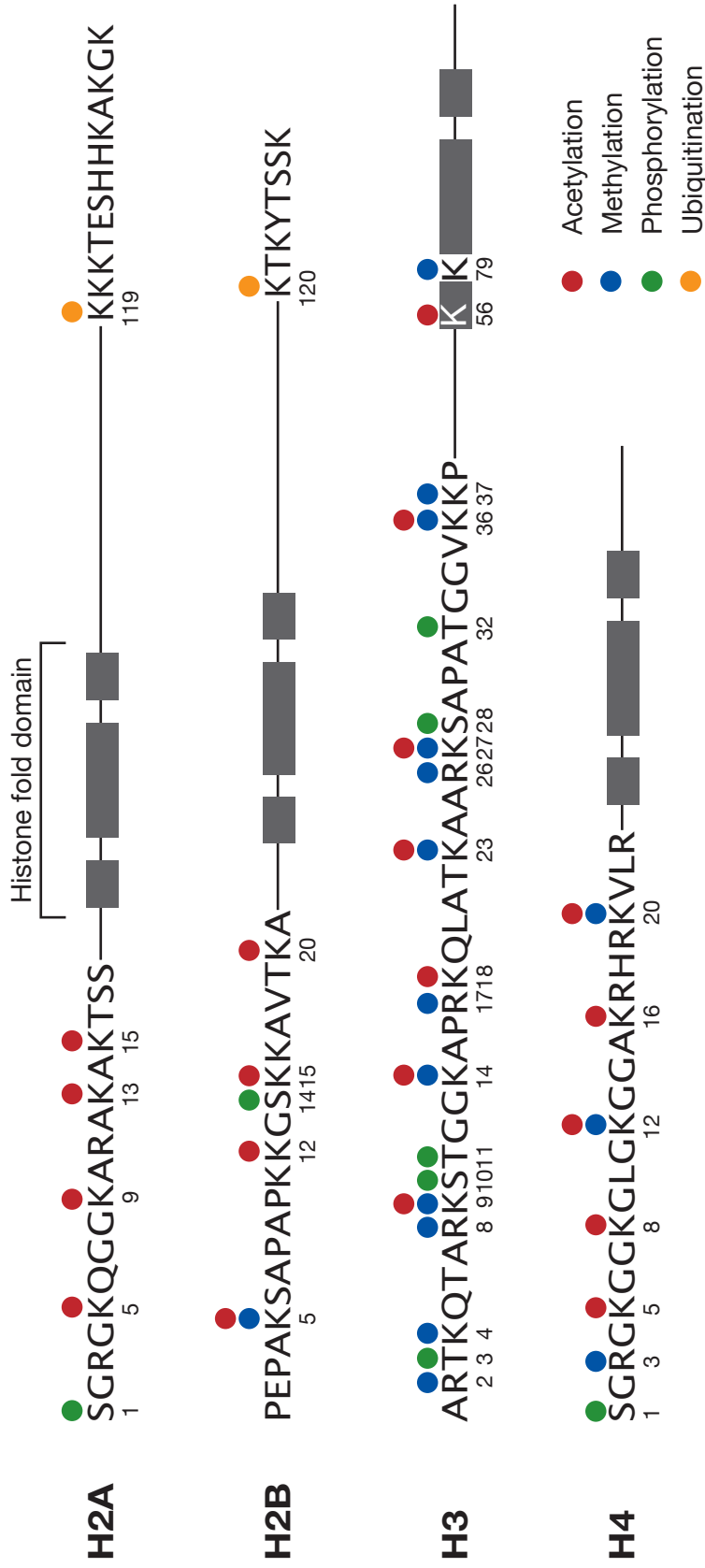


Figure 1.4 Post-translational modifications of human core histones. The helices of the histone fold domains are indicated by boxes and the post-translational modifications are coloured as follows: acetylation (red), methylation (blue), phosphorylation (green), ubiquitination (orange). The cores histones are not drawn to scale. Data from Ray-Gallet et al. (2005).

ated with regions of heterochromatin (Turner et al., 1992). Acetylated core histones also have roles in DNA replication and repair (Han et al., 2007; Celic et al., 2006). Bromodomain-containing proteins bind specifically to acetylated lysine residues in order to bring about these functional roles (Winston and Allis, 1999).

Methylation can occur on lysine and arginine residues by transfer of a methyl group from S-adenosyl methionine (Kim and Paik, 1965). Lysine methylation is performed by many methyltransferases that can act specifically on mono-, di- or tri-methylated residues (reviewed in Kouzarides, 2007), while lysine demethylases remove specific methylation marks. A number of arginine methyltransferases are known, but only one arginine demethylase has been identified to date (Chang et al., 2007). Methylated lysine residues are recognised by chromodomain-containing proteins (Jacobs et al., 2001), as well as proteins containing plant homeodomains (Shi et al., 2006) or chromo-like domains such as Tudor or MBT domains (Kim et al., 2006). These proteins tend to associate specifically with mono-methylated residues or di- and tri-methylated residues. Methylation has roles in a variety of processes. For example, histone H3K9 methylation recruits heterochromatin protein 1 to the promoters of euchromatic repressed genes (Schultz et al., 2002); H3K27 methylation is involved in X chromosome inactivation (Plath et al., 2003); and H4K20 has roles in heterochromatin formation and transcriptional repression via L3MBTL1 (Nishioka et al., 2002; Kalakonda et al., 2008) as well as in gene imprinting (Pannetier et al., 2008). In unicellular organisms H3K4, an activatory methylation mark, is more prevalent than in higher eukaryotes (Garcia et al., 2007), probably because a much higher proportion of unicellular genomes are transcriptionally active.

Phosphorylation of core histones is regulated by serine and threonine kinases and phosphatases, and is generally associated with sites of DNA damage and repair. For example, phosphorylated histone H2AX, a histone H2A sub-

type, is required to recruit repair factors at sites of DNA double-strand breaks, while its dephosphorylation facilitates the completion of DNA repair (Chowdhury et al., 2005). Phosphorylated residues are bound by 14-3-3 proteins (Furukawa et al., 1993).

Histone H2A ubiquitination is also thought to have roles in DNA repair (Bergink et al., 2006). Ubiquitination of histones H2A and H2B is regulated by ubiquitylases and deubiquitylases, although the process is not well understood. It has been suggested that the large size of the modification may have structural effects on chromatin (Moore et al., 2002). Histone H2A ubiquitination is associated with transcriptional repression (De Napoles et al., 2004), and histone H2B ubiquitination with transcriptional activation (Zhu et al., 2005).

Each core histone post-translational modification is suggested to contribute to a biological effect, by recruiting effector proteins, and leads to modification of processes such as transcription activation, chromatin condensation, DNA replication and DNA repair. This theory is known as the “histone code” (Strahl and Allis, 2000; Jenuwein and Allis, 2001). Single chemical modifications may be sufficient to cause a biological effect or they may act in combination with other modifications through “cross-talk”. For example, histone H4K20 methylation is dependent on the methylation of histone H3K9 (Kourmouli et al., 2004). In addition, some modifications may have context-specific effects. For example, methylation of histone H3K9 has been shown to activate transcription in some regions although it is usually a repressive mark (Vakoc et al., 2005).

1.2.2 Core histone subtypes

There are protein subtypes of core histones H2A, H2B and H3 that allow chromatin specialisation (Franklin and Zweidler, 1977 and reviewed by Kamakaka

and Biggins, 2005). The major core histone protein subtypes are expressed in S phase and involved in chromatin assembly, but other “replacement” subtypes can be incorporated into chromatin independently of DNA replication (Wu et al., 1982).

There are several “replacement” subtypes of histone H2A. Histone H2A-Bbd and macroH2A are present only in vertebrates. Histone H2A-Bbd is enriched in transcriptionally active regions (Chadwick and Willard, 2001a), while macroH2A1 and macroH2A2 are enriched in the inactive X chromosome (Chadwick and Willard, 2001b). H2AX has roles in DNA repair (Ward and Chen, 2001 and Section 1.2.1). H2A.Z has a variety of roles, for example, facilitating the folding of nucleosomal arrays but inhibiting the formation of highly condensed chromatin structures (Fan et al., 2002). H2A.Z also functions in the regulation of nucleosome turnover at barrier elements between heterochromatin and euchromatin (Dion et al., 2007).

Histone H2B has a testis- and sperm-specific subtype, called TSH2B (Zalensky et al., 2002). Histone H3.3, a “replacement” H3 subtype is associated with transcriptionally active regions (Ahmad and Henikoff, 2002), while CENP-A is the histone H3 subtype found in centromeric nucleosomes (Palmer et al., 1991). No subtypes of histone H4 have been reported.

1.2.3 DNA methylation

DNA is methylated on the cytosine of CpG dinucleotides by DNA methyltransferases, using S-adenosyl methionine as the methyl group donor. The level of DNA methylation varies between species, with *Saccharomyces cerevisiae* having none (Binz et al., 1998). It is only present in *Drosophila melanogaster* during early stages of development (Lyko et al., 2000), but is more prevalent in

mammals. The specificity of the DNA methylases is enhanced by small interfering RNA molecules (Kawasaki and Taira, 2004) or protein factors (Brenner et al., 2005). DNA methylation has roles in mammalian development (Okano et al., 1999) and is associated with regions of transcriptional repression, except in invertebrates where it is an activating mark (reviewed in Cedar, 1988; Field et al., 2004). It can function in repression by preventing the binding of transcription factors (Watt and Molloy, 1988) or through association of methyl binding domain-containing proteins, which recruit co-repressor complexes (Jones et al., 1998; Nan et al., 1998). There is co-operation between DNA methylation, histone H3K9 methylation and heterochromatin protein 1 to reinforce silent chromatin domains (reviewed by Fuks, 2005).

1.3 Linker histones

Linker histones are small, highly basic, lysine-rich proteins that have a highly conserved “winged-helix” globular domain (Ramakrishnan et al., 1993). This globular domain is flanked by basic N- and C-terminal tails, which show considerable variety in length and sequence.

Linker histones are not essential for the viability of lower eukaryotes, such as *S. cerevisiae*, *Aspergillus nidulans* and *Ascobolus immersus*, although linker histone deletion mutants may show a reduced life span (Ushinsky et al., 1997; Downs et al., 2003; Ramon et al., 2000; Barra et al., 2000). Linker histones are, however, essential for the viability of higher eukaryotes. For example, mice that are null for three linker histone subtypes die during embryogenesis although mouse embryonic cell lines can be propagated and contain 50% of the normal H1 levels (Fan et al., 2005). Mice null for two of the six linker histone subtypes are viable but there are compensatory effects restoring the wild-type

ratio of linker histone to core nucleosome (Fan et al., 2003).

1.3.1 The role of linker histones in transcriptional regulation and epigenetics

1.3.1.1 Linker histone variants

There is a wide range of species- and tissue-specific linker histone variants, which are regulated through differentiation and cell cycle-specific expression (Khochbin, 2001). The linker histone variants differ in mass, amino acid composition and sequence. The globular domains are relatively conserved compared with the basic tails, which vary in sequence and length.

The human linker histones have been studied extensively. To date eleven linker histone variants have been identified in humans (reviewed in Hapfel and Doenecke, 2009). Linker histones H1.1, H1.2, H1.3, H1.4 and H1.5 are ubiquitously expressed in somatic cells. H1x is also expressed ubiquitously but accumulates during the G1 phase of the cell cycle. Histones H1t, H1T2, H1LS1 and H1oo are expressed specifically in germ cells (H1t is also expressed in spleen cells). Histone H1.0 (H1^o) is expressed in terminally differentiated cells.

Linker histone variants have different affinities for DNA and chromatin, possibly caused by the differences in their C-terminal tails (De Lucia et al., 1994; Th'ng et al., 2005). In fluorescence recovery after photobleaching (FRAP) experiments, carried out by Th'ng et al., the length of the C-terminal tail correlated with affinity for chromatin *in vivo*, although an exception was H1.0, which has the shortest tail but moderate affinity. This could be explained, as the H1.0 tail has the highest density of basic residues, which would increase its association to DNA compared to a similar length, less basic tail. The variants were grouped as follows: low affinity (H1.1, H1.2), moderate affinity (H1.0, H1.3) and high

affinity (H1.4, H1.5). An *in vitro* study produced a slightly different result. This study determined linker histone variant affinity for chromatin in the presence of scaffold-associated region DNA to prevent precipitation: low affinity (H1.0), moderate affinity (H1.2, H1.5) and high affinity (H1.3, H1.4, H1.0) (Orrego et al., 2007).

Linker histone variants are located in different chromatin regions. The use of green fluorescent protein (GFP)-tagged linker histones in FRAP experiments demonstrated that histones H1.0, H1.1, H1.2 and H1.3 are enriched in euchromatin, while histones H1.4 and H1.5 are enriched in heterochromatin (Th'ng et al., 2005). The variants also have different effects on gene expression. Removal of a specific variant in mice caused particular effects on structure-dependent transgene expression (Alami et al., 2003). This indicates that the arrangement of linker histone variants within chromatin could allow fine-tuning of both chromatin structure and transcription.

A specialised linker histone variant used widely (and in this Thesis) is the erythrocyte-specific histone H5, which is exclusively found in birds, fish, amphibians and reptiles (Neelin et al., 1964). Histone H5 is different from the other chicken linker histones, having shorter N- and C-terminal tails and a differing globular domain sequence. It is similar to mammalian histone H1.0, although it has a higher arginine content and differences in the loop between helices II and III in the globular domain (see Section 1.3.2.1). The higher arginine content of histone H5 may account for its greater affinity for DNA (Clark and Thomas, 1988), four-way junction DNA (Varga-Weisz et al., 1994), and chromatin, relative to other linker histones (Kumar and Walker, 1980).

1.3.1.2 Post-translational modifications of linker histones

Like core histones, linker histones have a role in the “histone code”, with post-translational chemical modifications modulating their DNA and protein interactions, and affecting processes such as chromatin compaction levels and transcription. Many post-translational modifications of linker histones are known (reviewed in Happel and Doenecke, 2009). The first to be identified was phosphorylation (Balhorn et al., 1972) and further modifications reported include acetylation, methylation, N⁶-formylation and ubiquitination, in a variety of species including mammals, chicken and *Drosophila* (Wisniewski et al., 2007; Snijders et al., 2008; Villar-Garea and Imhof, 2008). A summary of the known linker histone posttranslational modifications for humans are shown in Figure 1.5 (Wisniewski et al., 2007).

The best-studied post-translational modification of linker histones is phosphorylation. It is a common modification, occurring at up to five sites on each of the five major human subtypes plus H1x (Wisniewski et al., 2007). The majority of these phosphorylation sites have cyclin-dependent kinase (CDK) consensus motifs, S/TPXR/K (Garcia et al., 2004). Linker histone subtypes are differentially phosphorylated, both relative to each other (Sarg et al., 2006), and throughout the cell-cycle (Bradbury et al., 1974; Hohmann et al., 1976; Gurley et al., 1995).

Initially it was thought that linker histone phosphorylation had a role in chromatin condensation, because phosphorylation levels increase during mitotic chromosome condensation (Yasuda et al., 1981). Also, dephosphorylation of linker histone (and histone H3) in cells arrested at metaphase causes decondensation of the chromosomes (Th'ng et al., 1994). However phosphorylated histone H1 is associated with chromatin decondensation at active replication foci (Alexandrow and Hamlin, 2005). The apparent inconsistency between the

effect of H1 phosphorylation during M-phase and at active foci could be explained by the removal of linker histone at M-phase being required to allow other molecules to compact the chromosomes, e.g. condensins. Indeed, on a molecular level, phosphorylation reduces the affinity of linker histone for DNA, especially the affinity of the C-terminal tail (Green et al., 1993; Hendzel et al., 2004), and FRAP experiments indicate that linker histones have a higher chromatin exchange rate when they are phosphorylated (Lever et al., 2000; Contreras et al., 2003).

Linker histone phosphorylation is associated with regulation of gene expression. Phosphorylated linker histones are enriched in active chromatin *in vivo* (Chadee et al., 1995). Gene activation is suggested to cause phosphorylation of the linker histone, reducing its affinity for the nucleosomes and allowing chromatin remodelling-complexes to modify nucleosome positions (Horn et al., 2002) opening up the chromatin for transcription initiation.

Acetylation and methylation occur at several sites in human, mouse and chicken linker histones (Wisniewski et al., 2007; Snijders et al., 2008). Acetylation can occur at sites within the globular domain that are important for DNA binding, as well as in the N- and C-terminal tails (Wisniewski et al., 2007). Deacetylation of lysine 26 in human linker histone has a role in SirT1-mediated heterochromatin formation (Vaquero et al., 2004). This residue can also be methylated, and then acts as a binding site for heterochromatin protein 1 and results in transcriptional repression (Daujat et al., 2005). However, this interaction does not occur if the neighbouring serine residue is phosphorylated, providing an example of a “phospho-switch” within the “histone code”.

Other post-translational modifications of linker histones have been observed, but their mode of action is not fully understood. For example histone H1 can be ubiquitinated, adding 76 amino acids to the protein, which would

be expected to have a structural effect within chromatin (Moore et al., 2002). In *Drosophila* a reduction in H1 ubiquitination reduces the expression from Dorsal-dependent genes (Pham and Sauer, 2000). Poly(ADP)-ribosylation of linker histones also causes relaxation of the chromatin structure (Poirier et al., 1982) and plays a role in maintaining the DNA methylation pattern (Zardo et al., 1997).

Reducing histone H1 content in mouse embryonic stem cells, and total suppression of histone H1 genes in *Arabidopsis thaliana*, lead to changes in DNA methylation within specific genomic regions (Fan et al., 2005; Wierzbicki and Jerzmanowski, 2005). However, the connection between linker histones and DNA methylation is currently unclear. In some assays histone H1 binds preferentially to methylated DNA (McArthur and Thomas, 1996) and causes stronger inhibition of transcription from methylated chromatin templates (compared to unmethylated) (Levine et al., 1993). However, other assays show no preference of histone H1 for methylated DNA, either alone or in nucleosomes (Campoy et al., 1995; Nightingale and Wolffe, 1995).

There are two non-enzymatic modifications known for linker histones. N⁶-formylation, which is thought to arise from oxidative DNA damage, occurs at lysines in all three domains of histone H1 and is thought to impede the function of linker histones by preventing acetylation or methylation at these residues (Jiang et al., 2007b). Deamidation of asparagines and glutamine residues (to aspartic acid and glutamic acid respectively) has also been observed (Snijders et al., 2008) and is thought to affect protein structure and stability (Lindner et al., 1998).

1.3.1.3 Linker histones and core histone post-translational modification

The relationship between linker histones and core histone post-translational modifications is not well understood. Core histone acetylation reduces the affinity of linker histones for nucleosomes and their ability to compact chromatin (Perry and Annunziato, 1991; Ridsdale et al., 1990). It also causes an increase in the dynamics of linker histones within chromatin (Misteli et al., 2000). Conversely, linker histones have been shown to inhibit core histone acetylation within nucleosomes, both *in vitro* and *in vivo* (Herrera et al., 2000), suggesting there may be a feedback mechanism between linker histone binding and core histone acetylation.

Histone H1-depleted mouse embryonic stem cells also show a four-fold reduction in acetylation of histone H4K12 (Fan et al., 2005). This is suggested to compensate for linker histone depletion by increasing the net positive charge on the H4 tail, neutralising the charges on the DNA to a greater extent, and creating a more compact chromatin structure. The histone H1-depleted cells also show a two-fold reduction in histone H3K27 tri-methylation. Cytoplasmic retention of a linker histone subtype in *Caenorhabditis elegans* causes a reduction in histone H3K9 and H3K27 methylation, and an increase in the activatory H3K4 methylation mark, causing desilencing of a silenced transgene (Jedrusik and Schulze, 2007).

1.3.1.4 Gene-specific effects of linker histones

Linker histones have long been considered to be general repressors of transcription (Schlissel and Brown, 1984; Weintraub, 1984). However, although linker histones are partially depleted at actively transcribed genes they are not absent (Nacheva et al., 1989; Kamakaka and Thomas, 1990; Krishnakumar et al., 2008).

Linker histones can be removed entirely in lower eukaryotes (Ramon et al., 2000), or levels reduced in higher eukaryotes (Fan et al., 2005), without global effects on transcription. This suggests they might only affect the transcription from a subset of genes to which they bind. For example, in mouse embryonic stem cells with 50% depletion of linker histones there are very few changes in gene-expression compared with wild-type cells (Fan et al., 2005). Only 38 gene targets had changes in expression of more than two-fold, and these showed both increases and decreases in expression. However, half of the somatic linker histone variants were still present indicating that the lack of a global effect on transcription could be due to the removal of only a subset of the linker histone variants. *S. cerevisiae* is viable when linker histone is completely absent and yet this still results in only gene-specific effects on transcription (see Section 1.5.4), suggesting that the gene-specific effects of linker histones seen by Fan et al. may not be down to the retention of a subset of the linker histone variants. Gene-specific effects of linker histones are not surprising, given the different binding of linker histone variants to euchromatin and heterochromatin regions (Section 1.3.1.1) and modification to linker histone action through post-translational modification of both linker and core histones (Sections 1.3.1.2 and 1.3.1.3).

Modification of linker histone binding to nucleosomes affects the regulation of transcription, both through its role in nucleosome positioning and through competition with other transcription factors (Section 1.3.2.3). For example, linker histone binding occludes the binding of USF and GAL4-AH transcription factors to nucleosomes (Juan et al., 1994). This was later shown to be due to reduction of the transient exposure of DNA binding sites on the nucleosome surface, rather than direct steric interference (Juan et al., 1997). Another role of linker histone-dependent chromatin condensation in transcrip-

tional regulation, in principle, could be the bringing together of distal regulatory DNA elements.

1.3.2 The role of linker histones in chromatin structure

1.3.2.1 The structure of linker histones

Histone H5 is an avian erythrocyte-specific linker histone that was used in the initial structural studies of the linker histone globular domain (Figure 1.6 and Ramakrishnan et al., 1993). The H5 globular domain shares structural similarity with sequence-specific DNA-binding proteins, such as HNF-3 γ , and is very similar to the globular domain of histone H1, although there are differences in the loop between helices II and III (Figure 1.6; Cerf et al., 1994).

The linker-histone globular domain consists of three α -helices and a three-stranded β -sheet. The domain contains two DNA-binding sites (Figure 1.6; Goytisolo et al., 1996), clusters of basic residues, that are highly conserved (Figure 1.7; Wells and McBride, 1989; Wells and Brown, 1991). Mutation of one DNA binding site abolishes the ability of linker histone globular domains to bind to chromatin correctly and to assemble tramline complexes through binding of two DNA molecules simultaneously (Goytisolo et al., 1996; Brown et al., 2006).

1.3.2.2 Linker histone binding in the nucleosome

Linker histones are generally present in approximately stoichiometric amounts relative to nucleosomes. For example, liver nuclei contain 0.8 molecules of linker histone molecules per nucleosome and chicken erythrocyte chromatin has about 1.3 linker histones (H1 and H5) for each core nucleosome (Bates and

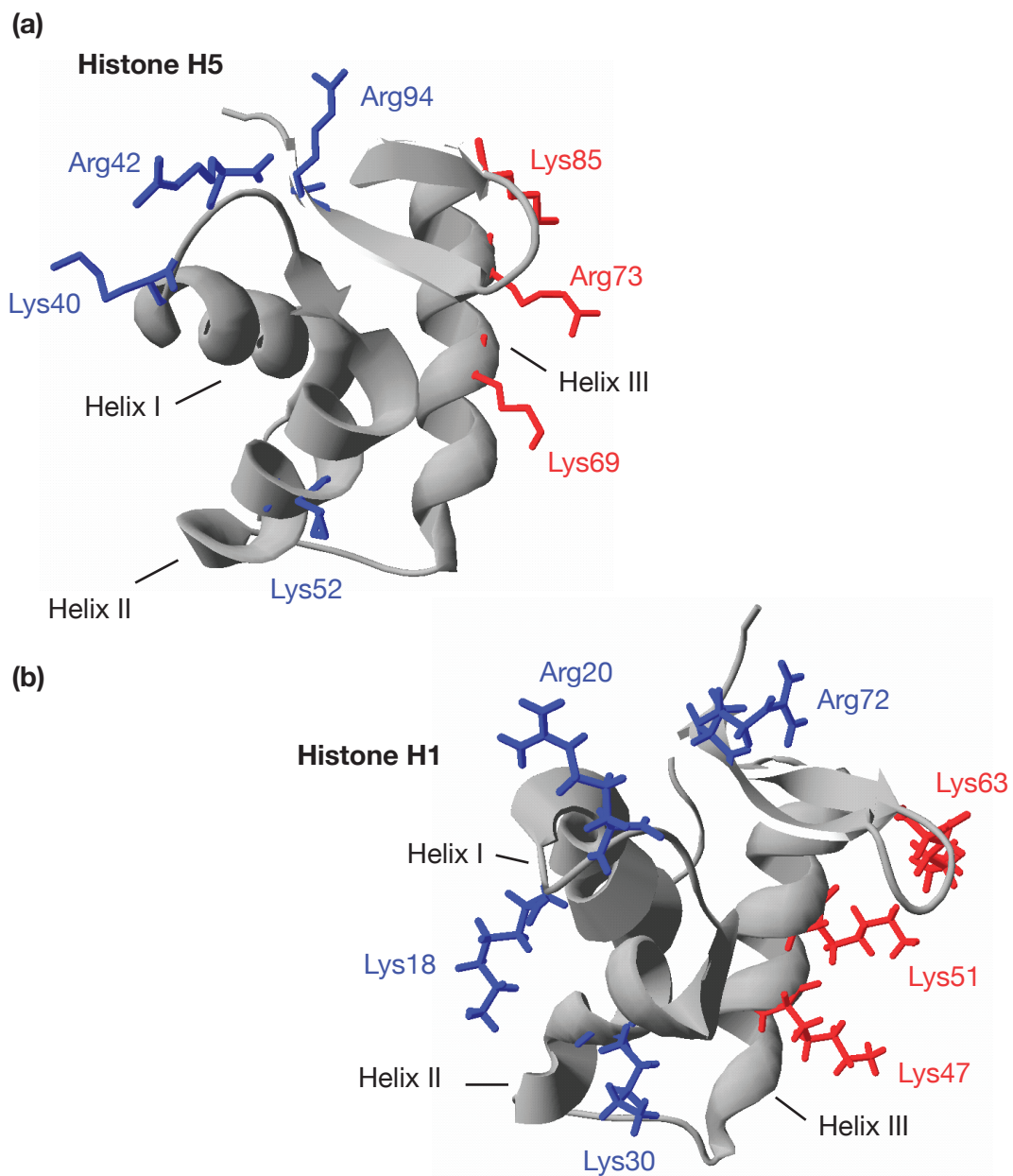


Figure 1.6 Structure of the globular domains of chicken linker histones H1 and H5. The putative DNA binding residues are marked as follows: site I (red), site II (blue). **(a)** X-ray crystal structure of chicken histone H5 (Ramakrishnan et al., 1993) **(b)** NMR structure of chicken histone H1, using residue numbering for the globular domain (Cerf et al., 1994). Images were generated using Swiss PDB viewer and pdb files: 1HST (H5) and 1GHC (H1).



Figure 1.7 Conservation of the DNA binding sites of linker histones. A multiple-sequence alignment of the globular domains of several linker histones. The secondary structure shown is based on the crystal structure of GH5 and is from Ali et al. (2004). The residues in colour are the putative DNA binding site residues, based on GH5 (Figure 1.6).

Thomas, 1981). Embryonic stem cells, however, contain only about 1 linker histone per 2 nucleosomes (Woodcock et al., 2006).

Linker histones bind asymmetrically to the nucleosome, near the DNA dyad. H5 makes contacts through DNA binding site I to chromatosomal DNA, and through the second DNA binding site to the nucleosome dyad (Figure 1.8a; Zhou et al., 1998). Linker histone H1 was also shown to bind at the nucleosome dyad in a DNase I protection assay (Staynov and Crane-Robinson, 1988) and, more recently, modelling of a histone H1 subtype suggested it binds to a nucleosome core in a very similar manner to histone H5 (Figure 1.8b and Brown et al., 2006). When a linker histone binds to the nucleosome core in this way its C-terminal tail is located at the point where DNA enters and exits the nucleosome. This allows the C-terminal tail to bind the linker DNA forming stem-loop structures (Figure 1.8c; Bednar et al., 1998; Sivolob and Prunell, 2003).

1.3.2.3 Linker histone binding to DNA in chromatin

Binding of linker histone to chromatin occurs through the globular domain (Allan et al., 1980; Zhou et al., 1998) and the isolated globular domain is sufficient to bind chromatin and protect chromosome-length DNA from nuclease digestion (Allan et al., 1980). The role of the linker histone N-terminal basic tails is unclear but they are thought to have a role in the positioning of the globular domain (Allan et al., 1986). The basic C-terminal tails have roles in chromatin binding and condensation (Allan et al., 1986; Hendzel et al., 2004); they are thought to act as poly-cations neutralising the charges of the linker DNA. The C-terminal tail of vertebrate histone H1 has been shown to adopt α -helical confirmation upon binding to DNA (Roque et al., 2005).

Linker histone binding to DNA in chromatin is strongly affected by the presence of the C-terminal basic tail, the removal of which reduces the affinity

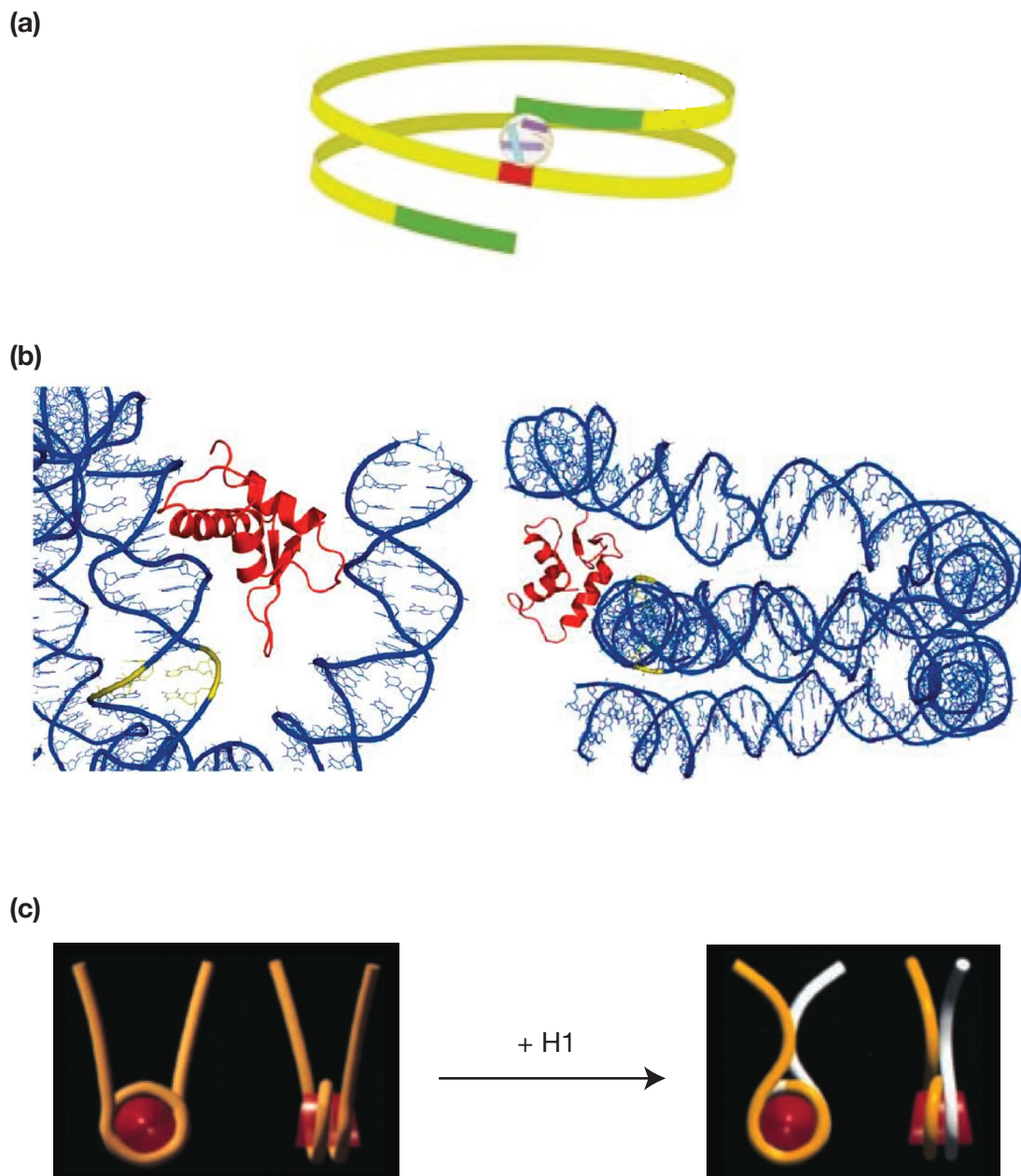


Figure 1.8 Binding of linker histone to the chromatosome. (a) A schematic of the position of GH5 on a chromatosome. Nucleosome dyad, red; Chromatosomal DNA, green; Nucleosomal DNA, yellow. From Zhou et al. (1998). (b) Two views of a molecular model of linker histone binding to the chromatosome. Chromatosomal and nucleosomal DNA, blue; nucleosome dyad, yellow; globular domain of histone H1, red. From Brown et al. (2006). (c) Models of entry and exit of DNA from the nucleosome in the absence and presence of linker histone. Addition linker histone causes the formation of various stem-loop in the DNA with differing cross-overs of the entry and exit DNA, of which one is shown. From Bednar et al. (1998).

for chromatin (De et al., 2002; Hendzel et al., 2004). Deletion of the N-terminal tail shows only a modest effect on chromatin binding. Hendzel and colleagues (2004) demonstrated that the S/TPKK phosphorylation sites in the C-terminal tail are particularly important for linker histone binding, as the substitution of threonine 152, which is in such a site, with glutamic acid had almost the same effect as truncating the tail at residue 151.

Linker histones bind cooperatively to linear DNA molecules in low concentrations of sodium chloride (Renz and Day, 1976; Clark and Thomas, 1988), producing an H1-rich and H1-poor species when added to DNA at an input ratio of less than 0.6 (Clark and Thomas, 1986). They show a preference for binding AT-rich DNA (Renz and Day, 1976) (such as scaffold-associated regions (Izaurralde et al., 1989) and the AT element of simian virus 40 DNA (Hendrickson and Cole, 1994)), *cis*-platin-damaged DNA (Yaneva et al., 1997) and other distorted DNA structures, such as four-way junctions (Varga-Weisz et al., 1994).

Linker histones have long been known to bind chromatin fragments dynamically (Caron and Thomas, 1981; Thomas and Rees, 1983). These observations have been supported by more recent studies using FRAP experiments in living cells. Histone H1 exchanged between chromatin regions continuously with residence times of several minutes, although the vast majority was bound at all times (Lever et al., 2000; Misteli et al., 2000). As well as the linker histone variant and the post-translational modifications of both linker histones and core histones (Section 1.3.1), the presence of site-specific (such as HNF-3 and MeCP2) (reviewed in Zlatanova et al., 2000) or global competitors (such as HMGB, HMGN, and HMGA proteins) (Catez et al., 2004) also affect the association of linker histone with chromatin.

Linker histones affect chromatin structure through nucleosome positioning. If underlying nucleosome positions are specified in the DNA sequence

the linker histones do not over-ride this but, when there are alternative positions available, they affect the relative distribution of nucleosomes (Meersseman et al., 1991). Linker histones inhibit short-range nucleosome mobility *in vitro* (Pennings et al., 1994), and depletion of linker histone in mouse embryonic stem cells reduces the nucleosome repeat length (Fan et al., 2005).

1.3.2.4 Linker histones and higher-order chromatin structure

Linker histones are required for maximal compaction of chromatin and stable formation of a regular “30 nm fibre” (Figure 1.3; Thoma et al., 1979; Hizume et al., 2005). Upon increasing ionic strength linker histone-depleted chromatin folds into structures that approach H1-mediated compaction levels, however the fibres lack order (Thoma et al., 1979; Yao et al., 1991). Depletion of three linker histone variants from mouse embryonic stem cells and analysis of the chromatin using electron microscopy showed that the chromatin was less compact than wild-type chromatin and had an irregular distribution of open 10 nm filament and more compact structures throughout the polynucleosomes (Fan et al., 2005). Depletion of histone H1 also causes elongation of metaphase chromosomes, preventing proper segregation of chromosomes during anaphase (Maresca et al., 2005).

As mentioned above (Section 1.3.2.3), the C-terminal domain of linker histones binds linker DNA through non-specific electrostatic interactions, causing charge-neutralisation. However, it functions in chromatin condensation through specific tail subdomains. Regions required for the formation of the stem-loop linker DNA structure (Figure 1.8c; Lu and Hansen, 2004) and the stabilisation of chromatin condensation (Bharath et al., 2002) have been identified and contain S/TPKK motifs. The positioning of these subdomains within the C-terminal tail, as well as the S/TPKK motifs themselves, determine tail function-

ality to a greater extent than the specific sequence of the subdomains (Bharath et al., 2002; Lu et al., 2009).

1.4 Yeast chromatin

The model organism *S. cerevisiae* is a unicellular budding yeast that is used in research because it is easily genetically manipulated. The basic cellular processes, such as replication, cell division and metabolism are conserved from yeast to mammals.

S. cerevisiae (hereafter called yeast) contains core histone proteins that are highly homologous with those of higher eukaryotes (Wells and McBride, 1989). It has two identical copies of histones H3 (Hht1p, Hht2p) and H4 (Hhf1p, Hhf2p) and two very similar subtypes of histones H2A (Hta1p, Hta2p) and H2B (Htb1p, Htb2p). Yeast also contains a H2A.Z homologue called Htz1p, which is enriched in nucleosomes at promoter regions and is involved in transcriptional regulation by preventing the spread of silent heterochromatin (Li et al., 2005; Meneghini et al., 2003). Nuclease digestion of yeast chromatin demonstrates that it is packaged into nucleosomes in a similar manner to higher eukaryotes (Thomas and Furber, 1976). Yeast chromatin is able to condense and form “30 nm fibres”, resembling those in higher eukaryotic chromatin, suggesting either the presence of a linker histone-like molecule or a subtly different fibre structure (Lowary and Widom, 1989). For a long time the presence of a yeast linker histone was debated, but the HHO1 gene product has now been identified as a *bone fide* linker histone (Landsman, 1996; Section 1.5). Hho1p chromatin levels are much lower than metazoan linker histones (Section 1.5.2; Chapter 3) and, as yet, there have been no other yeast linker histone variants identified, raising the question of whether the function of Hho1p in yeast chro-

matin is different from that of linker histones in metazoan chromatin.

Although there are similarities between yeast chromatin and that of higher eukaryotes there are also differences. The nucleosome repeat length in yeast (165 bp) (Thomas and Furber, 1976) is much shorter than that of higher eukaryotes, which mostly vary from 170–260 bp (van Holde, 1989). The majority of higher eukaryotic species and tissues have nucleosome repeat lengths around 188–196 bp, with chicken erythrocytes having 207 bp repeat length (Compton et al., 1976) and sea urchin sperm having 240 bp repeat length (Spadafora et al., 1976). There are also differences between putative nucleosome-positioning motifs determined for yeast, for which the 10 bp periodic AT-dinucleotides extend beyond the nucleosome core sequence, unlike those for chicken and *Drosophila* nucleosomes (Cui and Zhurkin, 2009).

A global assessment of yeast core histone post-translational modifications identified acetylation and methylation (Jiang et al., 2007a). Yeast chromatin is highly acetylated (Davie et al., 1981; Waterborg, 2000) but further studies are required to determine how other modifications in yeast compare with those in other organisms. Yeast-like chromatin, with short nucleosome repeat lengths, has been used to determine structural information about the nucleosome core (Luger et al., 1997; White et al., 2001) and higher-order structures (Schalch et al., 2005; Routh et al., 2008), however it remains to be determined whether yeast chromatin is a true model for that of higher eukaryotes. Central to this question is whether the non-canonical Hho1p linker histone functions in the same way as canonical linker histones.

1.5 The yeast linker histone

Whether *S. cerevisiae* contained a linker histone was unclear for a long time. As the nucleosome repeat length is so short, extensive binding of a linker histone would result in there being no linker DNA between nucleosomes. Also the yeast chromatin is mostly transcriptionally active, so it was thought that yeast may not require a linker histone (Davie et al., 1981; Waterborg, 2000). Early investigations were unable to identify a linker histone in yeast chromatin extracts (Moll and Wintersberger, 1976; Thomas and Furber, 1976), while a candidate H1-like protein (Sommer, 1978) was later shown to also be HMG-like and mitochondrial (Weber and Isenberg, 1980; Certa et al., 1984). However, anti-mouse histone H1 antibodies did suggest the presence of a linker histone-like protein in salt extracts from yeast (Srebrevna et al., 1987).

It was not until the *S. cerevisiae* genome was sequenced (Goffeau et al., 1996; Bussey et al., 1997) that a putative histone H1 orthologue was identified. Various linker histone sequences were compared with the yeast genomic sequence using local alignment searches against DNA in all six reading frames. One open reading frame with sequence homology to the globular domain of linker histones was identified and named HHO1 (Histone H One 1) (Landsman, 1996; Ushinsky et al., 1997). The systematic name of the gene is YPL127C. The HHO1 gene encodes Hho1p, a protein of 258 amino acids and a calculated molecular weight of about 28 kDa. The overall identity of Hho1p sequence compared to other linker histones was assessed at 40–57% (Ushinsky et al., 1997). Comparison of Hho1p protein with itself identified a second region with sequence homology to a linker histone globular domain (Landsman, 1996) making it structurally distinct from canonical linker histones (see Figure 1.9a; Section 1.3.2.1). The first “globular” domain, GI, is flanked by a basic N-terminal tail similar to those of canonical linker histones. There is a basic linker re-

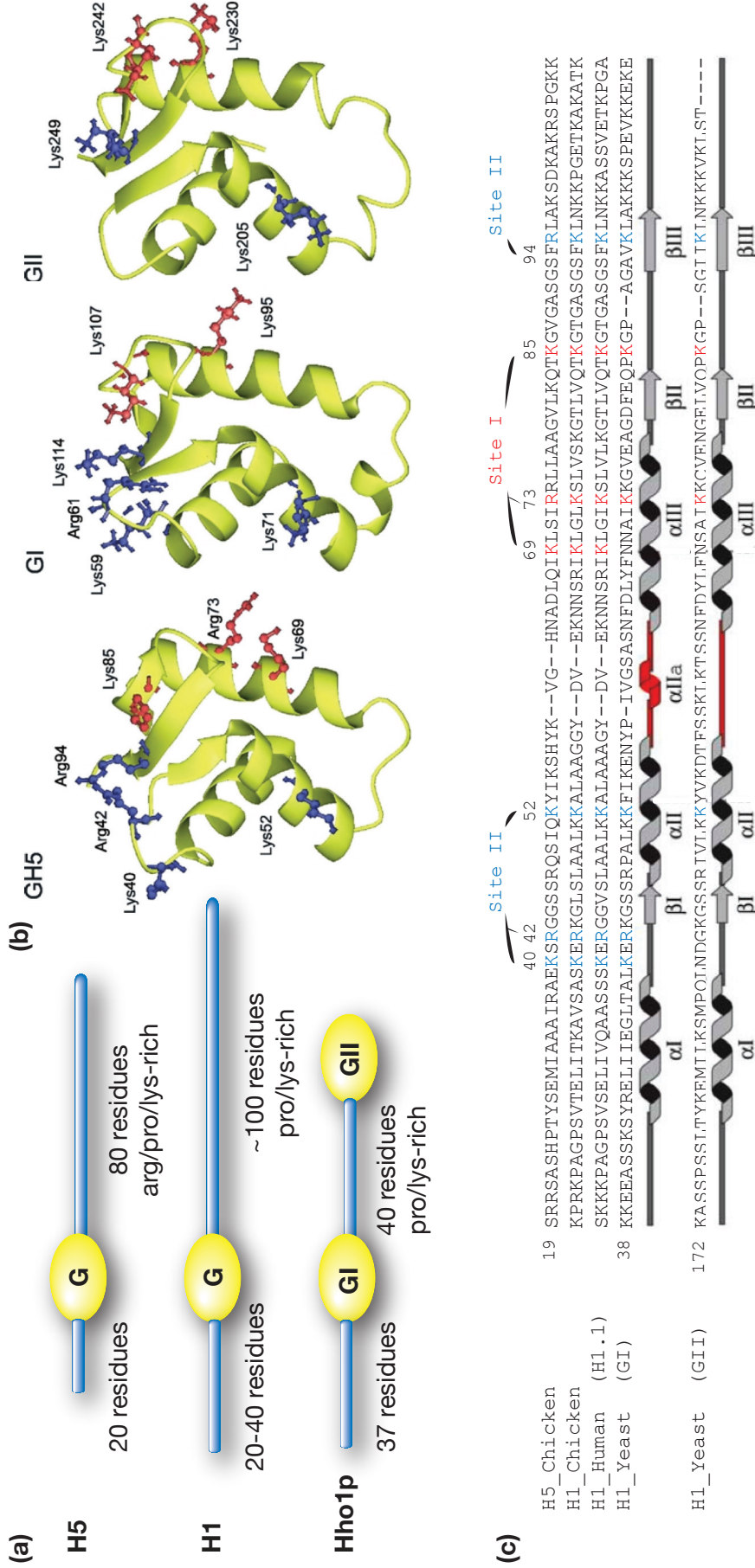


Figure 1.9 The yeast linker histone, Hho1p. (a) Cartoons showing the domain structures of Hho1p and canonical linker histones. (b) Ribbon diagrams of structures of the globular domain of histone H5 (GH5) and the two Hho1p domains that show homology to GH5, indicating the positions of the basic residues of the putative DNA binding sites. From Ali et al. (2004). (c) A multiple-sequence alignment of linker histone globular domains. The DNA binding site residues of histone H5 and the secondary structure of Hho1p domains, GI and GII, are indicated. Adapted from Sanderson et al. (2005).

gion between GI and the second “globular” domain, GII, that resembles the C-terminal tail of canonical linker histones in terms of its composition, being proline- and lysine-rich, but does not contain S/TPKK phosphorylation motifs. There is no C-terminal extension beyond GII. The biochemistry of the isolated “globular” domains is discussed in Section 1.5.5.

Initially it was unclear whether Hho1p functions as a true linker histone. Early evidence supporting the putative linker histone role of Hho1p demonstrated that it has similar electrophoretic and chromatographic properties to other linker histones (Patterton et al., 1998), and that Hho1p and the core histones are the only genes transcribed during S phase (Spellman et al., 1998). Hho1-GFP fusion protein localises to the nuclei of yeast cells (Ushinsky et al., 1997), and a fusion protein of Hho1p with two copies of human influenza hemagglutinin (HA) is acid-extracted from the nuclear fraction along with core histones (Freidkin and Katcoff, 2001). Hho1p is able to bind reconstituted core-dinucleosomes (Patterton et al., 1998) and confer a “chromatosome stop” of about 167 bp during digestion of chromatin by micrococcal nuclease (Patterton et al., 1998; Ali and Thomas, 2004). Like canonical linker histones (Section 1.3.2.3), Hho1p binds preferentially to non-linear DNA structures, such as supercoiled DNA (Ono et al., 2003) and four-way junction DNA (Ali and Thomas, 2004).

A yeast strain deleted for the HHO1 gene is viable and has no detectable defect in cell growth, replication, mating or sporulation (Ushinsky et al., 1997; Escher and Schaffner, 1997; Patterton et al., 1998). An HHO1 knock-out mutant, in a W303 background strain, showed a decreased lifespan (number of budding events) (Downs et al., 2003), while a similar assay in an S288C strain did not (Li et al., 2008). The viability of *hho1*-null yeast strains contrasts with the situation in more complex, higher eukaryotes, which require a number of linker histone

variants for their development (Section 1.3; Fan et al., 2001, 2003).

To date, Hho1p is the only linker histone identified with non-canonical domain structure. A linker-histone protein has yet to be identified in *Schizosaccharomyces pombe*, while the basic “linker histone-like” protein in *Tetrahymena thermophila* has no globular domain (Shen and Gorovsky, 1996) and cannot be considered a true linker histone.

1.5.1 Structural studies of Hho1p

Model structures for the GI and GII domains of Hho1p were produced using the crystal structure of the H5 globular domain (GH5) as a threading guide (Baxevanis and Landsman, 1998). The sequences of the Hho1p “globular” domains are compatible with the formation of the winged-helix motif, characteristic of canonical linker histone globular domains, and NMR studies confirmed that both isolated domains have structural similarity to GH5 (Figure 1.9b; Ono et al., 2003; Ali et al., 2004). The GII domain exists in slow equilibrium between two species: one folded and one “unfolded”. The equilibrium shifts to the folded form in the presence of high concentrations of tetrahedral anions, such as phosphate or perchlorate, which may mimic the presence of DNA (Ali et al., 2004). The GI and GII domains of Hho1p show structural differences, compared with GH5, in the loop connecting helices II and III (Ali et al., 2004). In GI it is longer and forms a short helix, whereas in GII it is slightly longer again but lacks the helix. The Hho1p domains also differ in the conservation of the basic residues in the DNA binding sites (Figure 1.9c). Both domains lack one of the basic residues in site I, while there are a further two residues in site II absent from the GII domain. Mutant forms of the GII domain were produced by replacing the loop region between helices II and III with that of GI (to give GII-L), introducing the two “missing” site II basic residues, or containing both modifications (Sander-

son et al., 2005). The loop domain was shown to be the cause of the instability of the GII domain, while introduction of the “missing” site II residues destabilised the protein.

Circular dichroism (CD) studies suggest that the N-terminal tail and linker regions of Hho1p are unstructured in aqueous solution (Ali and Thomas, 2004), and do not gain significant structure in the presence of sodium perchlorate anions (Osmotherly, 2006). NMR studies of the first two domains of Hho1p (the N-terminal tail and the GI domain, called NGI) also showed that the N-terminal tail is very flexible and unstructured (Ono et al., 2003). Addition of linear DNA to the sample did not cause any chemical shift changes, although peaks corresponding to three regions of the protein showing spectral broadening. This was attributed to weak, non-specific binding of the DNA.

1.5.2 Location of Hho1p in yeast chromatin

A genome-wide chromatin immunoprecipitation assay analysed on microarray chips (ChIP-chip) indicated that the abundance of Hho1p in yeast chromatin is much lower than that of the core histones, or the histone H2A variant Htz1p (Zanton and Pugh, 2006). The published measurements for the abundance of Hho1p in yeast range from 1 molecule per about 4 nucleosomes (Downs et al., 2003), to 1 per 37 nucleosomes (Freidkin and Katcoff, 2001). This is significantly lower than in higher eukaryotes and is discussed further in Section 3.1.

Despite its relatively low abundance, Hho1p is widely associated with the genome. The ChIP-chip assay indicates a relative exclusion of Hho1p from promoter regions of genes, especially at active genes (Zanton and Pugh, 2006). Hho1p is reported to associate with various regions including open reading frames, intergenic regions, centromeric regions, subtelomeric regions, regions

distal from telomeres, inducible genes, the ribosomal DNA (rDNA) locus and silent mating type loci (Ali, 2001; Downs et al., 2003; Veron et al., 2006). A preference of Hho1p for binding at rDNA loci was reported in a Southern blotting experiment (Freidkin and Katcoff, 2001). No enrichment in or exclusion from silent mating type loci or telomeres was identified in a chromatin immunoprecipitation (ChIP) study (Yu et al., 2009).

More recently the observed enrichment of Hho1p at rDNA loci was contradicted by the results of a genome-wide association study of Hho1p. This study showed an even distribution of Hho1p throughout the yeast chromatin during both exponential growth and in stationary phase (Schäfer et al., 2008). However comparison between the two growth conditions indicated that chromatin binding increased at the six loci tested, upon entry into stationary phase, although the cellular levels of Hho1p remained constant. Re-entry into exponential growth caused dissociation of Hho1p within two hours. Most yeast investigations are carried out on exponentially growing cells, when only a proportion of the Hho1p molecules will be associated with yeast chromatin, and this may explain why there are so few observations of global Hho1p function.

1.5.3 Effect of Hho1p on chromatin structure

Deletion of the HHO1 gene has no effect on the nucleosome repeat length of yeast chromatin (Patterton et al., 1998) or the nucleosome positioning in an array of stochastically positioned nucleosomes (Puig et al., 1999). This is in contrast to mice embryonic stem cells, which showed both global loosening of chromatin structure and a decrease in nucleosomal repeat length upon depletion of linker histone to about 50% of wild-type levels (Fan et al., 2005). A recent publication reported Hho1p-dependent compaction of chromatin in stationary phase yeast, but not in exponentially growing cultures, suggesting Hho1p has a

global role in chromatin compaction at specific times (Schäfer et al., 2008). For both growth phases, chromatin fragments were prepared from wild-type and *hho1*-null yeast strains and centrifuged through sucrose gradients. The more compact chromatin structures sediment more rapidly.

Hho1p suppresses homologous recombination (Downs et al., 2003) suggesting that Hho1p is involved in maintaining local chromatin structure, reducing the accessibility of the DNA to factors involved in recombination. At the rDNA locus, deletion of Hho1p increases recombination events (Li et al., 2008) and causes loosening of chromatin structure (Levy et al., 2008). This results in an increase in accessibility of rDNA to psoralen, an inter-strand cross-linker, and retardation in a gel-mobility-shift assay. Hho1p is also required for the establishment of silenced chromatin structures containing the HML silenced mating type loci, although it is not required to maintain this structure (Yu et al., 2009). The expression of genes that are transcriptionally-dependent on chromatin structure was unaltered in yeast strains either over-expressing or deleted for Hho1p (Escher and Schaffner, 1997). Thus, Hho1p may have specific and subtle functions in the regulation of chromatin compaction, even though the global effect is too subtle to be measured in most conditions.

1.5.4 Effect of Hho1p on transcription

There is conflicting evidence about the role of Hho1p in transcription regulation. In studies of the expression of reporter genes in wild-type and *hho1*-null strains, transcription from an *in situ* URA3 reporter gene with a minimal PHO5 promoter is not regulated by Hho1p (Patterton et al., 1998) whereas expression from an exogenous CYC1-lacZ reporter is Hho1p-dependent (Ushinsky et al., 1997).

Whole genome microarray analyses of transcription changes following deletion of the HHO1 gene demonstrate no general increase in the expression levels, indicating Hho1p is not a general repressor of transcription. One study showed a general but modest decrease in expression, with 27 out of over 6200 genes showing a reduction in mRNA levels of greater than 2-fold (Hellauer et al., 2001). The Hho1p-dependent genes were not of any particular function or class. Other microarray studies identified a small number of genes whose transcription increased and a small number whose transcription decreased upon deletion of HHO1 (Freidkin and Katcoff, 2001; Levy et al., 2008). The Hho1p-dependent genes varied between the studies, possibly due to different growth conditions or microarrays used. The studies do, however, suggest a role for Hho1p in gene-specific transcription. Freidkin and Katcoff (2001) saw no preferential binding of Hho1p to Hho1p-dependent genes, indicating that the transcription regulation may not occur through direct binding of Hho1p. An additional finding in this study was that Hho1p regulates its own transcription. A yeast strain expressing a mutant form of Hho1p containing the promoter and first 149 nucleotides showed no detectable phenotype but resulted in a substantial increase in levels of the truncated HHO1 transcript.

A further microarray study identified a number of genes from which, upon heat shock, Hho1p dissociates but there is no gene activation (Zanton and Pugh, 2006). In contrast, a negative-correlation between Hho1p binding and gene expression was shown in a wild-type yeast strain, both during exponential growth and at stationary phase (Schäfer et al., 2008). However, in an *hho1*-null strain the rank order of gene expression, compared with wild-type cultures, was retained, indicating that the association of Hho1p at these genes had no effect on their transcription level. This strongly suggests that the binding of Hho1p at a gene may be an effect of transcriptional activity of that gene, rather than being

involved in the regulation, and that Hho1p may be displaced from chromatin by the transcription machinery (Schäfer et al., 2008).

There is a differential effect of Hho1p on transcriptional silencing at the heterochromatic regions of the yeast genome. One study of Hho1p action used a yeast strain containing a mutant histone H4 (Y88G) (Yu et al., 2009). This mutation disrupts the binding of histone H4 to the H2A/H2B dimer, within the octamer. It causes temperature- and DNA damage-sensitivity as well as disrupted transcriptional silencing, but has no effect on gross chromatin structure (Santisteban et al., 1997). When Yu et al. (2009) deleted the HHO1 gene in the H4 Y88G strain, the defects in transcriptional silencing in telomeric and mating type loci of the H4 mutation were partially suppressed. An HHO1 knock-out strain shows no change in transcription of reporter genes inserted into silent mating type loci or telomeres in wild-type yeast strains (Escher and Schaffner, 1997; Patterson et al., 1998; Yu et al., 2009). This indicates that Hho1p may have a role in transcriptional silencing at heterochromatic regions, but at a level too subtle to be identified in a wild-type background.

Hho1p can inhibit the spread of silenced chromatin from heterochromatic regions, although it does not considerably decrease silencing within heterochromatin itself (Veron et al., 2006). This is in contrast to the linker histones in humans, which are recruited to sites of heterochromatin formation (Vaquero et al., 2004). Thus, although Hho1p is involved in the formation of compact chromatin structures that have reduced recombination (as described above), it also has a role in preventing the formation of transcriptionally silent chromatin structures.

At the rDNA locus the situation is even less clear. Hho1p is required for RNA polymerase (RNAP) I transcription of ribosomal RNA components from native rDNA and has been shown to reduce RNAP II transcription of a gene em-

bedded in the rDNA (Levy et al., 2008). However another group used a similar reporter system and saw no change in RNAP II transcription of the reporter gene upon deletion of HHO1 (Li et al., 2008). The conflicting results for RNAP II transcription at the rDNA require further investigation to determine the specific conditions or regions of the rDNA that have Hho1p-dependent effects.

This apparent contradiction between the roles of Hho1p in chromatin structure (Section 1.5.3), as well as the disparity with metazoan linker histone function described above, may result from the majority of the yeast genome being transcriptionally active. This requires chromatin (outside of the heterochromatic regions) to be protected from the very compact chromatin structures that cause transcriptional silencing. However, yeast may benefit from more modest compaction of the chromatin that reduces recombination events, preserving genome integrity without affecting gross chromatin structure.

1.5.5 Bi-functionality of Hho1p?

The presence of two domains in Hho1p with similarity to the H5 globular domain raises the question of whether it is a bi-functional linker histone. As illustrated in Figure 1.9, both Hho1p globular domains lack one basic (non-conserved) residue in DNA binding site I, while the GII domain also lacks two of the site II residues. Thus the GII domain may not have been expected to function as a linker histone globular domain, capable of binding close to the nucleosome dyad and conferring chromatosome protection.

In vitro, however, both isolated GI and GII domains of Hho1p bind to linear DNA, four-way junction DNA and chromatin, with GII having higher affinity presumably because it is more basic (Ali and Thomas, 2004). This suggests that the intrinsically disordered GII domain may fold in the presence of

DNA and that Hho1p could in principle act as a bi-functional linker histone, if GII also folds in the context of the full-length protein. The isolated GI domain protects chromosome-length DNA in a micrococcal nuclease digestion of bulk chromatin (Ali and Thomas, 2004). The GII domain also produces a “chromosome stop” but requires more specific reaction conditions, presumably because GII is less stably folded than GI (Sanderson et al., 2005). This demonstrates that the structural instability of GII is more important than its more basic nature in this assay.

It is not known whether both GI and GII domains of Hho1p are folded and functional within the yeast cell. In the context of the full-length protein each domain binds a four-way junction DNA molecule independently (Schäfer et al., 2005), indicating that Hho1p can be bi-functional *in vitro*. As mentioned in Section 1.5.3, Hho1p suppresses homologous recombination in yeast (Downs et al., 2003). The isolated GI and GII domains are not functional in this assay (Dr Jessica Downs, personal communication), however a truncation mutant (NGIL) does suppress homologous recombination indicating that the GII domain is not required for this function (Harvey and Downs, 2004). If the GII domain is engineered to be flanked by the basic N-terminal and linker regions (NGIIL) it can also function in this assay (Osmotherly, 2006), indicating that both “globular” domains are potentially functional and bind chromatin *in vivo*.

Domain deletion studies demonstrate that the isolated GII domain is sufficient to restore the transcriptional silencing of a reporter gene in the rDNA locus of an HHO1 deletion strain, unless the N-terminal tail is also present (Levy et al., 2008). If the N-terminal tail is present then both “globular” domains are required to restore wild-type transcription regulation. The mechanism of this system is not clear. Linker histone N-terminal tails are thought to have roles in positioning of globular domains at the nucleosome dyad (Allan et al., 1986), and

this appears to inhibit the function of the GII domain. However if the full-length Hho1p is present the N-terminal tail could position GI, leaving GII free to function in transcriptional silencing. The action of the GI domain, in the absence of the N-terminal tail was not tested. In another study, the GII domain was dispensable for suppression of the various phenotypic defects of the histone H4 Y88G mutant strain described in Section 1.5.3 (Yu et al., 2009). These studies suggest that the homologous GI and GII domains of Hho1p may have independent functions *in vivo*.

In view of the potential bi-functionality of Hho1p a bridging model has been described in which the linker histone binds to two nucleosome cores simultaneously (Ali and Thomas, 2004; Sanderson et al., 2005; Schäfer et al., 2005). Both GI and GII domains recognise the DNA conformation at the nucleosome dyad, mimicked by four-way junction DNA, which is where the globular domain of histone H5 binds (Section 1.3.2.2). The linker domain of Hho1p is long enough to bridge the distance between two core nucleosomes within chromatin (based on the tetranucleosome crystal structure (Schalch et al., 2005) which had a nucleosome repeat length equivalent to that in yeast) even if the entire linker assumed an α -helical conformation (Schäfer et al., 2005). If the “globular” domains bound adjacent nucleosome cores this would allow the basic linker domain to associate with any linker DNA. Mechanistically, if the folded GI domain bound a nucleosome core and the linker domain associated with linker DNA then the unbound GII domain would be located close to another nucleosome core, which could promote its concomitant folding and binding. It is also possible for the GII domain to bind chromatin first, promoting the binding of the GI domain.

In an alternative model the two domains bind within one nucleosome, to two symmetry-related sites at opposite sides of the DNA dyad. Binding of

Hho1p in this manner would cause the linker domain to form an extended hairpin loop that associates with the linker DNA, partially neutralising it (Schäfer et al., 2005). Only one of these two potential globular domain binding sites is bound by canonical histone H1 although the second, lower-affinity site can be occupied if excess linker histone is added (Nelson et al., 1979).

Hho1p may also bind chromatin in the same way as a canonical tripartite linker histone (Figure 1.8), with the GII domain remaining unfolded and acting as an extension to the linker domain. In principle either “globular” domain could bind the nucleosome core and leave the other free to interact with other protein factors, however it is more likely that the GI domain is bound as it would be positioned by the N-terminal tail. At present it is not clear which binding mechanism occurs for Hho1p and further investigation is required.

1.5.6 Roles of Hho1p in yeast

In summary of the literature reviewed, I offer two possible roles for Hho1p in yeast chromatin. Firstly, Hho1p has a protective role. Transcriptional down-regulation (for example, upon entry into stationary phase) increases the proportion of Hho1p molecules bound to chromatin, facilitating chromatin compaction. The compaction may not be great enough to modify the biochemistry of bulk chromatin, however local and subtle changes occur reducing recombination events. This compaction helps to maintain the integrity of the genome during periods of semiquiescence.

Secondly, Hho1p ensures that the yeast chromatin can be readily transcribed. Association of Hho1p with chromatin is displaced by the transcription machinery both upon re-entry into exponential growth and within the rDNA locus, indicating that Hho1p does not condense chromatin enough to prevent

transcription. This is an important function in yeast, as the majority of the genome is transcriptionally active at any one time. Hho1p also prevents the spreading of transcriptionally silent chromatin through its action at barrier elements and is required for efficient RNAP I transcription at the rDNA.

The two roles of Hho1p may appear contradictory, however the roles complement each other producing a finely balanced chromatin regulation, preserving the integrity of the genome but ensuring that transcription can be easily reinstated.

1.6 Introduction to work presented in this Thesis

It is important to understand how yeast chromatin may differ from that of higher eukaryotes because yeast is a widely used model organism. Many yeast cellular processes are conserved in higher eukaryotes; however, yeast chromatin may not be a good model for that of higher eukaryotes if Hho1p has different roles from metazoan linker histones. Therefore work described in this Thesis aims to characterise Hho1p further, both at a structural and functional level. In Chapter 2 the structure of the second “globular” domain of Hho1p, GII, is further investigated to consider the role of residual structure in this unstable domain. Homologues of histone H1 interacting-partners are investigated to determine whether they interact with Hho1p (Chapter 4).

It is also important to study how Hho1p binds to chromatin to allow the understanding of chromatin condensation in yeast. Chapter 3 considers the structural roles of Hho1p within chromatin, comparing the structural properties of chromatin arrays containing Hho1p or canonical linker histones.

The basic tail of canonical linker histones has important roles in DNA and chromatin binding. It is unstructured in solution but can gain secondary

structure when bound to DNA. It is subject to phosphorylation *in vivo*. The equivalent region in Hho1p, in terms of amino acid composition, is the basic linker between the GI and GII domains and the structure of this region is investigated in Chapter 5. The structural effect of phosphorylation on the linker domain of Hho1p is also studied, as well as the effect of phosphorylation on Hho1p interactions with DNA and chromatin.

Chapter 2

**Structural investigation of GII, the
second “globular” domain of Hho1p**

2 Structural investigation of GII, the second “globular” domain of Hho1p

2.1 Introduction

As discussed in Section 1.5, the *S. cerevisiae* linker histone, Hho1p, contains two domains, GI and GII, with sequence and structural similarity to the single globular domain of canonical linker histones. Ali et al. (2004) showed that the isolated domains have different stabilities, the GII domain exists as two forms in slow equilibrium and folding can be stabilised by the presence of tetrahedral anions that are thought to mimic DNA phosphates. Figure 2.1 shows ^1H - ^{15}N HSQC spectra of the GI and GII domains of Hho1p, and the effect of sodium phosphate concentration. GI is stably folded in 10 mM phosphate whereas at least 250 mM phosphate is required to stabilise the folded form of GII. The shift in the equilibrium from the two forms of GII to just the folded form, upon increasing phosphate concentration, is shown by the loss of peaks from the proton resonance “random coil region” (about 8.0–8.5 ppm). The amino-acid sequence of the loop region connecting helices II and III (see Figure 1.9c) in GII was shown to determine the relative stability of the folded form of the domain (Sanderson et al., 2005).

It is known that the GII domain is able to function as a linker histone globular domain both *in vitro* and *in vivo*, presumably gaining structure to achieve this (Section 1.5.5). CD studies demonstrated that Hho1p had a lower

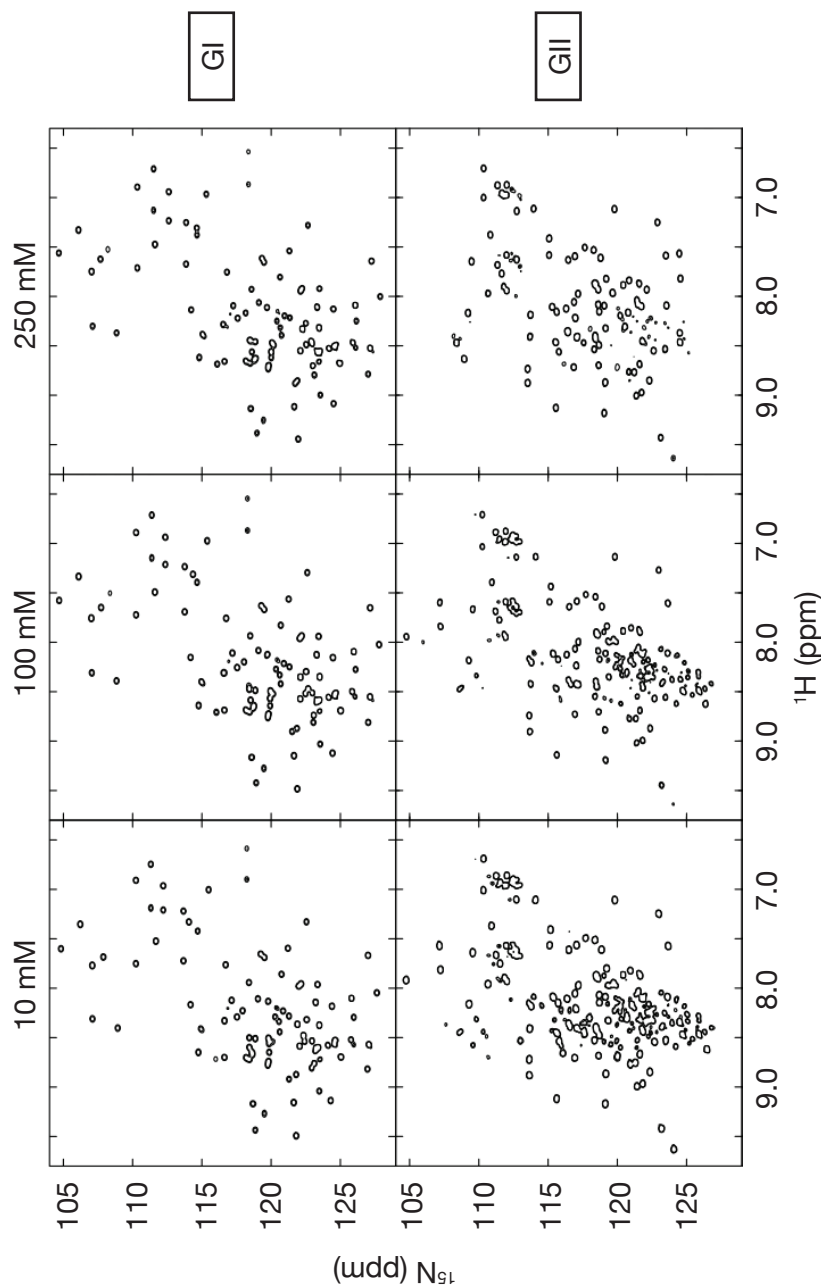


Figure 2.1 The effect of sodium phosphate concentration on the GI and GII domains of Hho1p. ^1H - ^{15}N HSQC spectra of GI and GII in buffers containing increasing concentrations of sodium phosphate. The spectra of the GI domain are almost identical in all the conditions, indicating no change in structure. There is a decrease in the number of peaks in the GI spectra, with increasing phosphate concentrations. In 10 mM and 100 mM phosphate GII exists in two forms, folded and “unfolded”, in slow equilibrium. In 250 mM phosphate the equilibrium shifts to the stably folded species, as indicated by a decrease in the number of peaks within the “random coil” region (proton resonances of about 8.0–8.5 ppm). From Sanderson et al. (2005).

percentage of α -helix than NGIL in 10 mM sodium phosphate buffer, suggesting the GII domain is not stably folded within Hho1p in these conditions (Ali and Thomas, 2004). Both GI and GII domains within Hho1p are able to bind independent four-way junction DNA molecules, in buffer conditions where the GII domain is stably folded (Schäfer et al., 2008). However, it is currently unknown whether the GII domain retains the ability to fold and bind DNA in the context of the full-length protein *in vivo*.

In this Chapter I confirm that the degree of GII folding in the context of Hho1p is similar to that of the isolated domain. Therefore I investigate the “unfolded” species of isolated GII domain, to determine if it contains residual structure relevant to the folded state and, if so, what the nature of the structure is. Residual structure is an indication that an intrinsically disordered protein has efficiently formed secondary structure, but requires specific conditions to support the packing of this secondary structure into a stable tertiary fold. Although the population of molecules is overall intrinsically disordered some members of the population will have the “correct” conformation. Selection of those molecules, for example by binding of a partner molecule, removes them from the pool of molecules and shifts the equilibrium towards the correct conformation (reviewed in Tsai et al., 2001a,b).

The dynamic nature of protein folding means that some structural elucidation techniques are more suitable than others for the investigation of residual structure in the GII domain. The techniques used to study intrinsically disordered proteins have been recently reviewed (Wright and Dyson, 2009). NMR spectroscopy is used, here, to investigate residual structure in the GII domain as it allows the study of low populations within a sample; and information about the dynamics and structural character of the protein ensemble are possible at a residue-specific level. If NMR is combined with paramagnetic spin labeling

the long-range interactions of a dynamic protein can be determined at a per residue resolution. This is in contrast to techniques such as CD and small angle X-ray scattering (SAXS) that have much lower resolution, although they provide useful information about secondary structure and ensemble envelopes respectively. Like NMR spectroscopy, X-ray crystallography can provide high resolution structural data, however the requirement for a homogenous crystalline sample means that no information about the dynamics of a sample is determined, making it unsuitable to study the highly dynamic GII domain.

2.2 Materials and methods

2.2.1 Bacteria

2.2.1.1 Bacterial growth media

The bacterial growth media used in this Thesis are listed in Table 2.1

2.2.1.2 Bacterial strains

The bacterial strains used in this Thesis are listed in Table 2.2

2.2.2 Plasmids

Plasmid pET17b-HHO1 contains the cDNA for full-length Hho1p (residues 1–258) under the control of a T7 promoter, as well as an ampicillin resistance gene and an origin of replication.

Plasmid pET17b-GII contains the cDNA for the second globular domain of Hho1p (residues 171–258) as well as pET17b features described above (Ali and Thomas, 2004).

Table 2.1: Bacterial growth media

Medium	Recipe
2xYT medium:	16 g tryptone, 10 g yeast extract, 5 g NaCl per litre
LB medium:	10 g tryptone, 5 g yeast extract, 10 g NaCl per litre
LB-agar plates	10 g tryptone, 5 g yeast extract, 10 g NaCl, 15 g agar per litre
M9 medium:	2 mM MgSO ₄ , 0.1 mM CaCl ₂ , 0.2% (w/v) glucose, 200 ml 5x M9 salts per litre (64 g Na ₂ HPO ₄ · 7H ₂ O, 15 g KH ₂ PO ₄ , 2.5 g NaCl, 5 g NH ₄ Cl per litre)
MOPS medium:	0.132 M K ₂ PO ₄ , 0.4% (w/v) glucose (or 0.1% when using ¹³ C-glucose), 100 ml 10x MOPS per litre (400 mM MOPS pH 7.4, 40 mM Tricine pH 7.4, 0.1 mM FeSO ₄ , 95 mM NH ₄ Cl, 2.76 mM K ₂ SO ₄ , 5 μM CaCl ₂ , 5.28 mM MgCl ₂ , 500 mM NaCl, 1 ml 10x micronutrients per litre (0.03 mM (NH ₄) ₆ (MO ₇) ₂₄ , 4 mM H ₃ BO ₃ , 0.3 mM CoCl ₂ , 0.1 mM CuSO ₄ , 0.8 mM MnCl ₂ , 0.1 mM ZnSO ₄)) (Neidhardt et al., 1974)
TB medium:	12 g tryptone, 24 g yeast extract, 4 ml glycerol, 100 ml [0.17 M KH ₂ PO ₄ , 0.72 M K ₂ HPO ₄] per litre

Table 2.2: Bacterial strains

<i>E. coli</i> strain	Genotype	Supplier
BL21(DE3)	F ⁻ <i>ompT hsdS_B</i> (r _B ⁻ , m _B ⁻) <i>gal dcm rne131</i> (DE3)	Novagen
BL21(DE3)pLysS	F ⁻ <i>ompT hsdS_B</i> (r _B ⁻ , m _B ⁻) <i>gal dcm</i> (DE3) pLysS (Cam ^R)	Novagen
DH5α	F ⁻ ϕ 80 <i>lacZ</i> ΔM15 Δ(<i>lacZYA-argF</i>)U169 <i>endA1 recA1 hsdR17</i> (r _k ⁻ , m _k ⁺) <i>supE44 thi-1 gyrA96 relA1 phoA</i> λ ⁻	Invitrogen
Rosetta(DE3)	F ⁻ <i>ompT hsdS_B</i> (r _B ⁻ , m _B ⁻) <i>gal dcm</i> (DE3) pRARE (Cam ^R)	Novagen

2.2.3 Expression and purification of Hho1p and the GII domain

2.2.3.1 Expression of ^{15}N -Hho1p

Plating the transformed cells onto LB-agar plates before growing the overnight cultures greatly reduced the expression levels of Hho1p. Therefore expression cultures of Hho1p or Hho1p-truncations were immediately grown in small liquid cultures following transformation.

E. coli Rosetta(DE3) cells were transformed with pET17b-HHO1 using heat shock (Sambrook et al., 1989) and grown overnight at 37 °C, without shaking, in TB medium supplemented with 50 $\mu\text{g}/\text{ml}$ carbenicillin (Melford Laboratories Ltd.). 5 ml of the overnight culture was used to inoculate 10 flasks (2 l) containing 500 ml of M9 medium, with ^{15}N - NH_4Cl as the sole nitrogen source and supplemented with 50 $\mu\text{g}/\text{ml}$ carbenicillin, and cultures were grown at 37 °C with shaking at 250 rpm to an OD_{600} of about 0.6. Protein expression was induced with 1 mM isopropyl β -D-thiogalactopyranoside (IPTG) and cultures were grown for a further 18 h at 18 °C with shaking at 50 rpm. Cells were harvested by centrifugation at 6000 g for 10 min at 4 °C and washed in 10 mM sodium phosphate pH 7.0, 150 mM NaCl, 1 mM dithiothreitol (DTT), 1 mM ethylenediaminetetraacetic acid (EDTA), 0.5 mM phenylmethylsulfonyl fluoride (PMSF). Pellets were stored at -20 °C.

2.2.3.2 Purification of Hho1p

The purification procedure is based on that described previously for Hho1p (Ali and Thomas, 2004). Pellets were resuspended in buffer B (10 mM sodium phosphate pH 7.0, 1 M NaCl, 1 mM DTT, 1 mM EDTA, 0.5 mM PMSF) supplemented with 1 $\mu\text{g}/\text{ml}$ leupeptin (Sigma-Aldrich), 1 $\mu\text{g}/\text{ml}$ aprotinin (Sigma-

Aldrich), 0.156 mg/ml benzamidine (Sigma-Aldrich), 1 μ g/ml pepstatin A (Sigma-Aldrich). Cells were lysed by two passes through a French press at 1000 psi and cell debris was removed by centrifugation at 35000 g for 30 min at 4 °C. The cell extract was filtered through a 0.2 μ m membrane (Millipore) and diluted 10-fold in buffer A (10 mM sodium phosphate pH 7.0, 1 mM DTT, 1 mM EDTA, 0.5 mM PMSF).

The diluted filtrate was loaded on to a HiTrap SP Sepharose HP cation-exchange column (GE Healthcare), which had been pre-equilibrated with buffer A. Bound proteins were eluted with a 10-column-volume linear gradient from buffer A to buffer B and fractions containing Hho1p, as identified by absorbance at 280 nm and SDS/18%-PAGE (Section 2.2.4.1), were collected. Ammonium sulphate was added slowly, while stirring the sample on ice, to a final concentration of 2.5 M and the resulting suspension was clarified by centrifugation at 6000 g for 20 min at 4 °C. The supernatant was loaded on to a HiTrap Phenyl Sepharose HP hydrophobic-interaction column (GE Healthcare), which had been pre-equilibrated with buffer C (10 mM sodium phosphate pH 7.0, 1 mM DTT, 1 mM EDTA, 2.5 M ammonium sulphate). Bound proteins were eluted with an eight-column-volume linear gradient from buffer C to buffer A, and fractions containing Hho1p, identified as described above, were collected.

The collected fractions were pooled and dialysed overnight against buffer A at 4 °C. If further purification of Hho1p was required the dialysed sample was loaded on to a Resource S cation-exchange column (GE Healthcare), which had been pre-equilibrated in buffer A, and bound proteins were eluted with a 50-column-volume linear gradient from buffer A to buffer B. The pooled fractions containing pure Hho1p were then dialysed as above. The purified Hho1p samples were concentrated at 4 °C using a 10 kDa cut-off Vivaspin 2 concentrator (Sartorius) and flash frozen in aliquots for storage at -80 °C.

2.2.3.3 Expression of ^{15}N -GII and ^{13}C , ^{15}N -GII

E. coli BL21(DE3) cells were transformed with pET17b-GII using heat shock, and grown overnight, with 250 rpm shaking, at 37 °C in LB medium supplemented with 50 $\mu\text{g}/\text{ml}$ carbenicillin. 5 ml of the overnight culture was used to inoculate 10 flasks (2 l) containing 500 ml of MOPS medium, with ^{15}N - NH_4Cl as the sole nitrogen source (plus 0.5 g/l ^{13}C -glucose as the sole carbon source when applicable) and supplemented with 50 $\mu\text{g}/\text{ml}$ carbenicillin. Cultures were grown at 37 °C with shaking at 250 rpm to an OD_{600} of about 0.6. Protein expression was induced with 1 mM IPTG and cultures were grown for a further 3 h. Cells were harvested and stored as described for Hho1p in Section 2.2.3.1.

2.2.3.4 Purification of the GII domain

The GII domain was purified using the same procedure as for Hho1p, (Section 2.2.3.2; Ali and Thomas, 2004). The pure GII samples were concentrated in a Vivaspin 2 concentrator with a 3 kDa cut-off.

2.2.4 Protein characterisation

2.2.4.1 SDS/polyacrylamide gel-electrophoresis

Vertical slab gels were run as described (Thomas and Kornberg, 1978). Unless otherwise stated, the gels contained 18% (v/v) polyacrylamide. Briefly, protein samples were denatured by boiling in SDS loading buffer (50 mM Tris-HCl pH 6.8, 100 mM DTT, 2% (w/v) sodium dodecyl sulfate (SDS), 0.1% (w/v) bromophenol blue, 10% (v/v) glycerol), loaded on to the gels and run at 35 mA in Tris/glycine buffer (140 g/l glycine, 30 g/l Tris base, 5 g/l SDS). Proteins were fixed in the gels (45% (v/v) methanol, 10% (v/v) glacial acetic acid) and vi-

sualised by staining with Coomassie Brilliant Blue R250 (0.5 g/l in 45% (v/v) methanol, 10% (v/v) glacial acetic acid) and destaining (5% (v/v) methanol, 7.5% (v/v) acetic acid).

2.2.4.2 Amino acid analysis

Accurate protein concentrations were determined by Mr Peter Sharratt (Protein and Nucleic Acid Chemistry Facility, Department of Biochemistry, University of Cambridge) using an Alpha II Plus Automatic Analyser (Pharmacia LKB).

2.2.4.3 Mass spectrometry

Electrospray ionisation time of flight (ESI-TOF) mass spectrometry was performed by Dr Len Packman (Protein and Nucleic Acid Chemistry Facility).

2.2.5 NMR spectroscopy

All NMR experiments were recorded by Dr Katherine Stott (Department of Biochemistry, University of Cambridge). Experiments were recorded on DRX500 or DRX600 spectrometers equipped with triple-resonance HCN probe heads and actively-shielded z-gradients. Data were processed using the AZARA suite of programs (v2.8, ©1993–2010 Wayne Boucher and Department of Biochemistry, University of Cambridge) and assignments were made using Analysis v2.1 (Vranken et al., 2005).

2.2.5.1 NMR sample conditions

NMR experiments on ^{15}N -Hho1p were carried out at 288 K on protein at about 500 μM in 10 mM sodium phosphate pH 7.0, 1 mM DTT, 1 mM EDTA, 0.5 mM

PMSE, 10% (v/v) $^2\text{H}_2\text{O}$. Data acquisition for GI and GII has been previously described (Sanderson et al., 2005).

NMR experiments on ^{15}N -GII and ^{13}C , ^{15}N -GII were carried out on proteins at about 1.4 mM and 2 mM respectively. Experiments were recorded at 273 K in 10 mM sodium phosphate pH 7.0, 1 mM DTT, 1 mM EDTA, 0.5 mM PMSE, 10% (v/v) $^2\text{H}_2\text{O}$. For the urea titration the protein sample was adjusted with a stock solution containing 10 mM sodium phosphate pH 7.0, 1 mM DTT, 1 mM EDTA, 9 M urea, to final concentrations of 1, 2 and 4 M urea. The sample containing 4 M urea was therefore diluted 1.8-fold compared to the original sample. ATSL-labelled sample was prepared as described (Section 2.2.5.5).

2.2.5.2 Chemical shift deviations from random coil

$^{13}\text{C}^\alpha$ chemical shift deviations from random coil, corrected for sequence context (Schwarzinger et al., 2001), were measured using Analysis (Section 2.2.5). The spectra were referenced against 4,4-dimethyl-4-silapentane-1-sulphonic acid. Because the chemical shift reference data were acquired at a much higher temperature than used in this study there is a systematic shift in values from zero.

For percentage helix calculations the baseline was calculated using the mean value for residues 2–5 and 85–87, for which the resonances of the two species are converged, giving a baseline of -0.80883 ppm. A resonance may be defined as 100% α -helix if it has a shift deviation of 3.1 ppm (Spera and Bax, 1991).

2.2.5.3 Heteronuclear NOE measurements

$\{^1\text{H}\}^{15}\text{N}$ NOE values were obtained at 600 MHz with either 4 s of ^1H saturation using a 120° pulse train or a 4 s delay prior to the first ^{15}N pulse (Farrow et al.,

1994). The $\{^1\text{H}\}^{15}\text{N}$ NOE values were calculated using the following formula:

$$\{^1\text{H}\}^{15}\text{NNOE} = \frac{I_{sat}}{I_{unsat}}$$

2.2.5.4 Chemical-shift difference measurements

Normalised changes in amide chemical shift (Zuiderweg, 2002) were measured using Analysis (Vranken et al., 2005) and analysed using Microsoft Excel. The following formula was used to combine differences in chemical shift with appropriate scaling:

$$\Delta\delta = \sqrt{(\Delta\delta_N \times 0.15)^2 + (\Delta\delta_H)^2}$$

2.2.5.5 ATSL-labelling of the GII domain

Cysteine 61 of the GII domain was labelled with (1-acetoxy-2,2,5,5-tetramethyl- δ -3-pyrroline-3-methyl) methanethiosulfonate (ATSL) (Toronto Research Chemicals), by adding it to the protein sample (approximately 1 mM sample in 10 mM sodium phosphate pH 7.0, 1 mM EDTA, 0.5 mM PMSF) at a 5-fold molar excess (from a 1.7x stock). The reaction was carried out under argon at 25 °C for 3 h. The sample was buffer exchanged into 10 mM sodium phosphate pH 7.0, 1 mM EDTA using a Vivaspin concentrator with 3 kDa cut-off and $^2\text{H}_2\text{O}$ was added to 10% (v/v).

2.3 Results

2.3.1 The GII domain of Hho1p exists as a folded and an “unfolded” species in the context of the full-length protein

Transformed *E. coli* BL21(DE3) cells must be inoculated straight into liquid medium, rather than selecting transformants on antibiotic and agar plates, to achieve appreciable expression of full-length Hho1p (data not shown). Using this protocol ^{15}N -Hho1p was produced and a ^1H - ^{15}N HSQC spectrum was recorded (Figure 2.2)

Comparing this spectrum of the full-length protein with spectra for the isolated domains (Sanderson et al., 2005), indicated that peaks overlap to a large extent (Figure 2.3). Therefore, the domains within the full-length protein are in chemical environments similar to those of the isolated domains. Extra residues occur in the unfolded region at around 8.5 ppm proton shift, due to the N-terminal tail and linker residues. The boxes highlight peaks that occur in both the Hho1p and the “unfolded” GII spectra, but which do not occur in the folded GII spectrum. There are no peaks that occur in both the Hho1p and folded GII spectra but not in the “unfolded” GII spectrum.

These data indicate that GII domain exists in an equilibrium between the folded and “unfolded” species in the context of the full-length protein in 10 mM sodium phosphate buffer, as for the isolated domain. As the protein context of the GII domain does not appear to change its structural character this suggests further study of the isolated GII domain would be relevant for understanding the domain in the context of full-length Hho1p.

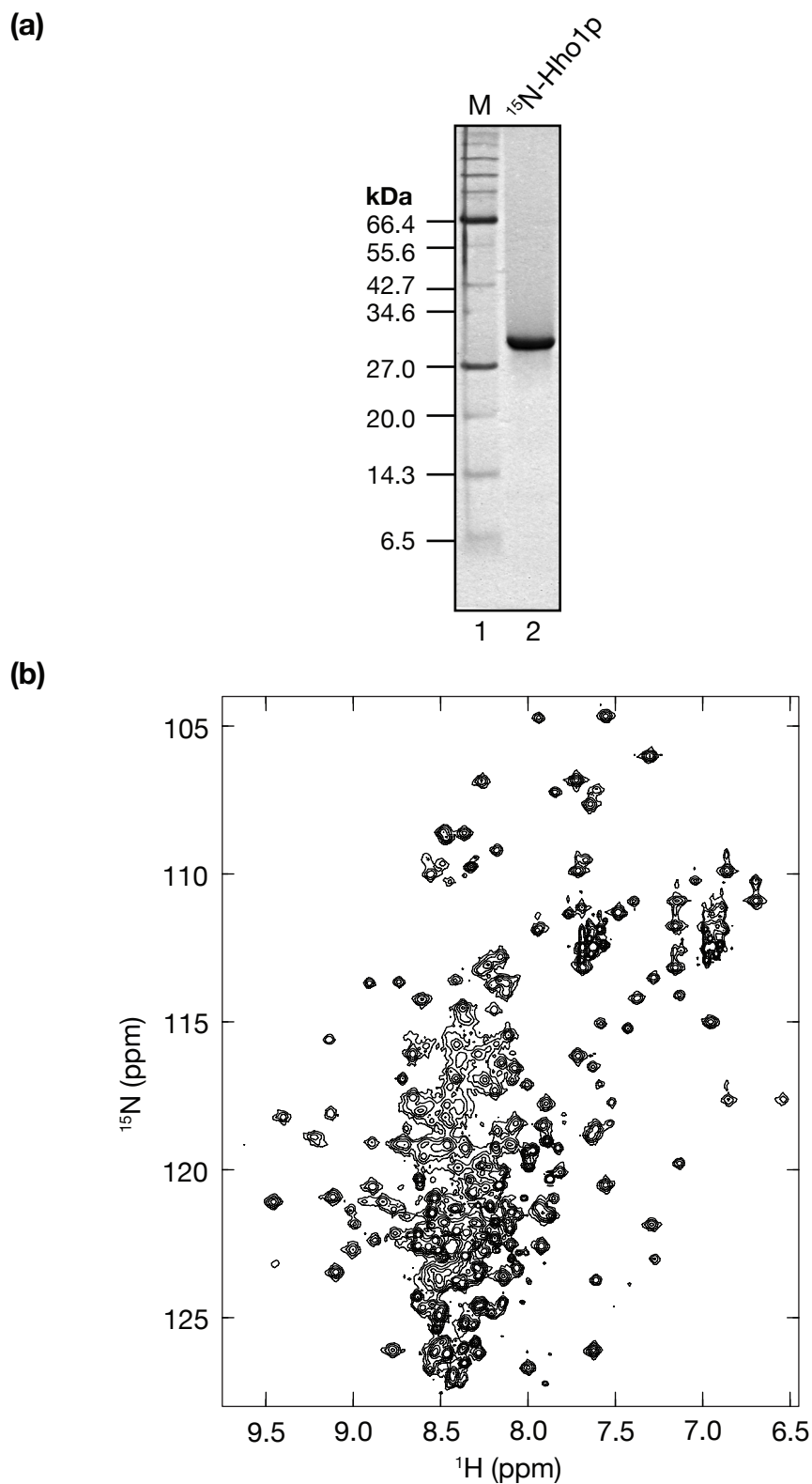


Figure 2.2 ^1H - ^{15}N HSQC spectrum of ^{15}N -labelled Hho1p. (a) SDS/18%-PAGE of ^{15}N -labelled Hho1p (lane 2). Lane 1, protein molecular weight markers. (b) ^1H - ^{15}N HSQC spectrum of ^{15}N -Hho1p, recorded at 500 MHz at 288 K in 10 mM phosphate buffer at pH 7.

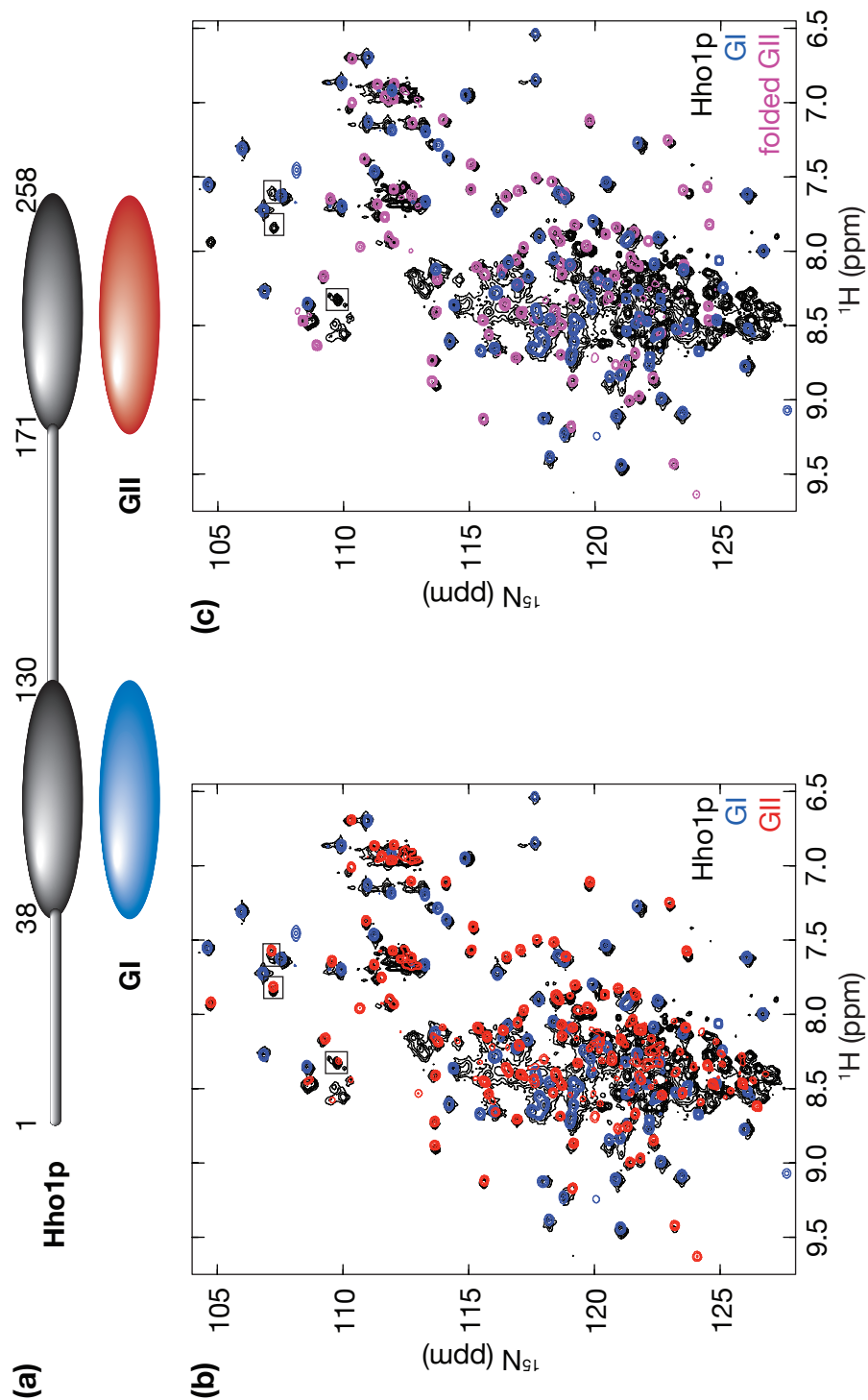


Figure 2.3 The GII domain of Hho1p exists as a folded and an “unfolded” species in the context of the full-length protein. (a) Schematic of the proteins used in these experiments. The residue numbers equivalent to the full-length protein are indicated. (b) Comparison of ^1H - ^{15}N HSQC spectra of ^{15}N -Hho1p (black), ^{15}N -GI domain (blue) and ^{15}N -GII domain (red), recorded at 500 MHz at 288 K in 10 mM sodium phosphate buffer at pH 7. (c) As (b) except containing the spectrum of the ^{15}N -GII domain in 250 mM sodium phosphate buffer (magenta). The tetrahedral anions cause the equilibrium to shift so the folded species dominates (magenta). GI and GII spectra are as published previously (Sanderson *et al.*, 2005).

2.3.2 Sequence-based disorder prediction indicates that the helices of the GII domain of Hho1p are less ordered than those in the GI domain

Comparison of sequence-based disorder predictions, using the VL3E DisProt Predictor of Intrinsically Disordered Regions (Peng et al., 2005) indicated that regions with low predictions of disorder in GII were similar to those in GI, although the GII regions were predicted to be more strongly disordered (Figure 2.4). For both domains the predicted disorder values for helices II and III were much lower than for helix I. It should be noted that the input window for this program is 15 residues, meaning the predictions for helices II and III of GI and GII could be affected by the different loop structures between helices II and III (in GI and GII) (Ali et al., 2004), as well as by the different sequences of the helices themselves.

Given how structurally unstable the GII domain is, relative to the GI domain (Ali et al., 2004), it was unexpected for the disorder prediction to be so similar. It is known that only a proportion of the GII domain has stable tertiary structure in 10 mM sodium phosphate buffers but a GII molecule, although disordered, may preferentially populate helical conformations, reflected in the disorder prediction values.

2.3.3 NMR assignments of the “unfolded” GII domain of Hho1p

To study the “unfolded” form of the GII domain, ^{15}N -GII and $^{13}\text{C},^{15}\text{N}$ -GII were produced (Figure 2.5a). The conditions in which NMR spectra were recorded were optimised using ^1H - ^{15}N HSQC spectra, so that the linewidths and intensity

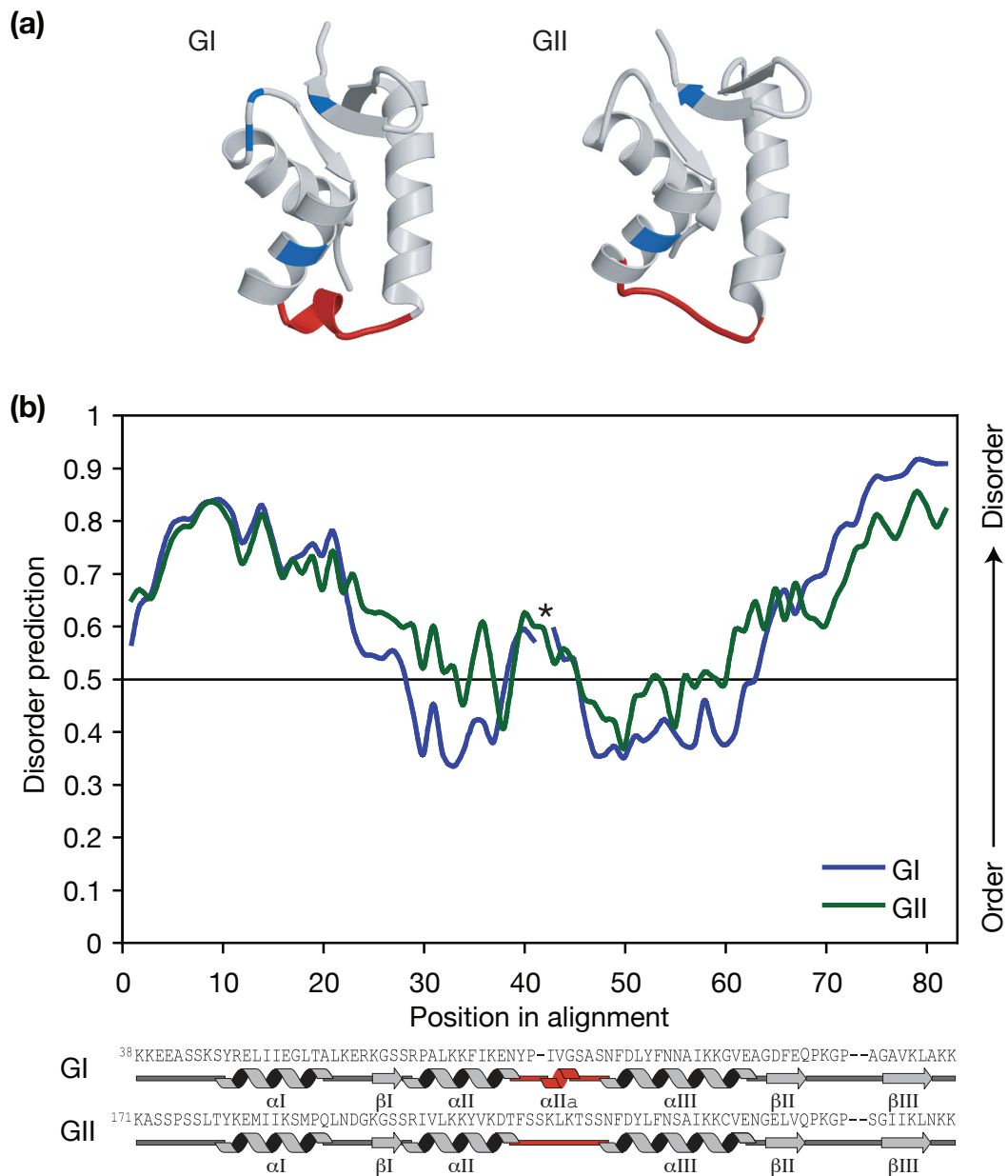


Figure 2.4 Structure and disorder predictions for the G1 and GII domains of Hho1p. (a) Ribbon diagrams of G1 and GII structures (Sanderson *et al.*, 2005). (b) Graph showing the disorder prediction for the G1 and GII domain sequences as determined by VL3E DisProt Predictor of Intrinsically Disordered Regions (Peng *et al.*, 2005). A value of 1 indicates disordered regions, and a value of 0 completely ordered regions. Secondary structure diagrams are to scale and highlight the difference in the loops between helices II and III (Sanderson *et al.*, 2005). Helices II and III are the most ordered regions of both domains, but G1 is more ordered than in GII in both helices. The G1 loop has one less residue than the GII loop, causing a break in the graph (marked with an asterisk)

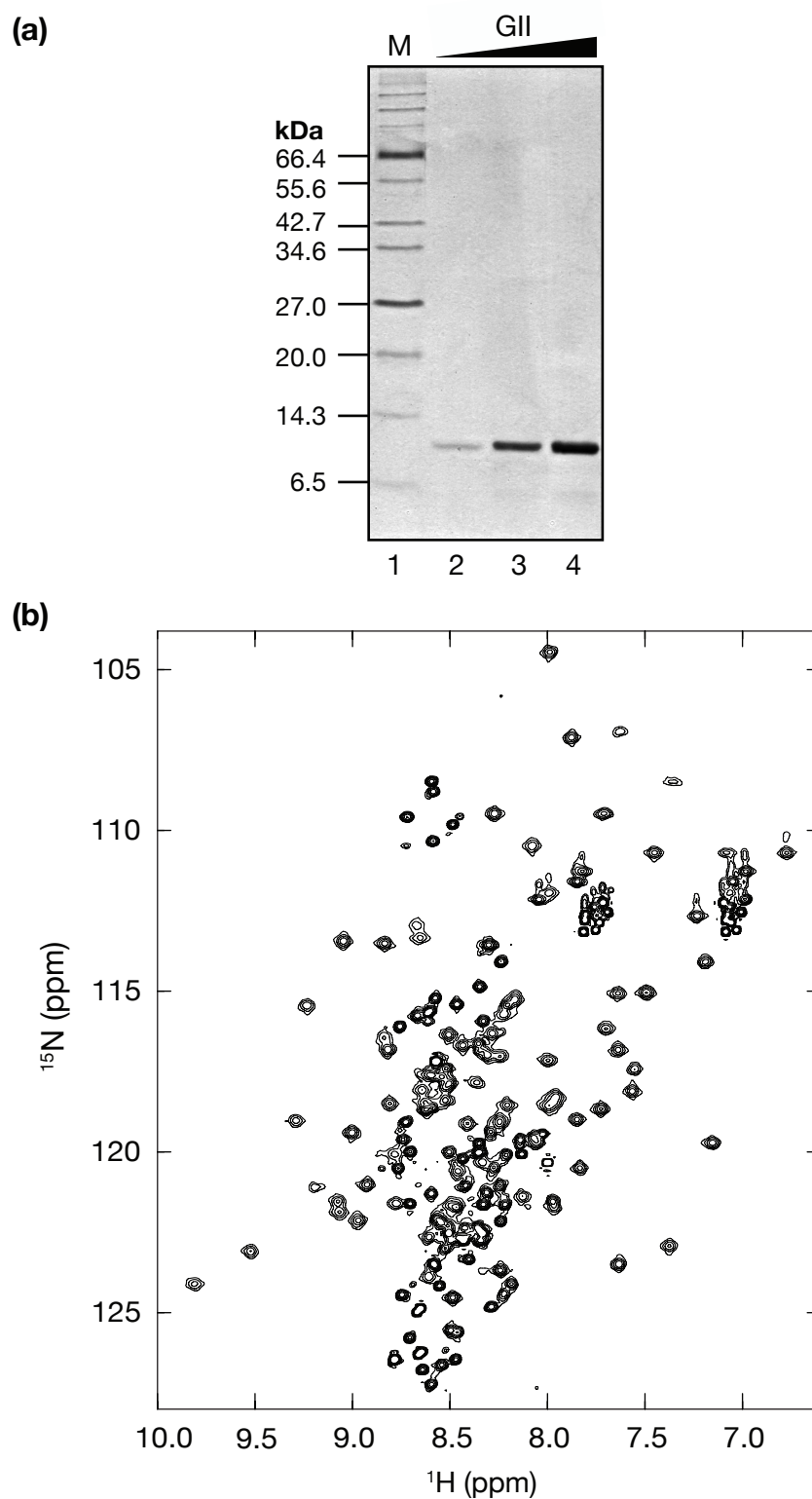


Figure 2.5 NMR spectroscopy of the GII domain of Hho1p in conditions where peaks from the “unfolded species” dominate. (a) SDS/18%-PAGE of ^{15}N -labeled GII. (b) ^1H - ^{15}N HSQC spectrum of ^{15}N -GII, recorded at 600 MHz at 273 K in 10 mM sodium phosphate buffer at pH 7.

of peaks due to the “unfolded” species were optimised in preference to those of the folded form (Figure 2.5b). HNCA, HNCACB, HN(CO)CA, HN(CO)CACB, HNN and HN(C)N experiments were used to sequentially assign the folded and “unfolded” species of GII. The magnetisation transfers for the experiments are shown in Figure 2.6.

The HNN and HN(C)N experiments were as described (Panchal et al., 2001). They are based on the HNCA and HN(CO)CA experiments but have an extra transfer to the nitrogen atoms with the result that the HNN has connectivity between the H^N_i and $N_{i, i+1}$ and $i-1$. The relatively slow relaxation of unfolded proteins means that the extra transfer does not cause an unacceptable loss of sensitivity in these systems. The experiments exploit two ^{15}N dimensions (which is the dimension with the greatest intrinsic dispersion of resonances in unfolded proteins) making them an excellent tool for assigning the “unfolded” form of the GII domain. Both the “unfolded” and folded species within the sample were assigned. Assignment was achieved through sequential steps along the backbone, using the triple-resonance experiments and HNN-based experiments to establish connectivity to about equal extents. The following percentages of resonances were assigned for the “unfolded” species: N (96.4%), H^N (96.4%), H^α (89.8%), C^α (97.7%) and C^β (97.6%). (See Appendix A for the resonance list of the “unfolded” species). The folded species was assigned in a similar manner but also used the published assignment for GII at 288 K and in 250 mM sodium phosphate as a guide (Ali et al., 2004). The following percentages of resonances were assigned for the folded species: N (96.4%), H^N (96.4%), C^α (96.6%) and C^β (94.0%).

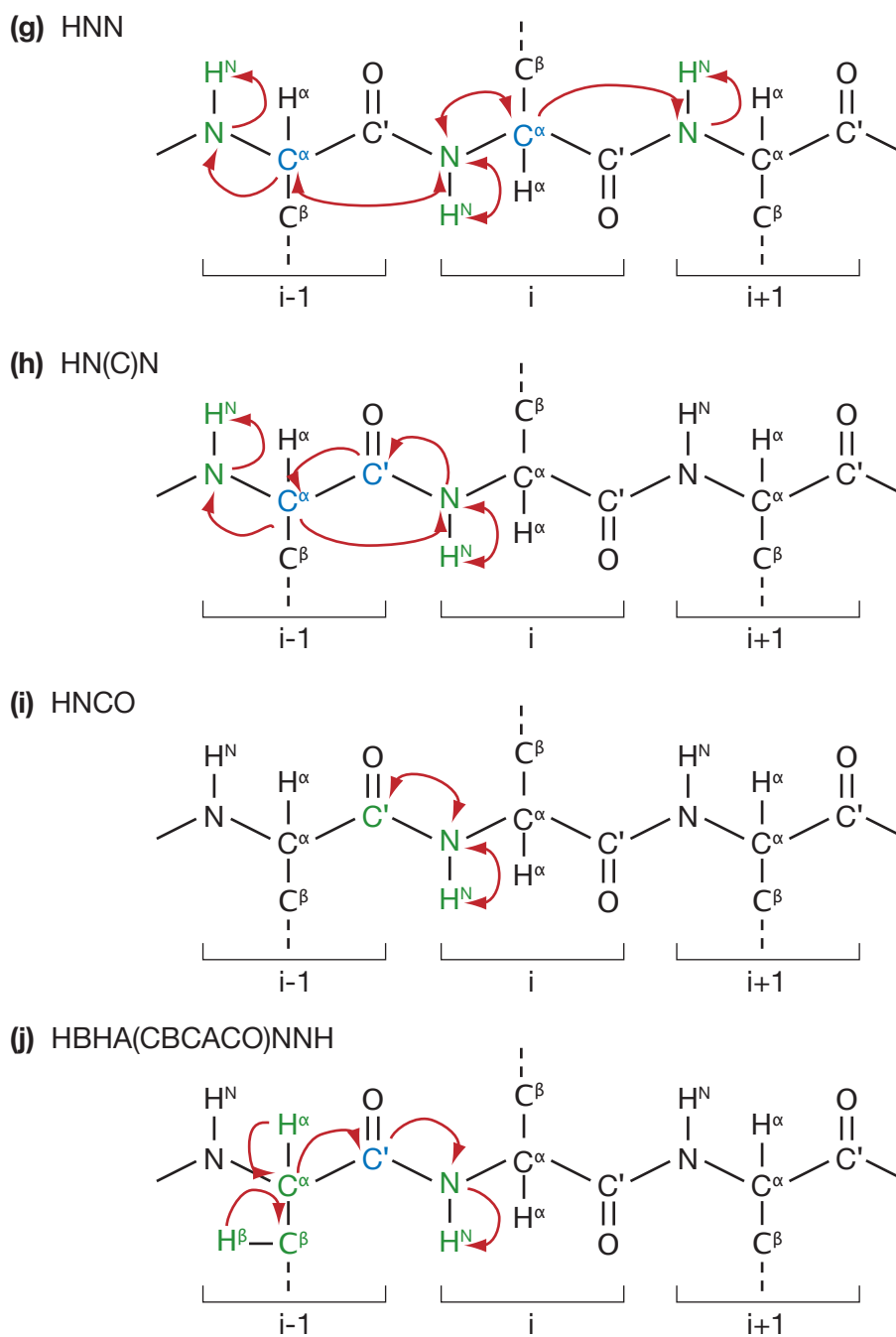


Figure 2.6 Magnetisation transfers of NMR experiments used in this Thesis. Green, observed atoms; Blue, atoms through which magnetisation is transferred, but which are not observed. (a) H-N HSQC (b) H-C HSQC (c) HNCA (d) HN(CO)CA (e) HNCACB (f) HN(CO)CACB (g) HNN (h) HN(C)N (i) HNCO (j) HBHA(CBCACO)NNH

2.3.4 The GII domain of Hho1p contains regions of residual structure

The C^α shift deviation from random coil values was measured for both the folded and “unfolded” GII species. It is well established that there is a correlation between secondary chemical shifts (deviations from random-coil values) and the secondary structure environment in which they are located (Wishart et al., 1991). It is also known that the sequence context of residues modifies the chemical shift of random coil resonances. Therefore, for unfolded or partially unfolded proteins it is important to use sequence-context corrected random coil values to calculate the chemical shift deviations from random coil (Schwarzinger et al., 2001).

The C^α shift deviations from random coil values are, as expected, much smaller for the “unfolded”, compared with the folded, form (Figure 2.7a). However some small but contiguous deviations occur around residues 8–18 and 50–68 for the “unfolded” resonances, indicating the presence of some residual structure. These deviations occur down-field, towards higher ppm values, and so are indicative of α -helical character (Wishart et al., 1991). Fully α -helical resonances show a shift deviation of 3.1 ± 1.0 ppm (Spera and Bax, 1991). The resonances defined to be within the helices of GII in previous NMR studies (Ali et al., 2004) were adjusted for the baseline and the percentage of α -helix was calculated. As expected the folded species within this sample showed an average more than 100% helical character (using this particular definition) over the three defined helices. The mean values of helical character for the “unfolded” form of GII were 25%, 5% and 21% for helices I, II and III, respectively, although there was variation across each helical region (Figure 2.7a). It is clear that there is considerable α -helical character in the regions corresponding to helices I and III of the GII domain in the “unfolded” species. This indicates that there is ei-

ther a subpopulation of GII molecules containing α -helices at these regions, or that the molecules contain α -helices a proportion of the time.

Heteronuclear nuclear Overhauser effect ($\{^1\text{H}\}^{15}\text{N}$ NOE) experiments were used to study the picosecond-nanosecond dynamics of the two GII species (Figure 2.7b). $\{^1\text{H}\}^{15}\text{N}$ NOE experiments measure the dynamics that are faster than, and independent of, the overall tumbling of a molecule; therefore they can identify secondary structure elements. The error bars for the “unfolded” species are smaller than those for the folded species because the “unfolded” peaks display a higher signal-to-noise ratio in the conditions used. The majority of the “unfolded” residues have $\{^1\text{H}\}^{15}\text{N}$ NOE values smaller than 0.6, indicating a dynamic structure with little or no stable secondary structure. However residues in the regions corresponding to helices I (residues 9–20) and III (residues 49–64) approach this value. These regions of reduced dynamics correlate with regions of positive C^α shift deviations from random coil and thus indicate the regions of residual structure.

2.3.5 Urea reduces, but does not abolish, residual structure in the GII domain of Hho1p

A urea titration was carried out on the GII sample to determine if structural character was lost, implying the presence of residual structure. Figure 2.8a shows the ^1H - ^{15}N HSQC spectra of ^{13}C , ^{15}N -GII in buffers containing 0, 1, 2 and 4 M urea. 1 M urea was sufficient to shift the equilibrium entirely to the “unfolded” form of GII, shown by the complete disappearance of the peaks due to the folded form at urea concentrations >0 M. The proton resonances shift down-field as urea is added, indicating a loss of helical character (Wishart et al., 1991), confirming residual structure in the sample in non-denaturing buffer

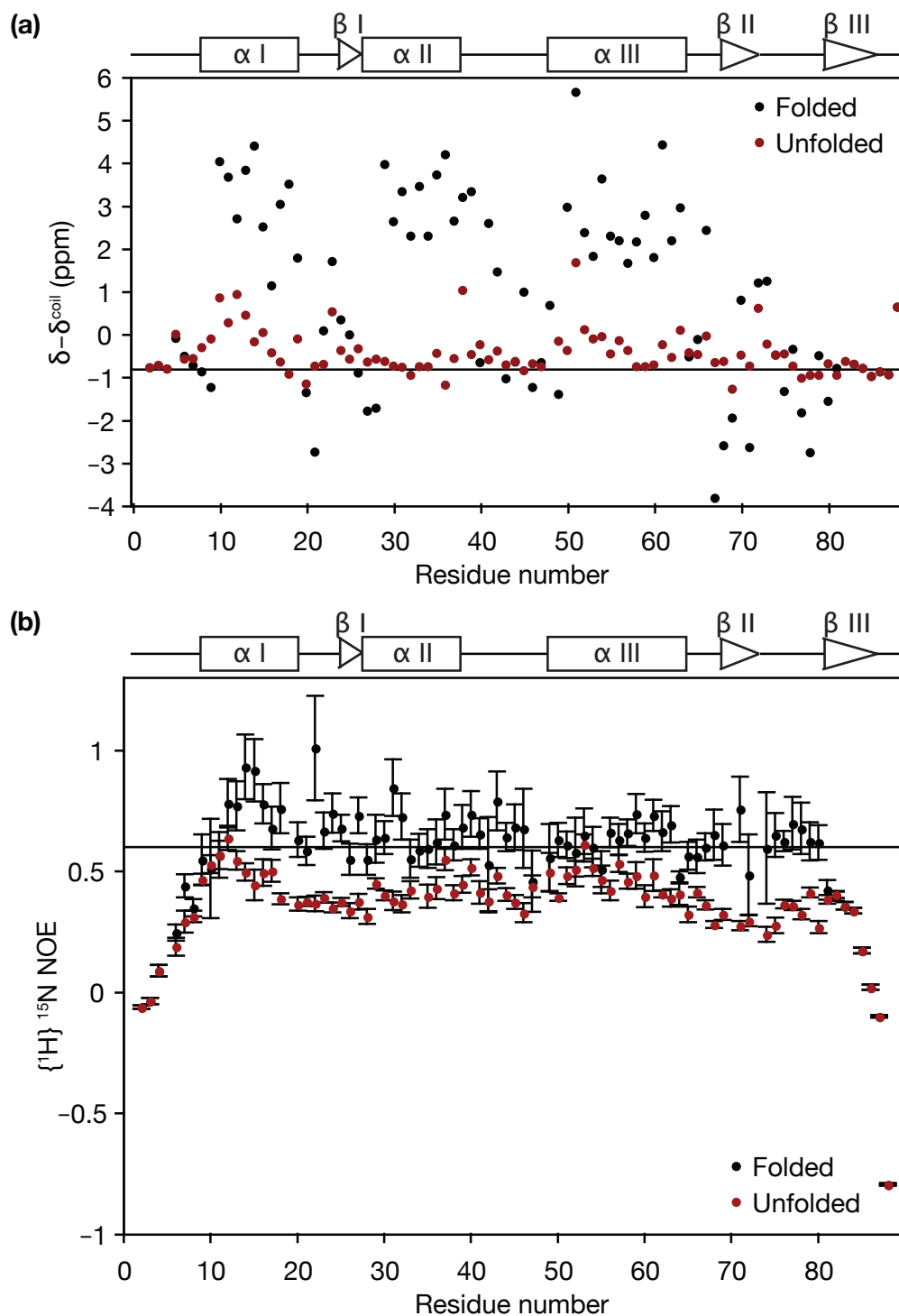


Figure 2.7 Comparison of the folded and “unfolded” forms of GII in 10 mM sodium phosphate. (a) C^α shift deviations from random coil for the two species of the GII domain, corrected for sequence context (Schwarzinger et al., 2001). There is a contiguous increase in the deviation around residues 8–18 and 50–59. The true baseline appears to be around -0.8 ppm, because this experiment was carried out at a very different temperature to that used to produce the random coil values (Schwarzinger et al., 2001). The secondary structure of the folded form is indicated. **(b)** Heteronuclear NOE values for the unfolded species are below 0.6; however regions corresponding to helices I and III approach this value.

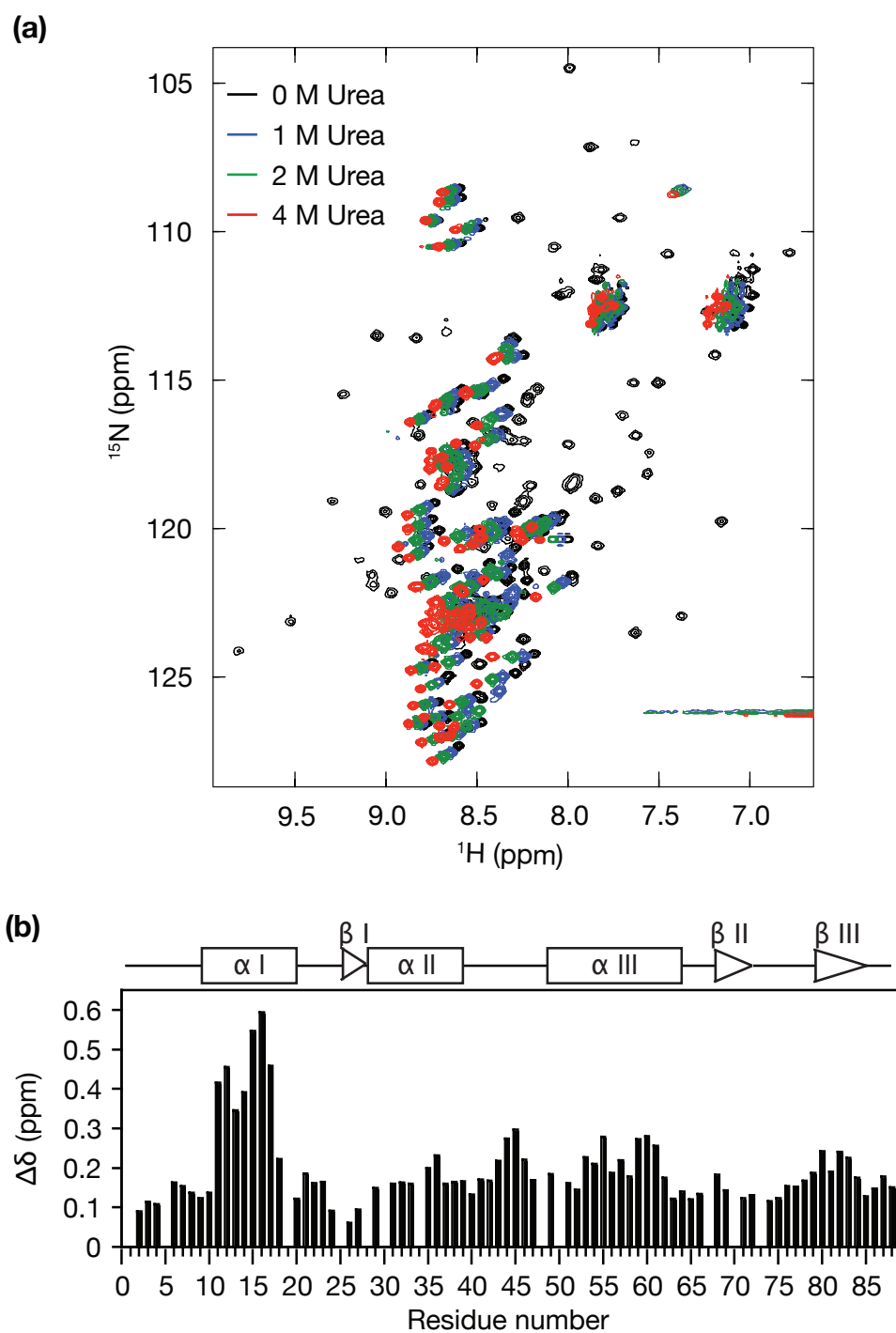


Figure 2.8 Urea titration into the GII domain of Hho1p. **(a)** ^1H - ^{15}N HSQC spectrum of $^{13}\text{C}^{15}\text{N}$ -GII, recorded at 500 MHz at 273K in 10 mM sodium phosphate pH 7. The samples contain urea, as indicated: none (black), 1 M (blue), 2 M (green), or 4 M (red). **(b)** Graphical representation of the size of the peak shifts upon addition of urea from 0 to 4 M. The secondary structure of the folded form of GII is indicated. The largest shifts occur around residues 11–17.

conditions. The combined peak shift differences were measured using the Analysis program (Vranken et al., 2005). A plot of peak shift differences between the GII domain in no urea and 4 M urea indicates that peaks due to residues 11–17 consistently shift further than the rest of the peaks (Figure 2.8b). The data in Figure 2.7 show that this is one of the regions showing α -helical character in non-denaturing buffer, and suggests that the residual structure in this region is vastly reduced in the presence of urea.

$\{^1\text{H}\}^{15}\text{N}$ NOE values decreased across most of the GII domain as the concentration of urea was increased (Figure 2.9). This indicates that GII becomes more dynamic as urea was added, suggesting that residual structure was being lost. The regions that contain residual structure in 0 M urea (residues 9–20 and 50–60) continue to have the highest $\{^1\text{H}\}^{15}\text{N}$ NOE values in 4 M urea, indicating that there may be residual structure in these regions that is persistent even in these denaturing conditions.

2.3.6 Contacts between helices I and III may be important in the packing of the GII domain of Hho1p

In principle, paramagnetic relaxation enhancement (PRE) could be used to identify interactions between residual secondary structure and tertiary elements within the dynamic GII domain. This would be investigated, in buffers containing 10 mM sodium phosphate, by determining which peaks due to the folded form were attenuated upon attachment of a paramagnetic tag (such as *S*-(2,2,5,5-tetramethyl-2,5-dihydro-1H-pyrrol-3-yl)methyl methane-sulfonothioate; MTSL) at a single location on the GII domain. The experiment was considered to be straightforward due to the presence of one cysteine residue within the GII domain at position 61 (corresponding to residue 231 of

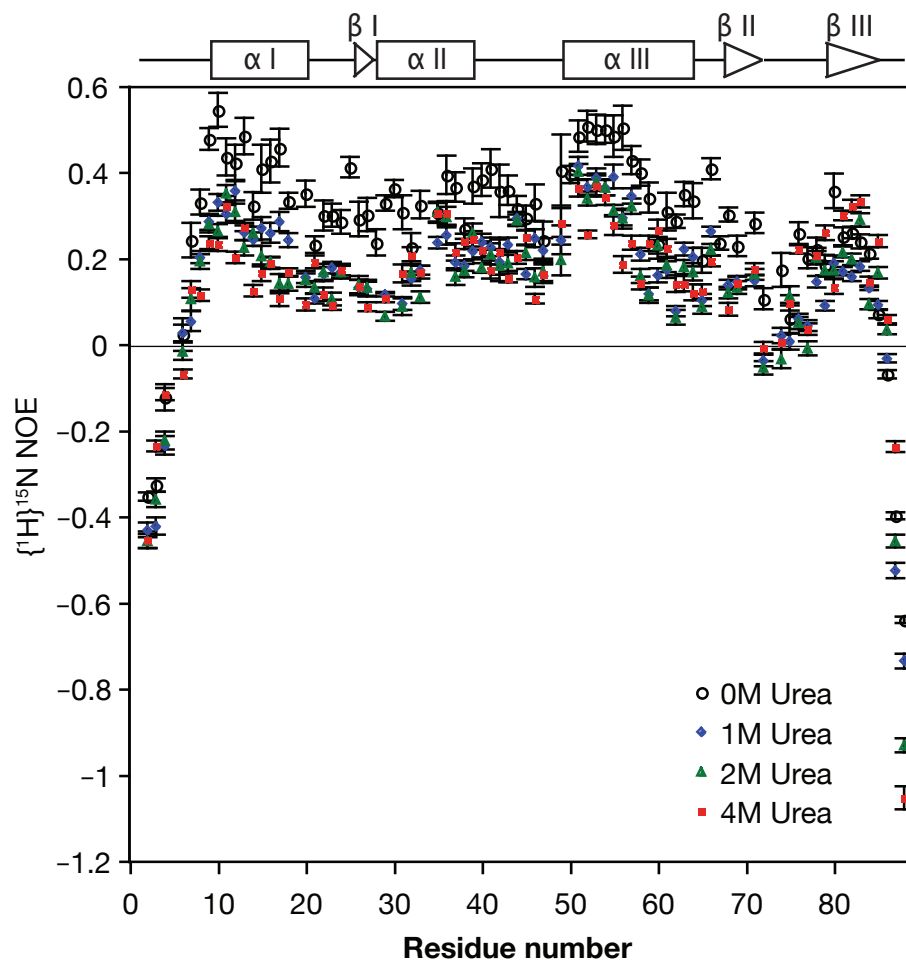


Figure 2.9 Heteronuclear NOE measurements for the GII domain of Hho1p in sodium phosphate buffer containing various concentrations of urea. Decreasing $\{^1\text{H}\}^{15}\text{N}$ NOE values upon addition of urea indicates that GII is becoming more dynamic. This suggests there is residual structure in the GII domain in 10 mM sodium phosphate buffers when urea is not present.

Hho1p).

Unfortunately, when the diamagnetic control tag (ATSL) was attached to the cysteine residue, the equilibrium shifted entirely to the “unfolded” form of GII (Figure 2.10a,b) meaning that no information could be gained about the dynamic equilibrium. However, although the PRE technique could not be used to study the folding of the GII domain, the effect of the modification suggests that the region containing cysteine 61 is involved in the packing of secondary elements or stability of the folded species. Cysteine 61 occurs towards the C-terminal end of helix III in the structured form of GII and is buried between helices I and III (Figure 2.10c). Evidently the addition of the ATSL-tag at cysteine 61 disrupts the packing between these helices and preventing the formation of the folded species.

2.4 Discussion

2.4.1 The GII domain exists as a folded and an “unfolded” species, both as an isolated domain and in the context of full-length Hho1p

NMR studies of ^{15}N -labelled full-length Hho1p indicate that the GI and GII domains retain the structural character of the isolated domains (Figure 2.3). Therefore, information gained from studies of the isolated domains can be applied to the regions within the full-length protein. Hho1p is a less attractive NMR subject than the isolated domains because the expression yields are lower and the samples degrade upon storage at 4 °C. More importantly, the larger number of residues and the presence of the unstructured regions (the N-terminal tail, the linker domain and the “unfolded” GII species), means Hho1p

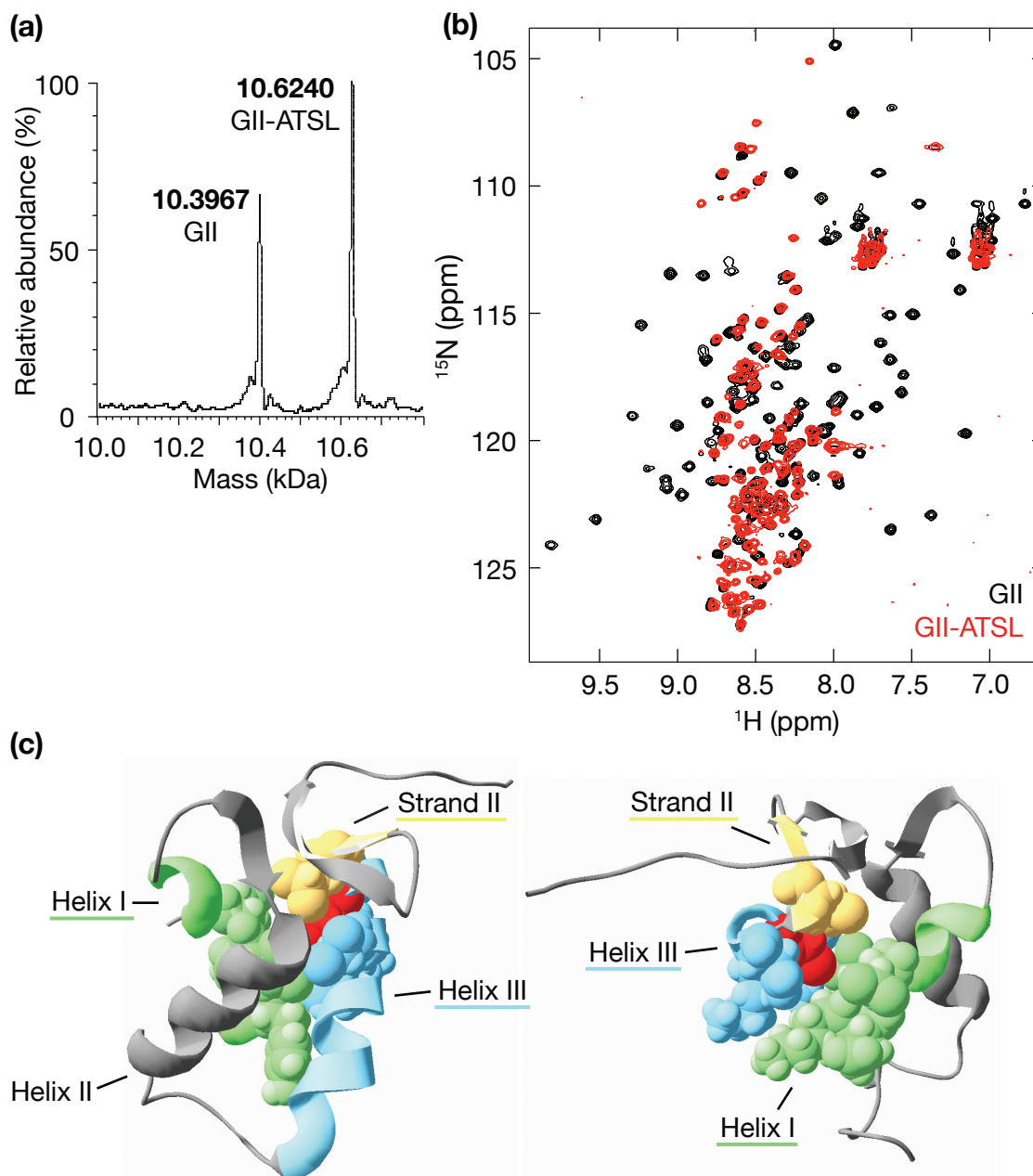


Figure 2.10 Attaching ATSL to the GII domain at cysteine 61 causes the equilibrium to shift to the “unfolded” species in 10 mM sodium phosphate buffer. (a) ESI-TOF mass spectrometry of GII-ATSL (^{13}C , ^{15}N -labelled) following treatment with 100 mM DTT for 10 minutes to remove the tag from some of the sample. The observed masses indicates there is one label per protein molecule. (b) ^1H - ^{15}N HSQC spectra of ^{13}C , ^{15}N -GII (black) and ^{13}C , ^{15}N -GII-ATSL (red), recorded at 600 MHz at 27 3K in 10 mM sodium phosphate buffer at pH 7.0. The ATSL-labeled sample has lost the dispersed resonances corresponding to the folded form of GII. (c) Two views of the structure of the GII domain, with the side chain of cysteine 61 marked in red. The backbone and selected sidechains of helices I and III and strand II are marked in green, blue and yellow respectively. Cysteine 61 is towards the C-terminal end of helix III and is buried within the side chains of residues in helices I and III and strand II. Images were created using SwissPDB viewer (1USS.pdb).

spectra show greater peak overlap than the spectra of the isolated domains.

2.4.2 The “unfolded” form of the GII domain of Hho1p contains regions of residual structure and may fold through interactions between these regions

Optimisation of the NMR conditions for the “unfolded” species of GII in 10 mM sodium phosphate buffer, by lowering the temperature, allowed the resonances for this species to be assigned. C^α shift deviations from random coil values and study of the backbone dynamics through $\{^1H\}^{15N}$ NOE measurements demonstrate regions of residual structure around residues 8–18 and 50–68 in the “unfolded” GII species, approximately where helices I and III occur in the folded form (Figure 2.7). Helices I and III have a much stronger helical character than helix II (25%, 21% and 5% respectively), despite the DisProt VL3E prediction suggesting that helices II and III should be more ordered than helix I (Figure 2.4b). The difference between the predicted and observed levels of order could be due to transient packing of helices within the “unfolded” GII domain. Helix I is predicted by the DisProt VL3E program to have low levels of intrinsic order, but packing with helix III could promote helix formation in helix I. A lack of transient packing interactions involving helix II could explain why its order prediction approaches that of helix III but only a small degree of helical-character was actually observed.

Residual structure in GII is confirmed by the ability to increase backbone dynamics by the addition of urea to the sample, presumable due to destruction of helical content (Figure 2.9). The presence of residual structure suggests that the GII domain is able to form secondary structure, but specific conditions are required to support packing of these elements into the tertiary struc-

ture. The residual structure in the GII domain explains how the folded and “unfolded” species exist in a dynamic equilibrium and allows rapid folding of the GII domain.

The addition of an ATSL-label at cysteine 61 causes the equilibrium to shift to the “unfolded” form (Figure 2.10), also suggesting a delicate equilibrium between the folded and “unfolded” GII species, which is disrupted by the bulky tag. This implies that the contacts between helices I and III, which show the strongest helical character in the “unfolded” GII, may be important in the packing of the GII domain. The residue in helix III of the GI domain that corresponds to cysteine 61 of GII is a glycine. This, along with the ATSL experiment, implies that the helical packing does not support a bulky group at this location.

Despite being partially unstructured in 10 mM sodium phosphate buffers the GII domain is able to protect chromatosomes from micrococcal nuclease (MNase) digestion in particular conditions (Sanderson et al., 2005). This implies that the equilibrium of GII species may move towards the folded form in the presence of DNA. Within the context of the full-length protein GII is relatively unstructured and exists as a dynamic ensemble of species (Figure 2.3). If the GI domain bound chromatin then the local DNA concentration would increase. This could allow selection of the the folded form of GII, producing a bi-functional linker histone (Section 1.5.5). This bi-functionality could explain why Hho1p is less abundant in chromatin than canonical linker histones (Bates and Thomas, 1981; Freidkin and Katcoff, 2001; Downs et al., 2003).

2.5 Summary

- Full-length Hho1p can be expressed in minimal medium and in quantities sufficient for NMR studies.
- The globular domains within full-length Hho1p have similar structural characters to the isolated domains.
- The “unfolded” GII domain species contains regions of residual structure around the residues corresponding to helices I and III of the folded domain.
- The residual structure is partially removed by the addition of urea, with the chemical shifts indicating a loss of alpha-helical character, especially around the residues corresponding to helix I.
- Adding a chemical tag to cysteine 61 disrupts the equilibrium between the “unfolded” and folded species of the GII domain. This demonstrates that packing between the helices I and III is important in the folding of the GII domain of Hho1p.

Chapter 3

Hho1p acts within chromatin in a similar manner to canonical linker histones

3 Hho1p acts within chromatin in a similar manner to canonical linker histones

3.1 Introduction

It is known that Hho1p binds throughout the *S. cerevisiae* genome (Downs et al., 2003; Ali, 2001), but it is unclear whether it is evenly distributed throughout the genome (Schäfer et al., 2008) or enriched at certain loci (Freidkin and Katcoff, 2001). Also contested is the abundance of Hho1p relative to core nucleosomes in the yeast cell. The published values range from one Hho1p molecule per 4 nucleosomes (Downs et al., 2003) to 1 per 37 nucleosomes (Freidkin and Katcoff, 2001). Both of these assays used yeast strains containing a tagged version of Hho1p, which could affect the expression or chromatin association of the protein. Furthermore, Freidkin and Katcoff estimated the number of nucleosomes in a yeast cell to be around 74,000, which is considerably higher than more recent measurements, indicating they underestimated the Hho1p : nucleosome ratio.

More recently, sequencing DNA immunoprecipitated by histone H3- and H4-antibodies has determined the number of nucleosomes in a yeast cell to be around 53,000 (Mavrich et al., 2008). The number of Hho1p molecules in a yeast cell has been measured at about 6500 (Ghaemmaghami et al., 2003). This study created TAP-tag fusion proteins that were expressed from the endogenous promoters and quantified by immunodetection, using an endoge-

nous protein as a loading control. These numbers would suggest a ratio of one Hho1p molecule for about every 8 nucleosomes. Finally, previous work in this laboratory measured the yeast cellular levels of Hho1p and nucleosome as about equal. In this assay untagged Hho1p and chicken erythrocyte chromatin were used to create standard curves, allowing quantification of the immunodetection of Hho1p and histone H4 in yeast whole-cell extract (Ali, 2001). Further investigation of the Hho1p to nucleosome ratio is required to determine which of the reported measurements is most accurate, since this will affect how we consider the role of Hho1p within chromatin.

Among the Hho1p binding models, described in Section 1.5.5, are two models that could explain why the reported Hho1p : nucleosome ratios are lower than for histone H1 : nucleosome levels in metazoans. If only one globular domain of Hho1p binds to a nucleosome core, the second globular domain might perhaps sterically interfere with the binding of another Hho1p molecule to the adjacent core nucleosomes. Alternatively Hho1p may bridge between two adjacent nucleosome cores, effectively halving the number of Hho1p molecules required to saturate the chromatin.

The potential for Hho1p to bridge two nucleosomes may allow a mechanism for condensation of the yeast chromatin. The yeast genome contains nucleosome-free regions (Bernstein et al., 2004; Lee et al., 2004) but otherwise the nucleosome repeat length is around 165 bp (Thomas and Furber, 1976). This is the length of DNA required for a chromatosome (i.e. there is no linker DNA present between the chromatosomes) raising the question of whether the chromatin could be further condensed. Analytical ultracentrifugation and electron microscopy indicate condensation of reconstituted chromatin with 167 bp nucleosome repeat length, upon addition of sub-stoichiometric amounts of linker histone H5 (Routh et al., 2008). Hho1p was shown to affect the com-

paction of yeast chromatin both at the rDNA locus and a region outside the rDNA (Levy et al., 2008). Psoralen cross-linking demonstrates the accessibility of DNA by intercalating with DNA and causing reduced gel mobility. The psoralen accessibility was lower in an *hho1*-null strain than in a wild-type yeast strain. Global compaction of yeast chromatin in stationary phase also appears to be mediated by Hho1p, as wild-type yeast chromatin was seen to sediment more rapidly through sucrose gradients than that from an *hho1*-null strain (Schäfer et al., 2008). In contrast, the nucleosome repeat length in yeast bulk chromatin does not change upon deletion of the HHO1 gene and there was no difference in the *in vivo* micrococcal digestion pattern in individual genes (Puig et al., 1999; Patterson et al., 1998). Taken together this indicates that Hho1p can affect chromatin structure albeit only at particular times or locations *in vivo*; presumably the effect is too subtle to be seen in assays on bulk chromatin. This may explain the observation that Hho1p can inhibit homologous recombination without producing a detectable effect on the global chromatin structure (Downs et al., 2003).

In this Chapter I aim to provide a definitive measurement of the Hho1p to nucleosome ratio in *S. cerevisiae* cells. Standard curves of non-tagged recombinant Hho1p and Hhf2p were used to allow semi-quantitative immunodetection of the proteins in whole-cell extract from a wild-type yeast strain. The wild-type yeast strain ensures natural Hho1p levels, while using non-tagged recombinant yeast proteins should ensure that antibody binding is consistent between the protein in the cell extract and the samples used to produce the standard curves. In addition, contacts made to core histones by Hho1p and canonical linker histones are compared. The compaction of reconstituted nucleosome arrays containing Hho1p and tripartite linker histones is also investigated.

3.2 Materials and methods

3.2.1 Yeast

3.2.1.1 Yeast growth medium

The yeast growth medium used in this Thesis is listed in Table 3.1

Table 3.1: Yeast growth medium

Medium	Recipe
YPAD medium:	10 g yeast extract, 20 g peptone, 20 g glucose, 48 mg adenine hemisulphate per litre

3.2.1.2 Yeast strains

The yeast strains used in this Thesis are listed in Table 3.2

Table 3.2: Yeast strains

<i>S. cerevisiae</i> strain	Genotype (-/-)	Supplier
HHO1-TAP	MAT α his3 Δ 1 leu2 Δ 0 met15 Δ 0 ura3 Δ 0 HHO1- TAP::HIS	Open Biosys- tems
HTZ1-TAP	MAT α his3 Δ 1 leu2 Δ 0 met15 Δ 0 ura3 Δ 0 HTZ1- TAP::HIS	Open Biosys- tems
W303-1B	MAT α { <i>leu2-3,112 trp1-1</i> <i>can1-100 ura3-1 ade2-1</i> <i>his3-11,15</i> } [<i>phi</i> ⁺]	Gift from Dr J. Downs, University of Sussex

3.2.2 Plasmids

Plasmid pET28b-HHF2 contains the cDNA for a full-length core histone H4 gene from *S. cerevisiae*, and was a gift from Dr Carl Wu (Center for Cancer Re-

search, U.S. National Institutes of Health). The coding sequence is native, without modifications or tags (Shen et al., 2003).

Plasmid pET17b-NGIL contains the cDNA for the N-terminal region (N-terminal tail, GI domain and linker region; residues 1-170) of Hho1p under the control of a T7 promoter, and an ampicillin resistance gene (Ali and Thomas, 2004).

The DNA arrays are contained in pUC18-based plasmids, and were provided by Dr Andrew Routh (MRC Laboratory of Molecular Biology, Cambridge). pUC18-167x25 and pUC18-197x25 are based on the Widom “601” DNA nucleosome positioning sequence (Lowary and Widom, 1998) and contain DNA repeat lengths of 167 and 197 bp respectively. The plasmids have been constructed as described previously (Routh et al., 2008) except that each array contains 25 tandem copies of the particular DNA sequence.

3.2.3 Proteins

3.2.3.1 Expression and purification of the yeast core histone H4, Hhf2p

E. coli Rosetta(DE3) cells were transformed with pET28b-HHF2 using heat shock (Sambrook et al., 1989). Following overnight growth on LB-agar plates at 37 °C colonies were picked and grown overnight, shaking, at 37 °C in LB medium supplemented with 25 $\mu\text{g/ml}$ kanamycin and 25 $\mu\text{g/ml}$ chloramphenicol (both from Melford Laboratories Ltd.) (see Section 2.2.1.1 for media recipes).

Ten flasks (2 l) containing 450 ml 2xYT medium, supplemented with the antibiotics above, were each inoculated with 5 ml of overnight culture and grown at 250 rpm at 37 °C. When an OD_{600} of about 0.6 was reached expression was induced with 1 mM IPTG and cultures grown for a further 4 h. Cells were harvested by centrifugation at 5000 g for 15 min at 20 °C (to reduce cell lysis),

then resuspended in 50 mM Tris-HCl pH 7.5, 100 mM NaCl, 1 mM EDTA, 1 mM benzamidine, and the cell suspension was flash frozen and stored at -20°C .

The cell suspension was thawed and the buffer supplemented with 1 $\mu\text{g}/\text{ml}$ leupeptin, 1 $\mu\text{g}/\text{ml}$ aprotinin, 0.156 mg/ml benzamidine, 1 $\mu\text{g}/\text{ml}$ pepstatin A and 0.5 mM PMSE. Cells were lysed by passing twice through a French press at 1000 psi and inclusion bodies (containing Hhf2p) were collected by centrifugation at 35000 g for 10 min at 4°C . The pellet was crushed and washed twice with TW buffer (wash buffer as described above, supplemented with 1% (v/v) Triton X100) and twice with wash buffer. The pellet was resuspended in DNase buffer (50 mM Tris-HCl pH 7.5, 2.5 mM MgCl_2 , 0.5 mM CaCl_2), and then DNase I (Sigma-Aldrich-Aldrich) was added to 2 $\mu\text{g}/\text{ml}$ and the sample was incubated at 37°C for 1 hour.

Inclusion bodies were collected by centrifugation as before and extracted by crushing the pellet in 50 mM Tris-HCl pH 8.8, 6 M guanidine hydrochloride, 25 mM DTT, incubation for 45 min at 25°C , with agitation, and centrifugation at 35000 g for 10 min at 4°C . The supernatant was taken and the pellet re-extracted. The supernatants were then combined and filtered through a 0.2 μm membrane (Millipore). The guanidine hydrochloride was removed by passing the sample over a HiPrep 26/10 desalting column (GE Healthcare), which had been pre-equilibrated with urea buffer (10 mM sodium phosphate, 8 M urea, 1 mM EDTA, 1 mM DTT, pH adjusted to 6).

Purification of Hhf2p was followed by SDS/18%-PAGE (Section 2.2.4.1). Fractions of sufficient purity were flash frozen and stored at -80°C . Accurate protein concentrations were determined by automated amino acid analysis (Section 2.2.4.2).

3.2.3.2 Expression and purification of Hho1p and NGIL proteins

Hho1p was expressed in TB medium (Section 2.2.1.1) using the conditions described in Section 2.2.3.1. NGIL was expressed in LB medium (Section 2.2.1.1), supplemented with 50 $\mu\text{g}/\text{ml}$ carbenicillin, using the same conditions as GII (Section 2.2.3.3), except it was expressed in BL21(DE3)pLysS cells (Section 2.2.1.2). Both proteins were purified as described for Hho1p (Section 2.2.3.2) except that NGIL was concentrated in a Vivaspin 2 concentrator with a 5 kDa cut-off (Sartorius).

3.2.4 Extraction of chromatin and linker histones from chicken erythrocytes

Chicken erythrocyte materials (nuclei, medium-length linker histone-depleted chromatin, core histone octamers, linker histones and 147 bp competitor DNA) were prepared as described (Thomas, 1998).

3.2.4.1 Isolation of chicken erythrocyte nuclei

5 ml of frozen chicken erythrocytes were thawed and lysed at 37 °C in 75 ml sucrose buffer A (15 mM Tris-HCl pH 7.5, 0.34 M sucrose, 15 mM NaCl, 60 mM KCl, 0.5 mM spermidine hydrochloride (Sigma-Aldrich), 0.15 mM spermine hydrochloride (Sigma-Aldrich), 15 mM 2-mercaptoethanol) containing 2.5 mM EDTA pH 8.0 and 0.5% (v/v) NP-40 (Hewish and Burgoyne, 1973). Lysed cells were filtered through two layers of muslin and the nuclei collected from the filtrate by centrifugation at 2000 *g* for 5 min at 4 °C. The pellet of nuclei was washed with sucrose buffer A until the supernatant was no longer pink and re-suspended in sucrose buffer A containing 0.25 mM PMSE. The absorbance of

the nuclear suspension was measured at 260 nm in 1 M NaOH and the volume of nuclei was adjusted with sucrose buffer A to give A_{260} of 50.

3.2.4.2 Preparation of medium-length chromatin by micrococcal nuclease digestion

The temperature of the nuclei (at $A_{260} = 50$) was raised to 37 °C and CaCl_2 was added to 1 mM. Micrococcal nuclease (Worthington: 15 U/ μl stock) was added at 2 μl per ml nuclei and the suspension was incubated for 3 min with swirling to produce medium-length chromatin. Digestion was stopped by addition of 0.1 M EDTA pH 8.0 to 10 mM and chilling the nuclei on ice.

Nuclei were collected by centrifugation at 2000 g for 10 min at 4 °C and the pellet drained well. The nuclei were lysed in 0.2 mM EDTA, in a volume at least equal the starting volume of nuclei, by incubation on ice for 2 h. Nuclear debris was removed by centrifugation at 2000 g for 5 min at 4 °C and the soluble chromatin in the supernatant taken. The typical yield was 1 ml of chromatin at $A_{260} = 20$ from 1 ml nuclei. ($A_{260} = 10$ corresponds to 1 mg/ml chromatin)

3.2.4.3 Size-fractionation of chromatin through sucrose gradients

5–30% sucrose gradients (30 ml) containing 10 mM Tris-HCl pH 7.5, 1 mM EDTA, 0.5 mM PMSF were prepared and allowed to settle for 2 h at 4 °C. A maximum of 3 ml or 100 A_{260} units of soluble chromatin was layered on to the gradients and fractionated by centrifugation at 16000 rpm in a Beckman SW28 rotor for 16 h at 4 °C. The rotor was allowed to decelerate without braking to avoid disturbing the gradients. Gradients were fractionated and about 0.2 A_{260} unit samples were taken for analysis. Proteins were precipitated with 25% Trichloroacetic acid (TCA: Fisher Scientific) on ice for 20 min. The proteins

were collected by centrifugation at 17000 g for 15 min at 4 °C and, for samples that contained sucrose, the TCA precipitation was repeated. Protein pellets were washed in acetone containing 10 mM HCl and then in acetone alone. Samples were analysed by SDS/20%-PAGE, and fractions containing chromatin were dialysed against buffer A (Section 2.2.3.2).

3.2.4.4 Salt-stripping of linker histones from chicken erythrocyte chromatin

Soluble chromatin was prepared (Section 3.2.4.2) and NaCl added to 0.65 M from a 2 M stock, quickly with constant swirling to avoid precipitation of the chromatin. The chromatin was fractionated in sucrose gradients, as in Section 3.2.4.3, but the gradients also contained 0.65 M NaCl. Centrifugation conditions for medium-length stripped chromatin were 22400 rpm in a Beckman SW28 rotor for 15 h at 4 °C. Gradients were fractionated and analysed as above and the fractions containing H1,H5-depleted chromatin were pooled and dialysed against buffer A (Section 2.2.3.2). Chromatin concentration was measured by absorbance at 260 nm.

3.2.4.5 Preparation of core histone octamers from linker histone-depleted chicken erythrocyte chromatin

Hydroxyapatite resin (1 ml per 20 A_{260} units chromatin) (Sigma-Aldrich) was pre-equilibrated with 10 mM sodium phosphate pH 7.0, 3 M KCl, 1 mM EDTA, 1 mM DTT. The linker histone-depleted chromatin was adjusted to 3 M KCl, from a 5 M stock, and was incubated with the hydroxyapatite resin for 30 min at 4 °C. The supernatant, containing core histone octamers, was removed and the resin washed twice in the buffer. Supernatant and wash fractions were combined and immediately concentrated in a Vivaspin concentrator with a 10 kDa

cut-off. Using KCl in the buffers allows the octamer concentration to be determined by automated amino acid analysis (Section 2.2.4.2) (M_r : 108486 Da)

3.2.4.6 Isolation of linker histones H1 and H5 from chicken erythrocytes

Linker histones were isolated from either chicken erythrocyte chromatin (Section 3.2.4.2) or nuclei (Section 3.2.4.1). Perchloric acid (PCA) was added to the chromatin or nuclei to a final concentration of 5% (v/v) and the sample was stirred on ice for 15 min. Precipitated proteins were collected by centrifugation at 10000 g for 10 min at 4 °C and the supernatant, on ice, was immediately brought to pH 7.0 with triethanolamine. The neutralised supernatant was dialysed against buffer A and the linker histones were further purified using a Hi-Trap SP Sepharose HP cation-exchange column as described (Section 2.2.3.2). The histone H1 (several variants) elutes at lower concentrations of NaCl than H5 (about 550 mM and 700 mM respectively).

3.2.4.7 Isolation of 147 base pair competitor DNA from linker histone-depleted chicken erythrocyte chromatin

A trial digestion was carried out using 10 A_{260} units of linker histone-depleted chromatin (Section 3.2.4.4) and 30 U micrococcal nuclease at 37 °C in 10 ml digestion buffer (10 mM Tris-HCl pH 7.5, 1 mM DTT, 1 mM $CaCl_2$). Samples (0.04 A_{260}) were taken at various time points (from 4 to 48 min) and the DNA extracted. The samples were diluted to 350 μ l with water, 50 μ l 10% (w/v) SDS was added and mixed well, then 100 μ l 5 M NaCl was added and the sample mixed again. Proteins were extracted twice using phenol:chloroform:isoamyl alcohol (25:24:1 (v/v)). The DNA was precipitated from the aqueous phase with at least 3 volumes of absolute ethanol and incubation at -80 °C for 1 hour. DNA was collected by centrifugation at 20000 g for 30 min at 4 °C and the pellet was

washed with 70% (v/v) ice-cold ethanol. DNA was analysed in 19 cm long 7%-polyacrylamide gels containing 0.3x TBE (Section 3.2.6.2).

Bulk chromatin digestion was carried out using conditions identified in the trial digestion to produce predominantly core particles containing about 147 bp DNA. The digested chromatin was passed through sucrose gradients (Section 3.2.4.3) by centrifugation at 28000 rpm in a Beckman SW28 rotor for 27 h at 4 °C and fractionated and analysed as described (Section 3.2.4.3). Fractions containing core particles were dialysed against 10 mM Tris-HCl pH 7.5, 1 mM EDTA, 1 mM DTT and 0.5 mM PMSF before concentration in a Vivaspin concentrator with 10 kDa cut-off. The DNA was then extracted as described for the trial digestion samples, except that the final DNA pellet was dissolved in TE buffer (10 mM Tris-HCl pH 8.0, 1 mM EDTA).

3.2.5 Isolation of yeast nuclei

Yeast nuclei were prepared using a protocol based on several previously published methods (Lowary and Widom, 1989; Thomas and Furber, 1976; Wintersberger et al., 1973).

A culture of yeast W303 cells (Section 3.2.1.2) was grown to an OD₆₀₀ of approximately 1, in 50 ml YPAD (Section 3.2.1.1) at 30 °C with shaking at 260 rpm. The cells were harvested by centrifugation at 2000 g for 5 min at 20 °C, resuspended in 40 ml pre-incubation buffer (50 mM potassium phosphate pH 7.5, 1 M sorbitol, 10 mM MgCl₂, 30 mM 2-mercaptoethanol, 0.5 mM PMSF) and incubated for 30 min at 30 °C with shaking at 300 rpm. Cells were collected by centrifugation at 3000 g for 5 min at 20 °C.

The cells were resuspended in 40 ml spheroplasting buffer (25 mM potassium phosphate pH 7.5, 25 mM sodium succinate pH 5.5, 1 M sorbitol,

10 mM MgCl₂, 10 mM 2-mercaptoethanol, 0.5 mM PMSF) supplemented with 20 mg Zymolyase 20-T (Seikagaku). The cell suspension was incubated at 30 °C with shaking at 260 rpm for 45-60 min, and the resulting spheroplasts collected by centrifugation at 3000 g for 5 min at 4 °C. The spheroplasts were washed twice with spheroplasting buffer.

Spheroplasts were resuspended in lysis buffer (20 mM potassium phosphate pH 7.5, 18% (w/v) Ficoll 400 (Sigma-Aldrich), 0.5 mM MgCl₂, 0.5% (v/v) NP-40, 1 mM PMSF, 1 µg/ml leupeptin, 1 µg/ml aprotinin, 0.156 mg/ml benzamidine, 1 µg/ml pepstatin A) at 4 °C. Unlysed spheroplasts and cells were collected by centrifugation at 4000 g for 10 min at 4 °C. The supernatant (containing mitochondria, vacuoles and membrane fragments) was taken and the nuclei were collected by centrifugation at 30000 g for 20 min at 4 °C. The supernatant was removed carefully from the top. The nuclei were washed in the buffer required for the subsequent experiments, for example 10 mM sodium phosphate pH 8.0 for the cross-linking reactions.

3.2.6 DNA characterisation

3.2.6.1 Agarose gel-electrophoresis

Unless otherwise stated, 0.9% (w/v) agarose gels containing 0.3x TBE (26.7 mM Tris base, 0.6 mM EDTA, 26.7 mM boric acid) were used. Glycerol was added to 5% (v/v) to the samples and a lane containing gel loading buffer (0.3X TBE, 5% (w/v) glycerol, 0.04% (w/v) bromophenol blue, 0.04% (w/v) xylene cyanol FF) was used to follow the progress of electrophoresis. Gels were run in 0.3x TBE at 10 V/cm. The DNA was visualised by staining with ethidium bromide, destaining in deionised water and illumination with 254 nm UV light.

3.2.6.2 Native PAGE

Unless otherwise stated 7% (w/v) polyacrylamide gels containing 0.3x TBE (Section 3.2.6.1) were run at 10 V/cm. Samples were prepared and the DNA was visualised as for agarose gels (Section 3.2.6.1).

3.2.7 Western blotting

3.2.7.1 Antibodies

Rabbit anti-Hho1 and anti-H1 polyclonal antibodies were raised in house. Rabbit anti-H3 polyclonal antibody was raised against a synthetic peptide from within residues 100 to the C-terminus of human histone H3 (Abcam: ab1791). Rabbit anti-H4 polyclonal anti-H4 polyclonal antibody was raised against a synthetic peptide from within residues 1-100 of human histone H4 (Abcam: ab7311).

The secondary antibody was a donkey anti-rabbit IgG horseradish peroxidase-conjugated (HRP) antibody (GE Healthcare).

3.2.7.2 Protein transfer and immunodetection

Proteins were separated by SDS/PAGE (Section 2.2.4.1) and transferred electrophoretically to nitrocellulose membrane (GE Healthcare) at 250 mA at 4 °C for 3 h in SDS transfer buffer (25 mM Tris base, 192 mM glycine, 20% (v/v) methanol, 0.1% (w/v) SDS). The membrane was blocked overnight at 4 °C on a rocking platform with 4% (w/v) dried skimmed-milk powder (Marvel™) in TBS-T (10 mM Tris-HCl pH 7.5, 150 mM NaCl, 0.05% (v/v) Tween 20), and then incubated with a primary antibody (Section 3.2.7.1) at the appropriate dilution in TBS-T/milk for 2 h at 25 °C or overnight at 4 °C with rocking. The membrane

was washed in TBS-T (3x 15 min), incubated with the secondary antibody at 1:5000 dilution in TBS-T/milk for 1 hour with rocking at 25 °C, then washed in TBS-T as above, and bound HRP-conjugated antibody was detected with enhanced chemiluminescence Western blotting reagents (GE Healthcare) and exposure to X-ray film (Konica Minolta).

3.2.7.3 Nitrocellulose membrane stripping

In order to re-probe the nitrocellulose membranes they were first stripped by incubation for 30 min at 50 °C with agitation in 50 mM Tris-HCl pH 6.8, 10 mM 2-mercaptoethanol, 2% (w/v) SDS. Membranes were rinsed well with dH₂O, washed in TBS-T (3x 15 min), and then re-probed (Section 3.2.7.2).

3.2.8 Chemical cross-linking

Chemical cross-linking was carried out essentially as described (Thomas, 1989) using 5 μ M protein samples (the equimolar mixture contained 5 μ M of each protein) in 10 mM sodium phosphate pH 8.0, 1 mM EDTA and 1 mM DTT, unless otherwise stated. An 11x dimethyl suberimidate (DMS: Pierce) stock solution was made in 100 mM triethanolamine and immediately added to the samples to the final concentration indicated. Samples were incubated at 25 °C for the indicated time and the reaction quenched by the addition of hot SDS loading buffer (Section 2.2.4.1). Samples were analysed by SDS/18%-PAGE (Section 2.2.4.1) and Western blotting with the indicated antibodies (Section 3.2.7).

3.2.9 Reconstitution of nucleosome arrays

3.2.9.1 Purification of DNA arrays

E. coli DH5 α cells (Section 2.2.1.2) in five flasks (2 l) containing 500 ml LB medium (Section 2.2.1.1) plus 50 μ g/ml carbenicillin was used to propagate pUC18-167x25 or pUC18-197x25 plasmids (Section 3.2.2). The plasmids were purified using a maxi-prep protocol involving equilibrium centrifugation in CsCl-ethidium bromide gradients (Sambrook et al., 1989). The ethidium bromide was removed with water-saturated butanol, and the DNA precipitated with 1/10 volume of 3 M NaAc pH 5.2, and three volumes of cold absolute ethanol at -80°C for 1 hour. The DNA was collected by centrifugation at 20000 g for 30 min at 4°C and washed with cold 70% (v/v) ethanol. The dry pellet was dissolved in dH₂O.

Plasmids were digested with *Eco* RV, *Dra* I, *Dde* I and *Hae* II (all from NEB) in NEB buffer 3 and BSA at 37°C overnight (120 units of each enzyme per mg plasmid DNA respectively). The long DNA arrays were separated from the shorter plasmid fragments by sequential precipitation with 5–8% PEG 6000 (Sigma-Aldrich) in 0.5 M NaCl. A stock solution of 30% PEG 6000 and 2.5 M NaCl was used to produce a final concentration of 5% PEG in the DNA solution, incubated on ice for 10 min and the precipitated DNA was collected by centrifugation at 25000 g for 10 min at 4°C . The supernatant was taken, the PEG concentration adjusted to 5.1% and the precipitation repeated. The process was repeated for PEG concentrations of 5.2%, 5.3%, 5.4%, 5.5%, 6.5%, 5.7%, 5.8%, 5.9%, 6.0% and 8.0%. Each pellet of precipitated DNA was dissolved in H₂O and analysed in 0.9% (w/v) agarose gels containing 0.3x TBE (Section 3.2.6.1). The samples containing the DNA arrays were precipitated as described above.

3.2.9.2 Reconstitution of nucleosome arrays by continuous salt dialysis

Chromatin was reconstituted using a continuous salt dialysis method described previously (Huynh et al., 2005). The point of stoichiometric octamer binding to positioning sequences in the DNA array was first determined through an octamer titration and assessment of reconstitution using gel-mobility-shift assay in 1% (w/v) agarose gels containing 0.3x TBE (Section 3.2.6.1).

Samples for reconstitution contained 1.2 pmol 25-mer DNA array (30 pmol octamer sites), sufficient chicken erythrocyte octamers to bind at each positioning sequence, 6 pmol 147 bp competitor DNA (crDNA) and the indicated molar ratio of linker histone in binding buffer (2.2 M NaCl, 10 mM Tris-HCl pH 7.5, 1 mM EDTA, 5 mM DTT, 0.5 mM PMSE, 1 mM benzamidine). The samples were incubated on ice for 30 min and then transferred to dialysis “buttons” (the cap of a 0.6 ml microfuge tube holds the sample, which is covered with dialysis membrane and sealed with a ring cut from the body of the tube). The buttons were placed in a dialysis bag containing 50 ml binding buffer and this was dialysed overnight at 4 °C against 5 litres of 10 mM Tris-HCl pH 7.5, 1 mM EDTA, 1 mM DTT. Reconstitution was assessed in gel-mobility-shift assays, typically with 0.2 pmol chromatin per lane using 0.9% (w/v) agarose gels containing 0.3x TBE (Section 3.2.6.1).

3.2.9.3 Fixing reconstituted nucleosome arrays with glutaraldehyde

To preserve the compaction state of the nucleosome arrays as they pass through the agarose gels the arrays were gently fixed. Glutaraldehyde (50% (v/v): Sigma-Aldrich) was added from a 1% stock to a final concentration of 0.1% (v/v) and samples were incubated on ice for 10 min before loading on to agarose gels (Section 3.2.6.1).

3.2.9.4 Folding of nucleosome arrays

Reconstituted chromatin samples (in “buttons”) were dialysed for 36–40 h at 4 °C against 10 mM triethanolamine pH 7.5, 1 mM MgCl₂. Gels were fixed with glutaraldehyde (Section 3.2.9.3) before running through agarose gels (Section 3.2.6.1).

3.2.9.5 *Ava I* digestion of nucleosome arrays

Chromatin for *Ava I* (NEB) digestion was reconstituted as in Section 3.2.9.2 except there was no EDTA in the buffers. The buffer conditions were adjusted to 50 mM NaCl and 2 mM MgCl₂, *Ava I* was added (typically 17000 U per pmol nucleosome array) and the samples were incubated at 37 °C for the indicated time. The digestion was stopped by the addition of EDTA to 10 mM and samples were kept on ice before analysis in agarose gels (Section 3.2.6.1).

3.2.9.6 Analytical ultra-centrifugation

Analytical ultra-centrifugation (AUC) experiments were carried out in collaboration with Dr Andrew Routh (MRC Laboratory of Molecular Biology, Cambridge).

Sedimentation coefficients were determined using a Beckman XL-A centrifuge with scanner optics (absorbing at 260 nm) and a Beckman AN60 rotor. Sedimentation runs were carried out at 19000 rpm for 2 h at 5 °C. Sedimentation coefficients were determined by a time-derivative method (Stafford, 1992), and differential apparent sedimentation coefficient distribution, $g(s^*)$ was calculated using the Dcdt+ data analysis program (v 2.05) (Philo, 2006). The sedimentation coefficients were corrected for buffer composition and temperature using the factors determined previously (Routh et al., 2008).

3.3 Results

3.3.1 Hho1p is less abundant than metazoan linker histones

In order to measure the relative levels of Hho1p and nucleosomes in yeast cells, without using tagged proteins or estimations of nucleosome content, a semi-quantitative protocol was devised. A range of amounts of recombinant Hhf2p (i.e yeast histone H4) and Hho1p were analysed by Western blotting using polyclonal anti-H4 and anti-Hho1 antibodies. Densitometry of these blots produced standard curves that were used to measure the amounts of the proteins in a wild-type yeast whole-cell extract (Figure 3.1). The standard curves were fitted to a linear trend line, and only blots where both standard curves have R^2 values greater than 0.925 were used. Table 3.3 shows the data produced and the calculations for the molar ratio of core histone octamers (assumed to be half the molar amount of Hhf2p) to Hho1p. There is about one molecule of Hho1p for every 5–10 nucleosome cores in yeast. There is variation of a factor of 2 between the samples but, despite repeating the experiment many times, a more precise measure could not be achieved (data not shown). The R^2 values for blots 1 and 2 were slightly higher (mean value: 0.975) than those of blots 3 and 4 (mean value: 0.960), indicating that the Hho1p may be present at around one molecule per every six nucleosomes.

Table 3.3: Ratio of core nucleosome to Hho1p in yeast cells

Blot	Amount (ng)		Amount (pmol)		Molar ratio octamer to Hho1p
	Hhf2p	Hho1p	Hhf2p	Hho1p	
1	52.3	12.0	4.6	0.4	5.4
2	62.5	10.7	5.5	0.4	7.1
3	65.4	9.9	5.8	0.4	8.0
4	77.2	9.1	6.8	0.3	10.3
Mean	64.4	10.4	5.7	0.4	7.7
Std. Dev.	10.2	1.2	0.9	0.0	2.1

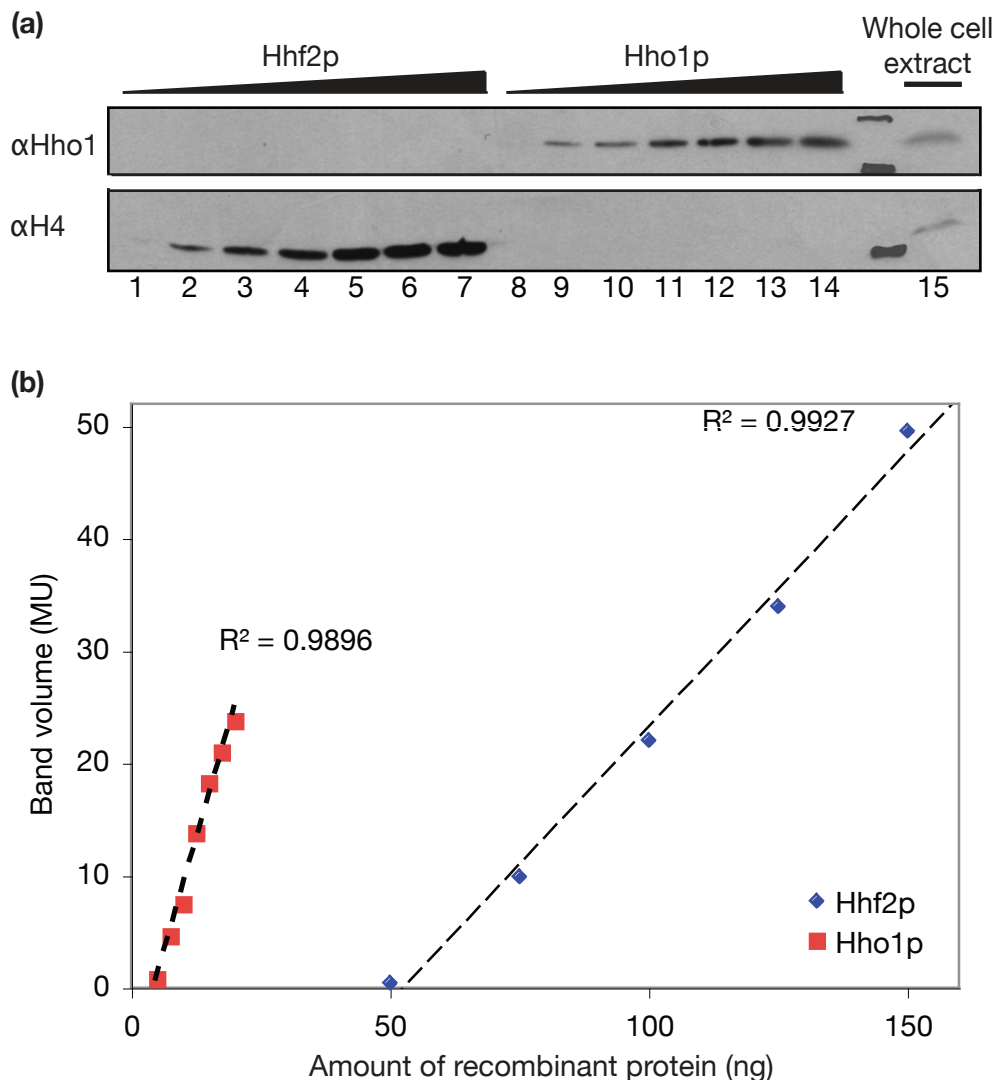


Figure 3.1 Determining the ratio of Hho1p to nucleosomes in yeast whole-cell extract through semi-quantitative Western blots. (a) Example of a blot probed with anti-H4 and then anti-Hho1 antibodies. Lanes 1-7 contain 50, 75, 100, 125, 150, 175, 200 ng recombinant Hhf2p respectively; lanes 6 and 7 were not used for the standard curve as densitometry indicated that the signal was saturated. Lanes 8-14 contain 5, 7.5, 10, 12.5, 15, 17.5, 20 ng recombinant Hho1p respectively. Lane 15 contains whole cell extract from 1 OD₆₀₀ *S. cerevisiae* W303. **(b)** Example of standard curves produced from densitometry of the Western blots in (a). R² values above 0.925 indicate the data are a good fit for the linear trend lines indicated.

3.3.2 Comparison of cross-linked products of chromatin containing Hho1p or canonical linker histones

Chemical cross-linking of linker histone-stripped chicken erythrocyte (CE) chromatin pre-incubated with equimolar amounts of chicken erythrocyte histone H1 or recombinant Hho1p produced similar patterns of products (Figure 3.2). Both chicken histone H1 and Hho1p cross-linked with chromatin produce a product of the size expected for a linker histone dimer, and Western blotting confirms that these products contain linker histone. The product of higher mobility than the putative dimer band is likely to contain Hho1p plus a core histone. Perchloric acid (PCA), which is widely used to extract linker histones, could not separate the cross-linked products containing just linker histones from those also containing core histones.

Yeast cells were treated to produce spheroplasts. The nuclei were extracted (Figure 3.3a; Section 3.2.5) and cross-linked with DMS. The cross-linking was followed by Western blotting, with anti-Hho1 antibody (Figure 3.3b). The products produced were of a similar size to those produced upon cross-linking of Hho1p bound to chicken erythrocyte chromatin. The dimer band is not as pronounced upon cross-linking nuclei, probably because Hho1p is present at less than 1 : 1 ratio to the nucleosomes in yeast nuclei whereas Hho1p was equimolar in the linker histone-depleted chicken erythrocyte chromatin bound with Hho1p. An anti-H3 blot indicates that none of the product bands around the size of the possible dimer band contain H3, and similar results were produced using an anti-H4 antibody (data not shown). However as antibodies were unavailable for core histones H2A and H2B, it is not known that the putative dimer band contains only Hho1p. It should also be noted that the cross-linking may destroy some of the epitopes recognised by the antibodies, therefore absence of signal does not necessarily mean absence of the antigen

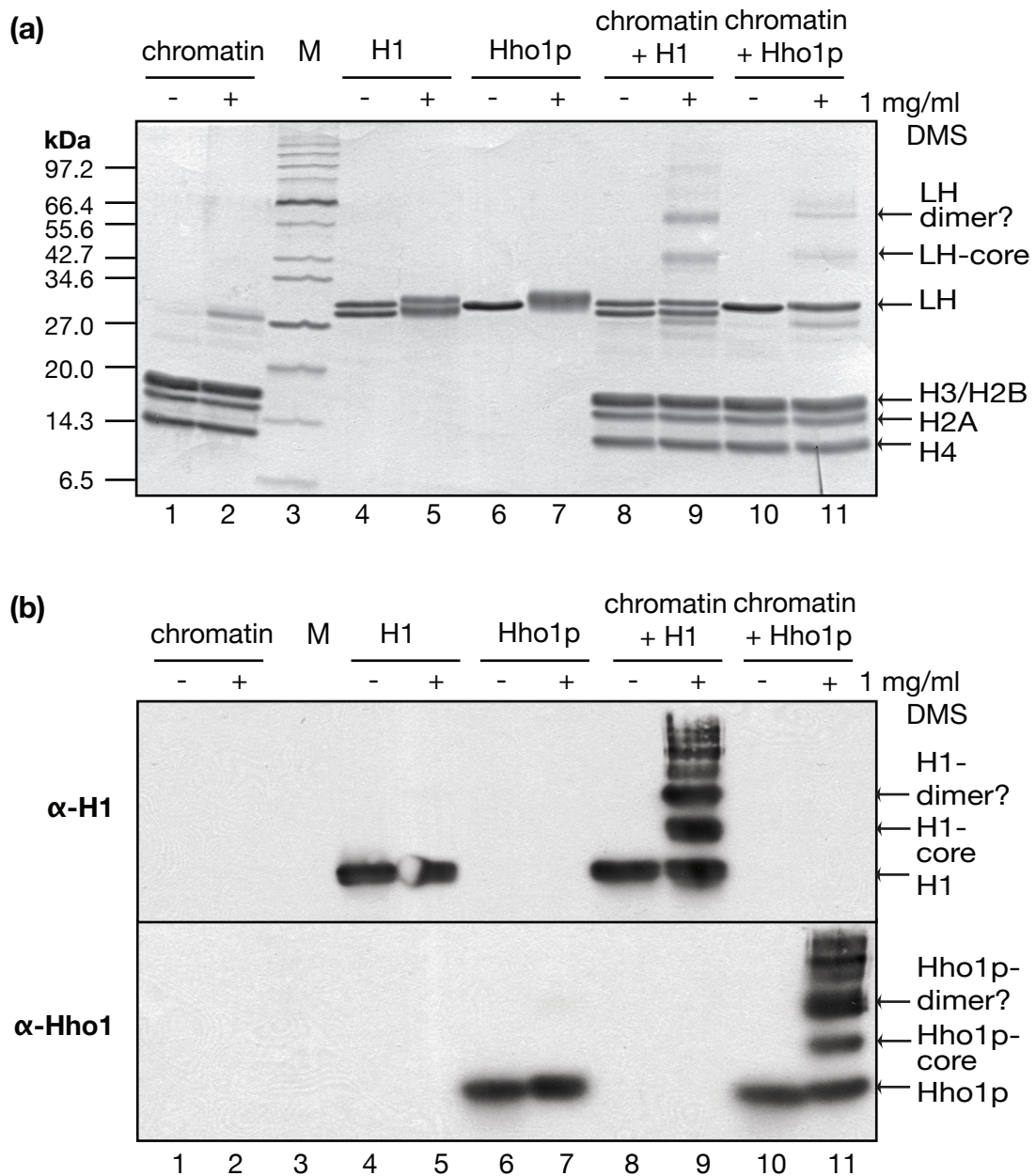


Figure 3.2 Cross-linking of linker histone-depleted chicken erythrocyte chromatin bound with linker histones. **(a)** SDS/18%-PAGE showing samples before (-) and after (+) treatment with 1 mg/ml DMS for 30 minutes. Similar sized products are formed for samples containing H1 (extracted from chicken erythrocytes) and recombinant Hho1p (lanes 9, 11) (LH: linker histone). Bands of the size expected for linker histone dimers are indicated with an arrow. Lane 3 contains protein molecular weight markers. **(b)** Western blots using anti-H1 and anti-Hho1. A similar pattern of linker histone-containing bands is produced for chromatin bound by H1 and Hho1p (lanes 9 and 11). Putative linker histone dimer bands are indicated for both samples.

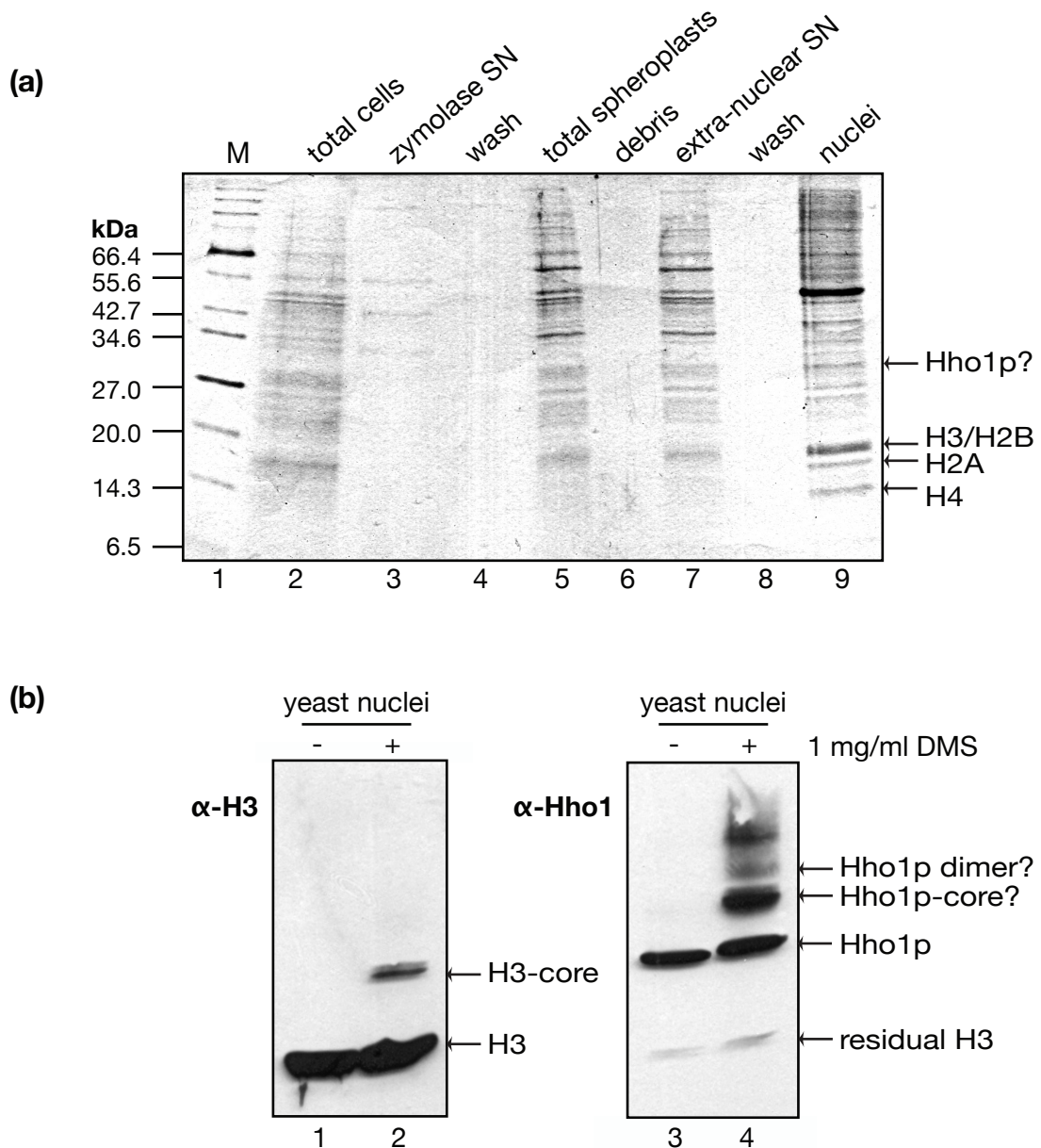


Figure 3.3 Cross-linking of *S. cerevisiae* nuclei shows a ladder of Hho1p-containing products. **(a)** SDS/18%-PAGE showing the preparation of yeast nuclei through spheroplasting and differential centrifugation. Bands corresponding to the expected sizes of core histones are enriched in the nuclear fraction (lane 9). Lane 1 contains protein molecular weight markers. **(b)** Western blots of yeast nuclei before (-) and after (+) treatment with 1 mg/ml DMS for 30 minutes. The yeast nuclei (lane 4) show a similar ladder of cross-linked products to Hho1p-bound to chicken erythrocyte chromatin (Figure 3.2b lanes 9, 11). A product that corresponds to the expected size of a Hho1p dimer is indicated. Some residual H3 signal is seen on the α -Hho1 blot (lanes 3, 4).

in the cross-linked products; however polyclonal antibodies were used to minimise this. Again, PCA extraction did not enrich for the Hho1p-only products (data not shown).

3.3.3 Hho1p-containing nucleosome arrays are structurally similar to those containing canonical linker histones

In order to study the compaction levels of chromatin containing various linker histone contents, reconstituted nucleosome arrays were used. The components used in these assays are shown in Figure 3.4. NGIL is a truncation mutant of Hho1p, which has the second globular domain removed. A stepwise decreasing salt-dialysis protocol was used to load octamer (isolated from chicken erythrocytes) on to the DNA arrays in the presence of mixed sequence competitor DNA (crDNA) (Figure 3.5). The DNA arrays contained 25 copies of the Widom “601” octamer positioning sequence with either 167 or 197 bp repeat lengths. 167 bp was used because it is similar repeat length to that measured for yeast chromatin (Thomas and Furber, 1976), while the longer linker DNA in the 197 bp repeats (essentially the “canonical” repeat length of about 200 bp) would emphasise any array compaction. Once the amount of octamer required to bind at equimolar ratio to the positioning sequences in the DNA arrays was determined these conditions were used for the further linker histone titrations.

Initially the reconstituted nucleosome arrays were run immediately in agarose gels (Figure 3.6), causing any compaction of the arrays to be lost. Therefore any gel shifts upon the addition of linker histone would be due to the change in mass of the array, allowing the binding of linker histone into the array to be determined. All of the linker histones caused the nucleosome arrays to be retarded in the gel, indicating binding of the linker histones. The arrays

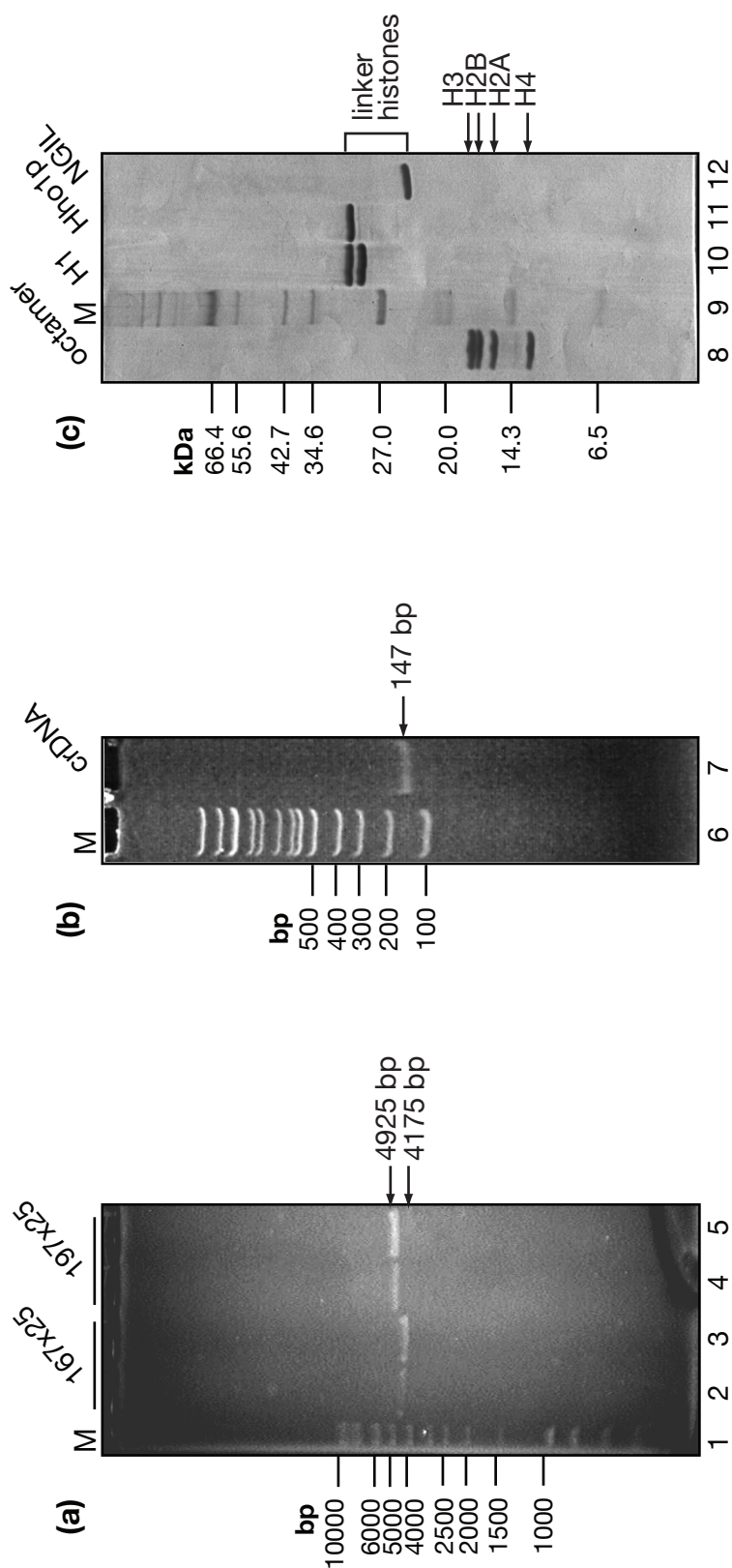


Figure 3.4 Nucleosome array reconstitution components. (a) 1% agarose gel containing 0.3x TBE, showing the two Widom “601” positioning sequence-derived DNA arrays used in the reconstitution assays. The repeat lengths are 167 bp (lanes 2, 3) and 197 bp (lanes 4, 5) and both arrays contain 25 repeats of this sequence. Lane 1 contains DNA size markers. (b) 7% acrylamide gel containing 0.3x TBE, showing the competitor DNA used in the reconstitution assays. The size of this band was more accurately determined on a longer gel by comparison with pBR322 DNA-MspI digest fragments (data not shown). Lane 6 contains DNA size markers. (c) SDS/20%-PAGE of proteins used in the reconstitution assays. Lane 9 contains protein molecular weight markers.

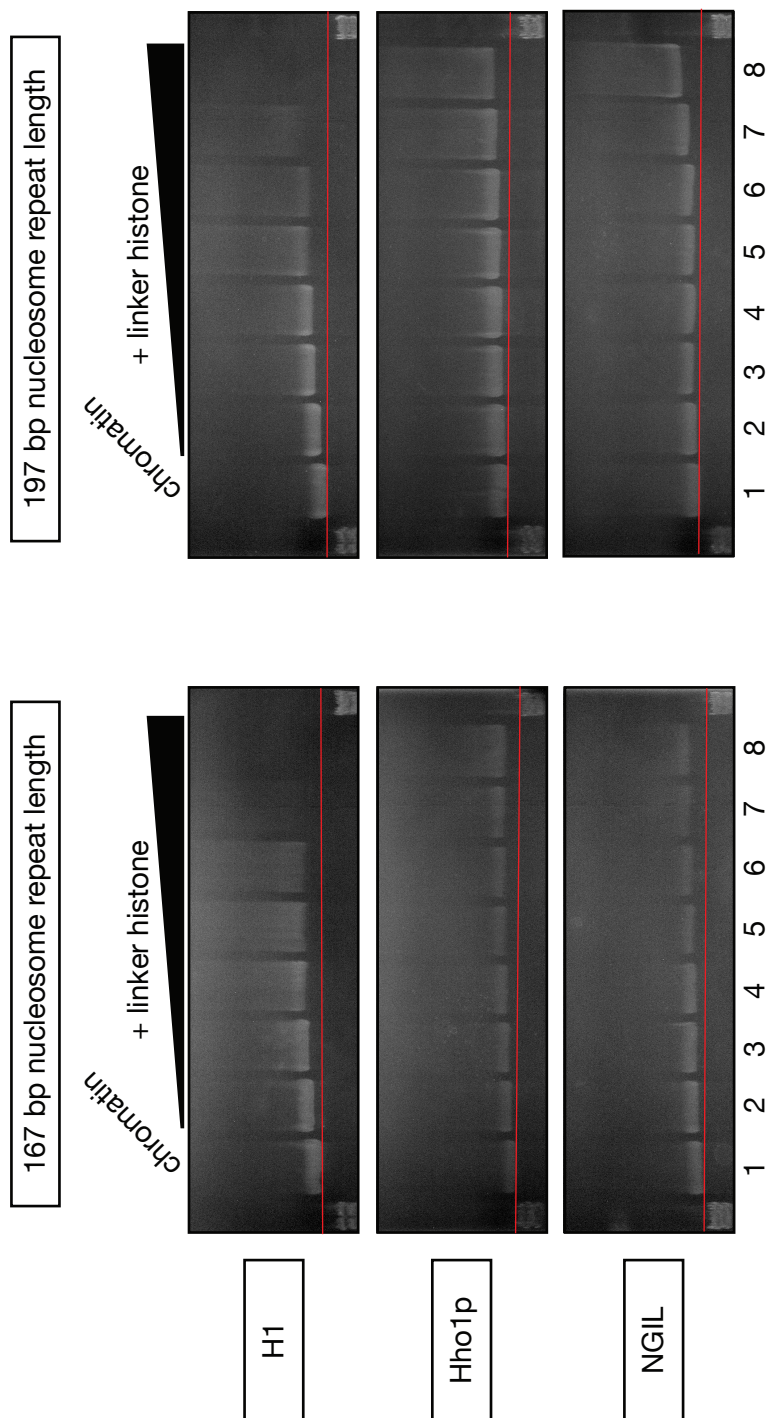


Figure 3.6 Titration of linker histones into nucleosome arrays. Nucleosome arrays with the DNA repeat length and the linker histone content indicated. The input molar ratio of linker histone to nucleosome are 0, 0.2, 0.4, 0.6, 0.8, 1, 1.5 and 2 for lanes 1-8 respectively. All reconstructions were carried out in the presence of 147 bp competitor DNA to control loading of octamer on to the arrays. All arrays were analysed in 0.9% agarose gels containing 0.3x TBE. A decrease in gel mobility is seen upon addition of linker histone (the lines indicate the position of equal mobility though the gel, using the molecular weight markers as a guide). Lanes 7 and 8 for the 167 bp arrays and lane 8 of the 197 bp arrays are empty due to precipitation of the chromatin.

containing chicken erythrocyte histone H1 precipitated at lower linker histone input ratios than those containing Hho1p or NGIL. H1-containing arrays are completely precipitated in lane 7 and 8 for 167 and 197 bp repeat lengths respectively, while neither of the Hho1p- or NGIL-containing arrays were precipitated in the same conditions, suggesting that H1 has a higher affinity for the nucleosome arrays. The 197 bp repeat nucleosome arrays were more soluble than the 167 bp repeat arrays.

By gently fixing the nucleosome arrays with glutaraldehyde before analysing them in the gels, the compaction state of the nucleosome arrays could be studied (Figure 3.7). The arrays were compacted by addition of linker histone, as indicated by their faster mobility in the gels with increased linker histone content, with the effect being much more obvious for the arrays with 197 bp repeat length. The arrays containing histone H1 were compacted more strongly than those containing Hho1p and NGIL, which barely shift. This is likely to be partially due to the higher affinity of histone H1 for the nucleosome arrays, meaning more H1 than Hho1p or NGIL would be bound within the chromatin for a given input ratio. However the Hho1p- and NGIL- containing nucleosome arrays were beginning to precipitate in lanes 7 and 8, indicating that no further compaction of these arrays would be expected upon addition of linker histone. There is no appreciable difference between the Hho1p- and NGIL-containing nucleosome arrays, suggesting the second globular domain of Hho1p is not required for compaction of the array.

Dialysing nucleosome arrays into buffers containing magnesium chloride causes the arrays to fold into the “30 nm fibre state” (Huynh et al., 2005). Following folding arrays were fixed to preserve their structure during electrophoresis (Figure 3.8). Compaction of the linker histone-free arrays (lanes 1) can be seen by comparing their sizes relative to the DNA markers in Figures

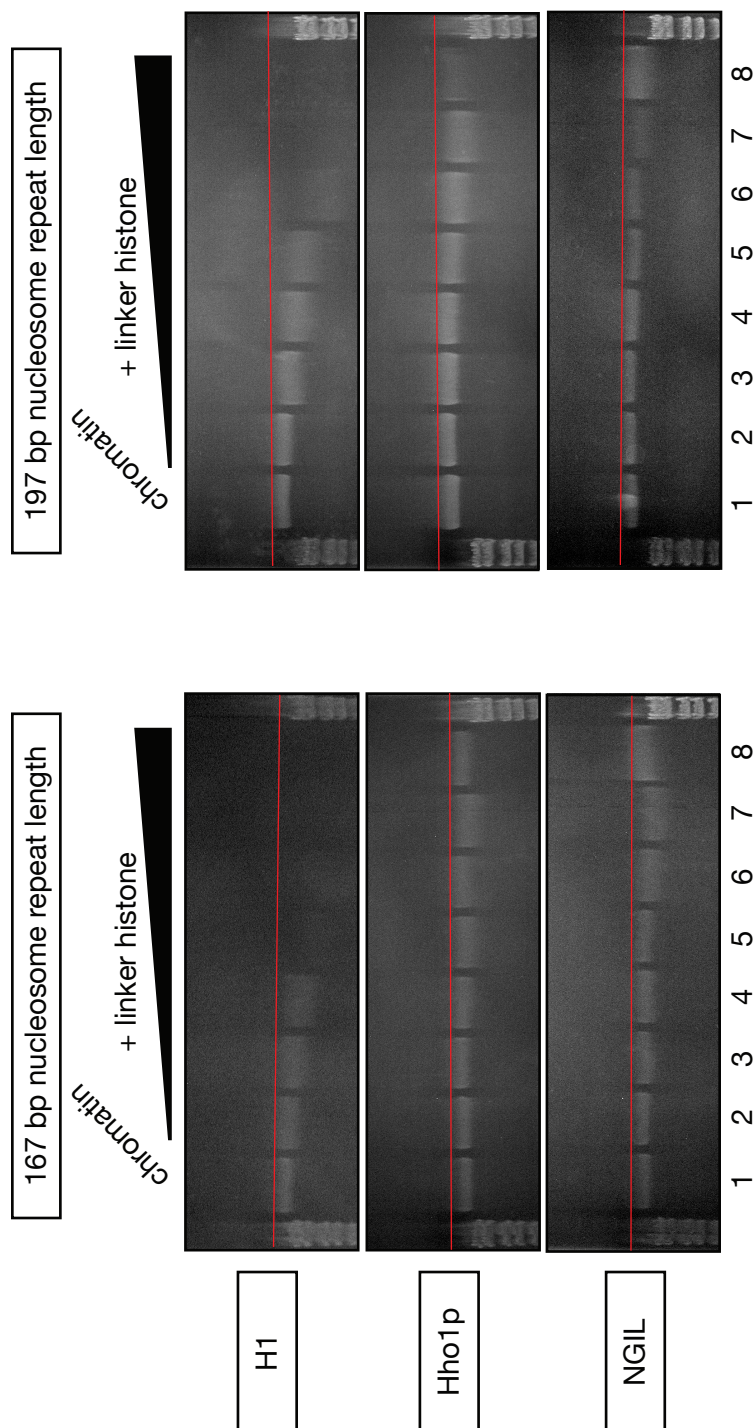


Figure 3.7 Compaction of nucleosome arrays upon addition of linker histone. Nucleosome arrays with the DNA repeat length and linker histone content indicated. The input molar ratio of linker histone to nucleosome are 0, 0.2, 0.4, 0.6, 0.8, 1, 1.5 and 2 for lanes 1-8 respectively. All reconstitutions were carried out in the presence of 147 bp competitor DNA to control loading of octamer on to the arrays. Arrays were fixed with 0.1% glutaraldehyde on ice for 10 minutes to preserve their compaction level as they migrated through the gel. All arrays were run in 0.9% agarose gels containing 0.3x TBE. The lines indicate the position of equal mobility through the gel, using the molecular weight markers as a guide. Arrays containing H1 are more highly compacted than those containing Hho1p or NGIL, for a given input ratio, as indicated by their faster mobility in the gels. H1-containing arrays also precipitate at lower input ratios than with Hho1p or NGIL.

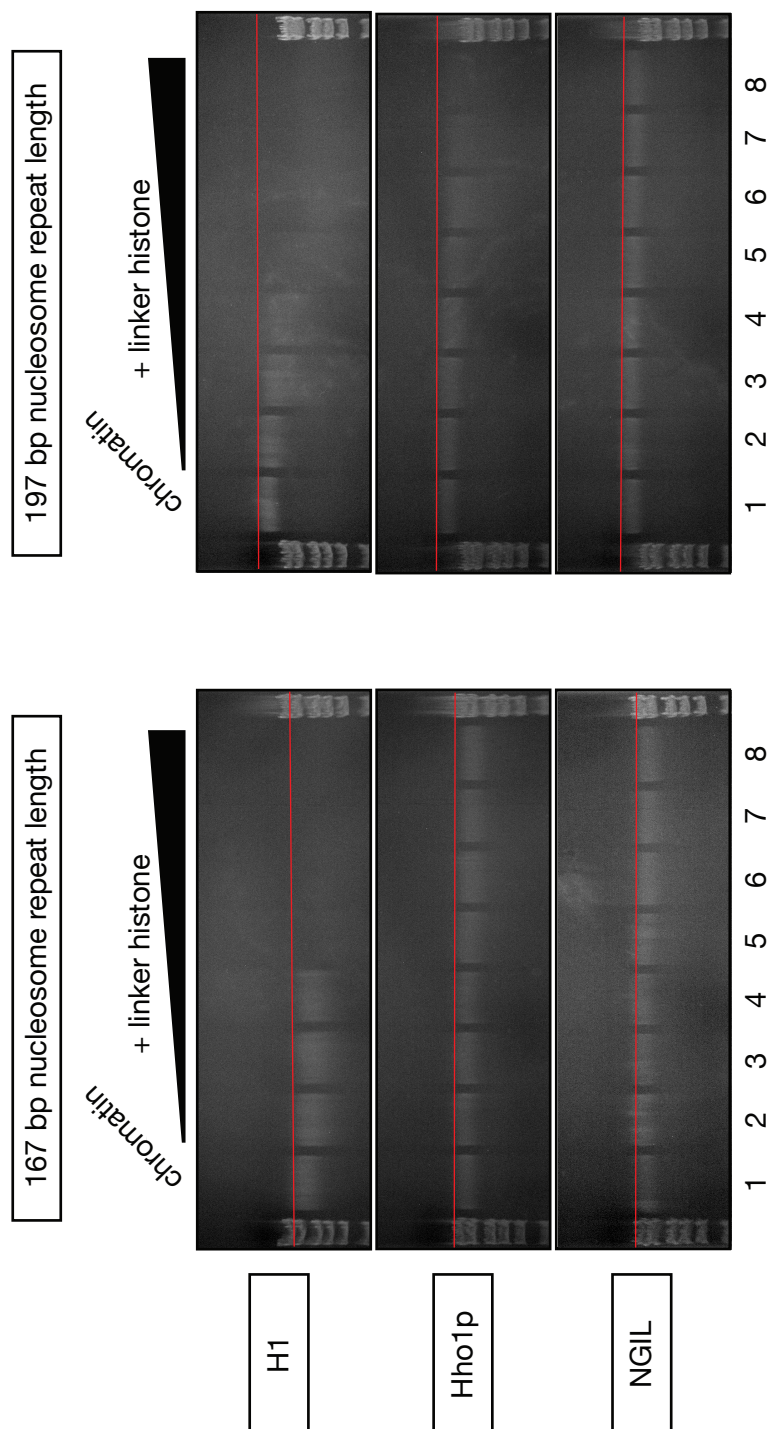


Figure 3.8 Folding of nucleosome arrays containing linker histone. Nucleosome arrays with the DNA repeat length and linker histone content indicated. The input molar ratio of linker histone to nucleosome are 0, 0.2, 0.4, 0.6, 0.8, 1, 1.5 and 2 for lanes 1-8 respectively. All reconstitutions were carried out in the presence of 147 bp competitor DNA to control loading of octamer on to the arrays. Reconstituted arrays were folded in buffer containing 1 mM MgCl₂. Arrays were fixed with 0.1% glutaraldehyde on ice for 10 minutes to preserve their structure as they migrated through the gel. All arrays were run in 0.9% agarose gels containing 0.3x TBE. The lines indicate the position of equal mobility through the gel, using the molecular weight markers as a guide. There is no significant change in the mobility of folded arrays containing Hho1p or NGIL, although addition of H1 cause a slight increase in gel mobility.

3.7 and 3.8. Addition of linker histones in the folded arrays had little effect on the nucleosome array gel-mobility. Only addition of histone H1 to nucleosome arrays with 197 bp repeat length caused noticeable compaction of the folded arrays. This suggests that Hho1p has no appreciable effect on the gross structure of the “30 nm fibre” formed in buffers containing magnesium chloride.

As it was not possible to clearly show differences between the folded nucleosome arrays reconstituted with the different linker histones by electrophoretic mobility shift assays, analytical ultracentrifugation was used to compare the arrays quantitatively, in collaboration with Dr Andrew Routh (MRC Laboratory of Molecular Biology, Cambridge). The 167 bp repeat length DNA arrays were used as this is the nucleosome repeat length of yeast (Thomas and Furber, 1976). Histone H5 was used, rather than chicken erythrocyte histone H1, to allow comparison with earlier data produced by Dr A. Routh (personal communication). Figure 3.9a shows an example of the raw data that is produced as the boundary of the chromatin samples moves along the cell during centrifugation. In most cases the transformed data indicated that there were two species in the chromatin samples: a larger, well-defined species and a more varied species, which is likely due to fragmentation and aggregation of the arrays (Figure 3.9b). The sedimentation coefficients of the more defined species for each array were plotted against the input ratio of linker histone, and distinct trend lines for each linker histone were identified by fitting the data to a linear function. However the large variation in the data suggests that the differences may not be significant (Figure 3.9c). This lack of a significant difference between the compaction of the folded nucleosome arrays containing the various linker histones is consistent with the results observed in the gel-mobility-shift assay (Figure 3.8).

To probe the structure of the nucleosome arrays digestion with *Ava I*

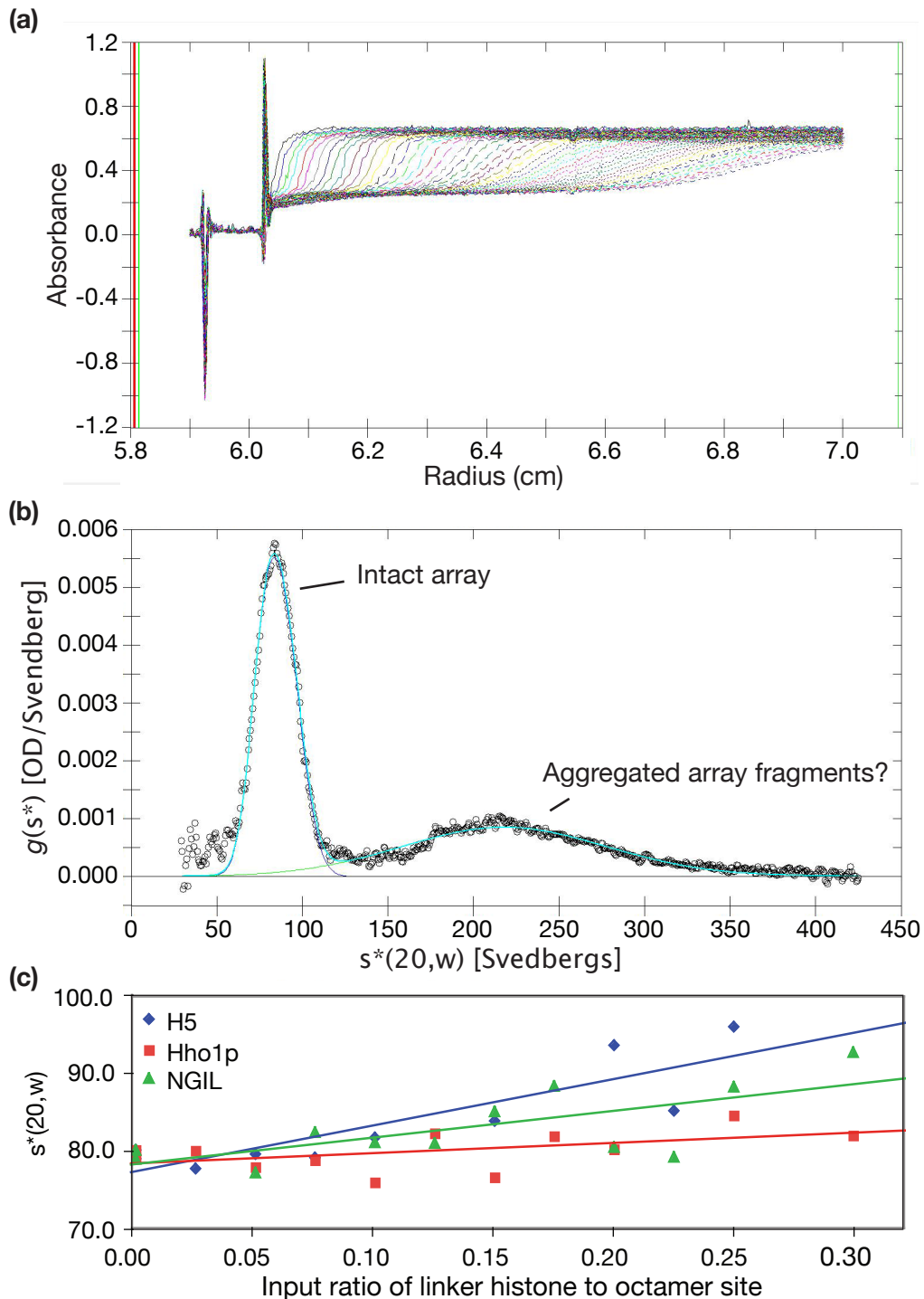


Figure 3.9 Analysis of folded nucleosome arrays by analytical ultracentrifugation. (a) Example of the raw data produced during analytical ultracentrifugation showing the boundary of the nucleosome arrays moving from left to right during consecutive scans. (b) Example of the transformed data showing two species. One species is tightly defined with an $s^*(20,w)$ of about 85. The other species shows a broader distribution of smaller species that appear to be aggregating. (c) Sedimentation coefficients of folded 167 bp repeat 25-mer nucleosome arrays containing linker histones as indicated. The individual data points are plotted. H5 from chicken erythrocyte nuclei was used as a positive control to allow comparison with data from Dr A. Routh (personal communication).

restriction endonuclease was used as there is a recognition site between each repeat of the positioning sequence in the DNA array (see Figure 3.5). Nucleosome arrays containing chicken erythrocyte histone H1 or H5 precipitated in the buffer conditions required for *Ava I* activity. This is likely due to the 2 mM MgCl₂ in the buffer, which has been previously shown to cause precipitation of reconstituted nucleosome arrays containing histone H5 (Huynh et al., 2005). Therefore digestion of the arrays containing an input ratio of one molecule per nucleosome of Hho1p or NGIL was compared to that with no linker histone, or just the DNA array alone.

Figure 3.10 shows time courses for *Ava I* digestion of these arrays. The DNA array produced a ladder of products as the array was digested, while the nucleosome arrays produced less distinct intermediate products, probably because the nucleosomes reduce the accessibility of *Ava I* to the recognition sites. A band corresponding to 167 bp DNA (an individual repeat of the array) increases upon *Ava I* digestion for all arrays. This indicates that *Ava I* is able to displace both linker histone and octamer from the DNA array in these conditions. Chromatin containing Hho1p may protect the intact array from *Ava I* digestion for longer than chromatin containing either NGIL or no linker histone (the intact arrays persist for at 120, 40 and 40 minutes respectively).

To look for evidence of bridging by Hho1p the nucleosome arrays used above were digested to completion using *Ava I* (Figure 3.11a). If Hho1p were bridging between two nucleosomes it may cause dinucleosomes to be protected from *Ava I* digestion. The size of products for the Hho1p-containing, NGIL-containing and no linker histone arrays are equivalent, giving no indication of bridging two nucleosomes by Hho1p. Fixing the arrays gently with 0.1% glutaraldehyde on ice before digestion for various times (samples fixed for 10 min are shown in Figure 3.11b) caused larger products to remain after *Ava I*

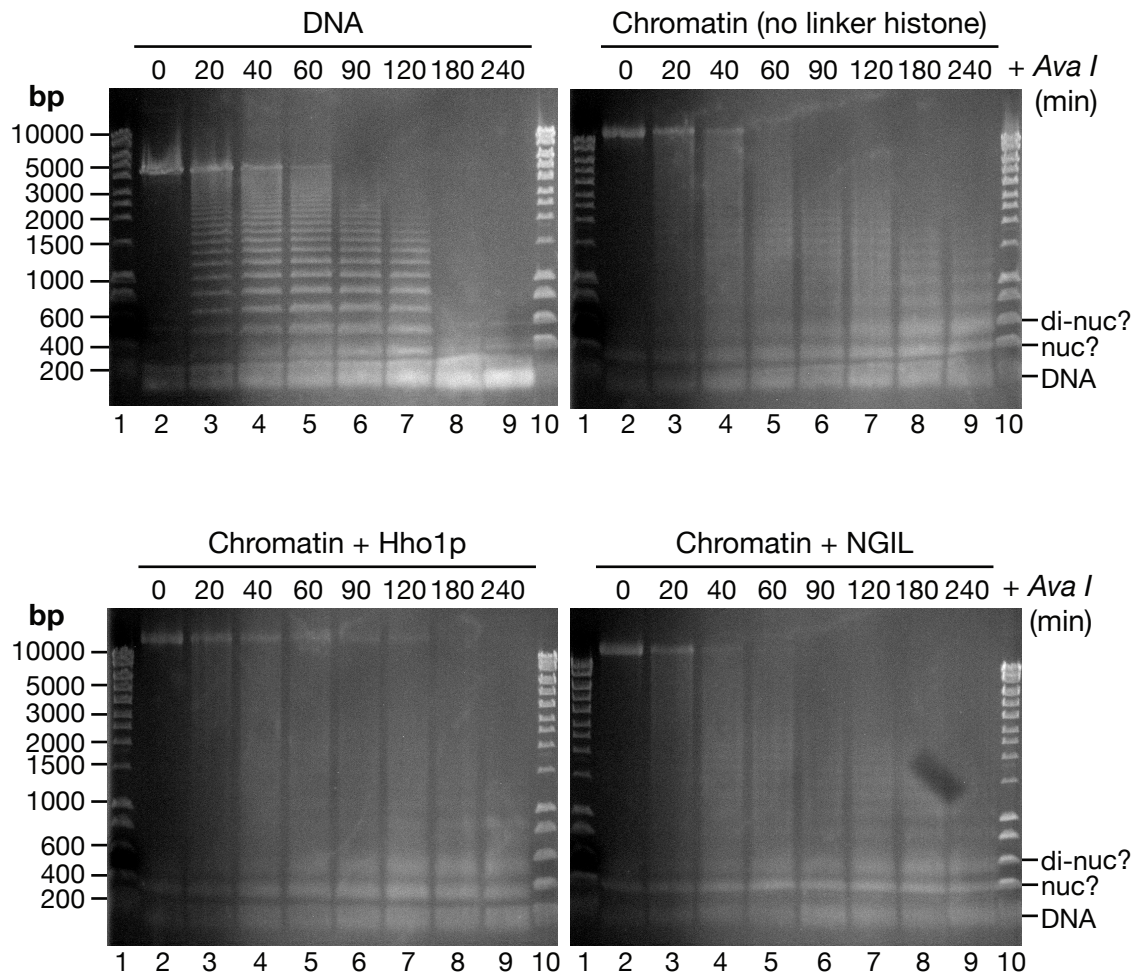


Figure 3.10 Hho1p may protect nucleosome arrays from digestion by *Ava I*.

Time courses are used to compare the relative protection of the *Ava I* sites in the indicated nucleosome and DNA arrays (167 bp repeat length, 25-mer arrays) during partial *Ava I* digestion. Linker histones are present at an equimolar input ratio to nucleosome core. Samples are run in 0.9% agarose gels containing 0.3x TBE. Lanes 1 and 10 contain DNA size markers. The intact Hho1p-containing arrays persists longer upon *Ava I* digestion (lane 7) than chromatin without linker histone or containing NGIL (lanes 4).

digestion, presumably due to histone tails being cross-linked to DNA and other nucleosomes, but there were no obvious differences in the products from the different arrays.

3.4 Discussion

3.4.1 Hho1p is present at about 1 molecule per 5–10 nucleosomes and may form dimers upon cross-linking of yeast chromatin

To understand the roles of Hho1p within yeast chromatin it is important to know its abundance. Previous measurements have made use of yeast strains with tagged proteins in the genome or have estimated the number of nucleosomes in a yeast cell, producing ratios that vary from one in four nucleosomes (Downs et al., 2003) to one in 37 nucleosomes (Freidkin and Katcoff, 2001). Using semi-quantitative Western blotting, a ratio of about one Hho1p per every 5–10 nucleosomes was obtained and the quality of data suggest that Hho1p may be present at the more abundant end of that range (Figure 3.1; Table 3.3). This estimate is compatible with the genome-wide association of Hho1p seen by Schäfer and colleagues (2008), in which a ChIP-chip assay showed that all of the yeast open reading frames (about 6400) were bound by Hho1p.

Hho1p, like histone H1, may form dimers upon cross-linking both *in vitro*, when bound to chicken erythrocyte chromatin, and within yeast nuclei. The intensity of the putative Hho1p dimer band produced was lower for cross-linking in yeast nuclei compared to that in chicken erythrocyte chromatin containing one molecule of Hho1p per nucleosome (Figures 3.2 and 3.3). This is consistent with the ratio of Hho1p to nucleosome being lower than one to one,

as determined in Section 3.3.1.

3.4.2 Hho1p increases the compaction of reconstituted nucleosome arrays; the second globular domain does not seem to be required

Studying the role of Hho1p in chromatin structure was challenging, as comparison with canonical linker histones was complicated by differences in their affinity for the nucleosome arrays (Figure 3.6). The affinities of Hho1p and NGIL for the nucleosome arrays were not appreciably different in this assay. This is slightly surprising due to previous observations of binding to DNA-cellulose, which showed 50% elution of protein at about 430 mM, 400 mM and 280 mM NaCl (for H1, Hho1p and NGIL respectively) (Ali and Thomas, 2004). Hho1p increases the compaction of nucleosome arrays slightly, but so does NGIL, indicating the second globular domain is not required (Figure 3.7). However, chicken erythrocyte histone H1 compact the reconstituted nucleosome arrays more strongly than both the Hho1p proteins. When Hho1p or NGIL were included in the folded nucleosome arrays there was no obvious increase in the compaction, while inclusion of chicken erythrocyte histone H1 only caused visible compaction in the nucleosome arrays with 197 bp repeat length (Figure 3.8). To determine if these observations were due to the low resolution of gel-shift-mobility assays, the folded nucleosome arrays with 167 bp repeat lengths were also compared using analytical centrifugation. The nucleosome arrays were prone to fragmentation, and the sedimentation coefficients measured did not form a tight trend with the linker histone input ratio. Therefore, it would be advisable to repeat these analytical ultracentrifugation experiments using longer nucleosome arrays, which appear to be more stable (Dr A. Routh,

personal communication) and have been shown to compact significantly upon inclusion of histone H5 (Routh et al., 2008).

Probing the structure of the reconstituted nucleosome arrays with *Ava I* restriction endonuclease allowed the Hho1p- and NGIL-containing arrays to be distinguished, as arrays containing Hho1p may be more resistant to *Ava I* digestion (Figure 3.10). The GII domain may cause occlusion of the *Ava I* site either by binding at the site itself (in the linker DNA) or binding an adjacent nucleosome to the GI domain. It is unlikely that the GII domain would bind the linker DNA because the isolated GII domain binds a nucleosome dyad and provides chromosome protection (Sanderson et al., 2005). No evidence of nucleosome bridging by Hho1p was detected by digesting with *Ava I* to completion (Figure 3.11). However this may be because the *Ava I* was able to displace the linker histone and octamer, releasing 167 bp length DNA of an individual repeat of the nucleosome positioning sequence plus linker DNA. One alternative explanation for the difference in *Ava I* partial digestion of Hho1p- and NGIL-containing nucleosome arrays could be that the full-length protein, with two globular domains, has a greater affinity for the chromatin than NGIL. This may be expected because each molecule of Hho1p has two DNA binding domains, however the binding of Hho1p and NGIL to chromatin appeared to be similar in the gel-mobility-shift assays (Figure 3.6). Therefore, nucleosome bridging by Hho1p is the most likely of these explanations and further efforts should be made to look for its occurrence.

3.5 Summary

- Hho1p is present at around one molecule per 5 to 10 nucleosomes. This is within the range of values previously published and is consistent with a relatively low cellular level (relative to core histones) but presence on every open reading frame in the yeast genome.
- The pattern of products produced by cross-linking Hho1p- and H1-containing chromatin is similar. Similar sized Hho1p-containing products are also produced by cross-linking yeast nuclei, but with a lower level of the putative linker histone dimer, consistent with substoichiometric amounts of Hho1p in yeast chromatin.
- Hho1p binds reconstituted nucleosome arrays with lower affinity than canonical linker histones. Despite this making comparison of the nucleosome arrays more difficult, Hho1p appears to cause less compaction of the arrays before they start precipitating, than histone H1.
- The second globular domain of Hho1p does not appear to be required for compaction of nucleosome arrays but may increase the resistance of an intact 25-mer nucleosome array to *Ava I* digestion. This tentatively suggests Hho1p may bridge between nucleosomes, protecting the linker DNA.

Chapter 4

Hho1p interactions with chromatin proteins

4 Hho1p interactions with chromatin proteins

4.1 Introduction

Reported Hho1p interactions come mainly from high-throughput studies that have looked for either genetic interactions (Collins et al., 2007; Wilmes et al., 2008) or physical interactions (Krogan et al., 2006; Tarassov et al., 2008). However these interactions do not necessarily occur directly between Hho1p and the other protein component. For example, an interaction between Hho1p and Srm1p (also called Prp20p) was identified by immunoprecipitation of yeast whole-cell extract using a Srm1-protein A bait complex (Dilworth et al., 2005). A number of chromatin-associated proteins were immunoprecipitated, including all four core histones. This suggests an entire chromosome could have been immunoprecipitated and that the interaction between Hho1p and Srm1p may not be direct. There is currently no published report of a direct interaction between Hho1p and a non-histone protein *in vitro*, however the literature does provide some suggestions for candidate Hho1p-interacting partners. Metazoan linker histones have been shown to interact with high mobility group (HMG) box proteins (Shooter et al., 1974; Carballo et al., 1983) and a homologue of the *S. cerevisiae* protein Sir2p (SirT1) (Vaquero et al., 2004), while Hho1p is known to share functions with Sir2p and Htz1p suggesting they may co-localise and/or functionally interact to bring about these shared functions (detailed below).

The domain structures of these proteins are shown in Figure 4.1.

There are several yeast proteins that contain HMG box domains. Rox1p binds with sequence-specificity (Balasubramanian et al., 1993), while Abf2p is mitochondrial (Diffley and Stillman, 1991), and Nhp10p (also called Hmo2) has been identified as part of the INO80 chromatin remodelling complex (Morrison et al., 2004), which is directly involved in DNA repair. Spp41p and Ixr1p are large proteins with only a small proportion containing similarity to an HMG box domain. Therefore none of the proteins discussed so far are considered to be HMGB1 homologues. Hmo1p and Nhp6ap are potential HMGB1 homologues, however, and were investigated in this Chapter.

Hmo1p contains a region with homology to the B box of HMGB1 and a region that has been suggested to be A-box-like (Lu et al., 1996). It contains a weakly acidic region C-terminal to the B box, flanked by a further basic tail. Hmo1p is found at rDNA loci and appears to alter the accessibility of individual rDNA genes to RNA polymerase I transcription (Gadal et al., 2002). As Hho1p is also known to be present and have functions at rDNA loci (Levy et al., 2008) there may be a direct interaction with Hmo1p. However a more recent paper has shown that Hmo1 is associated with the actively transcribed rDNA regions, which are largely devoid of nucleosomes (Merz et al., 2008). As Hho1p is known to bind the nucleosome dyad it suggests Hmo1p and Hho1p could occur within different parts of the rDNA, without directly interacting.

Nhp6ap contains just one HMG box, but is the most abundant HMG-box protein in yeast (Kolodrubetz and Burgum, 1990). It contains an HMG B-like domain and is highly homologous to, and functionally redundant with, Nhp6bp. Collectively they are called Nhp6p. Nhp6p binds to DNA without sequence-specificity and causes sharp bending of the DNA (Paull and Johnson, 1995). It binds nucleosomes *in vitro* and has roles in recruitment of chromatin

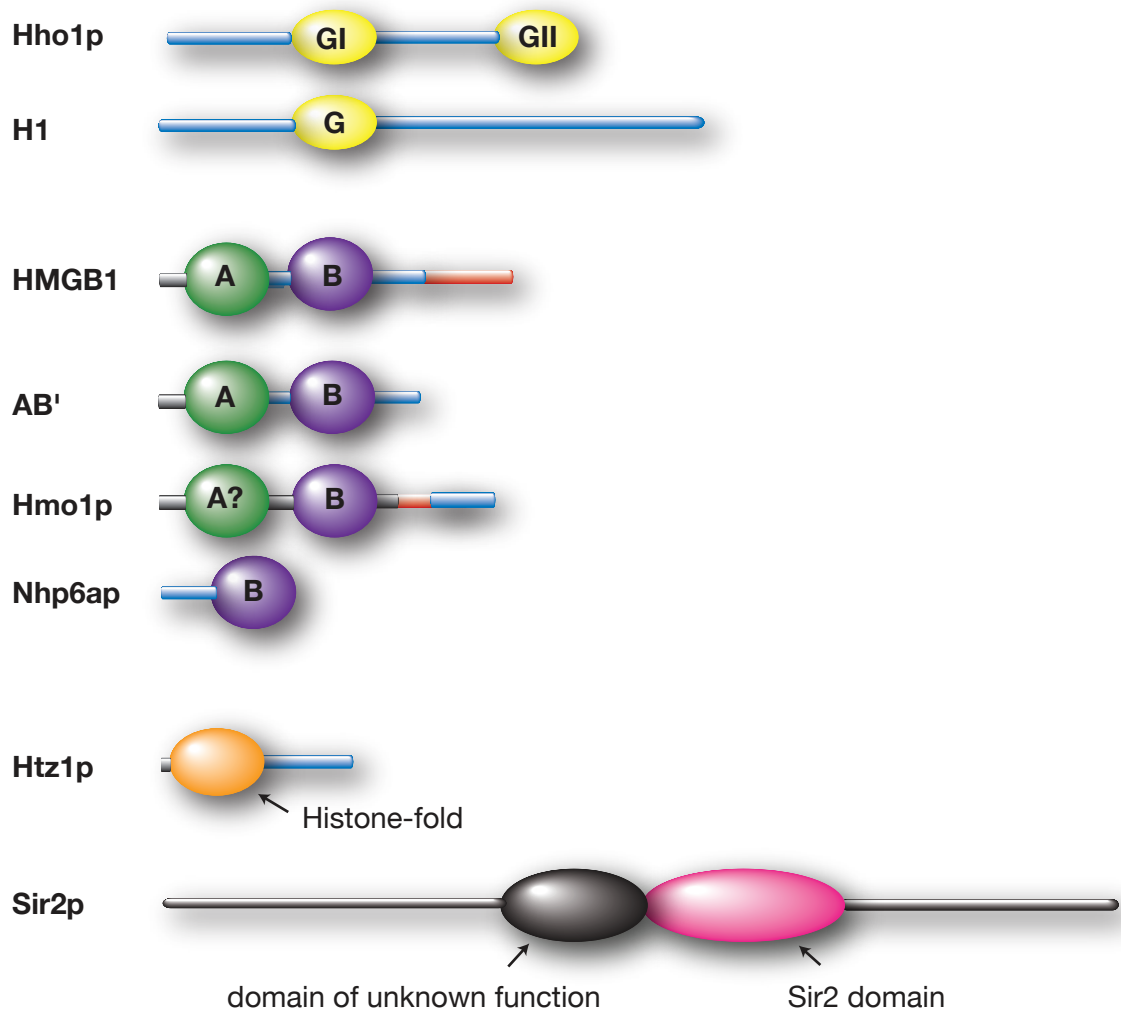


Figure 4.1 Cartoons indicating the domain structure of proteins used in this Chapter. Domains sharing structural and/or functional homology are the same colour. Basic linkers and tails are light blue, acidic linkers and tails are red.

remodelling complexes (Formosa et al., 2001; Szerlong et al., 2003). Nhp6ap is thought to be the homologue of metazoan HMGB1, which interacts with histone H1 through its acidic C-terminal tail (Cato et al., 2008). Nhp6ap, however, does not contain this acidic region suggesting that any interaction with Hho1p would occur in a different manner. An interaction between Hho1p and Nhp6ap was reported in a split-ubiquitin screen (Xue and Lehming, 2008). This study also saw an interaction between Hho1p and Nhp6bp, which did not occur in pull-down assays. The interaction between Hho1p and Nhp6ap has not been verified *in vitro*, therefore further investigation is required.

Sir2p is an NAD-dependent histone deacetylase that is involved in silencing transcription at rDNA loci, silent mating type loci and telomeres (Imai et al., 2000). It is also involved in regulation of recombination and lifespan of the yeast (Gottlieb and Esposito, 1989; Kaeberlein et al., 1999). Hho1p is also enriched on rDNA (Freidkin and Katcoff, 2001) and has roles in silencing and recombination, suggesting that Hho1p and Sir2p may function in similar pathways. When the SIR2 gene is deleted, Hho1p association at rDNA loci is reduced (Li et al., 2008), suggesting Sir2p has a role in Hho1p localisation. Sir2p acts as part of the RENT complex in its roles at rDNA loci (Huang and Moazed, 2003). Another component of the RENT complex, Fob1p, interacts with Hho1p as shown through affinity-capture mass spectrometry using a Fob1-TAP tagged strain (Huang et al., 2006). The *C. elegans* homologues function together to propagate a specialised subtelomeric chromatin state but were not seen to directly interact (Wirth et al., 2009). The human homologues of Hho1p and Sir2p, histone H1 and SirT1, interact through the N-terminus of SirT1 (Vaquero et al., 2004). Thus, Sir2p is a strong candidate to have a direct interaction with Hho1p.

Htz1p is an *S. cerevisiae* histone H2A subtype and a homologue of histone H2A.Z. It has roles in nucleosome positioning and preventing the spread

of silenced chromatin (Guillemette et al., 2005; Meneghini et al., 2003). Hho1p also has roles in barrier elements, and this is partially dependent on the presence of Htz1p (Veron et al., 2006). Interactions between Hho1p and Htz1p have been detected in a protein-fragment complementation assay and by affinity-capture mass spectrometry; however it is unknown if the interaction is direct (Tarassov et al., 2008; Lambert et al., 2009). Further investigation is required to determine if this interaction is direct and occurs *in vitro*.

In the work described in this Chapter, interactions of Hho1p with chromatin proteins are sought. Chemical cross-linking and gel filtration are used to look for interactions between Hho1p and Hmo1p, Nhp6ap or Sir2p *in vitro*. The interaction between Hho1p and Htz1p, is studied using co-immunoprecipitation and chemical cross-linking assays. qPCR studies look for co-localisation of Hho1p and Htz1p at positions across the ADH2 and PHO5 genes. Unfortunately, only the interaction between Hho1p and Sir2p was observed, and investigation of this interaction was hampered by difficulties in sample preparation.

4.2 Materials and methods

4.2.1 Plasmids

Plasmid pET11a-NHP6A contains the cDNA of the full-length *S. cerevisiae* NHP6A gene and was kindly provided by Prof Reid Johnson (University of California, Los Angeles) (Paull and Johnson, 1995).

Plasmid pGex4T-HTZ1 contains the cDNA of the *S. cerevisiae* HTZ1 gene with an N-terminal glutathione-S-transferase (GST) tag. The GST-fusion protein is thrombin cleavable, leaving five amino acids at the N-terminus of the

Htz1p. Plasmid pGex4T-HTZ1 was a gift from Dr Mark Churcher (MRC Laboratory of Molecular Biology, Cambridge).

Plasmid pGex4T-1-SIR2 (pDM111a) contains the cDNA of the *S. cerevisiae* SIR2 gene with an N-terminal GST tag. Cleavage with thrombin leaves five amino acids at the N-terminus of Sir2p. Plasmid pGex4T-1-SIR2 was a gift from Prof Danesh Moazed (Harvard Medical School, Boston) Tanny et al. (1999).

4.2.2 Proteins

4.2.2.1 HMGB1

Purified recombinant rat HMGB1 was provided by Miss Laura Cato (Department of Biochemistry, University of Cambridge).

4.2.2.2 Hmo1p

Purified recombinant Hmo1p was provided by Miss Varsha Jagadeshm (Department of Biochemistry, University of Cambridge).

4.2.2.3 Expression and purification of Nhp6ap

Nhp6ap was expressed using the same conditions as GII (Section 2.2.3.3). *E. coli* cell extract was produced using the protocol described for Hho1p (Section 2.2.3.2). Contaminating proteins were precipitated by slowly adding ammonium sulphate to a final concentration of 2.5 M while stirring on ice. The resulting suspension was clarified by centrifugation at 6000 g for 20 min at 4 °C. The supernatant was loaded onto a HiTrap Phenyl Sepharose HP hydrophobic-interaction column, which had been pre-equilibrated with buffer C (Section 2.2.3.2). Bound proteins were eluted with a 12-column-volume linear gradi-

ent from buffer C to buffer A and fractions containing Nhp6ap, as assessed by absorbance at 280 nm and SDS/18%-PAGE (Section 2.2.4.1), were collected.

The fractions were dialysed overnight against buffer A at 4 °C and loaded on to a Resource S cation-exchange column, which had been pre-equilibrated in buffer A. Bound proteins were eluted with a 50-column-volume linear gradient from buffer A to buffer B (Section 2.2.3.2). The fractions containing pure Nhp6ap were pooled and dialysed as above. The purified Nhp6ap sample was concentrated at 4 °C using a 3 kDa cut-off Vivaspin 2 concentrator and flash frozen in aliquots for storage at -80 °C.

4.2.2.4 Expression and purification of Htz1p

E.coli BL21(DE3) cells (Section 2.2.1.2) were transformed with pGex4T-HTZ1 and grown at 37 °C with shaking at 260 rpm in LB medium (Section 2.2.1.1) supplemented with 50 µg/ml carbenicillin. When the OD₆₀₀ reached about 0.6, expression of GST-Htz1 was induced with 0.5 mM IPTG and cultures were grown for a further 3 h. Cells were harvested by centrifugation at 5000 g for 10 min at 4 °C. Cells are washed in 10 mM sodium phosphate pH 8.0, 140 mM NaCl and the pellets were stored at -20 °C.

Cells were thawed and resuspended in 10 mM sodium phosphate pH 8.0, 1 M NaCl, 1 mM DTT, 0.5 mM PMSE, 1 µg/ml leupeptin, 1 µg/ml aprotinin, 0.156 mg/ml benzamidine, 1 µg/ml pepstatin, lysed by passage through a French press twice at 1000 psi, and cell debris was then removed by centrifugation at 35000 g for 30 min at 4 °C. The cell extract was filtered through a 0.2 µm membrane (Millipore) and bound to Glutathione Sepharose 4B media (GE Healthcare), pre-equilibrated in GST wash buffer (10 mM sodium phosphate pH 8.0, 140 mM NaCl), for 1 h at 25 °C. The GT-beads with bound proteins were washed thoroughly with GST wash buffer, thrombin (50 U) was added and

the sample was incubated overnight at 4 °C.

The cleaved Htz1p remained bound to the Sepharose beads, and needed guanidine hydrochloride for elution. The GST and other contaminants were removed from the beads by incubating in urea buffer (8 M urea, 20 mM sodium phosphate pH 8.0, 1 mM DTT) for 15 min, at 25 °C, followed by two further washes of the beads with urea buffer. Htz1p was then eluted from the beads by incubating for 1 h at 25 °C with 6 M Gu-HCl, 20 mM Tris-HCl pH 7.5, 10 mM DTT. The beads were washed with guanidine hydrochloride buffer and the eluted fractions were dialysed first against 10 mM Tris-HCl pH 7.5, 1 M Gu-HCl, 5 mM 2-mercaptoethanol and 0.2 mM PMSF and then again against 5 mM 2-mercaptoethanol and 0.2 mM PMSF. Htz1p was concentrated in a CentriplusRC concentrator (Millipore) with a 3 kDa cut-off, which contains a cellulose-based membrane as Htz1p binds to polyethersulfone membrane.

4.2.2.5 Expression and purification of Sir2p

E. coli BL21(DE3) cells (Section 2.2.1.2) containing pGex4T-1-SIR2 were grown in LB medium (Section 2.2.1.1), supplemented with 50 µg/ml carbenicillin, at 37 °C and 250 rpm until the OD₆₀₀ reached about 0.6. Following induction with 1 mM IPTG the temperature was reduced to 16 °C and the cultures were grown overnight. Cells were harvested by centrifugation at 5000 g for 10 min at 4 °C and washed with ice-cold binding buffer (10 mM sodium phosphate pH 8.0, 350 mM NaCl). The pellets were stored at -20 °C.

E. coli cell extract was produced using the protocol described for Hho1p (Section 2.2.3.2) except that the buffer used was at pH 8.0. GST-Sir2 was bound to GT-beads, which had been pre-equilibrated in binding buffer, for 1 h at 25 °C and washed three times with binding buffer. Thrombin digestion, using 50 U enzyme, was carried out overnight on the bead-bound sample at 4 °C. The

cleaved Sir2p was released into the supernatant, and the beads were washed in binding buffer. The supernatant and washes were concentrated at 4 °C in a Vivaspin 2 concentrator with a 10 kDa cut-off. Aliquots were flash frozen and stored at –80 °C.

4.2.3 Chemical cross-linking

Chemical cross-linking was carried out as described in Section 3.2.8. For cross-linking with 1-ethyl-3-[3-dimethylaminopropyl]carbodiimide (EDC: Pierce) the samples were prepared in 10 mM sodium phosphate buffer at pH 7.0. A 3x stock solution of EDC was prepared in 10 mM sodium phosphate pH 7.0.

4.2.4 Western blotting

Western blots were carried out as described in Section 3.2.7.

4.2.4.1 Antibodies

Anti-Hho1 and donkey anti-rabbit IgG HRP-conjugated antibodies are described in Section 3.2.7.1. Rabbit anti-Htz1 antibody was raised against a synthetic peptide of residues 117-134 of the *S. cerevisiae* Htz1p (Upstate). Anti-Sir2 (γ -80) is a rabbit polyclonal antibody raised against residues 1–80 of *S. cerevisiae* Sir2p (Santa Cruz Biotechnology).

4.2.5 Analytical gel filtration

For the Hho1p and Nhp6ap experiment a Superdex 75 10/300 GL gel filtration column (GE Healthcare) was pre-equilibrated in 10 mM sodium phosphate pH 7.0, 150 mM NaCl, 1 mM DTT and 1 mM EDTA. For Hho1p and

Sir2p a Superdex 200 10/300 GL gel-filtration column (GE Healthcare) was pre-equilibrated in 10 mM sodium phosphate pH 8.0, 175 mM NaCl and 1 mM EDTA.

Samples were prepared containing one or both proteins at 10 μ M or 17 μ M (for the Nhp6ap and Sir2p experiments respectively), in the same buffer, and incubated on ice for 30 min. The elution of proteins from the Superdex column was followed by absorbance at 280 nm.

4.2.6 Co-immunoprecipitation

4.2.6.1 Anti-Hho1 immunoprecipitation

Cultures of wild-type W303 yeast (Section 3.2.1.2) were grown in YPAD (Section 3.2.1.1). Cells were harvested by centrifugation at 2000 g for 5 min at 4 °C, washed in ice cold PBS (4.3 mM Na₂HPO₄, 1.47 mM KH₂PO₄, 137 mM NaCl, 2.7 mM KCl, adjusted to pH 7.4), and then resuspended in ice cold RiPA buffer (10 mM sodium phosphate pH 7.0, 140 mM NaCl, 1 mM EDTA, 0.5% (v/v) NP-40, 0.5% (w/v) sodium deoxycholate, 0.1% (v/v) SDS) supplemented with 1 μ g/ml leupeptin, 1 μ g/ml aprotinin, 0.156 mg/ml benzamidine, 1 μ g/ml pepstatin A. Cells were lysed and chromatin sheared on ice with pulses of sonication at 60% amplitude (15x 10 sec). Cell debris was removed by centrifugation at 16000 g for 5 min at 4 °C.

The whole-cell extract was pre-cleared with Protein A Sepharose beads (Zymed) for 1 h at 4 °C and the beads were removed by centrifugation at 3000 g for 1 min at 4 °C. At this point an input sample was taken and the rest of the supernatant was divided between the negative control (pre-immune serum) and positive immunoprecipitation (anti-Hho1 serum) reactions. The samples were incubated for 4 h at 4 °C and bound on to Protein A-Sepharose beads by incu-

bating overnight at 4 °C.

The beads were collected by centrifugation at 3500 g for 1 min at 4 °C and washed twice successively in each of the following ice cold buffers: RiPA buffer, PBS and TE buffer (10 mM Tris-HCl pH 8.0, 1 mM EDTA). Proteins were eluted from the beads by incubation at 25 °C for 10 min in 50 mM Tris-HCl pH 8.0, 10 mM EDTA, 1% (w/v) SDS. The elution was repeated and the supernatants combined.

4.2.6.2 HTZ1-TAP immunoprecipitation

Immunoprecipitation was carried out as in Section 4.2.6.1 with the following modifications. The yeast strain used was HTZ1-TAP (Section 3.2.1.2). The negative control used Protein A Sepharose beads and the positive immunoprecipitation used IgG sepharose beads (GE Healthcare), which were incubated in the whole-cell extract at 4 °C for 18 h.

4.2.7 Chromatin immunoprecipitation assay

The ChIP assay was carried out in collaboration with Dr Edwige Hiriart (MRC Laboratory of Molecular Biology, Cambridge).

4.2.7.1 Culture growth, cross-linking and whole-cell extract

HTZ1-TAP and HHO1-TAP yeast strains (Section 3.2.1.2) were grown in YPAD medium (Section 3.2.1.1) at 30 °C and 220 rpm. Yeast cells were cross-linked for 10 min at 25 °C by adding 1 mM EDTA, 140 mM NaCl and 1% (v/v) formaldehyde. Cross-linking was stopped by addition of 125 mM glycine with swirling for 5 min at 25 °C. Cells were harvested by centrifugation at 2000 g for 5 min at 4 °C and washed in ice cold PBS (Section 4.2.6.1).

Pellets were resuspended in RiPA buffer (Section 4.2.6.1) supplemented with 1 $\mu\text{g}/\text{ml}$ leupeptin, 1 $\mu\text{g}/\text{ml}$ aprotinin, 0.156 mg/ml benzamidine, 1 $\mu\text{g}/\text{ml}$ pepstatin A. Cells were lysed by “bead blasting” for four 15-second pulses at 55% power and the lysate sonicated for six 10-second pulses. Cell debris was removed by centrifugation at 16000 g for 5 min at 4 °C and the supernatant was taken.

4.2.7.2 TAP-tag precipitation

Whole-cell extracts were pre-cleared with Protein A Sepharose beads for 30 min at 4 °C, and the beads removed by centrifugation at 3000 g for 1 min at 4 °C. Samples were removed for “input” and the rest of the sample was divided between a negative control (using Protein A Sepharose beads) and positive immunoprecipitation (using IgG Sepharose beads). The samples were incubated for 3 h at 4 °C and the beads collected by centrifugation at 3000 g for 1 min at 4 °C.

Beads were washed twice successively in each of the following buffers: RiPA buffer (Section 4.2.6.1), RiPA buffer with 0.5 M NaCl, ChIP wash buffer (10 mM Tris-HCl pH 8.0, 0.25 M LiCl, 0.5% (v/v) NP-40, 0.5% (w/v) sodium deoxycholate, 1 mM EDTA) and TE buffer (Section 4.2.6.1). Chromatin was eluted from the beads by incubation for 10 min at 25 °C with elution buffer (Section 4.2.6.1). Beads were collected by centrifugation at 16000 g for 2 min at 25 °C and the elution was repeated. Samples were taken and analysed by Western blotting (Section 3.2.7) using an anti-TAP antibody (Open Biosystems).

4.2.7.3 Purification of DNA

Formaldehyde cross-links in the input and precipitated samples were reversed by addition of NaCl to 200 mM and incubation at 65 °C overnight. The samples were deproteinised by addition of 100 μ g proteinase K (BDH) for 1.5 h at 37 °C. DNA was then extracted using phenol:chloroform:isoamyl alcohol and precipitated with absolute ethanol as described in Section 3.2.4.7. The DNA pellets were dissolved in TE buffer (Section 4.2.6.1).

4.2.7.4 PCR analysis

The primers used for these analyses are listed in Table 4.1.

Table 4.1: Primers used for PCR analyses of Hho1p and Htz1p localisation

Gene	Position		Sequence
ADH2	-1	F	5'-CAGAGGAGAGCATAGAAATGGGGTT-3'
		R	5'-AGTAAGAGTATTTTCGAGTGTGAAAAAAGTC-3'
	+1	F	5'-AATAGAATATCAAGCTACAAAAAGCATAAC-3'
		R	5'-CCGTTGGATTCGTAGAAGATAAT-3'
	+5	F	5'-AATTGTTTACCTCGCTCGG-3'
		R	5'-AGCCTTAACGACTGCGCTA-3'
PHO5	A	F	5'-TGTTCCCTTGGTTATCCCATCGC-3'
		R	5'-GCAATTATTACTTGGATGCCCTCC-3'
	H	F	5'-CCTAACTTTTTGACCACCGCTG-3'
		R	5'-TGATTTCAACAAGAGAACCCTGGAC-3'
	J	F	5'-GGGAACTCAAAGAACTGGCATC-3'
		R	5'-ACTCTCCGAGGGGAATTGTACC-3'

The input, a ten-fold dilution of the input, the negative ChIP and positive ChIP samples for each of strains were used as templates in PCR reactions using each of the primer sets. DNA was amplified using Taq DNA polymerase (Biolone). The PCR products were analysed in 2% (w/v) agarose gels containing 0.5x TBE (44.4 mM Tris base, 1 mM EDTA, 44.4 mM boric acid) (Section 3.2.6.1).

4.3 Results

4.3.1 Searching for Hho1p-interacting partners

Anti-Hho1 immunoprecipitation was used to enrich Hho1p from yeast whole-cell extract or nuclear extract, however no other proteins co-purified with Hho1p that were visible on Coomassie-stained SDS/polyacrylamide gels (data not shown). This could be because the Hho1p/antibody interaction out-competed any interactions between Hho1p and other yeast proteins, or because that there are no strongly interacting partners for Hho1p. Also, GST-Hho1p was used for pull-down assays in yeast whole-cell and nuclear extracts, immobilising by means of glutathione-agarose beads, but again no interacting partners were identified on Coomassie-stained SDS/polyacrylamide gels (data not shown).

Through collaboration with Prof Charles Boone's laboratory (University of Toronto), genetic interactions with Hho1p were sought using a proteome-wide synthetic gene analysis (SGA) data set (Tong et al., 2004). This assay uses a deletion array of yeast strains and scores the growth defects of progeny produced by crossing these with yeast containing a second mutation (Tong and Boone, 2006). A computer-based scoring system estimates the relative growth rate of an individual colony, comparing the double mutant strains to wild-type controls. This determines if there is a genetic link between the two mutated genes. Hho1p had not been screened against the deletion array, however it had been brought up in other screens (data not shown). Unfortunately the scores from these screens were too weak to have been reported as potential interactions (in the *Saccharomyces* Genome Database) and so these candidates were not investigated further.

In order to attempt to identify potential candidates for Hho1p-

interacting partners I focussed on proteins whose metazoan homologues interact with histone H1, and those that share functions with Hho1p (discussed in Section 4.1).

4.3.2 Investigation of Hho1p interaction with HMG box proteins, Hmo1p and Nhp6ap

Initially the interaction of Hho1p with HMGB1 was compared with that of histone H1 with HMGB1, which requires the C-terminal tail of HMGB1 (Figure 4.2). The acidic tail of HMGB1 was required for cross-linking of Hho1p and HMGB1 with DMS. Cross-linked products are formed for Hho1p with full-length HMGB1 (lane 13) but not with the AB' form of HMGB1, which lacks the acidic tail (lane 17) (see Figure 4.1 for domain structure). This reduces the likelihood that Hho1p will interact with Hmo1p or Nhp6ap as they don't contain any strongly acidic regions.

Hmo1p formed a smear of products when cross-linked with either DMS or EDC (Figure 4.3a and b respectively; lanes 8). This self-association of Hmo1p had been previously reported in a yeast two-hybrid assay (Dolinski and Heitman, 1999). Addition of histone H1 or Hho1p to the reaction did not change the pattern of cross-linked products produced (compare lanes 8 with lanes 13 and 17) suggesting that Hmo1p does not interact with either linker histone in solution. The positive control reactions between linker histones and HMGB1 demonstrate that the cross-linking conditions were suitable to produce discrete product bands (lanes 11 and 15).

An interaction between Hho1p and Nhp6ap was also investigated using cross-linking with DMS and EDC. Initial studies using DMS did not produce discrete cross-linked product bands (Western blots showed a smear of

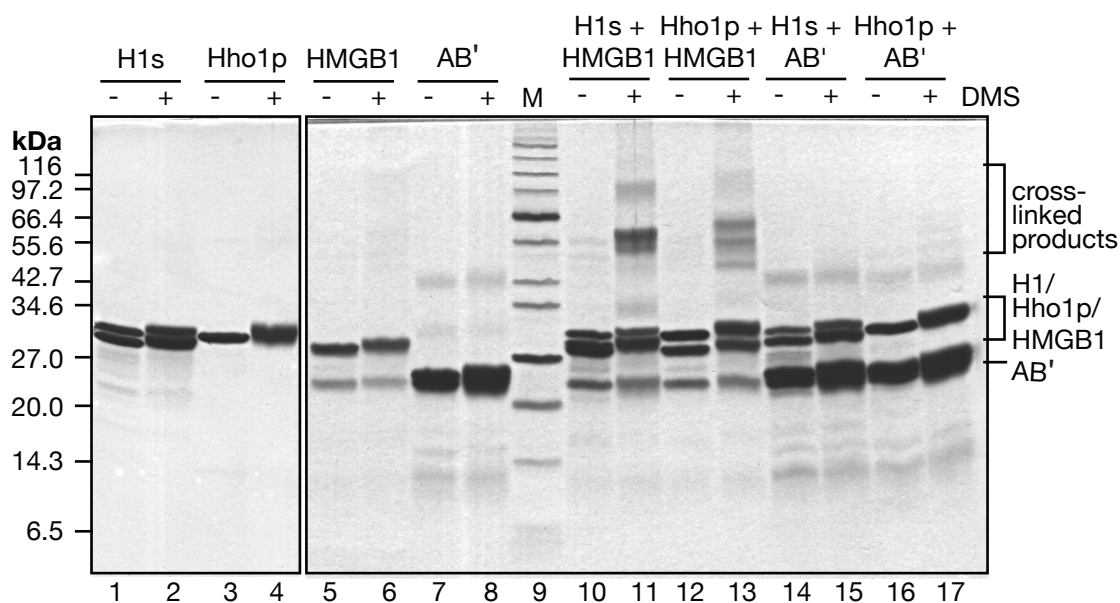


Figure 4.2 The acidic tail of HMGB1 is required for cross-linking to both histone H1 and Hho1p. SDS/18%-PAGE of proteins before (-) and after (+) cross-linking with 2 mg/ml DMS for 20 minutes at 25 °C. Lane 9 contains molecular weight markers. Histone H1 was extracted from chicken erythrocytes; the other proteins are recombinant. There is some degradation of HMGB1 to AB' seen in lanes 5-6 and 10-13. The cross-linked products for H1 and HMGB1 (lane 11) consist of a heterodimer and heterotrimer. The cross-linked products for Hho1p and HMGB1 (lane 13) may consist of a heterodimer and two homodimers, although the homodimers were not seen in the samples containing just one of the proteins (lanes 4 and 6). It is also possible that all three bands could be heterodimers, each with a different portion of Hho1p cross-linked to the HMGB1 molecule (e.g. G1 domain, GII domain or both domains).

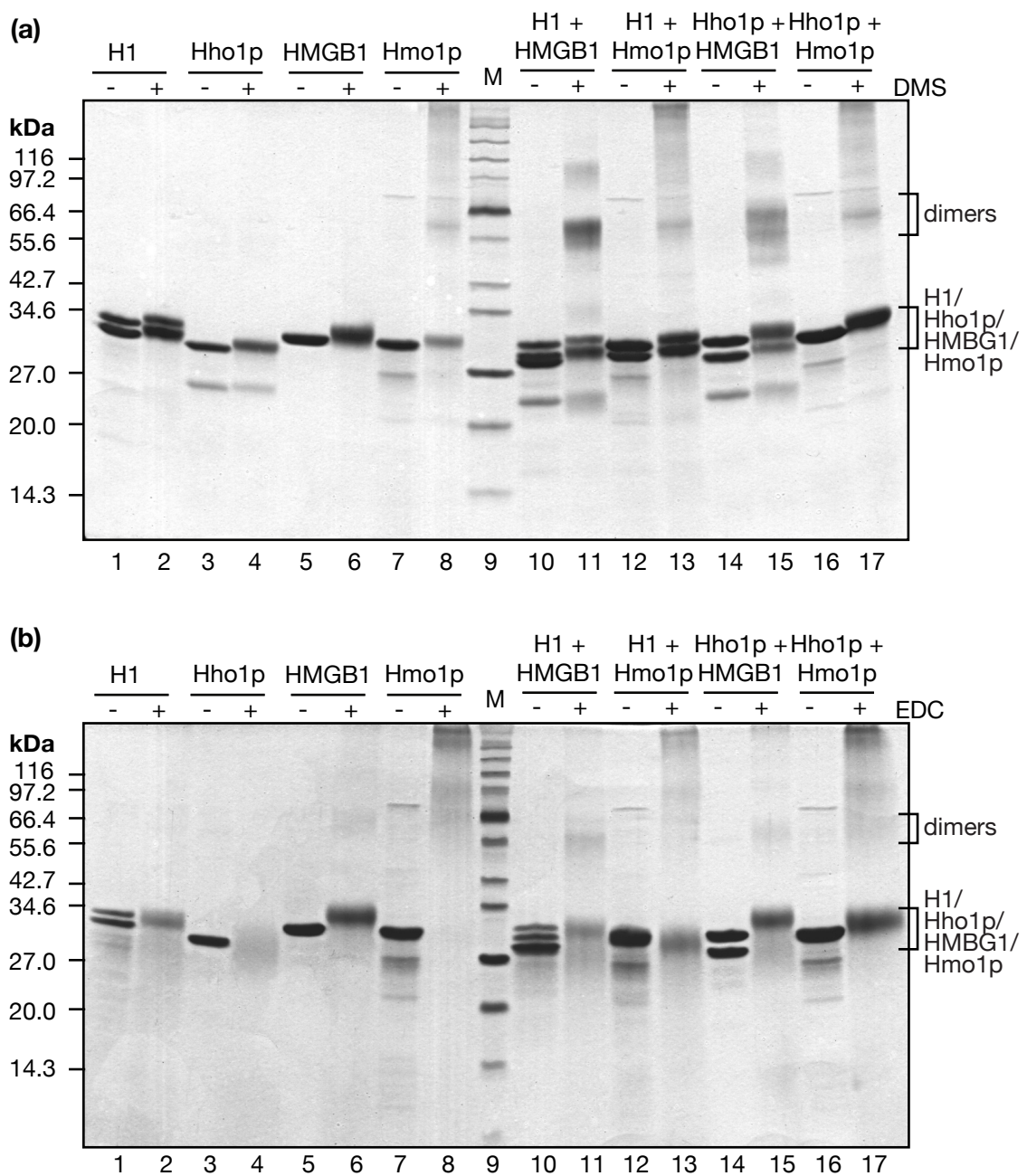
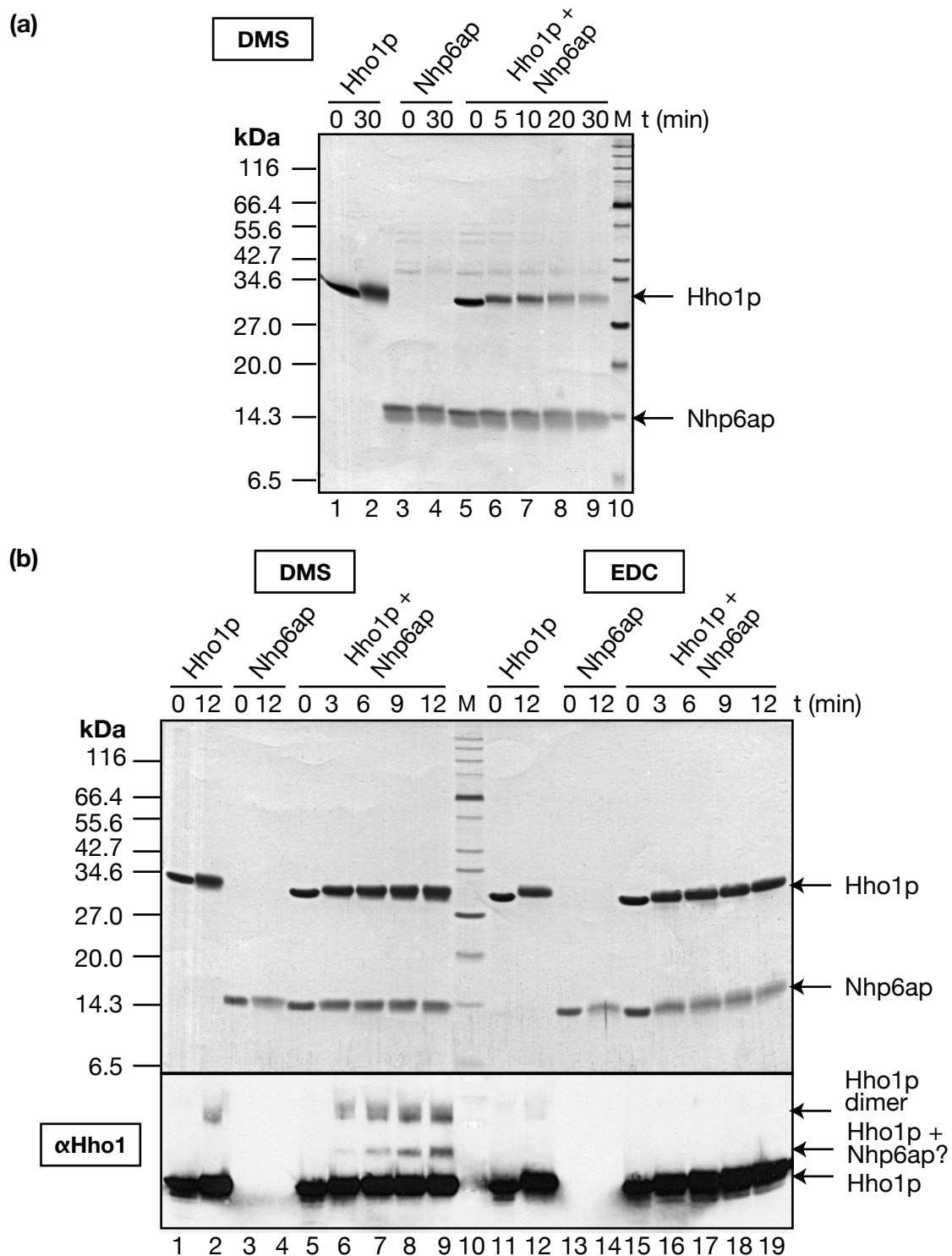


Figure 4.3 Hmo1p does not cross-link to histone H1s or Hho1p in solution. **(a)** SDS/18%-PAGE of proteins before (-) and after (+) cross-linking with 2 mg/ml DMS for 20 minutes at 25 °C. Lane 9 contains molecular weight markers. Histone H1 was extracted from chicken erythrocytes; the other proteins are recombinant. There is slight contamination of the Hmo1p samples by a protein of around 70 kDa. Lanes 1–8 contain the individual proteins; only Hmo1p forms cross-linked products, showing a smear of aggregation products. Lanes 11 and 15 are positive controls for cross-linking between HMGB1 and the linker histones, showing dimer products. Lanes 13 and 17 indicate that the presence of linker histone does not change the pattern of Hmo1p cross-linked products. **(b)** As in (a) but cross-linking with 24.2 mg/ml EDC for 20 minutes at 25 °C. The dimer products (lanes 11 and 15) for cross-linking of HMGB1 with linker histone is less pronounced than in (a).

Hho1p-containing products, data not shown) but the amount of unmodified Nhp6ap and, more noticeably, Hho1p decreased throughout the reaction (Figure 4.4a; compare lanes 2 and 4 with lane 9). In order to try to capture discrete cross-linked products by Western blotting, the cross-linking was carried out for shorter time-periods (Figure 4.4b). EDC cross-linker was also used to see if the bands of cross-linked products were more discrete. Under these conditions no cross-linking was seen on the Coomassie-stained gels, however the Western blot indicated a small proportion of DMS cross-linked products that contained Hho1p and are the size expected for an Hho1p-Nhp6ap dimer (Figure 4.4b; lanes 6–9). Unfortunately an anti-Nhp6a antibody was not available to verify if the product also contains Nhp6ap. The amount of putative Hho1p-Nhp6ap complex suggests the interaction is very weak. Levels are lower than that of the Hho1p dimer product, which is known to be an insignificant proportion of the sample and is not thought to be biologically relevant. The putative Hho1p-Nhp6ap cross-linking product was not observed using EDC at pH 7 (Figure 4.4b; lanes 16–19) or disuccinimidyl suberate (DSS) at pH 7.0 or pH 8.0 (data not shown).

Gel-filtration was also used to look for an interaction between Hho1p and Nhp6ap in 150 mM sodium chloride (Figure 4.5). The molar extinction coefficient of Nhp6ap is higher than that of Hho1p ($10810 \text{ M}^{-1} \text{ cm}^{-1}$ and $7680 \text{ M}^{-1} \text{ cm}^{-1}$ respectively) but this does not explain the large difference in the height of the Hho1p and Nhp6ap peaks. The Hho1p peaks has a long tail and therefore Hho1p presumably associates with the column matrix. In an equimolar (input) mixture of Hho1p and Nhp6ap the major peak sometimes eluted slightly ahead of the equivalent peak in the Nhp6ap-only sample, as shown in Figure 4.5, however this was not consistent. It should also be noted that the association of Hho1p with the column matrix will mean that the actual ratio of



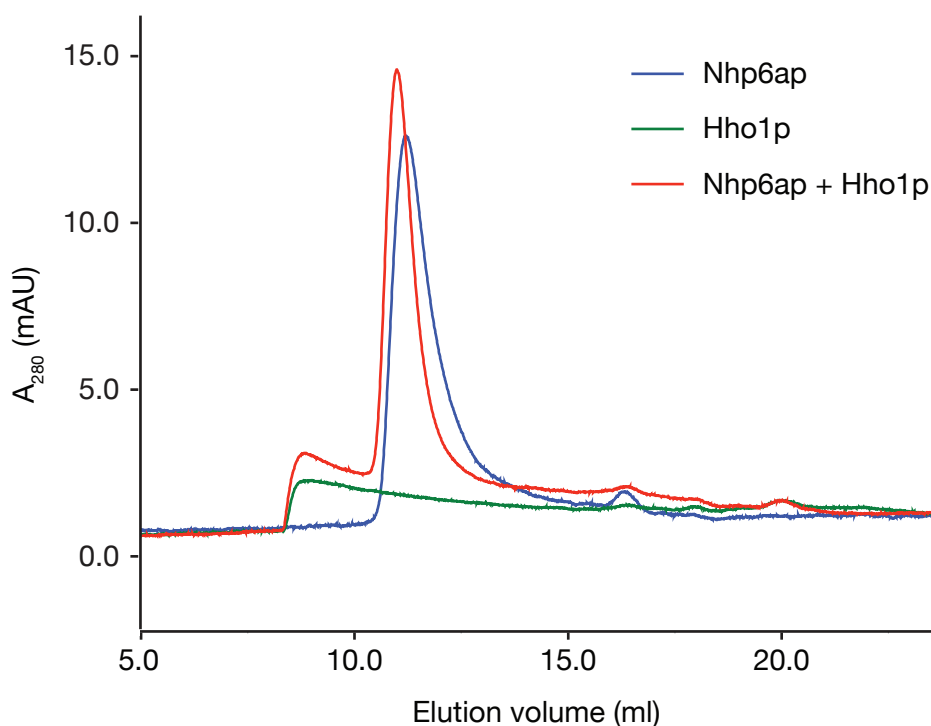


Figure 4.5 Gel-filtration of Hho1p and Nhp6ap. Elution profiles from a Superdex 75 column run in the presence of 150 mM NaCl. The Nhp6ap trace is blue, Hho1p alone is green, and the red curve is a 1:1 molar mix of both proteins. Hho1p associates with the column matrix as indicated by the long tail of the Hho1p only peak. This means that the actual ratio of Hho1p to Nhp6ap, as it passes through the column, is lower than the input ratio. The molar absorption coefficient of Hho1p is lower than that of Nhp6ap, which also contributes to the very different peak heights. The mixture sample indicates the presence of some unbound Hho1p as determined by the characteristic tail of the elution profile. The major peak eluted slightly ahead of the Nhp6ap peak (blue) in the Nhp6ap-only sample (red), although this was not consistent.

Hho1p to Nhp6ap, as it passes through the column, is lower than the input ratio. Chemical cross-linking in 150 mM NaCl was identical to that in Figure 4.4. If the salt concentration was increased to 200 mM the elution profile of Hho1p sharpened, however the major peak of the mixture no longer eluted ahead of that in the Nhp6ap-only sample (data not shown). The absence of a significant interaction as judged by either gel-filtration or chemical cross-linking indicates, at best, a very weak interaction between Hho1p and Nhp6ap that is unlikely to be biologically relevant.

4.3.3 Investigation of Hho1p interaction with Htz1p

A direct interaction between Hho1p and Htz1p was not seen in pull-down assays using either GST-Hho1p or GST-Htz1p as bait (data not shown). However, the assays were carried in salt concentrations above physiological levels (as Hho1p directly bound the glutathione-agarose beads in lower salt conditions) and this could have disrupted any protein-protein interactions.

Co-immunoprecipitation assays were carried out in yeast whole-cell extract, either using an Htz1-TAP tagged strain or by probing a wild-type yeast strain with anti-Hho1 antibodies (Figure 4.6). The TAP immunoprecipitation very clearly showed that the Htz1-TAG was immunoprecipitated, but not the Hho1p (lanes 4 and 5). The anti-Hho1 immunoprecipitation was slightly less clear as not all of the Hho1p was immunoprecipitated (lanes 9 and 10), however all the Htz1p remains in the unbound fraction suggesting that no co-immunoprecipitation occurred.

Chemical cross-linking studies were carried out using Hho1p and Htz1p (Figure 4.7). The Htz1p sample contained some contaminants (lanes 3–9), at least some of which are probably GST-Htz1p that was carried over from the

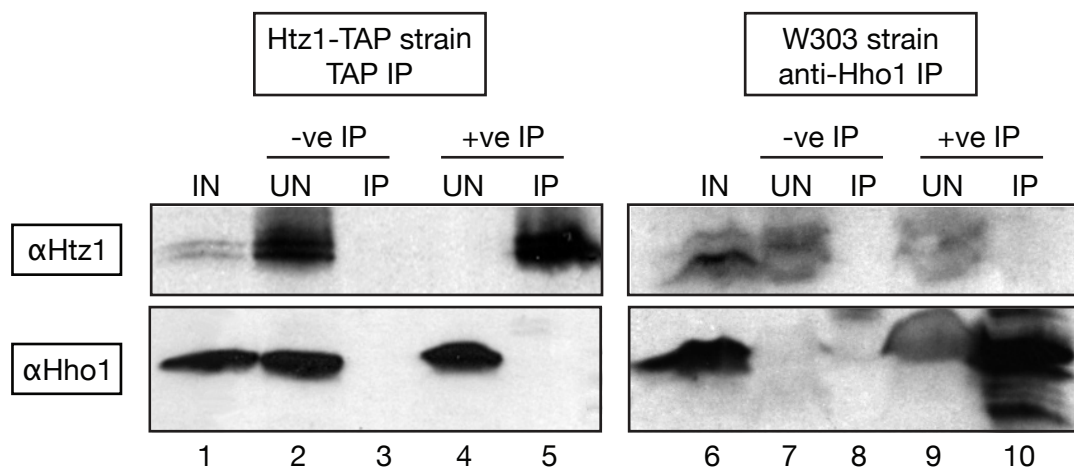


Figure 4.6 Hho1p and Htz1p immunoprecipitations from *S. cerevisiae* whole cell extract. Immunoprecipitated fractions were analysed by SDS/18%-PAGE and Western blotting with the antibodies indicated. The Htz1-TAP strain has a TAP-tag on the genomic copy of HTZ1, allowing its precipitation with IgG-sepharose. IN: pre-cleared input, UN: unbound, IP: immunoprecipitated. Lane 7 shows degradation of the unbound Hho1p in the negative IP control, but bands are still visible. There is no evidence of co-immunoprecipitation of Hho1p and Htz1p.

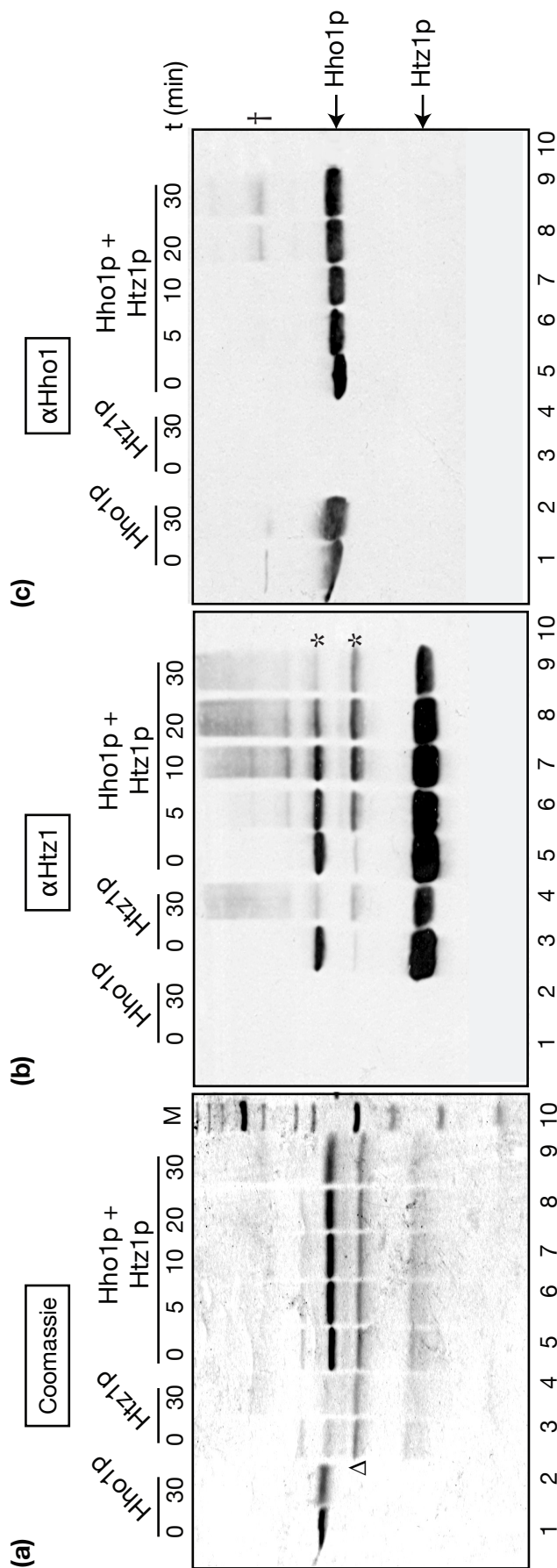


Figure 4.7 Chemical cross-linking of recombinant Hho1p and Htz1p. There appear to be no cross-linked products containing both Hho1p and Htz1p. **(a)** SDS/18%-PAGE of proteins before and after cross-linking with 2 mg/ml DMS at 25 °C. Lane 10 contains molecular weight markers. The Htz1p bands stain less strongly than the Hho1p bands, although equal molar amounts are loaded. The Htz1p samples contain a contaminant (marked with Δ). **(b)** As for (a) but a Western blot of a duplicate of the gel probed with α Htz1p. The Htz1p-contaminants detected by the anti-Htz1p antibody are likely to be GST-Htz1p from the purification process and a degradation product (marked with an asterisk). Cross-linking involving Htz1p is seen in both the Htz1p-only (lane 4) and mixture samples (lanes 6–9). **(c)** The Western blot from (b) stripped and re-probed with anti-Hho1p antibody. A small amount Hho1p dimer is produced in the Hho1p only sample and the mixture (marked with a cross).

purification process, as well as degradation products of this fusion protein. Cross-linking reactions containing the Htz1p sample showed a smear of cross-linking products in the anti-Htz1 Western blot (panel b, lanes 4 and 6–9). Small amounts of Hho1p dimer were seen in the anti-Hho1 Western blot (panel c, lanes 1, 2, 8 and 9). However, none of the cross-linked products contained both Hho1p and Htz1p suggesting that Hho1p and Htz1p did not interact directly in solution. Similar results were produced by EDC cross-linking (data not shown).

The relative association of Htz1p and Hho1p within two genes was investigated in ChIP assays, in collaboration with Dr Edwige Hiriart (MRC Laboratory of Molecular Biology, Cambridge). No suitable anti-Htz1p antibody was available to allow immunoprecipitation from wild-type yeast extracts, therefore a HTZ1-TAP genomically-tagged yeast strain was used. As the TAP tag includes protein A it would be immunoprecipitated by antibodies, therefore an anti-Hho1 immunoprecipitation could not be carried out in the HTZ1-TAP strain. An HHO1-TAP strain was used so that the two immunoprecipitations were carried out using strains with the same background character.

The association of Htz1p and Hho1p with regions of the ADH2 and PHO5 genes was assessed qualitatively (Figure 4.8). Regions corresponding to the –1 positioned nucleosome (in the promoter) as well as the +1 and +5 positioned nucleosomes in the open reading frame of the ADH2 were investigated. The PHO5 positions correspond to the promoter (position A), the open reading frame (position H) and the region after the open reading frame (position J). Qualitative comparison of the signals for the immunoprecipitated samples and the input material was made (with reference to the diluted input and negative immunoprecipitation controls) to identify the relative enrichment or depletion of Htz1p or Hho1p at these positions (Figure 4.8b). The data were interpreted cautiously as some of the PCR reactions, those producing the strongest signals,

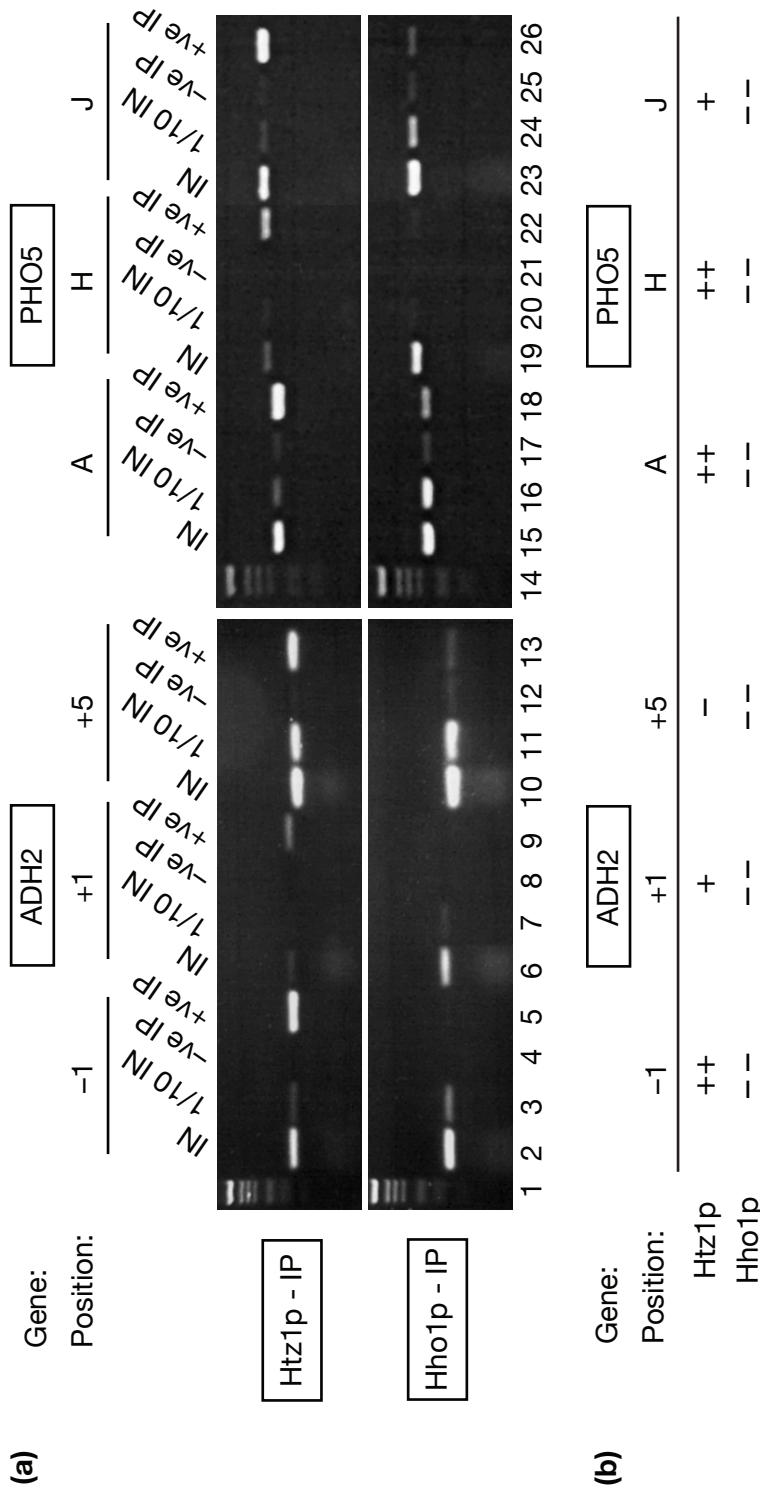


Figure 4.8 PCR analysis of Hho1p and Htz1p association with regions of the ADH2 and PHO5 genes in *S. cerevisiae*. **(a)** PCR products for the primer sets and DNA samples indicated, analysed in 2% agarose gels containing 0.5x TBE. Primer sets corresponding to: the first nucleosome upstream of the ADH2 transcription initiation site (lanes 2-5); the first nucleosome in the ADH2 open reading frame (lanes 6-9); the fifth nucleosome in the ADH2 open reading frame (lanes 10-13); within the promoter of the PHO5 gene (lanes 15-18); a position within the PHO5 open reading frame (lanes 19-22); after the PHO5 open reading frame (lanes 23-26). IN, total DNA; 1/10 IN, ten-fold dilution of total DNA; -ve IP, negative control for the immunoprecipitation indicated (giving the background PCR signal); +ve IP, immunoprecipitated material. **(b)** Qualitative comparison of amounts of immunoprecipitated material to input material, with reference to 1/10 IN and negative control signals. ++: enrichment; +: slight enrichment; -: slight depletion; --: depletion.

may have reached saturation.

There was more Htz1p present at each location than Hho1p and the relative association of Htz1p and Hho1p to regions throughout the ADH2 and PHO5 genes were different. Htz1p levels decreased over the length of the genes, whereas the Hho1p levels were depleted throughout the genes. This is consistent with a genome-wide study that saw promoter enrichment of Htz1p but not Hho1p (Zanton and Pugh, 2006). Further PCR analyses indicated that Hho1p was present at all these locations (producing more signal than the negative immunoprecipitation controls) but the signals were greatly depleted compared to the input sample (data not shown). There is no evidence of co-localisation, which may have been inferred if both Hho1p and Htz1p showed similar patterns of localisation across the genes.

4.3.4 Investigation of Hho1p interaction with Sir2p

Chemical cross-linking studies using Hho1p and Sir2p suggested a direct interaction of these proteins in solution (Figure 4.9). The Sir2p sample was not very pure, as observed in the anti-Sir2 Western blot (panel b, lane 3). Degradation was shown to occur during expression, and reduction of expression time had no appreciable effect on degradation the Sir2p produced. The Sir2p-only sample forms a cross-linked product that is visible on the anti-Sir2 Western blot (marked with an asterisk; panel b, lane 4). There is a product of slightly lower molecular weight that only occurs in the mixture samples (panel b, lanes 7–13). This band also contains Hho1p, as shown in the anti-Hho1 Western blot (panel c, lanes 7–13). It is difficult to determine a stoichiometry for the complex, as the range of Sir2p degradation products have caused a broad distribution of cross-linked products. This product is also visible in the Coomassie-stained gel and the band extends to approximately the 116 kDa molecular weight marker,

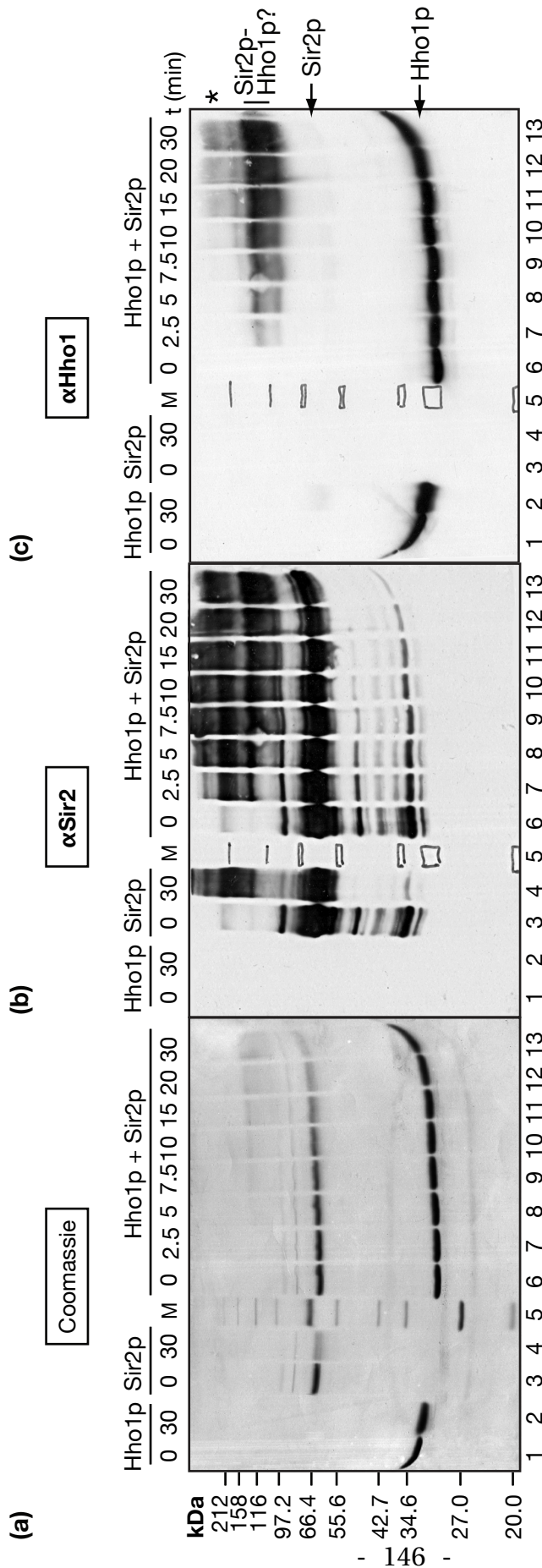


Figure 4.9 Chemical cross-linking of Hho1p and Sir2p in solution. (a) SDS/15%-PAGE of proteins cross-linked with 2 mg/ml DMS at 25 °C in buffer containing 175 mM NaCl. Lane 5 contains molecular weight markers. A cross-linked product occurs in samples containing both Hho1p and Sir2p (lanes 6–13). (b) Samples and gel as in (a), followed by Western blotting with anti-Sir2 antibody. The marker (lane 5) is hand annotated. Although the Sir2p is degraded and (Sir2p)_n product is formed (marked with an asterisk), the potential Sir2p-Hho1p product contains Sir2p. (c) Samples and gel as for (a), followed by Western blotting with anti-Hho1 antibody. The marker (lane 5) is hand annotated. The potential Sir2p-Hho1p product contains Hho1p.

which suggests that multiple Hho1p molecules may bind Sir2p. Hho1p is only contained in the Hho1p-Sir2p complex, while Sir2p is also contained in (Sir2p)_n products. This explains the differential loss of stain upon cross-linking for the bands corresponding to Sir2p and Hho1p in panel a.

Gel-filtration was carried out in the same buffer conditions as the cross-linking (Figure 4.10). The Hho1p peak is much sharper on this column, in the higher concentrations of sodium chloride, compared with the gel-filtration with Nhp6ap (Figure 4.5). The elution profile of the equimolar mixture showed a peak that may eluted slightly earlier than the peak in the Sir2p-only sample. The shift was very small, but consistent. The lack of a large shift in the gel filtration peaks could result from Hho1p nesting within the larger Sir2p protein, causing the apparent size of the complex to be very similar to that of Sir2p alone. However, for this to occur the Sir2p must be in a relatively extended conformation, and a larger difference in elution volume for Sir2p and Hho1p might therefore be expected. Thus, no strong conclusions regarding an interaction between Hho1p and Sir2p can be determined from this gel-filtration data.

Unfortunately purification difficulties and the instability of recombinant Sir2p samples precluded further investigation of the interaction between Hho1p and Sir2p.

4.4 Discussion

4.4.1 General searches for Hho1p-interacting partners

Identification of Hho1p-interacting partners from whole-cell or nuclear extracts proved difficult. This is partially due to the low cellular level of Hho1p. Co-immunoprecipitation of Hho1p-interacting partners may have been inhibited

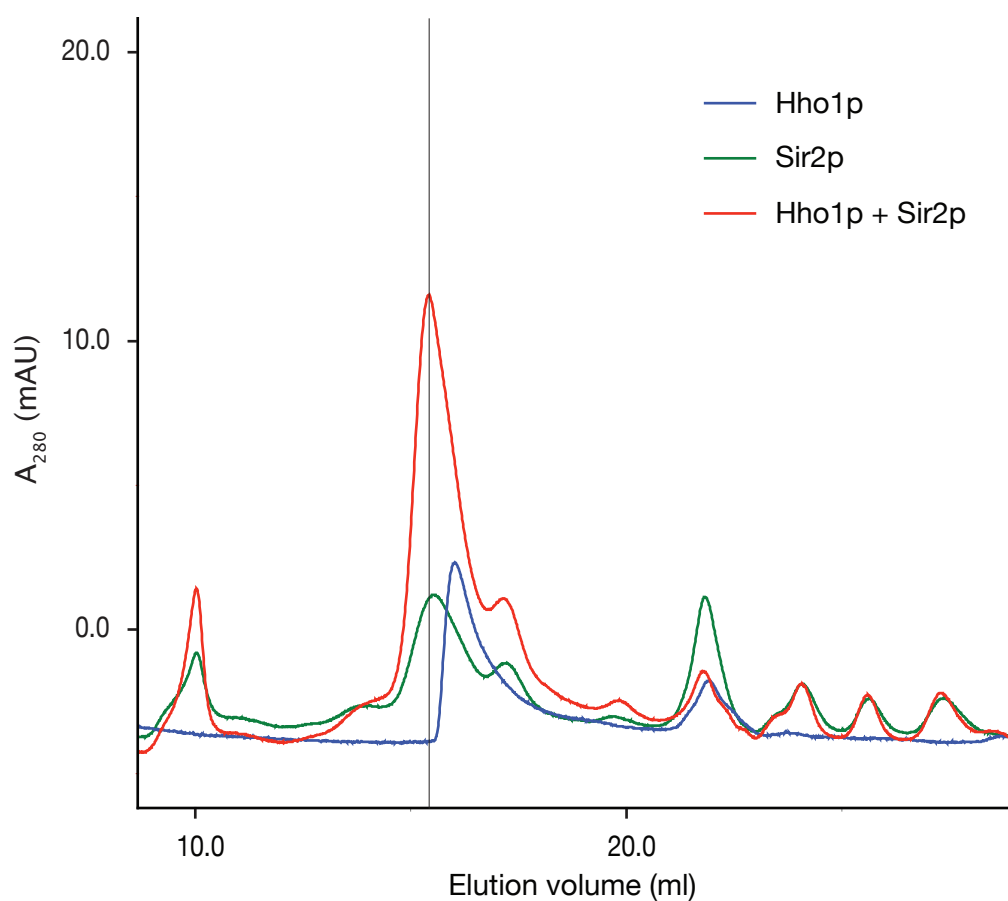


Figure 4.10 Gel-filtration of Hho1p and Sir2p. Elution profiles from a Superdex 200 column run in 175 mM NaCl. The Hho1p trace is blue, Sir2p alone is green, and the red curve is a 1:1 molar mix of both proteins. The mixture trace may possibly suggest a slightly earlier elution of the major species compared to the Sir2p-alone peak, as highlighted by the vertical line. This shift is very small but is consistent.

ited by the antibody-Hho1p interaction out-competing other Hho1p-protein interactions. GST-Hho1p pull-downs from yeast extracts were also unsuccessful, possibly because many protein-protein interactions do not persist at higher salt concentrations necessary because Hho1p interacts with the sepharose beads in physiological salt conditions.

The synthetic gene analysis data did not produce any candidates for proteins that genetically interact with Hho1p. If Hho1p was not required at all for survival in the assay growth conditions, a deletion that caused lethality in combination with the HHO1 deletion must also have been lethal as a single deletion.

Proteome-wide mass spectrometry studies have identified Hho1p from whole-cell extracts (e.g. Li et al., 2007) suggesting that an affinity-capture mass spectrometry assay could be sensitive enough to identify interacting partners (reviewed in Sinz, 2003). This assay involves the enrichment of Hho1p, and its interacting partners, through co-immunoprecipitation, followed by elution from the antibody and analysis using mass spectrometry. This assay would require the development of suitable anti-Hho1 antibodies, as the antibody used in this Chapter may out-compete other interactions with Hho1p (Section 4.3.1). Raising antibodies against smaller regions of the Hho1p molecule means the antibody interactions would be less likely to occur at the binding site of the interaction-partners, reducing the probability of Hho1p-protein interactions being out-competed by the Hho1p-antibody interaction.

4.4.2 Hho1p does not appreciably interact with Hmo1p, Nhp6ap or Htz1p, but does cross-link with Sir2p in solution

Hho1p does not interact with the HMGB1 homologues, Nhp6ap and Hmo1p. This was somewhat expected as Hho1p, like linker histone H1, was shown to interact with HMGB1 through its C-terminal acidic tail (Figure 4.2) and neither Hmo1p nor Nhp6ap contains a strongly acidic region. No known yeast HMG box-containing protein contains a strongly acidic tail. This suggests that there may be no interaction with Hho1p that is analogous to that of metazoan histone H1 and HMGB1.

Hmo1p is associated with rDNA loci (Gadal et al., 2002), which suggests that it could be involved in the same processes as Hho1p. However results described above suggest there is no direct interaction between these proteins. Although DMS cross-linking did produce a consistent product that could contain both Hho1p and Nhp6ap (Figure 4.4), it occurs at such low levels that it is unlikely to be of biological relevance.

Nhp6ap was reported to interact with Hho1p in a large-scale protein-fragment complementation assay (Tarassov et al., 2008). This is not necessarily inconsistent with the lack of interaction observed in the work described here (Figures 4.4 and 4.5) as the interaction seen in the protein-fragment complementation assay could have been indirect. The fusion proteins have 10 residue linkers between the yeast proteins and the reporter fragments allowing “near-neighbours” to be detected up to 82 Å apart. Verifying this protein-fragment complementation data in a smaller-scale experiment will determine whether the potential interaction between Nhp6ap and Hho1p is worth pursuing further.

Htz1p and Hho1p are both components of chromatosomes, therefore if they occur at the same locations within the genome they might be expected to interact. However, despite the reported interactions described in Section 4.1, work described in this Chapter offers no evidence of either a direct interaction between Hho1p and Htz1p or co-localisation of these proteins on the ADH2 and PHO5 genes.

TAP-tagged yeast strains were used for the chromatin immunoprecipitation study because there was no suitable anti-Htz1 antibody available for use in co-immunoprecipitation from wild-type yeast cells. The TAP-tag contributes an extra 21 kDa to the protein, a large proportion of the fusion protein, which might in principle affect the localisation of the proteins. A ChIP-chip study indicated that Htz1p is enriched in promoter regions (relative to intergenic regions) while Hho1p is relatively excluded from promoters (Zanton and Pugh, 2006). This is consistent with the data in Figure 4.8, suggesting that the TAP-tag did not cause aberrant localisation.

Htz1p, like Nhp6ap, was suggested to be an interaction-partner of Hho1p in the large-scale protein-fragment complementation assay (Tarassov et al., 2008). Again, this could be because Hho1p and Htz1p are “near-neighbours” rather than interacting directly and is not necessarily inconsistent with the lack of a direct interaction found here.

A protein interaction partner identified for Hho1p in the work described here is Sir2p, an NAD-dependent deacetylase that has roles in rDNA and silencing (Imai et al., 2000). Unfortunately the bacterial expression system used here is not optimal for production of Sir2p, resulting in samples that degraded both during expression and during storage. The sirtuin family of proteins have been expressed more successfully using the baculovirus expression system (for example, Cubizolles et al., 2006). Therefore the interaction between Sir2p and

Hho1p should be investigated further using recombinant Sir2p from this alternative source.

4.5 Summary

- Co-immunoprecipitation and synthetic gene analyses did not identify protein interaction partners for Hho1p.
- Hho1p does not interact directly with Hmo1p, Nhp6ap or Htz1p, *in vitro*.
- Hho1p cross-links with Sir2p *in vitro*. A pure and stable supply of Sir2p is required to allow further investigation of this interaction.

Chapter 5

Investigation of phosphorylation of Hho1p — biochemistry and linker domain structure

5 Investigation of phosphorylation of Hho1p — biochemistry and linker domain structure

5.1 Introduction

S. cerevisiae is a popular model organism often used to validate proteome-wide approaches to detect post-translational modifications. Currently the *Saccharomyces* Genome Database lists 62 literature references to “large-scale protein modification” experiments. Various modifications have been studied on a proteomic scale, for example methylation, palmitoylation, phosphorylation, sumoylation and ubiquitination (Pang et al., 2010; Roth et al., 2006; Li et al., 2007; Wohlschlegel et al., 2004; Radivojac et al., 2010). However, despite this extensive research, only three post-translational modifications have been reported for Hho1p - all of which are phosphorylations: of serine 130 in the linker domain and of serines 173 and 174 at the beginning of the second globular domain (Li et al., 2007; Holt et al., 2009).

Much more is known about post-translational modification of canonical linker histones, which have long been known to be phosphorylated and acetylated. More recently methylation, N-formylation and ubiquitination of linker histones have also been identified (Figure 1.5; reviewed in Happel and Doenecke, 2009).

Of the known post-translational modifications of linker histones, the most-studied modification is phosphorylation (discussed in Section 1.3.1.2). Histone H1 phosphorylation varies throughout the cell cycle (Talaszi et al., 1996). It affects cell-cycle progression, chromatin condensation and DNA replication (Gurley et al., 1978; Roth and Allis, 1992; Alexandrow and Hamlin, 2005). Also, phosphorylated linker histones are enriched at transcriptionally active chromatin sites, as indicated by the co-localisation of phosphorylated H1b with sites of RNA processing and gene activation in indirect immunofluorescence assays (Chadee et al., 1995). Most phosphorylation occurs on S/TPKK motifs, which are located in the C-terminal tail of histone H1 (Garcia et al., 2004; Deterding et al., 2008). Sea urchin sperm H1 is unusual, having several of these motifs in the N-terminal tail (Strickland et al., 1980).

In aqueous solution canonical linker histone C-terminal tails are largely unstructured, but form α -helix upon binding DNA (Roque et al., 2005) and in the presence of tetrahedral anions or trifluoroethanol (Clark et al., 1988). Phosphorylation of the C-terminal tail of histone H1 causes a decrease in α -helix and an increase in β -sheet character (Roque et al., 2008).

Hho1p does not contain any S/TPKK motifs, raising the question of whether its phosphorylation is regulated by kinases similar to those acting on canonical linker histones. The linker domain of Hho1p has more sequence variation than the C-terminal tail of canonical linker histones, raising the question of whether the structural character of these domains is different. There are indications that the Hho1p linker domain, like the canonical C-terminal tails, is unstructured in aqueous solution (Ali and Thomas, 2004; Osmotherly, 2006), as CD studies demonstrate a less α -helical character in proteins containing the linker domain, compared with the isolated GI domain, but this has yet to be studied in detail. In this Chapter I aim to investigate the structure of, and the

effect of phosphorylation on, the linker domain of Hho1p using NMR. The unmodified and phosphorylated linker domains are assigned using conventional triple-resonance experiments alongside the HNN/HN(C)N experiments which are particularly suited for assignment of unstructured proteins. Shift deviations from random coil, heteronuclear NOEs and temperature-dependence of proton shifts are used to determine the transient structure and fast dynamics of the unmodified and phosphorylated domain. The degree to which the peaks shift and the original peak is attenuated upon phosphorylation is additionally used to determine the sites of phosphorylation.

The effect of phosphorylation on the biochemical properties of Hho1p and various Hho1p-truncation proteins is also addressed. The domains in which phosphorylation events by CDK2/Cyclin A occurred are determined. Binding to linear DNA, four-way junction DNA and chromatin are used to compare unmodified and phosphorylated Hho1p-truncation proteins.

5.2 Materials and methods

5.2.1 Plasmids

Plasmid pET17b-GI contains the cDNA for the GI domain of Hho1p, plus the first 13 residues of the linker domain, (residues 38-130) under the control of a T7 promoter, and an ampicillin resistance gene (Ali and Thomas, 2004).

Plasmid pET17b-LGII contains the cDNA for the last 40 residues of the linker domain and the GII domain of Hho1p (residues 131-258) under the control of a T7 promoter, and an ampicillin resistance gene. This plasmid was generated by Dr Andy Sanderson (Department of Biochemistry, Cambridge).

5.2.1.1 Cloning of pET17b-HHO1-linker

The linker domain (residues 118-170 of Hho1p) was amplified from the pET17b-HHO1 plasmid using a forward primer with a flanking *Nde I* site and a start codon at the 5'-end, and a reverse primer containing a stop codon and *Xho I* site at the 3'-end. The sequences are listed in Table 5.1. The PCR reaction used KOD hot-start DNA polymerase (Merck), 40 °C primer-annealing temperature, and 30 sec extension at 72 °C.

Table 5.1: Primers used to clone the linker domain of Hho1p

Primer	Sequence
Forward:	5'-AAACTGCATATGAAGAAATCTCCAGAAGTAAAGAA-3'
Reverse:	5'-AAGGCGACTCGAGTTACTTGGCGGTAACAGTAGGC-3'

The PCR product and pET17b-HHO1 were digested with *Nde I* (NEB) and *Xho I* (NEB) for 3 h at 37 °C and the digestion products purified using a QIAquick PCR clean-up kit (Qiagen). The digestion products were analysed in a 1% (w/v) agarose gel containing 0.3x TBE (Section 3.2.6.1) and the bands corresponding to the PCR insert and linearised vector were excised and purified using a QIAquick gel-extraction kit (Qiagen).

Vector and insert were ligated at a 5:1 molar ratio for 3 h at 25 °C using T4 DNA ligase (NEB). The ligation reactions were used to transform *E. coli* DH5 α cells (Section 2.2.1.2) and the cells were grown overnight at 37 °C on LB-agar plates (Section 2.2.1.1) supplemented with 50 μ g/ml carbenicillin. Single colonies were grown at 37 °C, with shaking at 250 rpm, overnight in 5 ml LB medium (Section 2.2.1.1) supplemented with 50 μ g/ml carbenicillin. The plasmid DNA (pET17b-HHO1-linker) was extracted using a QIAquick miniprep kit (Qiagen) and its sequence was verified by DNA sequencing (Section 5.2.9).

5.2.2 Proteins

5.2.2.1 Expression and purification of Hho1p and Hho1p-truncation proteins

Hho1p was expressed in TB medium using the conditions described in Section 2.2.3.1. GI, GII, NGIL and LGII were expressed in LB medium, supplemented with 50 $\mu\text{g}/\text{ml}$ carbenicillin, using the same conditions as GII (Section 2.2.3.3), except that NGIL was expressed in BL21(DE3)pLysS cells. All proteins were purified as described for Hho1p (Section 2.2.3.2) except they were concentrated in Vivaspin 2 concentrators with appropriate sized molecular weight cut-offs (Sartorius) (MWCO used: Hho1p, 10 kDa; GI and GII, 3 kDa; NGIL and LGII, 5 kDa).

5.2.2.2 Expression and purification of ^{13}C , ^{15}N -linker domain of Hho1p

Plasmid pET17b-Hho1-linker (Section 5.2.1.1) was used to transform *E. coli* BL21(DE3) cells (Section 2.2.1.2) and pre-cultures were grown overnight in LB medium (Section 2.2.1.1) supplemented with 50 $\mu\text{g}/\text{ml}$ carbenicillin at 37 °C with shaking at 250 rpm. Ten flasks (2 l) containing 500 ml MOPS medium (Section 2.2.1.1), with ^{15}N - NH_4Cl as the sole nitrogen source, 0.5 g/l ^{13}C -glucose as the sole carbon source and supplemented with 50 $\mu\text{g}/\text{ml}$ carbenicillin, were each inoculated with 5 ml pre-culture and grown at 37 °C and 220 rpm until the OD_{600} was about 0.6. Expression of the linker domain was induced with 1 mM IPTG and growth was continued for a further 3 h. Cells were harvested by centrifugation at 6000 g for 10 min at 4 °C and washed in the sodium phosphate buffer described in Section 2.2.3.1.

Cell extract, was prepared as described for Hho1p (Section 2.2.3.1), and the Hho1p linker domain was extracted with a final concentration of 5% (v/v) PCA for 10 min with stirring on ice. The precipitated proteins were collected by

centrifugation at 10000 g for 10 min at 4 °C and the supernatant was immediately neutralised with triethanolamine before dialysis overnight at 4 °C against buffer A (Section 2.2.3.2).

The sample was filtered through a 0.2 μ m membrane (Millipore) and about 2.5 mg protein was loaded onto a Mono S cation-exchange column (GE Healthcare), which had been pre-equilibrated with buffer A. (The protein concentration was assessed by absorbance at 230 nm using a coefficient ($\epsilon = 15130$) determined using amino acid analysis data (Section 2.2.4.2). The bound proteins were eluted over a 50-column-volume linear gradient from buffer A to 60% buffer B (Section 2.2.3.2). The fractions were analysed by SDS/20%-PAGE (as Section 2.2.4.1, except that the gels were not fixed before staining) and those fractions containing pure linker domain were combined. The sample was concentrated in a Vivaspin 2 concentrator with a 3 kDa cut-off and buffer exchanged into 10 mM sodium phosphate pH 6.0, 1 mM EDTA, 1 mM DTT.

5.2.3 Phosphorylation of Hho1p and Hho1p-truncation proteins

Phosphorylation was carried out using recombinant CDK2/cyclin A. This was expressed and purified by Dr Rebecca Michael (Department of Biochemistry, Cambridge) using plasmids pET12d cyclin A-3 and pGex3C CDK2 from Dr Tim Hunt (Cancer Research UK, Clare Hall Laboratories, South Mimms).

For small-scale phosphorylation reactions protein samples (Hho1p, GI, GII, NGIL and LGII) were prepared at 50 μ M in 20 mM Tris-HCl pH 7.5, 10 mM MgCl₂, 5 mM ATP. CDK2/cyclin A (8 μ l/ml) was added and the sample was incubated at 30 °C for 16 h. Residual ATP was removed by buffer exchanging the proteins into buffer A (Section 2.2.3.2) using a Vivaspin 2 concentrator with an

appropriate molecular weight cut-off (MWCO used: Hho1p, 10 kDa; GI and GII, 3 kDa; NGIL and LGII, 5 kDa).

For large-scale phosphorylation of the linker domain NMR sample, the linker domain was phosphorylated at 260 μ M in 50 mM Tris-HCl pH 7.5, 10 mM MgCl₂ and 25 mM ATP. CDK2/cyclin A (20 μ l/ml) was added and the sample incubated at 30 °C for 14 h. The sample was buffer exchanged into 10 mM sodium phosphate pH 6.0, 1 mM EDTA, 1 mM DTT.

5.2.4 HEPES/Histidine gel-electrophoresis

HEPES/Histidine gels were run as described by (Paulson et al., 1992).

The HEPES/Histidine gels contained 10% (v/v) polyacrylamide and the running buffer contained 12 g/l HEPES and 30 g/l L-histidine. Protein samples (0.15 nmol of Hho1p, GI, GII, NGIL and LGII, or 2.6 nmol of the linker domain) in buffer A (Section 2.2.3.2) or 10 mM sodium phosphate pH 6.0, 1 mM EDTA, 1 mM DTT were incubated for 5 min at 37 °C in an equal volume of HEPES/Histidine loading buffer (125 mM N-Cyclohexyl-2-aminoethanesulphonic acid pH 9.0, 480 mg/ml urea, 10 mg/ml cysteamine hydrochloride, 1 mg/ml pyronine Y). Gels were stained and destained as described for SDS/18%-PAGE (Section 2.2.4.1).

5.2.5 DNA cellulose assay

DNA cellulose (0.05 g per sample: Sigma-Aldrich) was pre-equilibrated with “no salt buffer” (10 mM Tris-HCl pH 7.5, 1 mM EDTA, 1 mM DTT, 15 μ g/ml bovine serum albumin (BSA: PAA laboratories)). Protein samples (Hho1p, GI, GII, NGIL and LGII: 20 μ g in 0.5 ml “no salt buffer”) were incubated with the DNA cellulose for 2 h at 4 °C, turning end on end. The bead suspensions were then

packed into 1 ml plastic columns, run under gravity, the flow-through collected and the columns washed with 0.5 ml “no salt buffer”. The columns were washed with “no salt buffer” (see above) supplemented with increasing concentration of NaCl (100, 150, 200, 250, 300, 350, 400, 450, 500, 550, 600, 650, 700, 800 or 1000 mM: 2x 0.5 ml washes for each NaCl concentration). The wash fractions were collected, precipitated with 25% (w/v) TCA and the pellets washed as described in Section 3.2.4.3. The samples were analysed by SDS/18%-PAGE (Section 2.2.4.1) and densitometry of the Coomassie-stained protein bands. The BSA in the buffers was used to normalise the amount of Hho1p-related protein in the lanes, to account for any protein loss during the TCA precipitation step.

5.2.6 Four-way junction DNA gel-shift assay

5.2.6.1 Synthesis of four-way junction DNA

The 15 bp-arm four-way junction DNA was assembled from four 30 bp oligonucleotides, as described (Webb and Thomas, 1999). The oligonucleotides used for this four-way junction are listed in Table 5.2.

Table 5.2: Four-way junction DNA oligonucleotides

Oligonucleotide	Sequence
Strand 1:	5'-GAATTCAGCACGAGTCCTAACGCCAGATCT-3'
Strand 2:	5'-AGATCTGGCGTTAGGTGATACCGATGCATC-3'
Strand 3:	5'-GATGCATCGGTATCAGGCTTACGACTAGTG-3'
Strand 4:	5'-CACTAGTC GTAAGCCACTCGTGCTGAATTC-3'

Junctions were formed by incubating equimolar amounts of the four strands in TE buffer (Section 3.2.4.7) at 95 °C for five min and cooling slowly to 4 °C. The concentration of the labelled four-way junction was determined from the absorbance at 260 nm. Assembly of the junction was checked by 8%-PAGE in 0.3x TBE buffer (Section 3.2.6.2).

5.2.6.2 Gel-shift assays with four-way junction DNA

Samples (20 μ l) contained 10 mM Tris-HCl pH 7.5, 50 mM NaCl, 6% (v/v) glycerol, 100 pmol four-way junction DNA and either 0, 50, 100, 150 or 200 pmol of the proteins (Hho1p, NGIL or LGII). The samples were incubated for 30 min at 25 °C and analysed by 8%-PAGE in 0.3x TBE (Section 3.2.6.2).

5.2.7 Sucrose gradient assay for binding of Hho1p and Hho1p-truncation proteins to chromatin

Linear sucrose gradients (12 ml) were poured containing 10 mM sodium phosphate pH 7.0, 1 mM EDTA, 0.25 mM PMSF and 5-30% sucrose. Gradients were allowed to settle for 2 h at 4 °C. One A_{260} unit (equivalent to about 0.5 nmol of core nucleosomes) of medium-length H1,H5-depleted chromatin (Section 3.2.4.4) was incubated with Hho1p, NGIL or LGII for 30 min on ice in 10 mM sodium phosphate pH 7.0, 1 mM EDTA and 0.25 mM PMSF (100 μ l total volume). Input samples (1/10 volume) were set aside at 4 °C and the rest was layered onto the gradients. Centrifugation was carried out at 22400 rpm in a Beckman SW40 rotor for 16 h at 4 °C. No braking was used to avoid disturbing the gradients. Gradients were fractionated and about 0.2 A_{260} units analysed by SDS/18%-PAGE (Section 2.2.4.1) following two rounds of 25% TCA precipitation to remove the sucrose (Section 3.2.4.3).

5.2.8 NMR studies of the ^{13}C , ^{15}N -labelled linker domain of Hho1p

All NMR experiments were recorded by Dr K. Stott (Section 2.2.5).

^{13}C , ^{15}N -linker domain NMR experiments were carried out at 273 K on proteins at about 2 mM in sodium phosphate buffer (Section 5.2.2.2), supplemented with 10% (v/v) $^2\text{H}_2\text{O}$. Following the phosphorylation reaction (Section 5.2.3) the linker domain was concentrated and buffer exchanged back into the sodium phosphate buffer.

Chemical shift deviations from random coil (Section 2.2.5.2), heteronuclear NOE experiments (Section 2.2.5.3) and changes in chemical-shift measurements (Section 2.2.5.4) were carried out as described previously. Additionally, changes in chemical-shifts of the C^β resonances and peak loss upon phosphorylation were also measured using Analysis (Section 2.2.5) and analysed using Microsoft Excel.

The temperature-dependence of amide proton shifts (Baxter and Williamson, 1997) was obtained from ^1H - ^{15}N HSQC spectra recorded at 273, 278, 288 and 298 K. Amide proton shifts were measured using Analysis (Section 2.2.5) and analysed using Microsoft Excel. Proton shifts were fitted to a linear function and the gradient taken as the measure of temperature-dependence. Errors were obtained from the estimated covariance matrix (Vranken et al., 2005), producing error values that are analogous to standard deviations.

5.2.9 DNA sequencing

DNA sequencing was carried out by Mr John Lester (DNA Sequencing Facility, Department of Biochemistry, University of Cambridge) using an Applied Biosystems 3730xl DNA Analyser.

5.3 Results

As yet, the *in vivo* post-translational modifications of Hho1p are not fully known. To investigate this, efforts were made to extract Hho1p from yeast cells for study using mass spectrometry. In my hands, Hho1p could not be enriched from yeast whole-cell extract using 5% perchloric acid (PCA) extraction (as used for canonical linker histones), salt extraction (as used by Srebrevna et al. (1987)), or affinity purification using anti-Hho1 antibody (data not shown). A 1% PCA extract produced soluble Hho1p, however other proteins also remained soluble and Hho1p levels were too low to allow further purification (data not shown).

Being unable to determine Hho1p post-translational modifications *de novo* I searched the literature for proteomic post-translation modification studies mentioning Hho1p. One study reported phosphorylation events at a serine in the linker domain and at two serines in the start of the GII domain, with one more potential site also in the GII domain (Li et al., 2007). Therefore I determined to investigate the *in vitro* phosphorylation of Hho1p.

5.3.1 Phosphorylation of Hho1p and Hho1p-truncation proteins by CDK2/Cyclin A

Casein Kinase II (NEB), Calmodulin-Dependent Protein Kinase II (NEB) and Cyclin-Dependent Kinase 2-Cyclin A (recognition motifs: SXXE/D, RXXS/T and S/TPXR/K respectively) were tested for their ability to phosphorylate full-length Hho1p *in vitro* (data not shown). CDK2/Cyclin A was most efficient and was used to phosphorylate Hho1p and a variety of Hho1p-truncation proteins (Figure 5.1). Figure 5.2 shows a HEPES/Histidine gel containing the protein samples before and after CDK2/Cyclin A treatment, and mass spectrometry indicating the number of phosphorylation events that occurred.

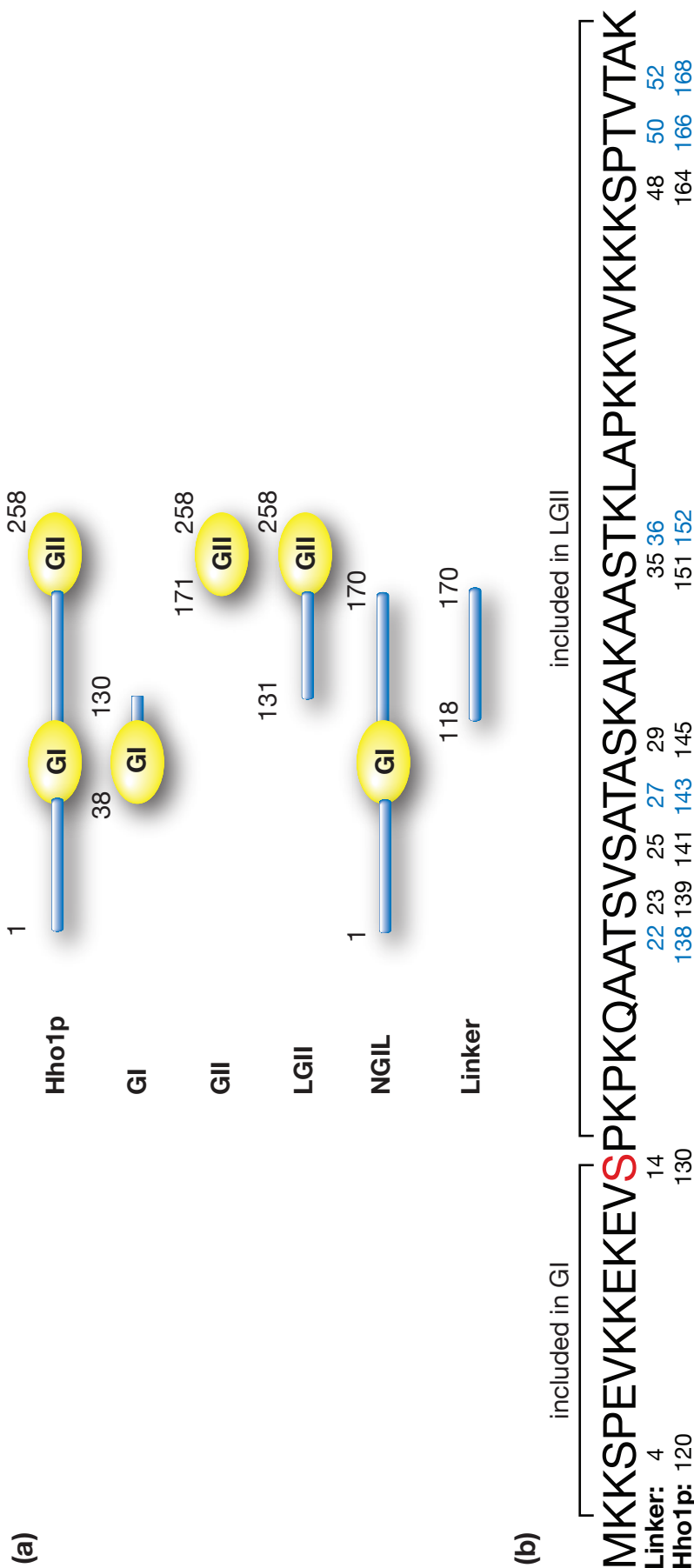


Figure 5.1 Hho1p and Hho1p-truncation proteins used in this Chapter. (a) Schematics indicating the domain structure of Hho1p and Hho1p-truncation proteins, with residue numbers corresponding to the full-length protein. The GI domain contains a few of the unstructured linker residues at its C-terminus and LGII is missing some linker residues at the N-terminus, because the original domain boundaries were determined by trypsin digestion (Ali and Thomas, 2004). (b) The protein sequence of the linker domain, as cloned into pET17b-HHO1-linker, containing all the unstructured residues between the GI and GII domains as determined by NMR studies (Ali *et al.*, 2004). The residue numbers of the serine and threonine (blue) residues are indicated and the serine that was seen to be phosphorylated *in vivo* by Li *et al.* (2007) is marked in red. It should be noted that two serine residues in this linker are also contained in the original GI protein (residues 120 and 130) and therefore absent from the LGII protein.

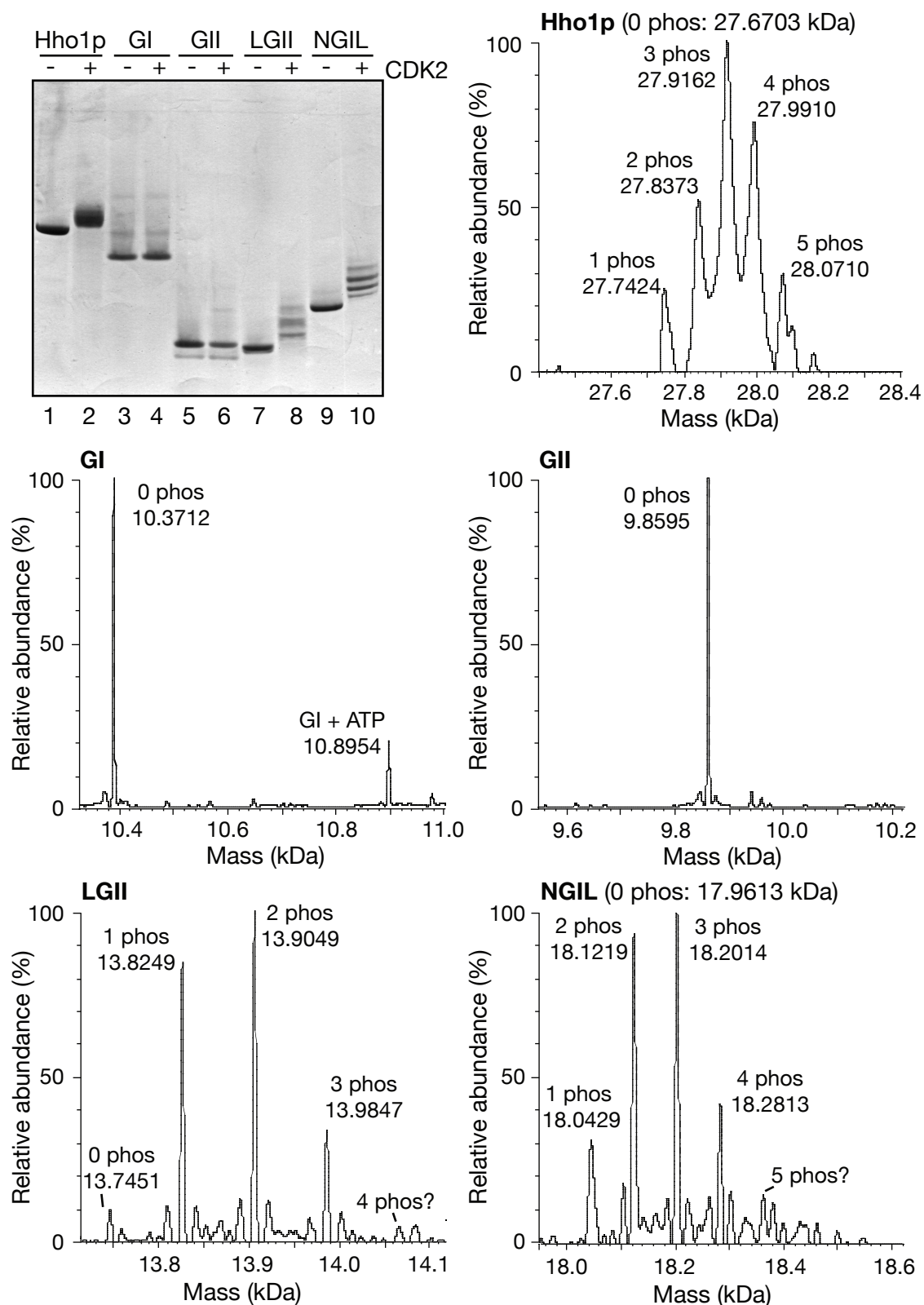


Figure 5.2 Phosphorylation of Hho1p and Hho1p-truncation proteins using CDK2/Cyclin A. HEPES/Histidine/10%-PAGE of the indicated proteins before and after treatment with CDK2/Cyclin A. Each lane contains 0.15 nmol protein. ESI-TOF mass spectrometry of the proteins following treatment with CDK2/Cyclin A. The labelled peaks are the mass of the unmodified domain plus a multiple of about 80 Da, indicating the number of phosphorylation events that have occurred.

Neither the isolated GI nor GII domains are phosphorylated, although some of the GI domain bound ATP. According to the proteomic data of Li and colleagues (2007) the GII domain is phosphorylated *in vivo*, indicating this may require a different kinase or greater sequence context than supplied by the isolated GII domain. NGIL contains the same number of phosphorylation events as full-length Hho1p, supporting the observation that the GII domain is not phosphorylated by this kinase. Therefore, the data suggest that the majority of the phosphorylation events happen in the linker domain (3 or 4 sites), while the N-terminal tail is phosphorylated once or twice.

5.3.2 Effect of phosphorylation on the interaction of Hho1p and domain deletion mutants with DNA and chromatin

The effect of phosphorylation on the binding of full-length Hho1p, NGIL and LGII to DNA and chromatin was studied. (The isolated globular domains were not studied because they were not phosphorylated by CDK2/Cyclin A). Initially interaction with DNA-cellulose was investigated. Unmodified and phosphorylated forms of each protein were bound to DNA-cellulose and washed with buffers containing increasing concentrations of sodium chloride (Figure 5.3). Densitometry analysis indicated that the phosphorylated form of each protein eluted at lower concentrations of salt than the unmodified version, demonstrating that phosphorylation reduces the affinity of these proteins for linear DNA. The effect of phosphorylation is small for all the proteins, probably because the change in net charge is small. It is not clear why a larger decrease in affinity for DNA-cellulose is seen upon phosphorylation of Hho1p compared with NGIL.

Binding of the proteins to four-way junction DNA, which mimics the nucleosome dyad, was studied in electrophoretic mobility shift assays (Fig-

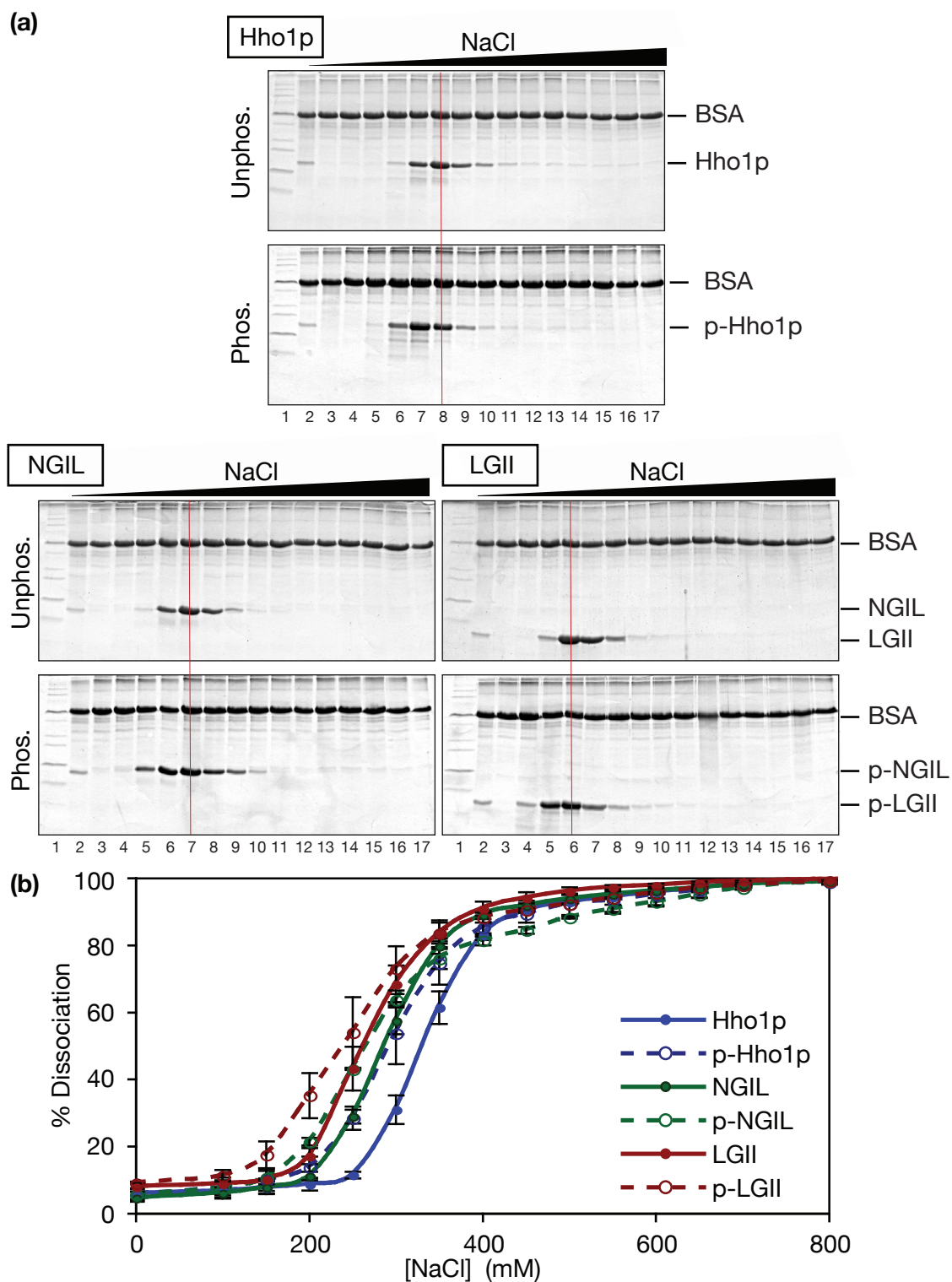


Figure 5.3 Effect of phosphorylation on the dissociation of Hho1p and Hho1p-truncation proteins from DNA-cellulose with increasing concentration of NaCl. **(a)** SDS/18%-PAGE of samples eluted from DNA-cellulose with increasing NaCl concentrations (0, 100, 150, 200, 250, 300, 350, 400, 450, 500, 550, 600, 650, 700, 800, 1000 mM NaCl, lanes 2-17). Vertical lines indicate the peak fractions of the unphosphorylated protein. **(b)** The dissociation of the samples with increasing NaCl washes, as measured by densitometry of the Coomassie-stained gels in (a) and normalised with respect to BSA. Error bars are \pm one standard error ($n=2$).

ure 5.4). Hho1p appears to preferentially bind two molecules of four-way junction DNA, as the higher band occurs even when the input ratio of Hho1p to four-way junction is less than one. As the concentration of Hho1p is increased a band corresponding to one Hho1p per DNA molecule is formed for unphosphorylated Hho1p, although a discrete product of this size is not formed with phosphorylated Hho1p. At an input ratio of two Hho1p per DNA molecule the samples precipitate. Densitometry analysis of the gel indicates that phosphorylation increases the affinity of Hho1p for four-way junction DNA (Figure 5.4b). The affinity of NGIL for four-way junction DNA also increases upon phosphorylation. The gel-shift assay indicates that phosphorylation promotes the formation of complexes containing two NGIL molecules and one DNA molecule, compared with unphosphorylated NGIL. The story is less clear for LGII as the bands produced are less well defined. The densitometry indicates that the affinity of LGII for four-way junction DNA is reduced upon phosphorylation, while the gel suggests that phosphorylation promotes the solubility of species containing more than one LGII molecule. The differential effect of phosphorylation upon binding of Hho1p, NGIL and LGII shows that there is a more complex effect on the proteins than simply the addition of negative charge, which would be expected to reduce the affinity for DNA.

Phosphorylation had no effect on the binding of Hho1p, NGIL or LGII to chromatin in a sucrose gradient binding assay (Figure 5.5). All of the proteins remained bound to chromatin, independent of their phosphorylation state, indicated by the absence of linker histone at the top of the gradient (lanes 10). The LGII band runs at the same size as the H3/H2B band, however the absence of LGII in the top fraction indicates that it is bound to the chromatin. All the linker histone remained associated with the chromatin in assays containing 50 and 80 mM sodium chloride also (data not shown).

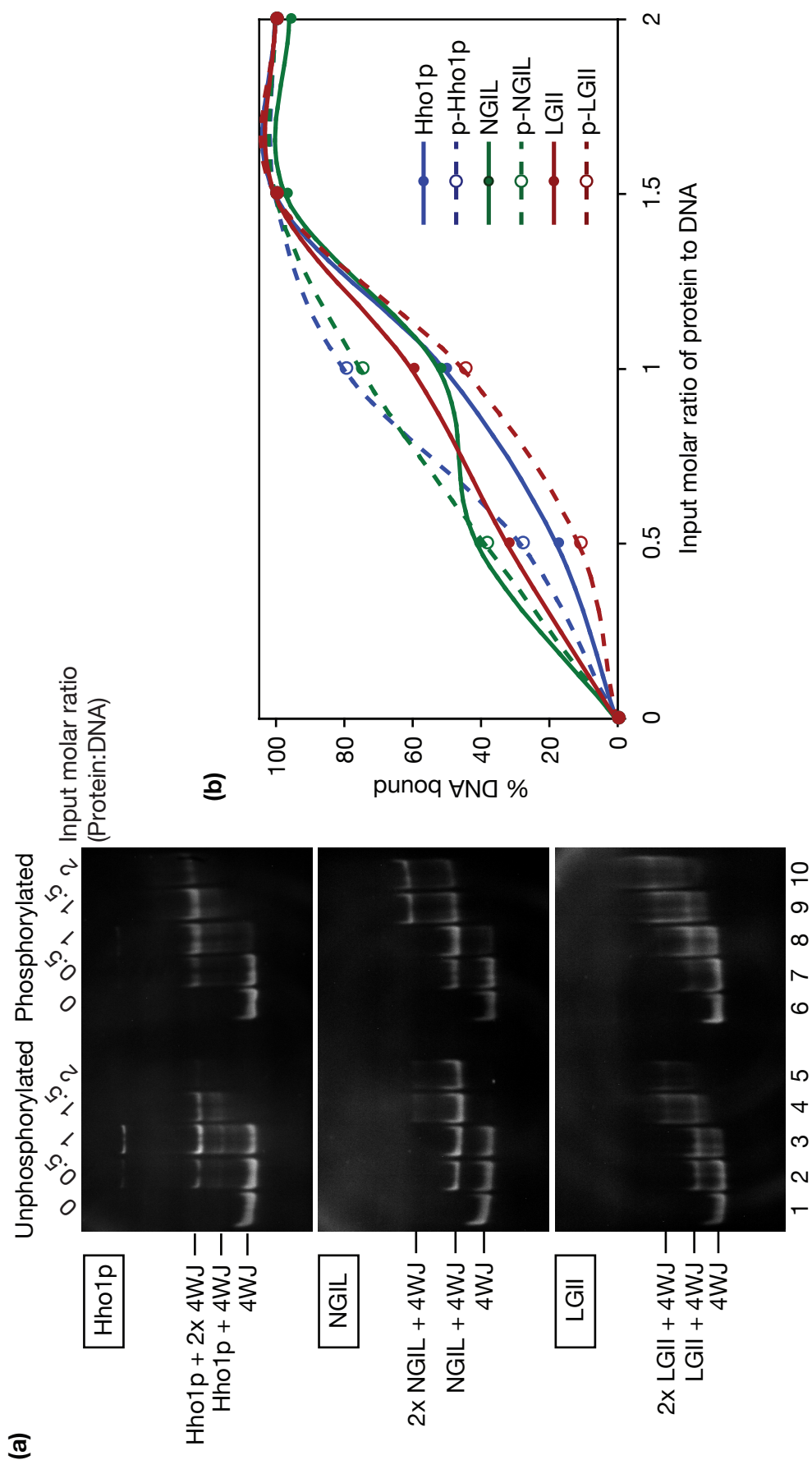


Figure 5.4 Effect of phosphorylation on Hho1p and Hho1p-truncation proteins binding to four-way junction DNA. (a) 8%-PAGE containing 0.3x TBE showing 15 bp-arm four-way junction DNA bound by the indicated proteins. **(b)** The percentage of DNA bound by protein, as measured by densitometry of the gel in (a).

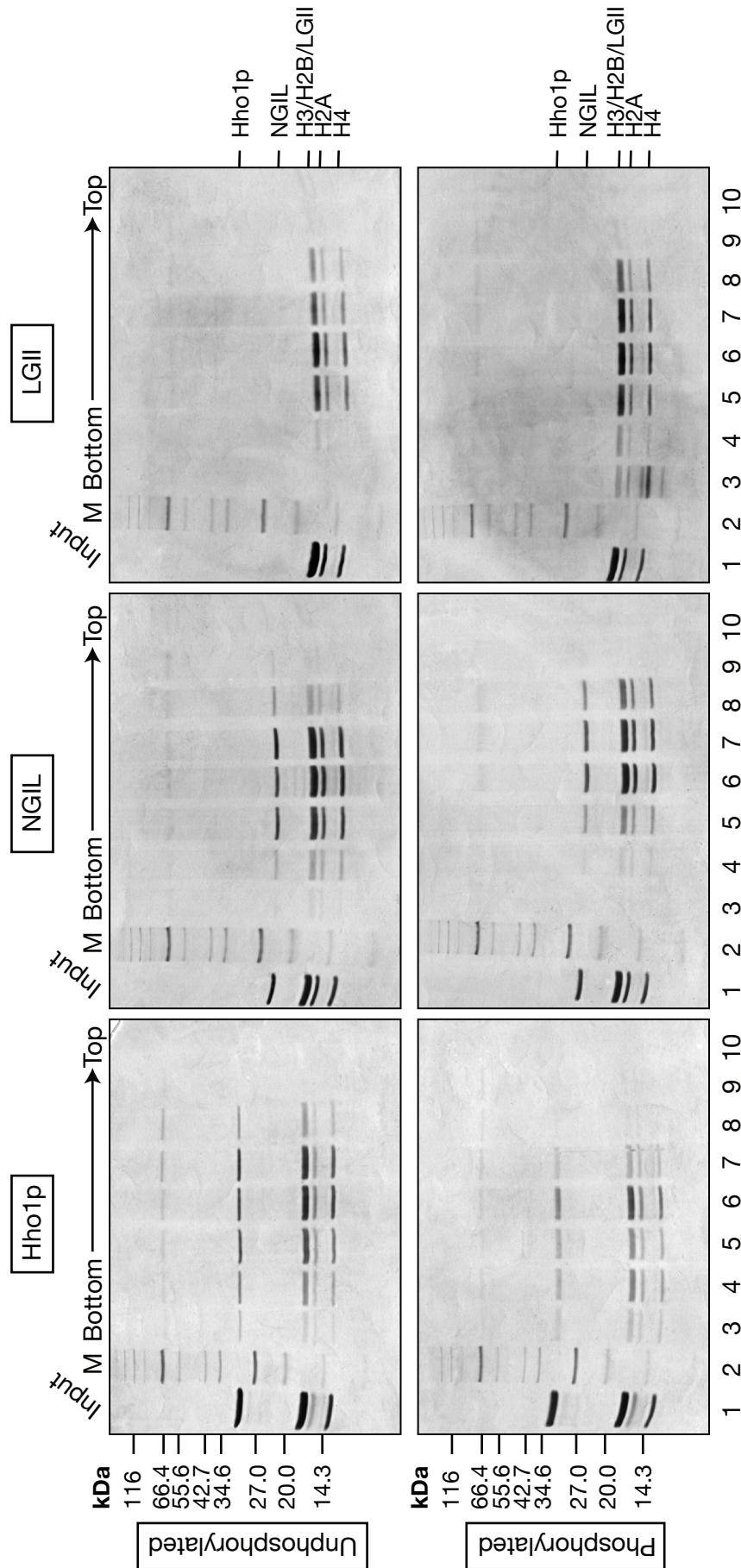


Figure 5.5 Phosphorylation has no effect on affinity of Hho1p and Hho1p-truncation proteins for chromatin in sucrose gradient assays. SDS/18%- PAGE of Hho1p, NGIL and LGII, pre-incubated with stripped chicken erythrocyte chromatin and separated in 5–30% sucrose gradients. The input ratio was about one linker histone molecule per core nucleosome. Lanes 1 contain input sample; lanes 2, protein molecular weight markers. Lanes 3–10, fractions from the bottom to top of the sucrose gradient as indicated.

5.3.3 Structural effects of phosphorylation on the linker domain of Hho1p

5.3.3.1 Predicted structural character of the linker domain of Hho1p

The majority of phosphorylation events by CDK2 on Hho1p appeared to occur in the linker region (Section 5.3.1). The VL3E DisProt Predictor of Intrinsically Disordered Regions suggested that the linker region (in red) is almost entirely disordered (Figure 5.6a) (Peng et al., 2005). Comparison of the disorder prediction for the linker domain in the context of full-length Hho1p and the isolated domain show some differences. This is due to the large input window for the program (15 residues) but implies that the isolated domain may have a slightly different character to that region in the context of the full-length protein. However, the disorder values of both are consistently above 0.9, predicting that they are almost entirely disordered (Figure 5.6b). Secondary structure prediction of the linker domain was carried out using the PSIPRED secondary structure prediction method (Jones, 1999; Bryson et al., 2005). Figure 5.6c indicates α -helix predictions for residues 5–9, 20–35 and 41–44 plus a very short β -strand for residues 51–52. The strongest helix prediction is for residues 30–34, which are predicted with 60% confidence. The predictions for both secondary structure and disorder could be explained if the secondary structure elements were transient or occurred only in specific conditions.

5.3.3.2 Production of the linker domain of Hho1p

The linker domain of Hho1p was cloned into the pET17b plasmid and optimal expression conditions were determined (Figure 5.7). Extraction trials indicated that the linker domain was soluble in 5% PCA and the linker was purified further over a Mono S ion exchange column (Figure 5.8). The linker domain has no

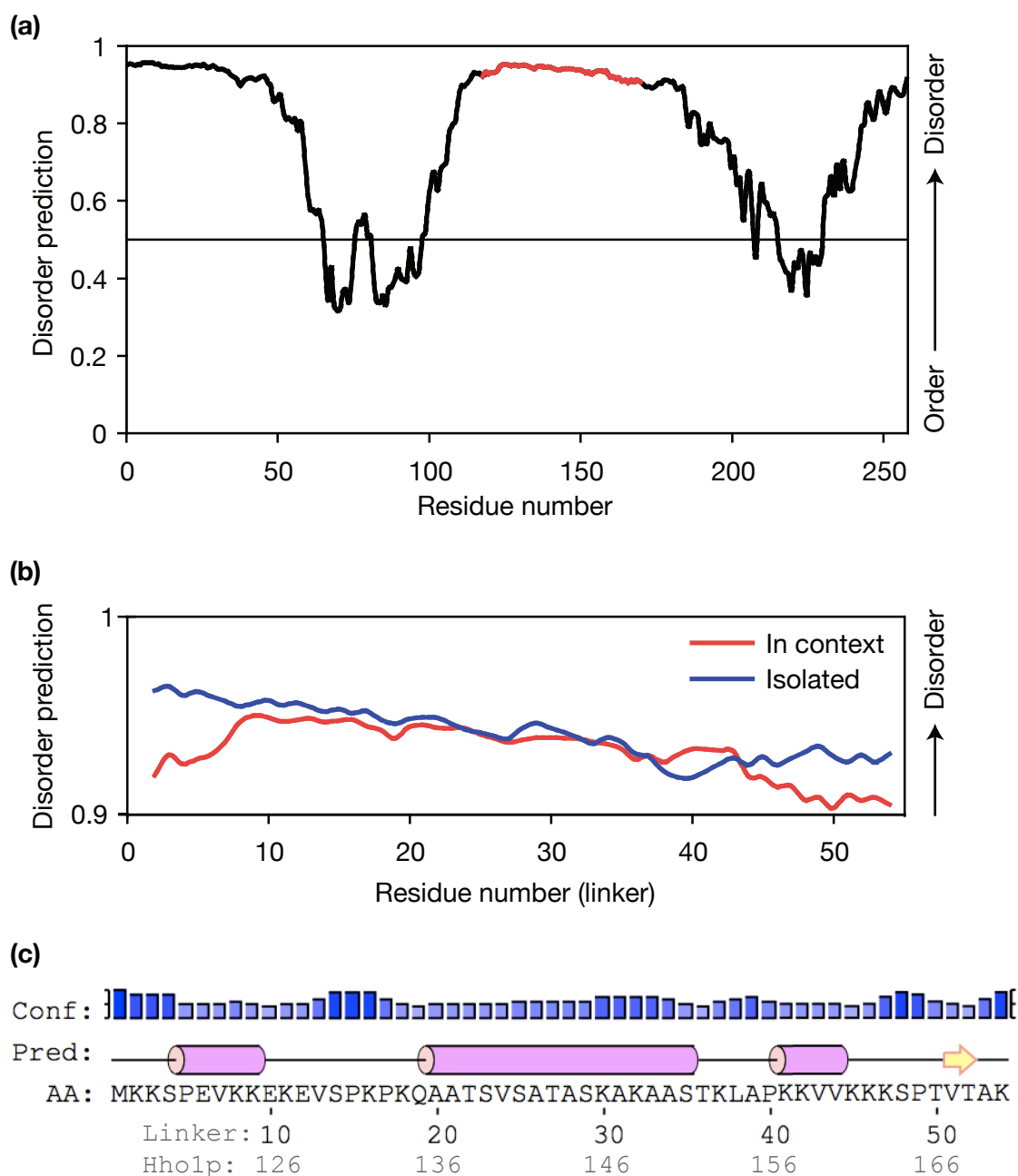


Figure 5.6 Disorder and secondary structure prediction for the linker domain of Hho1p. (a) Disorder prediction for Hho1p as determined by the VL3E DisProt Predictor of Intrinsically Disordered Regions program. Disordered regions take a value of 1 and completely ordered regions a value of 0 (Peng *et al.*, 2005). The linker region is highlighted in red and the high disorder prediction values suggest it is disordered. (b) Comparison of disorder predictions for the linker region when calculated in the context of full-length Hho1p and as an isolated domain. (c) Secondary structure prediction for the linker domain of Hho1p, using the PSIPRED programme v3.0 (Jones, 1999; Bryson *et al.*, 2005). Regions of predicted α -helix are indicated by a pink cylinder and β -strands by yellow arrows. The confidence in the prediction is indicated by the height of the blue bars.

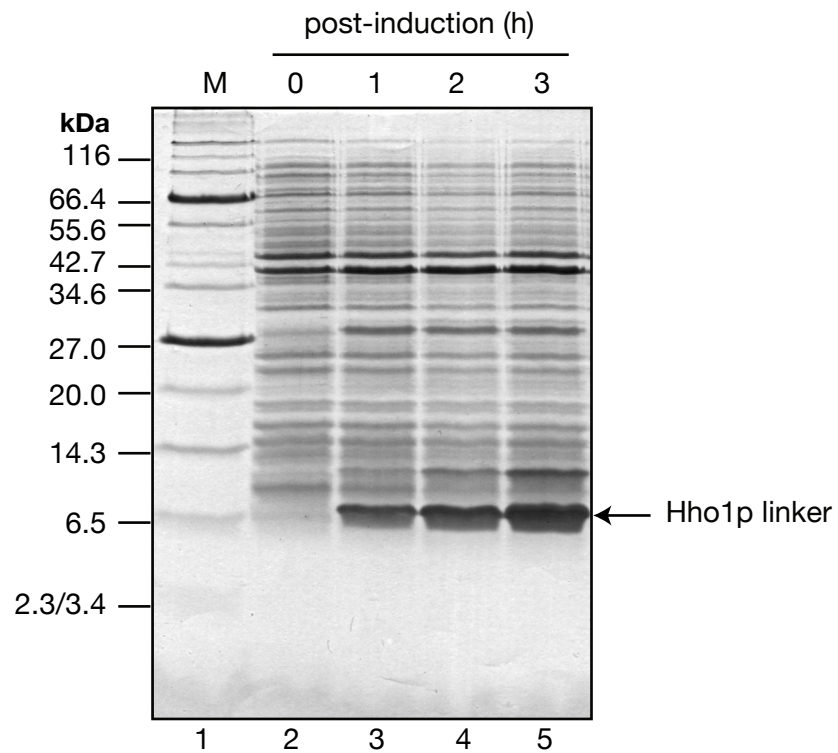


Figure 5.7 Expression of the linker domain of Hho1p. SDS/20%-PAGE containing 0.2 OD₆₀₀ of BL21(DE3) cells transformed with pET17b-HHO1-linker, before induction (lane 2) and at 1, 2 and 3 hours (lanes 3-5) after induction with 1 mM IPTG. Lane 1, protein molecular weight markers.

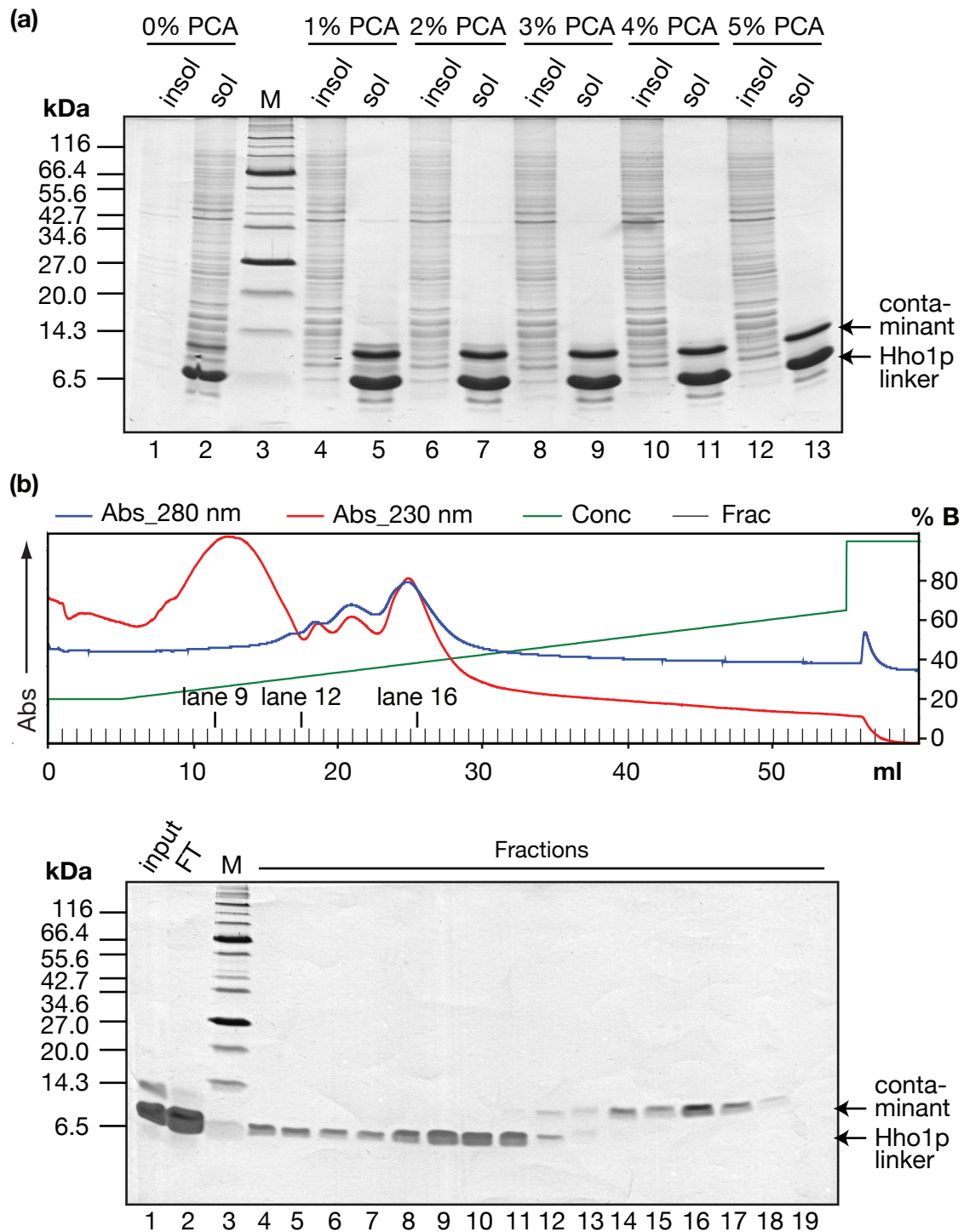


Figure 5.8 Purification of the linker domain of Hho1p. **(a)** SDS/20%-PAGE of cell extract samples, following extraction with the indicated concentration of PCA on ice for 10 minutes. Lanes 1, 4, 6, 8, 10 and 12, insoluble material. Lanes 2, 5, 7, 9, 11, 13, soluble material. Lane 3, protein molecular weight markers. **(b)** Fractionation of 5% PCA-soluble material using a Mono S column. FPLC trace of the elution profile and SDS/20%-PAGE of input, flow-through and elution fraction samples. The fractions in lanes 9, 12 and 16 of the gel are indicated on the elution trace. Lane 3, protein molecular weight markers.

absorbance at 280 nm, but absorbs at 230 nm due to the peptide backbone. A slightly larger contaminant absorbs at both 230 and 280 nm, allowing the elution of these proteins to be followed using the ratio of absorbance at 230 and 280 nm (Figure 5.8b: 0–18 ml, linker; 18–30 ml, contaminant). To allow separation of the linker from the slightly larger contaminant the maximum amount of protein that can be bound to the Mono S column is about 2.5 mg.

5.3.3.3 NMR studies of the linker domain of Hho1p

A $^{13}\text{C},^{15}\text{N}$ -linker sample was produced, using the protocol described above, and NMR spectra were recorded at 600 MHz at 273 K (Figure 5.9). Originally it was planned to record the experiments in a Tris buffer containing 10 mM magnesium chloride, so that the phosphorylation could be followed in real time. This produced spectra with very broad and weak peaks (data not shown) so a magnesium ion-free, sodium phosphate buffer was used (Section 5.2.2.2). HNCA, HNCACB, HN(CO)CA, HN(CO)CACB, HNCO, HNN, HN(C)N and $^1\text{H}-^{13}\text{C}$ HSQC experiments were used to assign the linker domain. The magnetisation transfers for the experiments are shown in Figure 2.6. The 3D HNN/HN(C)N strategy was applied in addition to conventional triple-resonance experiments because it uses two ^{15}N dimensions to produce greater dispersion of unstructured resonances (Section 2.3.3 and Panchal et al., 2001). Triple-resonance and HNN-based experiments were used, to about equal extents, to establish connections along the peptide backbone. The following percentages of resonances were assigned: N (95.9%), H^{N} (95.9%), H^{α} (57.4%), C' (97.9%), C^{α} (98.1%) and C^{β} (98.1%). The resonances for Ser4 and Ser48 overlapped entirely (these are Ser120 and Ser164 in full-length Hho1p; see Figure 5.1b). See Appendix B for the resonance list of the linker domain of Hho1p.

Shift deviations from random coil were measured for C' , C^{α} , H^{α} , H^{N}

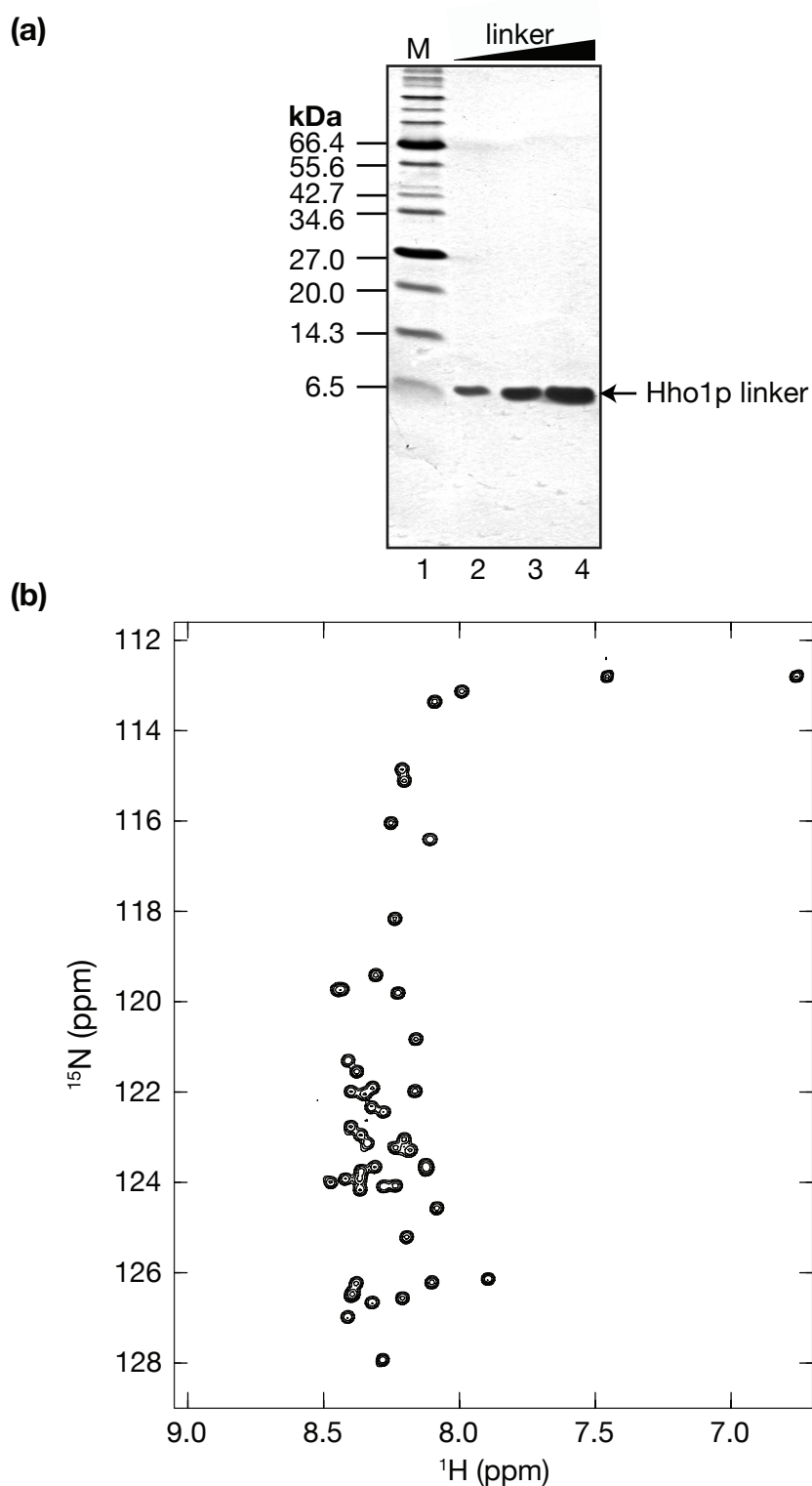


Figure 5.9 NMR spectroscopy of the linker domain of Hho1p. (a) SDS/20%-PAGE of the ^{13}C , ^{15}N -labelled linker domain NMR sample. Lane 1, molecular weight markers. (b) ^1H - ^{15}N HSQC spectrum of ^{13}C , ^{15}N -linker, recorded at 600 MHz at 273 K in 10 mM sodium phosphate buffer at pH 6.0.

and N resonances. There are systematic shifts in values from zero because the chemical shift reference data were acquired at a much higher temperature than that used in this study. The resonances showed small deviations from sequence context-dependent random coil NMR shifts (Schwarzinger et al., 2001), indicating there are no fully structured regions in the linker domain (Figure 5.10). However, around residues 24–38 there is a contiguous region of deviations from the C' , C^α and H^N random coil shifts. The H^N values decrease and the C^α and C' values increase for this region (assuming true baselines of around 0.2, -0.2 and 0 respectively) which is characteristic of α -helical character (Wishart et al., 1991). This region overlaps significantly with a region of helix predicted by the PSIPRED method (Figure 5.6c).

The dynamics of the Hho1p linker domain were studied using heteronuclear NOE measurements (Figure 5.11a). All of the $\{^1H\}^{15}N$ NOE measurements are below 0.6, indicating a linker that is dynamic on a picosecond-nanosecond time-scale and therefore contains with little or no stable secondary structure.

Temperature-dependent amide proton chemical shifts are indicators of hydrogen bonding and are shown in Figure 5.11b. As the temperature of a sample is increased the magnitude of thermal fluctuations rises, resulting in increased distances between atoms. This results in up-field shift of the amide proton resonances in α -helices as they move towards their random coil values. Those residues that are hydrogen-bonded are less susceptible to temperature-dependent structural changes, which is reflected in smaller up-field shifts. If a temperature-dependent amide proton shift is less negative than -4.5 ppb/K it is considered to be stably hydrogen-bonded (Baxter and Williamson, 1997). None of the amide proton shifts is above -4.5 ppb/K, indicating there are no stable hydrogen bonds within the linker domain. This suggests that none of

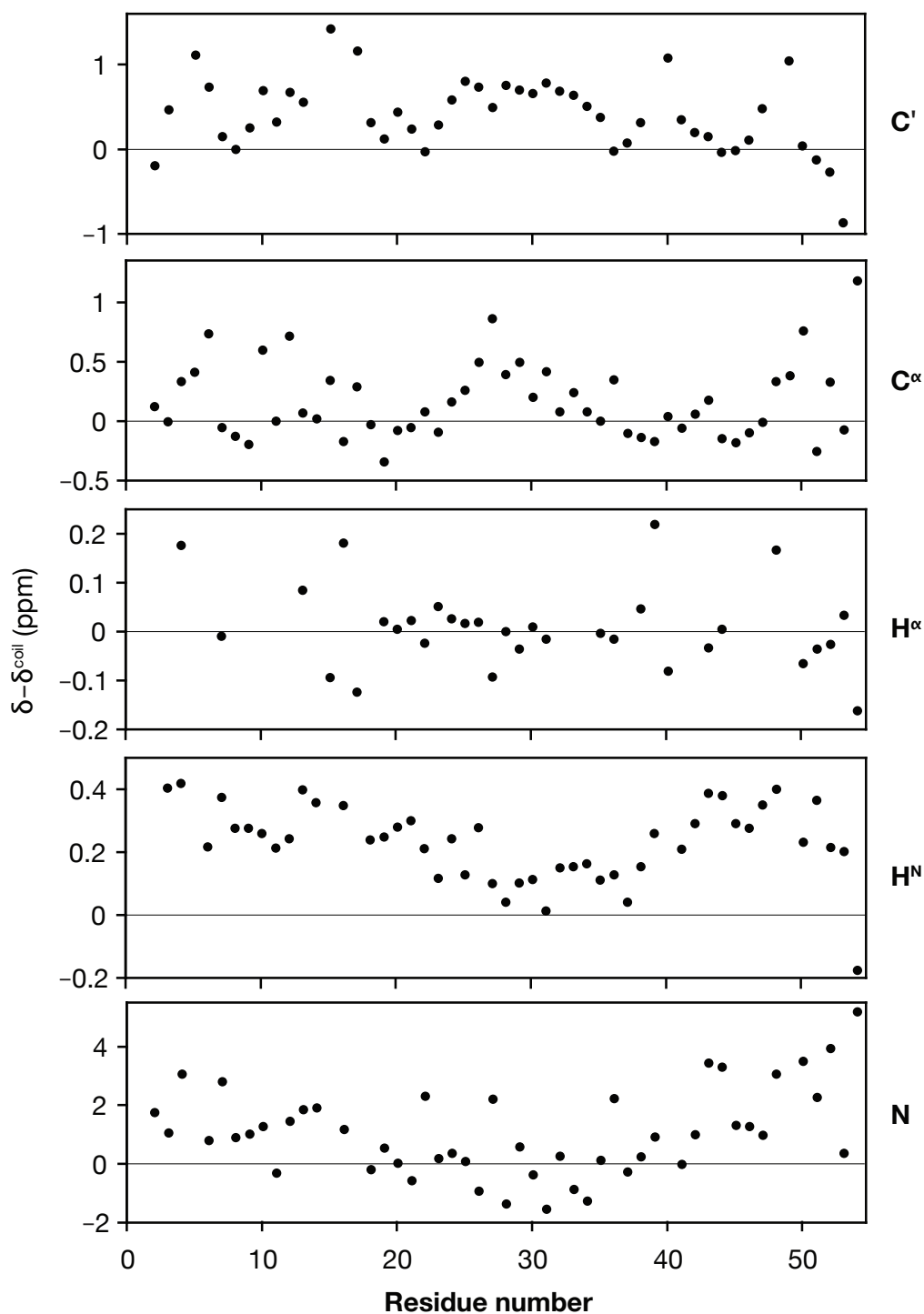


Figure 5.10 Shift deviations from random coil for the linker domain of Hho1p. C', C^α, H^α, H^N and N nuclei chemical shift deviations from random coil, corrected for sequence context (Schwarzinger *et al.*, 2001). A region with small but consistent deviations from the random coil shifts is apparent around residues 25-35 in the C', C^α and H^N panels. The true baselines are offset from zero because these experiments were recorded at much lower temperatures than the random coil values.

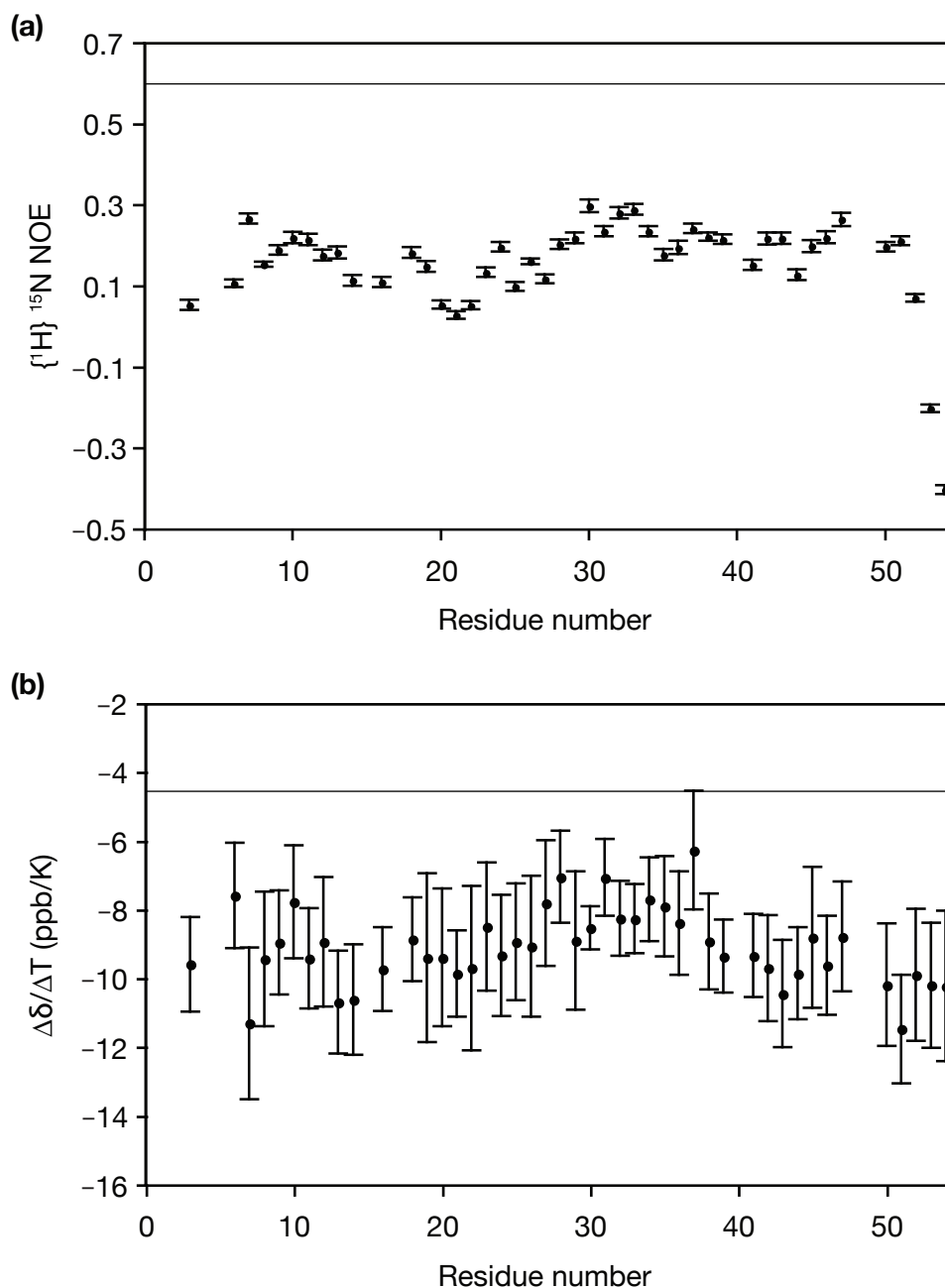


Figure 5.11 Analysis of the dynamics of the linker domain of Hho1p. (a) Heteronuclear NOE measurements are below 0.6, indicating a broadly dynamic linker domain, although the region between residues 25 and 35 does have slightly higher NOE values. (b) Temperature dependence of amide proton chemical shifts, obtained from ^{15}N -HSQC spectra acquired at 273, 278, 288 and 298 K. Values are more negative than -4.5 ppb/K, indicating that none of the amide protons is stably hydrogen-bonded (Baxter and Williamson, 1997).

the predicted helices (Figure 5.6c) is fully formed in the isolated linker domain. Despite these general characteristics, the data show slight increases in $\{^1\text{H}\}^{15}\text{N}$ NOEs and amide proton shifts for the region around residues 24–38, demonstrating that this region is slightly less dynamic than the rest of the linker. This is in line with the chemical shift deviation data in Figure 5.10.

5.3.3.4 The linker domain of Hho1p is phosphorylated at Ser4, Ser14 and Thr27 by CDK2/Cyclin A

The double-labelled linker sample was phosphorylated using CDK2/Cyclin A and the product analysed in HEPES/Histidine gels and by mass spectrometry (Figure 5.12). Only a proportion of the linker is shifted in the gel, suggesting only partial phosphorylation, however the mass spectrometry indicates that all of the linker domain is phosphorylated at least once. The phosphorylation could not be taken to completion; a mixture of phosphorylation states persisted with one, two or three phosphorylation events per molecule of linker domain.

The phosphorylated sample was used to record a $^1\text{H}^{15}\text{N}$ -HSQC spectrum at 600 MHz and 273 K (Figure 5.13a). There are a number of differences between this and the unphosphorylated $^1\text{H}^{15}\text{N}$ -HSQC spectrum, suggesting that there may be multiple phosphorylation events and potentially widespread changes in structural character of the linker domain upon phosphorylation. Of particular interest are the three new peaks that have appeared outside the “random coil region” (8.0–8.5 ppm proton resonance) (Figure 5.13a). Prior to the assignment of the phosphorylated species (see below) it was assumed that these peaks are likely candidates for phosphorylation sites, as three phosphorylation events were seen in the mass spectrometry data (Figure 5.12).

Aside from these peaks, some peaks shift and some peaks attenuate and a new peak appears. Therefore the phosphorylated species was assigned *ab ini-*

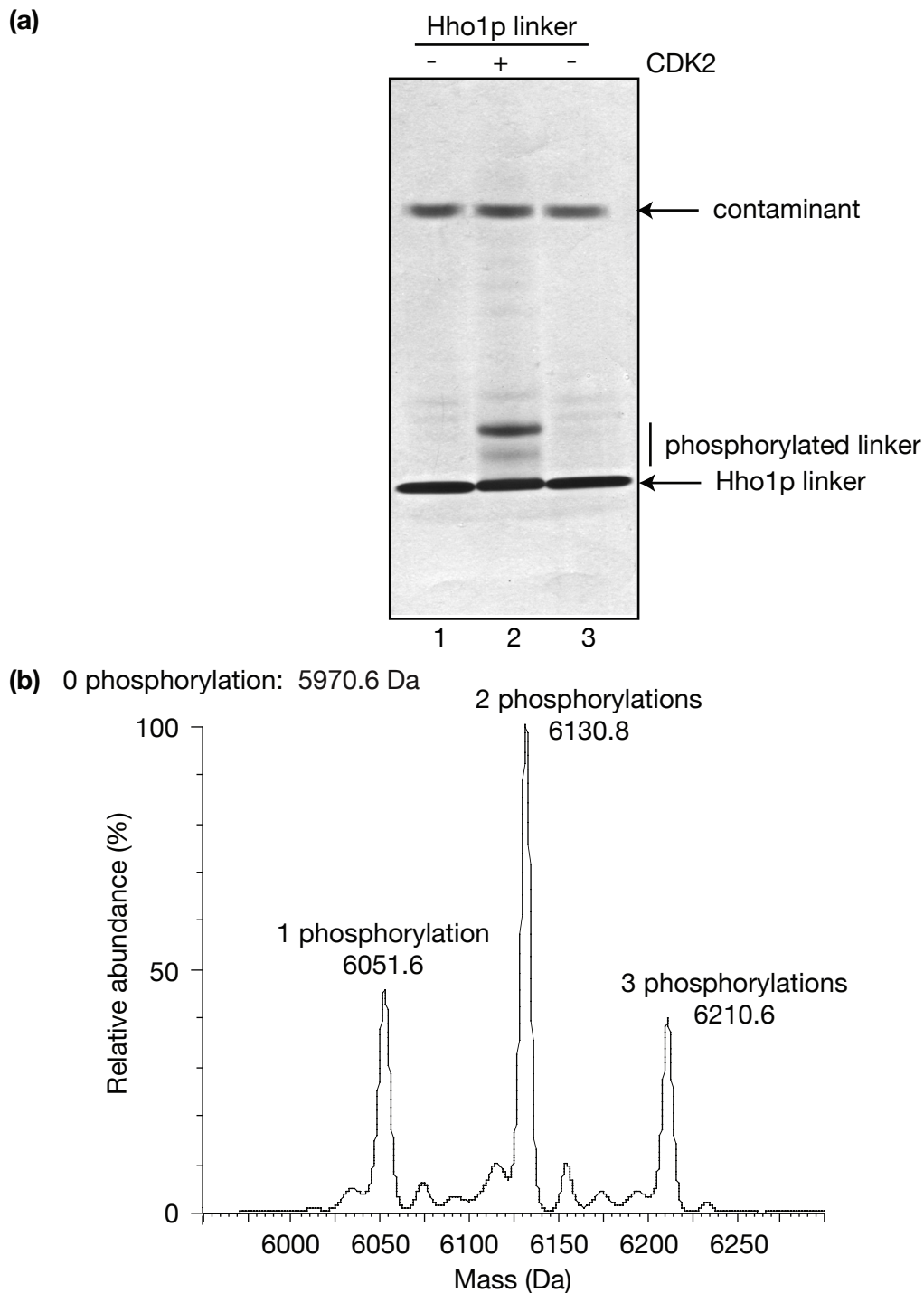


Figure 5.12 Phosphorylation of the linker domain of Hho1p. **(a)** HEPES/Histidine/10%-PAGE of linker domain of Hho1p before and after treatment with CDK2/Cyclin A. Each lane contains about 2.6 nmol protein. The linker domain stains relatively poorly with Coomassie blue, compared with the similar-sized contaminant. Amino acid analysis indicated the linker is in great excess over the contaminant. **(b)** ESI-TOF mass spectrometry of the linker domain following treatment with CDK2/Cyclin A. The peaks indicated are equivalent to the unmodified linker domain plus a multiple of about 80 Da, indicating the number of phosphorylation reactions. All of the linker has been phosphorylated at least once, although a large proportion shows no change in gel mobility in (a).

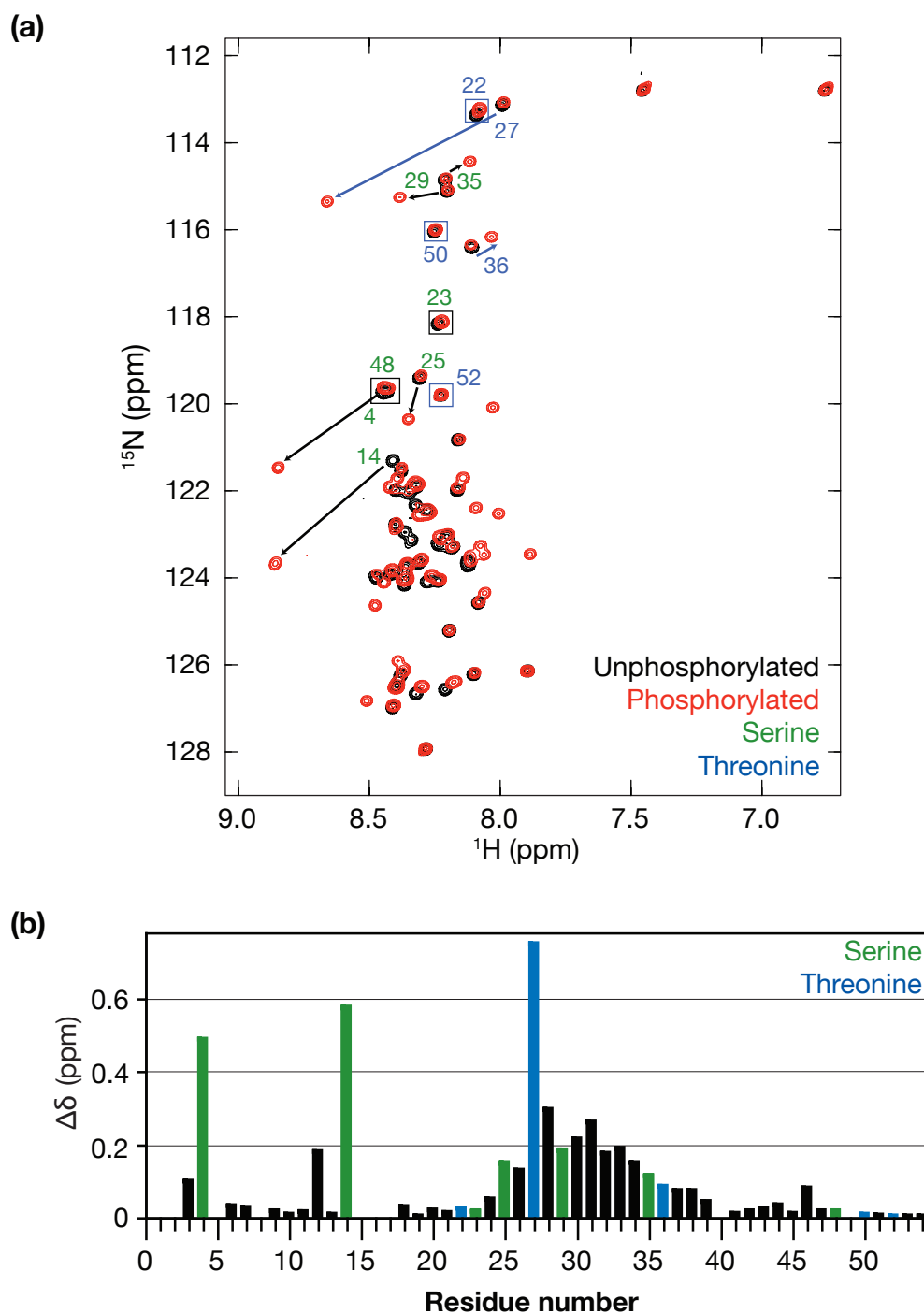


Figure 5.13 NMR peak shifts upon phosphorylation of the linker domain of Hho1p. (a) ^1H - ^{15}N HSQC spectra of ^{13}C , ^{15}N -linker and phosphorylated ^{13}C , ^{15}N -linker indicating movement of the serine (green) and threonine (blue) peaks upon phosphorylation. (b) Combined chemical-shift distances in the ^1H - ^{15}N HSQC spectra upon phosphorylation.

tio using HNCA, HNCACB, HN(CO)CA, HN(CO)CACB, HNCO, HNN, HN(C)N, HBHA(CBCACO)NNH and ^1H - ^{13}C HSQC experiments. The new peaks were assigned as if full phosphorylation had occurred. The sites of phosphorylation were assumed not to interact, based on the lack of “doubling” of the new peaks. This was proved correct as all of the new peaks could be accounted for by a single phosphorylated species. Assignment was achieved through sequential steps along the backbone, using the triple-resonance experiments and HNN-based experiments to establish connectivity to about equal extents. The following percentages of resonances were assigned: N (95.9%), H^{N} (95.9%), H^{α} (55.6%), C' (97.9%), C^{α} (98.1%) and C^{β} (98.1%). See Appendix C for the resonance list of the phosphorylated linker domain of Hho1p.

Upon phosphorylation peak duplication occurred for 17 residues: Ser4, Glu6, Ser14, Val24, Ser25, Thr27, Ala 28, Ser29, Lys30, Ala31, Lys32, Ala33, Ala34, Ser35, Thr36, Lys37 and Leu38. In each case there was one peak very close to that in the unphosphorylated linker spectrum and another peak that was assigned as the phosphorylated form. Duplication of peaks was seen due to the incomplete phosphorylation of the sample (Figure 5.12). The “additional” resonances assigned to Ser4 showed no overlap with those of the Ser4,48 “unphosphorylated” resonance set. No “additional” resonances were observed for Ser48. The unphosphorylated peak position for some residues is masked by overlapping peaks in the phosphorylated ^1H - ^{15}N HSQC spectrum. The following residues are likely to have duplicated, but masked, peaks due to the distance of the new peak from the unphosphorylated position: Lys3, Glu12, Lys18, Ala26 and Lys46.

The combined shift distances of the ^1H - ^{15}N -HSQC peaks upon phosphorylation were measured to indicate which residues of the linker domain are affected most strongly by phosphorylation (Figure 5.13b). The residues which

showed the greatest shifts in their $^1\text{H}^{15}\text{N}$ -HSQC peak upon phosphorylation were Ser4, Ser14 and Thr27. The ^1H resonances shift down-field, indicating potential phosphorylation events as demonstrated in previous peptide studies (Hoffmann et al., 1994). In addition to these peaks some of the neighbouring peaks are also shifted, but to a smaller extent. The region from residues 24–38 also showed chemical shift differences upon phosphorylation. This region contains several serine and threonine residues, so it is important to determine if the shift differences were due to multiple phosphorylation events or to a structural change in this region.

The C^β resonances were then studied to determine if they could report on the phosphorylation events. The C^β is closer to the phosphorylation event than the other nuclei assigned. If a chemical-shift change is induced by a structural change it is likely to affect the C^α and C^β shifts to a similar extent, so structural effects can be screened. The ^1H - ^{13}C HSQC was studied (Figure 5.14a) and peak shifts were identified for Ser4, Ser14, Ser25, Ser29 and Thr27. The shift differences were quantified using the triple resonance experiments as the peaks were less overlapped (Figure 5.14b). Ser4, Ser14 and Thr27 show clear C^β shift differences upon phosphorylation, compared with the other residues, which supports the assumption of phosphorylation at these sites, based on the combined amide shift difference (Figure 5.13b).

As noted above, the ^1H - ^{13}C HSQC also identified peak shifts for Ser25 and Ser29. The quantitative chemical-shift data indicated that the Ser25 shift is not appreciable, compared with Ser4 and Ser14, but Ser29 showed a significant, and positive, shift of C^β resonance upon phosphorylation. Ser29 occurs within the identified region of transient structure (Section 5.3.3.3), which undergoes structural change upon phosphorylation, as will be detailed in Section 5.3.3.5. Briefly, Ser29 showed the largest increase in C^α resonance of all the

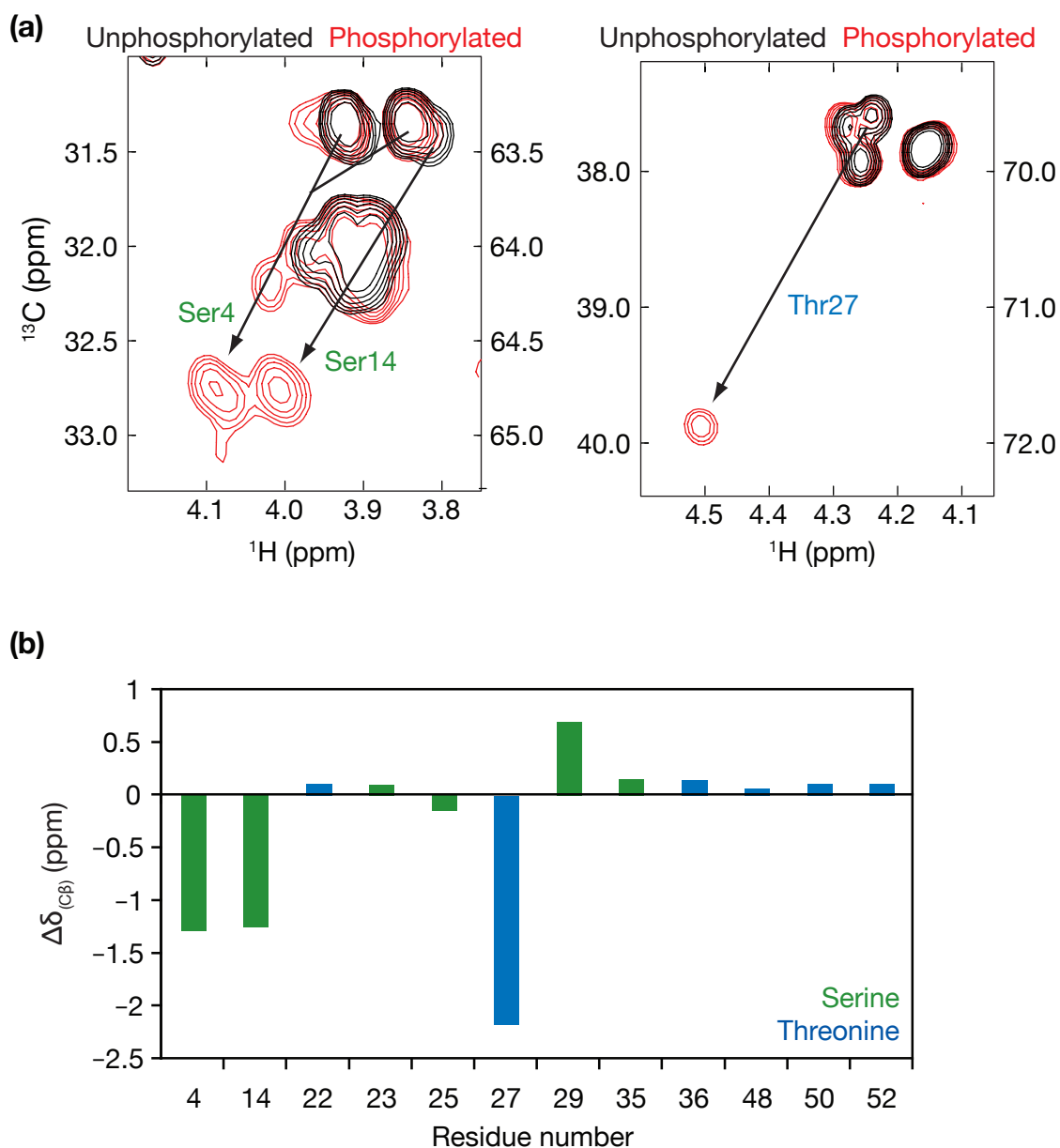


Figure 5.14 Using C^β resonances to report on phosphorylation of residues in the linker domain of Hho1p. (a) ^1H - ^{13}C HSQC spectra showing serine and threonine C^β resonances, with the shifts upon phosphorylation indicated. Two carbon resonance axes are marked because the spectra were folded. The smaller values are the aliased frequencies and the larger values are the true frequencies. (b) Shift in the C^β chemical-shifts of the serine and threonine residues upon phosphorylation: serine (green); threonine (blue).

linker residues upon phosphorylation, almost twice that of the C^β resonance shift. This indicates that the residue's environment is more changed near the backbone of the protein than near the potential site of phosphorylation and would be consistent with a change in secondary structure, rather than a phosphorylation event.

The peak duplication data can be considered quantitatively for each residue by considering peak loss upon phosphorylation at the site of the unphosphorylated peak. The data for each serine and threonine residue in the linker domain is shown in Figure 5.15a. As the “unphosphorylated” resonances for Ser4 and Ser48 overlap, they are considered as a set. Because the chemical shifts are affected by structural changes (detailed in Section 5.3.3.5), the data for residues 24–38 cannot be used to infer phosphorylation events. To try to separate Ser4 and Ser48 using peak loss data, the “nearest neighbours” were considered (Figure 5.15b). The “nearest neighbours” are the closest residues which were assigned in the ^1H - ^{15}N HSQC with well defined peaks. Lys3 does have some overlap in the phosphorylated spectrum but it was the only available data on the N-terminal side of Ser4. The overlap would cause an overestimation of the ratio of peak volumes for this residue. The “nearest neighbours” of Ser4 and Ser14 had less than 50% of the peak retained at the unphosphorylated position, including Lys3. This is in contrast to the neighbours of Thr22, Ser23, Ser48, Thr50 and Thr52, which show almost no peak loss upon phosphorylation. These data suggest that Ser4 and 14 are phosphorylated, while Thr22, Ser23, Ser48, Thr50 and Thr52 are not, supporting the observations from the amide and C^β chemical-shift difference data (Figures 5.13b and 5.14b).

Taken together these data demonstrate that the phosphorylated residues in the linker domain of Hho1p are Ser4, Ser14 and Thr27 (residues 120, 124 and 143 of Hho1p respectively).

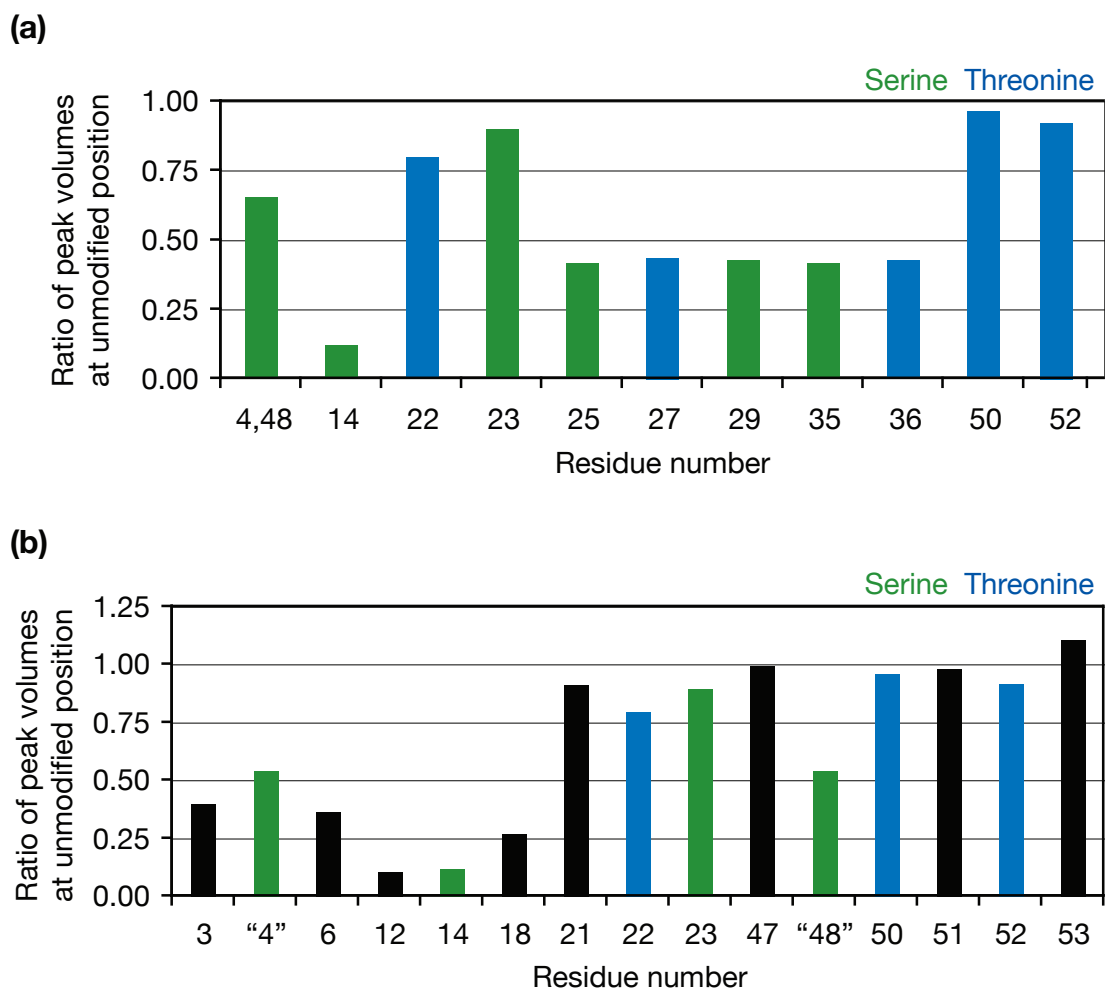


Figure 5.15 ^1H - ^{15}N HSQC peak loss upon phosphorylation of the linker domain of Hho1p. The ratio of peak volumes of the phosphorylated spectrum to unmodified spectrum for (a) each serine and threonine position assigned to the unmodified linker, and (b) serines 4, 14, 23 and 48, and threonines 22, 36, 50 and 52, plus their nearest neighbouring residues (corrected for sample concentration).

5.3.3.5 Effect of phosphorylation on the structure of the linker domain of Hho1p

C' , C^α , H^α , H^N and N shift differences from random coil were measured for the phosphorylated linker and compared with data for the unphosphorylated species (Figure 5.16). In most cases the shift values are similar for the unphosphorylated and phosphorylated linker domains, although H^α is more variable. Residues 24–36 show a larger deviation from random coil values for all nuclei upon phosphorylation of the linker domain, and the region is divided into two sub-regions showing different shift patterns. Residues between about 27 and 36 show amide proton resonances that shift up-field upon phosphorylation (residues 30–36) while the C^α and C' resonances shift down-field (residues 27–36). This could indicate a gain of α -helical character (Wishart et al., 1991; Spera and Bax, 1991). Residues between 24 and about 27 show resonances that shift in the opposite direction, indicating a loss of helical structure at this subregion.

The dynamics of the phosphorylated linker domain were studied using heteronuclear NOE measurements and temperature-dependent amide proton chemical shifts (Figure 5.17). As for the unphosphorylated domain, all of the $\{^1H\}^{15}N$ NOE measurements remain below 0.6 upon phosphorylation, indicating that no fully structured regions are formed. However there is a significant increase in the $\{^1H\}^{15}N$ NOE values for residues 3–6, 13–19 and 25–31 compared with the unphosphorylated species. The region of the predicted α -helix discussed above (residues 24–38) matches with one of the regions of decreased mobility identified by the $\{^1H\}^{15}N$ NOE analysis (residues 25–31). There is no other indication of a change in structure around residues 3–6 and 13–19, although this includes phosphorylated serine residues 4 and 14. The amide proton shifts remain below -4.5 ppb/K, indicating that no stable hydrogen bonds are formed upon phosphorylation (Baxter and Williamson, 1997). The values do

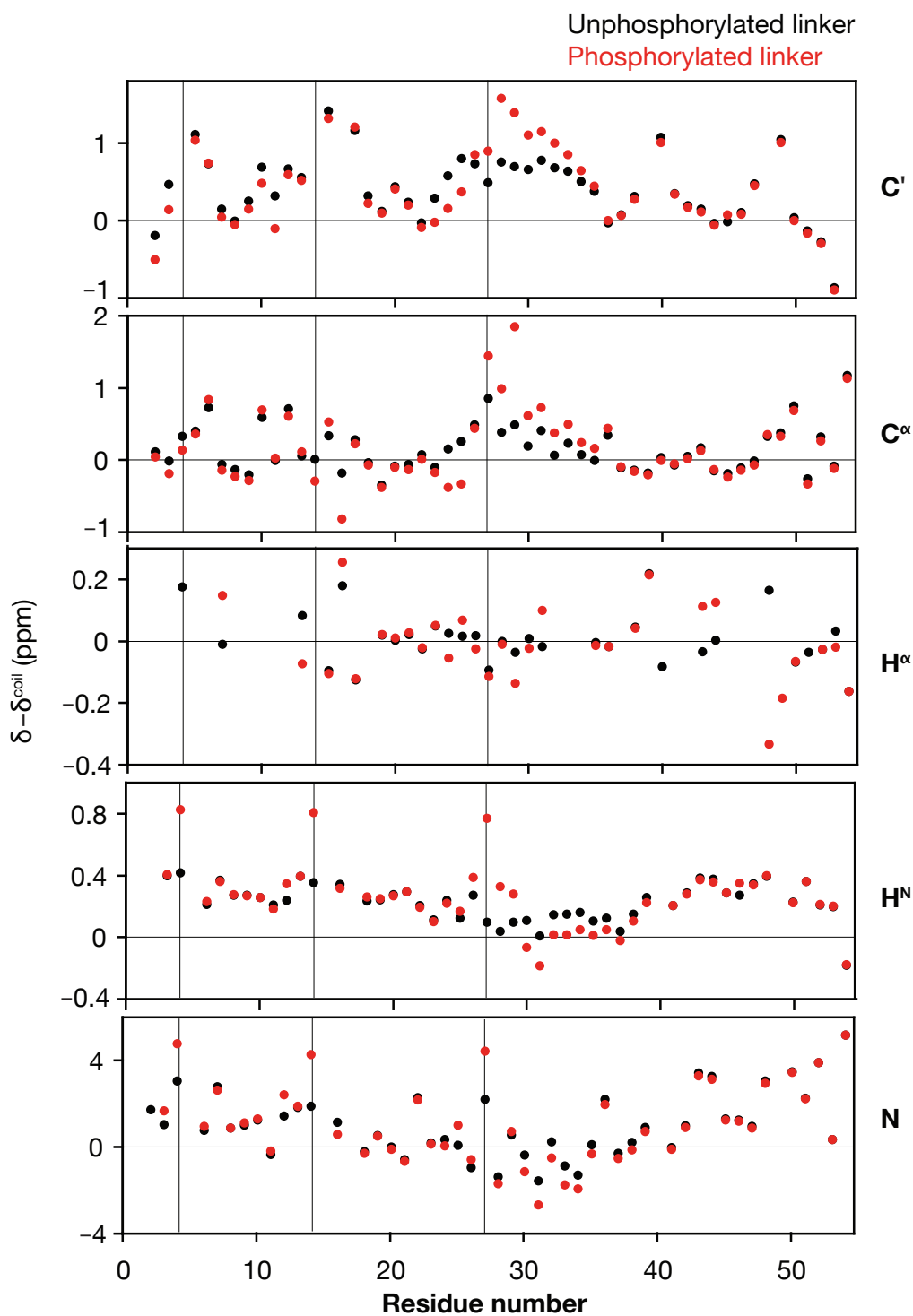


Figure 5.16 Shift deviations from random coil for the unphosphorylated and phosphorylated linker domain of Hho1p. C', C^α, H^α, H^N and N nuclei chemical shift deviations from random coil, corrected for sequence context (Schwarzinger *et al.*, 2001). Ser4, Ser14 and Thr27 are marked with vertical lines. The true baselines are offset from zero because these experiments were recorded at much lower temperatures than the random coil values. The region of transient structure identified previously (residues 24–36) shows changes in chemical shift deviations upon phosphorylation.

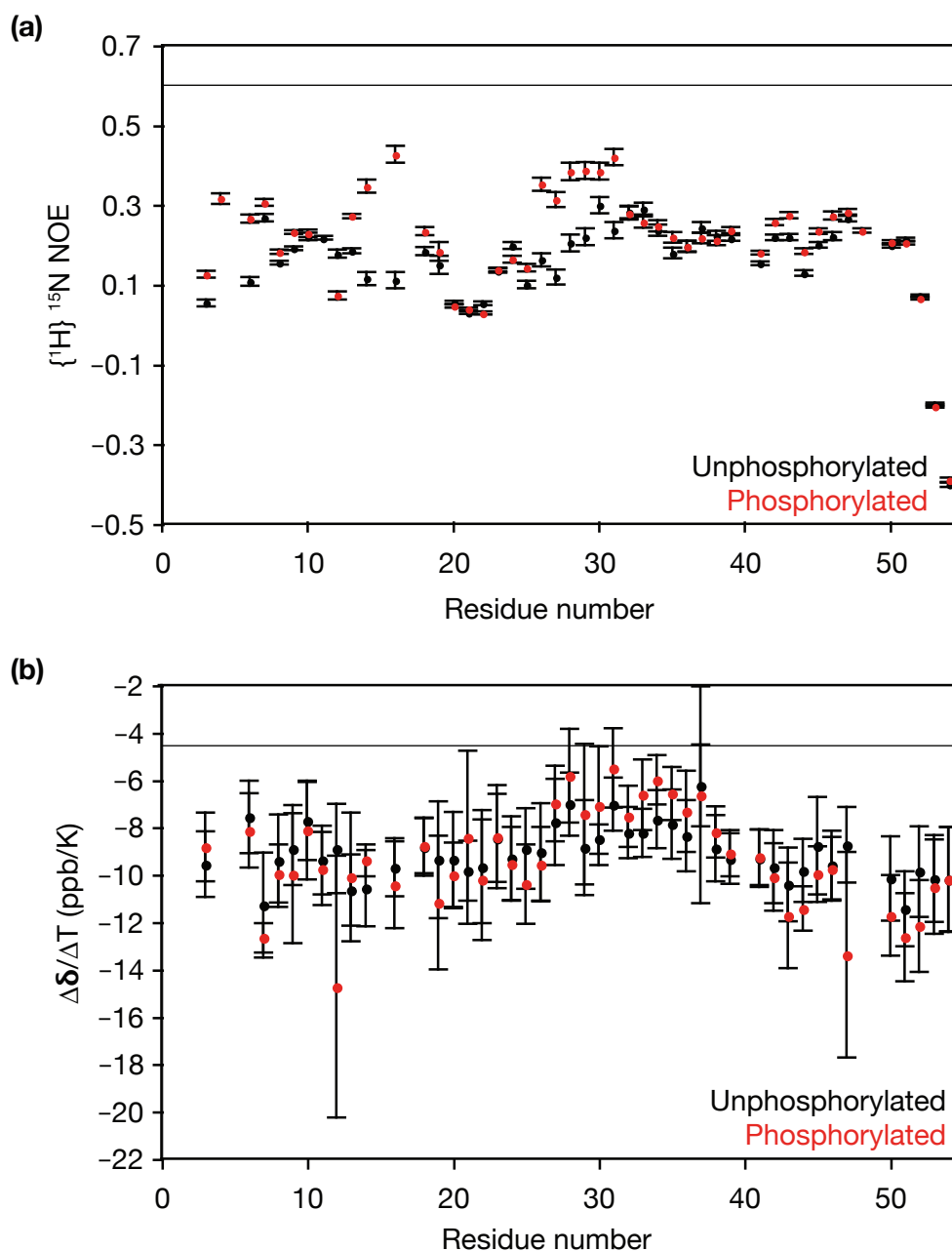


Figure 5.17 Analysis of the dynamics of the unphosphorylated and phosphorylated linker domain of Hho1p. (a) Heteronuclear NOE measurements remain below 0.6 following phosphorylation, indicating the linker domain remains mostly unstructured. Residues 3–6, 13–19 and 25–31 have significantly higher NOE values in the phosphorylated form indicating a reduction in fast (ps-ns) dynamics. (b) Temperature dependence of amide proton chemical shifts, obtained from ^{15}N -HSQC spectra acquired at 273, 278, 288 and 298 K. Values are more negative than -4.5 ppb/K, indicating none of the amide protons is stably hydrogen-bonded (Baxter and Williamson, 1997). There is a contiguous stretch of increased values around residues 25–35.

however increase slightly, especially over residues 20–36, but they are all within one standard error of the value for the unphosphorylated linker, and any difference in hydrogen bonding between the unphosphorylated and phosphorylated linker domain is therefore small and transient.

The experiments in Figures 5.16 and 5.17 demonstrate that the region of weak structure gains α -helical character at residues 27–36, but loses α -helical character in the residues immediately preceding this upon phosphorylation of the linker domain.

5.4 Discussion

Difficulties in extraction of Hho1p from yeast whole-cell or nuclear extracts hindered investigation of its post-translational modifications. This is an important question to address in order to understand if Hho1p is modified in similar ways to canonical linker histones (Section 1.3.1.2). The study by Li and colleagues (2007) successfully identified phosphorylation of Hho1p by mass spectrometric analysis of yeast whole-cell extract, suggesting that a similar procedure could be used to identify further Hho1p post-translational modifications in a proteome-scale study.

5.4.1 Phosphorylation of Hho1p by CDK2/Cyclin A occurs mainly in the linker domain

CDK2/Cyclin A phosphorylation of Hho1p, *in vitro* seemed a good starting point to investigate the effect of phosphorylation on the properties of Hho1p and the structure of the linker domain, as yeast contains a functional CDK2 homologue, Ime2p (Szwarcwort-Cohen et al., 2009). The CDK2/Cyclin A-treated

Hho1p is phosphorylated at more sites than were identified by Li and colleagues (2007). This could be because that study used α -factor arrested yeast cells, and phosphorylation states are known to vary with cell cycle and growth phase. This suggests that other kinases would produce a different pattern of phosphorylation events in Hho1p. These should be identified and the action on Hho1p studied, in order to elucidate the effect of all the naturally occurring phosphorylation events on Hho1p.

It should be noted that the phosphorylation events in the GII domain, identified by Li et al. were not observed for *in vitro* CDK2/Cyclin A phosphorylation of the isolated domain. The study by Holt et al. (2009) indicates that the phosphorylation of Ser174 is Cdk1-dependent. Analysis of various Hho1p regions suggested that the majority of phosphorylation events by CDK2/Cyclin A occur in the originally-defined linker region (residues 131–170). This corresponds to residues 15–54 of the linker domain used for structural work in this Chapter, which was phosphorylated only once (Thr27). At least two further phosphorylations occur in the context of the LGII protein (Figure 5.2), and it is unclear whether they occur in the originally-defined linker region or GII domain. In contrast, the phosphorylation of linker residues Ser4 and Ser14 (identified in Section 5.3.3.4) are contained in the GI protein, which doesn't show any phosphorylation by CDK2/Cyclin A (Figure 5.2), although Ser14 is the C-terminal residue of the GI protein and therefore may not be expected to be modified. This indicates that the phosphorylation of Hho1p and Hho1p-truncation proteins by CDK2/Cyclin A is context-dependent and demonstrates that further work is required to valid all of the CDK2/Cyclin A phosphorylation sites in Hho1p. Section 5.3.3.4 suggests that both amide and C^β chemical shift differences report on phosphorylations (Figures 5.13 and 5.14).

5.4.2 Phosphorylation affects the biochemistry of Hho1p and Hho1p-truncation proteins

Phosphorylation affects the affinity of Hho1p and Hho1p-truncation proteins for DNA. For linear DNA, phosphorylation reduces the affinity of the protein for the DNA. This could be because phosphorylation adds negative charge to a protein, making it less basic and reducing electrostatic affinity for DNA. Alternatively there could be a change in the structure of the protein upon phosphorylation, which could also affect affinity for DNA. Work described in this Chapter indicates there are some changes in structure of the linker domain upon phosphorylation, which have the potential to cause a considerable change in binding affinity.

Understanding the effect of phosphorylation on the affinity of Hho1p and Hho1p-truncation proteins for four-way junction DNA is more complex, with Hho1p and NGIL affinities increasing but LGII affinity appearing to decrease upon phosphorylation. This suggests that the interaction of LGII with four-way junction DNA may be controlled by the electrostatic association or that phosphorylation may destabilise the GII domain. There must be a structural effect of phosphorylation on Hho1p and NGIL to cause both the different effect to LGII, and the different effect of phosphorylation on binding to linear or four-way junction DNA. Further investigation is required to understand the specific phosphorylations that contribute to the different effects of phosphorylation on the properties of NGIL and LGII.

The chromatin binding assay was not able to distinguish between the unphosphorylated and phosphorylated proteins but, given that phosphorylation did affect DNA binding, this is probably due to the low resolution of this technique. Creation of yeast strains containing various GFP-tagged Hho1p re-

gions in place of the genomic copy of the HHO1 gene could allow FRAP to be used to compare the chromatin-binding properties quantitatively. In a similar manner to Lever et al. (2000) the effect of treating the cells with kinase inhibitors could provide insight into how phosphorylation modifies the dynamics of the Hho1p regions in chromatin.

5.4.3 The linker domain of Hho1p is mainly unstructured, but may have some helical character around residues 24–38

As predicted by the VL3E DisProt Predictor of Intrinsically Disordered Regions the isolated linker domain of Hho1p is mostly unstructured. The PSIPRED prediction method suggests several regions of α -helical structure, with the region around residues 30–34 being predicted with most confidence (Figure 5.6c).

The conclusions from the NMR data support the α -helix prediction for a region containing residues 24–38. Data in Figure 5.10 indicate a contiguous region of small chemical shift deviations from sequence-corrected random coil values. This indicates that the linker domain of Hho1p is not stably folded, but shows regions of transient structure or folding. The direction of the H^N , C^α and C' deviations indicate α -helical character in this region. Temperature-dependent amide proton shifts indicated that no stable hydrogen bonds occur within the linker domain (Figure 5.11), so none of the predicted helices are fully stable. However the values for residues 24–38 are less negative than those for the surrounding sequence, indicating a less dynamic structure at this region, with the potential for transient bonding to stabilise a structural element. $\{^1H\}^{15N}$ NOE values for the linker domain indicate that it is dynamic on a picosecond-nanosecond timescale, i.e. that the residues move independently and faster

than the overall tumbling of the domain (Figure 5.11). Regions around residues 10 and 30 show an increase in $\{^1\text{H}\}^{15}\text{N}$ NOE values relative to the rest of the linker domain, indicating that these regions are also less flexible and may contain transient structure.

Thus, the linker domain of Hho1p is a dynamic molecule in aqueous solution, with little or no structure at most regions. However the region around residues 24–38 has reduced fast dynamics and increased structural character, with both chemical shift deviations from random coil and the PSIPRED program predicting α -helical character.

5.4.4 Phosphorylation of the linker domain by CDK2/Cyclin A occurs at three sites

The linker domain residues that are phosphorylated *in vitro* by CDK2/Cyclin A are Ser4, Ser14 and Thr27. These were initially identified by their large combined chemical-shift distances upon linker domain phosphorylation (Figure 5.13). More conclusive data comes from considering the difference in C^β resonances upon phosphorylation (Figure 5.14). There was also significant peak loss at the “unphosphorylated” resonances of Ser4 and Ser14 and their “nearest neighbours”, indicating that a large proportion of the molecules were modified (Figure 5.15). The most dramatic peak loss in the ^1H - ^{15}N HSQC spectra upon phosphorylation occurs for Ser14, indicating that this residue is likely to be fully phosphorylated. It is of note that this is the phosphorylation event (equivalent to residue 130 of Hho1p) identified in yeast extracts by Li and colleagues (2007).

It is interesting to note that the regions that surround the phosphorylation events all show an increase in $\{^1\text{H}\}^{15}\text{N}$ NOE values upon phosphorylation (Figure 5.17). The changes around Thr27 may be due to the increase in

secondary structure at this region. However, there is no appreciable change in temperature-dependent amide proton chemical shifts, or shift deviation from random coil in the regions around Ser4 and Ser14, yet these also show increases in $\{^1\text{H}\}^{15}\text{N}$ NOE upon phosphorylation. Therefore, the change in picosecond-nanosecond dynamics at these regions may be a direct effect of the phosphorylation event, and not necessarily an indication of wider structural change.

Ser4 and Ser14 are both followed by a proline in the linker sequence; this is also true for Ser48, which is not phosphorylated. None of the threonine residues are followed by a proline. The optimal sequence context for CDK2 phosphorylation is S/TPXR/K (refined from the data in Songyang et al., 1994), but sub-optimal residues at position 4 are also recognised (Stevenson-Lindert et al., 2003). It could perhaps be argued that the sequence context of Ser4 and Ser14 (SPEVKK and SPKPK respectively) are closer to the optimal sequence than that of Ser48 (SPTVTAK) because they contain lysine residues within one residue of position 4 of the consensus sequence. The proximity of Ser48 to the C-terminus of the linker domain may also reduce the binding of the kinase at this position, depending on what contacts are required for CDK2 binding relative to its catalytic site. None of the threonine residues have an optimal CDK2 recognition motif, including Thr27, which is phosphorylated. It is clear however, that there is specificity of phosphorylation of the linker domain by CDK2/Cyclin A, as only three of the twelve serine and threonine residues are phosphorylated, even though none of the residues is in the optimal sequence context.

5.4.5 Phosphorylation of the linker domain by CDK2/Cyclin A changes the helical character of residues 24–38

Phosphorylation affected the structure of residues other than those directly modified. The changes were small and localised to the region containing residues 24–38, which had the most structural character in the unphosphorylated linker and showed peak duplication of all residues. The subregion of residues following Thr27 gained more α -helical character and became less dynamic upon phosphorylation, as seen in the shift deviation from random coil and $\{^1\text{H}\}^{15}\text{N}$ NOE values (Figures 5.16 and 5.17). However there was little effect on the temperature-dependent amide proton chemical shifts, suggesting that no stable α -helices were formed. The other residues at the start of this region show little change in their fast dynamics and a loss of α -helical character upon phosphorylation.

Thr27, which is phosphorylated by CDK2/Cyclin A, is located in the interior of this region of potential α -helix at approximately the boundary between the two subregions. The effect of phospho-serine on α -helix structures has been determined, and usually results in destabilisation of the helix when located in the helix interior (Andrew et al., 2002). However, if a basic residue occurs within the helix at a position that can interact with the phosphorylated residue a salt bridge can form, stabilising the helix (Errington and Doig, 2005). In the linker domain there is a lysine residue at the $i+3$ position to Thr27, and the side-chains of Lys30 could interact with the phospho-threonine if they were in an α -helix. A salt bridge between phosphorylated Thr27 and Lys30, could cause the stabilisation identified for the transient α -helical structure around residues 27–38, while destabilising the transient structure that immediately precedes the threonine residue in the unphosphorylated species.

Identification of the kinase that phosphorylates Hho1p *in vivo* will be important to verify the biological relevance of the effects of phosphorylation studied in this Chapter. Also, phosphorylation of Ser4 and Thr27 have not yet been identified for Hho1p *in vivo*. It is especially important to verify whether Thr27 phosphorylation occurs naturally, because it occurs within the region of transient structure in the linker domain and is therefore likely to affect the properties of Hho1p.

5.4.6 Comparison of the effect of phosphorylation on the linker domain of Hho1p and the C-terminal tail of histone H1

A similar structural investigation to that described in this Chapter has been carried out on the C-terminal tail of chicken erythrocyte linker histone H1.11L (Dr K. Stott, L. Cato, Dr J. O. Thomas, unpublished data). Both the histone H1 tail and Hho1p linker are mainly unstructured (Figure 1.9) but the linker domain has greater sequence complexity than the H1 tail. The H1 C-terminal tail does not contain a region of transient structure similar to that identified for the Hho1p linker domain in this Chapter, but has been shown to adopt α -helical conformation upon binding to DNA (Roque et al., 2005).

Phosphorylation events occur at the three S/TPKK sites within the histone H1 tail and these residues show the greatest change in shift deviation for the C $^{\alpha}$, H N and N nuclei, with smaller changes in the neighbouring residues. The changes were less pronounced and more localised than for Thr27 in the Hho1p linker domain. The histone H1 tail showed little change in dynamics upon phosphorylation, with only the phosphorylated residues and neighbouring residues being affected. This was also true for the Hho1p linker domain

at the sites of phosphorylation, although the effect was longer-range around Thr27 due to the induced α -helix in this region.

A major difference between the effect of phosphorylation on the Hho1p linker domain and the histone H1 C-terminal tail is that the former domain shows a change in α -helical character in the region 24–38. The gain of α -helical character in this sub-domain is in contrast to the situation for the histone H1 C-terminal tail, which, in another study, showed a slight loss of α -helix upon phosphorylation (Roque et al., 2008). The different effects of phosphorylation could occur because Hho1p linker does not contain T/SPKK sequences, which tend to form β -turn motifs in crystal structures (Suzuki, 1989). The difference in the structural effect of phosphorylation suggests that phosphorylation may have a different function, or at least a different mechanism of function, for the two types of linker histone. Therefore it is important that the region of transient structure in the Hho1p linker domain be further investigated to understand its role in the function of Hho1p, and the function of Hho1p compared with canonical linker histones.

5.5 Summary

- CDK2/Cyclin A phosphorylates Hho1p *in vitro*. The majority of phosphorylation events appear to occur in the linker domain, and phosphorylation is context-dependent.
- Phosphorylation reduces the affinity of Hho1p, NGIL and LGII for linear DNA.
- Phosphorylation increases the affinity of Hho1p and NGIL, and may decrease the affinity of LGII, for four-way junction DNA.
- Phosphorylation showed no effect on the binding of Hho1p, NGIL and LGII to chromatin in sucrose gradient sedimentation assays.
- The linker domain of Hho1p can be expressed in minimal medium and purified on an NMR-scale. It can be phosphorylated *in vitro* by CDK2/Cyclin A.
- Ser4, Ser14 and Thr27 of the Hho1p linker domain are phosphorylated by CDK2/Cyclin A. Ser14 is phosphorylated to the greatest extent, and is the phosphorylation event that has been identified for yeast *in vivo*.
- Residues 24–36 of the linker domain contains some residual structure, which changes upon phosphorylation. Residues 27–36 increase in α -helical character, while residues 24–26 lose α -helical character.

Chapter 6

Concluding Remarks

6 Concluding remarks

This Thesis aims to further our knowledge of the yeast linker histone, Hho1p, in terms of its structure and function within chromatin. Uniquely among linker histones, Hho1p contains two domains, GI and GII, with sequence homology to the globular domain of H5, as well as an unstructured N-terminal tail and a linker domain. Hho1p has similar properties to canonical linker histones *in vitro* (Section 1.5) and both isolated GI and GII domains appear to be functional linker histone globular domains (Section 1.5.5). This has led to the suggestion that Hho1p could act as a bifunctional linker histone, possibly bridging two nucleosomes.

There is currently no direct evidence for nucleosome bridging by Hho1p *in vivo* or *in vitro*. It is known that the length of the linker domain is sufficient to allow bridging, and both globular domains, in the context of a full-length Hho1p molecule, are able to bind independent four-way junction DNA molecules (Schäfer et al., 2005). Work presented in this Thesis was unable to conclusively demonstrate bridging in low resolution assays that compared the digestion of nucleosome arrays containing Hho1p or NGIL (Chapter 3). To directly address the question of nucleosome bridging, chromatin structure needs to be studied at greater resolution. For example, reconstituted chromatin has been studied using atomic force microscopy (AFM), demonstrating a solenoid structure in which the individual nucleosomes can be observed (Liu et al., 2001). AFM would be a complementary high-resolution technique to the more widely used electron microscopy studies (Section 1.1.2), as samples can be stud-

ied in aqueous conditions (although affixed to a surface).

Linker histones are required for the maximal and ordered compaction of chromatin into the “30 nm fibre” (Section 1.3.2.4). No obvious requirement of the GII domain for the compaction of nucleosome arrays by Hho1p was observed using gel-shift assays (Chapter 3). This argues against a nucleosome bridging role for Hho1p, which would predict that about half the input ratio of Hho1p would be required to cause equivalent compaction compared with an NGIL-containing array. However, because gel-shift assays are low resolution and indicated very little compaction of both Hho1p- and NGIL-containing arrays, AUC should be used to look for more subtle differences between Hho1p- and NGIL-dependent compaction of “unfolded” nucleosome arrays.

For nucleosome bridging to be a valid model, the GII domain must be able to fold in the context of full-length Hho1p. NMR studies in Chapter 2 suggest that the structural properties of the GII domain are context-independent. Therefore, studies that demonstrate the isolated GII domain can function as a linker histone globular domain, both *in vitro* and *in vivo* (Section 1.5.5), can be extended to the GII domain within full-length Hho1p. Thus, the nucleosome bridging model remains a possibility and should be pursued further in order to understand Hho1p and its role in yeast chromatin.

Our understanding of the stability of the GII domain is extended by work in Chapter 2, which demonstrates that secondary structure elements are present in the “unfolded” species. Therefore the instability of the GII domain results from less stable packing of the secondary structure elements into the folded species, rather than the formation of the secondary structure elements *per se*. Domain-swap mutants (of the GI loop into the GII domain) had previously identified the loop between helices II and III as the cause of the instability of the GII domain (Sanderson et al., 2005), suggesting the GII loop may disrupt

helix packing. A further domain-swap experiment could be carried out to test this, substituting the loop of GII into the GI domain and determining if the helix packing of the GI domain is disrupted.

While it is known that Hho1p is less abundant than core histones in yeast, the published ratios vary (Section 3.1). I reassessed this question in Chapter 3, determining a ratio of one Hho1p molecule for every 5–10 nucleosomes in the yeast W303 strain. A recent paper, however, has increased the complexity of this question. Schäfer et al. (2008) saw an increase in Hho1p binding to chromatin upon entry into stationary phase, while the cellular level of Hho1p remained constant. This indicates that measurement of cellular Hho1p levels relative to core histones does not equate to the functional ratio of Hho1p bound to nucleosomes in yeast chromatin. To determine the functional ratio, the abundance of Hho1p and core histone should be measured for isolated yeast chromatin extracts, so the unbound Hho1p is removed. Measuring Hho1p to nucleosome stoichiometry in this manner, at different stages of the cell-cycle and in different growth phases, will produce a more complete picture of Hho1p to nucleosome stoichiometry in yeast.

Further work is required to elucidate the protein interactions of Hho1p. The interaction with Sir2p, described here, is the first reported evidence of a direct interaction partner of Hho1p *in vitro* (Chapter 4). This interaction was not pursued here due to difficulties in producing Sir2p in the bacterial expression system, however baculovirus-expressed Sir2p has been successfully produced (Cubizolles et al., 2006). Once a suitable sample of Sir2p is produced, it could be used to determine if Hho1p interacts with the N-terminus of Sir2p, in a similar manner to the interaction between the human homologues, histone H1 and SirT1 (Vaquero et al., 2004). Unlike the metazoan homologues, H1 and HMGB1, Hho1p and Nhp6ap or Hmo1p do not interact *in vitro* (Chapter 4). This appears

to be due to the absence of a strongly acidic region in the HMG box proteins, as Hho1p interacts with the acidic tail of HMGB1 in a similar manner to metazoan histone H1 (Cato et al., 2008). Because the interaction of Hho1p with HMGB1 is similar to that of H1 with HMGB1, this suggests that it is valid to search for candidate Hho1p-interacting partners based on the interactions of metazoan linker histones.

Phosphorylation is known to reduce the affinity of linker histone for DNA and increase its exchange rate on chromatin (Green et al., 1993; Hendzel et al., 2004). The N-terminal tail of linker histones has been implicated in the correct placement of the H1 globular domain at the nucleosome dyad (Allan et al., 1986). Hho1p and NGIL, but not LGII, show increased affinity for four-way junction DNA upon phosphorylation (Chapter 5), suggesting phosphorylation of the N-terminal tail of Hho1p may facilitate the positioning of Hho1p on the DNA molecule. The different effect of phosphorylation on Hho1p, NGIL and LGII binding to four-way junction DNA also raises the possibility that phosphorylation could be used to change Hho1p from a bi- to mono-functional linker histone, with phosphorylation causing regions in the LGII domains to be less tightly associated with the chromatin while the protein remains anchored by regions in the NGIL domains.

The gain in α -helix upon phosphorylation of the Hho1p linker domain (Chapter 5) will shorten the length of the domain that can contact DNA in chromatin and may reduce the affinity of the protein for DNA. This is consistent with the observed decrease in affinity of LGII for linear and four-way junction DNA but is not consistent with the increased affinity of NGIL for four-way junction DNA (Chapter 5). The different effect of phosphorylation on these two linker-containing proteins suggests that regions outside of linker residues 27–38 are also be affected by phosphorylation.

An extension of work presented in this Thesis would be to study the effect of phosphorylation on the ability of Hho1p to compact reconstituted nucleosome arrays. Gross structural changes could be investigated by gel-shift-mobility assays, while AUC would allow quantitative study of more subtle effects. It would be important to ensure the amount of unmodified and phosphorylated linker histone bound in each array-type was equal by adjusting for their different affinities for chromatin. Routh et al. (2008) quantified the relative amount of H5 bound in reconstituted chromatin arrays by using H5 samples that had been radiolabelled on less than one in 1500 molecules.

Work presented in this Thesis highlights ways in which Hho1p differs from canonical linker histones (compaction of nucleosome arrays, protein interactions and transient structure in the linker domain). This increases the number of known differences between yeast and metazoan chromatin (Section 1.4). Thus, caution is required when using yeast as a model organism to study chromatin, and more work is required to understand exactly how yeast chromatin differs from that of higher eukaryotes.

Appendices

A - NMR resonances of the “unfolded” species of the GII domain of Hho1p

Residue	H ^N	N	H ^α	C ^α	C ^β
2 Ala	8.78	126.47	4.33	52.00	18.79
3 Ser	8.61	115.67	4.45	57.77	63.33
4 Ser	8.61	118.66	4.80	56.04	62.56
5 Pro				63.10	31.60
6 Ser	8.58	115.23	4.48	58.07	63.15
7 Ser	8.50	117.83	4.44	58.21	63.15
8 Leu	8.40	123.33	4.41	55.22	41.83
9 Thr	8.30	13.58	4.29	61.74	69.51
10 Tyr	8.42	122.36	4.40	59.19	38.09
11 Lys	8.24	121.11	4.05	57.01	32.54
12 Glu	8.21	120.12	4.09	57.07	29.66
13 Met	8.42	121.06	4.29	56.12	31.88
14 Ile	8.22	121.65	3.98	61.32	37.38
15 Leu	8.22	124.42	4.28	55.44	41.66
16 Lys	8.28	120.51	4.26	56.30	32.42
17 Ser	8.20	115.43	4.42	57.95	63.27
18 Met	8.33	122.78	4.81	53.01	31.89
19 Pro				62.81	31.62
20 Gln	8.77	120.51	4.32	54.98	29.06
21 Leu	8.58	123.58	4.31	54.79	41.83
22 Asn	8.73	119.07	4.73	52.71	38.26
23 Asp	8.43	120.21	4.55	53.80	40.38
24 Gly	8.60	108.47	3.94,3.94	45.21	
25 Lys	8.36	120.01	4.30	56.16	32.17
26 Gly	8.72	109.56	3.99,3.99	45.00	
27 Ser	8.46	115.39	4.47	58.01	63.26
28 Ser	8.60	117.60	4.47	58.12	63.08
29 Arg	8.46	122.67	4.29	55.75	30.27
30 Ile	8.35	122.74	4.11	60.70	38.01
31 Val	8.54	126.64	4.05	61.78	32.25
32 Leu	8.59	127.22	4.35	54.44	41.87
33 Lys	8.50	122.75		55.86	32.64
34 Lys				55.71	32.77
35 Tyr	8.55	122.31	4.54	57.66	38.39
36 Val	8.18	124.11	3.97	61.41	32.77
37 Lys	8.50	125.53	4.15	56.15	32.56

Residue	H ^N	N	H ^α	C ^α	C ^β
38 Asp	8.57	122.13	4.60	53.94	40.67
39 Thr	8.24	114.09	4.23	61.62	69.14
40 Phe	8.47	121.71	4.59	57.92	38.84
41 Ser	8.35	116.63	4.39	58.10	63.16
42 Ser	8.52	117.94	4.44	58.34	63.06
43 Lys	8.40	122.57	4.29	56.06	32.27
44 Leu	8.24	122.15	4.30	54.74	41.78
45 Lys	8.51	122.30		55.91	32.44
46 Thr	8.35	114.85	4.38	61.28	69.42
47 Ser	8.52	117.42	4.47	57.96	63.35
49 Asn	8.50	119.99	4.65	53.07	38.16
50 Phe	8.35	120.00	4.50	57.92	38.84
51 Asp	8.32	121.25	4.48	54.55	40.15
52 Tyr	8.14	119.63	4.39	58.52	37.66
53 Leu	7.97	121.54	4.10	55.16	41.44
54 Phe	8.07	119.56	4.45	58.06	38.87
55 Asn	8.29	119.37	4.64	52.90	38.29
56 Ser	8.33	115.94	4.29	58.56	62.93
57 Ala	8.29	124.82	4.29	52.42	18.51
58 Ile	8.02	119.45	4.04	60.85	37.86
59 Lys	8.46	125.61	4.26	55.86	32.46
60 Lys	8.52	123.00	4.28	55.90	32.58
61 Cys	8.59	121.29	4.49	58.22	27.64
62 Val	8.51	122.47	4.12	62.09	32.17
63 Glu	8.75	124.44	4.29	56.17	29.75
64 Asn	8.74	119.61	4.68	52.99	38.28
65 Gly	8.58	108.79	3.93,3.93	45.11	
66 Glu	8.35	119.73	4.30	55.93	29.91
67 Leu	8.42	122.66	4.36	54.68	41.75
68 Val	8.36	122.37	4.07	61.78	32.15
69 Gln	8.71	125.71	4.60	52.97	28.39
70 Pro				62.50	31.75
71 Lys	8.70	121.61	4.32	55.82	32.74
72 Gly	8.48	109.81	4.18,4.01	44.06	
73 Pro				62.75	31.66
74 Ser	8.75	116.08	4.45	58.18	63.40
75 Gly	8.58	110.31	3.94,3.94	44.87	
76 Ile	8.13	120.05	4.11	60.71	38.03
77 Ile	8.47	126.46	4.10	60.50	37.88
78 Lys	8.64	126.77	4.29	55.65	32.54
79 Leu	8.55	124.15	4.33	54.52	41.94
80 Asn	8.70	120.00	4.67	52.62	38.31
81 Lys	8.55	122.18	4.26	55.92	32.54
82 Lys	8.51	122.55	4.24	55.93	32.46
83 Lys	8.59	123.51	4.30	55.84	32.52

Residue	H ^N	N	H ^α	C ^α	C ^β
84 Val	8.43	122.74	4.05	61.74	32.46
85 Lys	8.66	126.29	4.31	55.66	32.63
86 Leu	8.67	125.00	4.41	54.54	41.95
87 Ser	8.57	117.19	4.53	57.78	63.39
88 Thr	8.00	120.30	4.15	62.84	70.11

B - NMR resonances of the linker region of Hho1p

Residue	H ^N	N	H ^α	C'	C ^α	C ^β
2 Lys		124.71		176.46	56.67	33.44
3 Lys	8.78	124.00		176.81	56.41	33.54
4 Ser	8.74	119.73	4.77		57.00	63.24
5 Pro				176.99	63.42	32.50
6 Glu	8.68	121.54		176.74	56.63	30.61
7 Val	8.54	123.23	4.08	176.36	62.54	33.02
8 Lys	8.70	126.49		176.61	56.46	33.26
9 Lys	8.67	123.92		176.90	56.42	33.44
10 Glu	8.70	122.76		176.70	56.58	30.63
11 Lys	8.63	122.33		176.82	56.64	33.30
12 Glu	8.67	122.94		176.62	56.59	30.67
13 Val	8.58	122.43	4.24	176.47	62.46	33.12
14 Ser	8.71	121.29			56.68	63.36
15 Pro			4.47	177.01	63.16	32.35
16 Lys	8.64	123.13	4.59		54.56	32.58
17 Pro				177.15	63.19	32.57
18 Lys	8.70	121.99		177.02	56.65	33.29
19 Gln	8.65	122.03	4.33	175.85	55.72	29.99
20 Ala	8.68	126.23	4.31	177.89	52.63	19.55
21 Ala	8.66	123.75	4.38	178.38	52.80	19.49
22 Thr	8.39	113.35	4.38	174.89	62.02	70.16
23 Ser	8.54	118.16	4.54	174.90	58.51	64.03
24 Val	8.47	121.98	4.18	176.89	62.81	33.00
25 Ser	8.61	119.41	4.46	175.13	58.74	63.84
26 Ala	8.70	126.45	4.39	178.77	53.40	19.40
27 Thr	8.29	113.13	4.26	175.12	62.77	69.82
28 Ala	8.40	126.21	4.35	178.64	53.26	19.28
29 Ser	8.51	115.11	4.40	175.38	59.10	63.78
30 Lys	8.49	123.29	4.32	177.05	56.88	33.18
31 Ala	8.39	124.57	4.28	178.45	53.09	19.25
32 Lys	8.46	120.83		177.12	56.69	33.28
33 Ala	8.50	125.21		178.10	52.89	19.34
34 Ala	8.51	123.05		178.44	52.90	19.31
35 Ser	8.51	114.85	4.51	175.43	58.70	63.90
36 Thr	8.41	116.40	4.36	174.79	62.39	69.90
37 Lys	8.43	123.71		176.69	56.61	33.24

Residue	H ^N	N	H ^α	C'	C ^α	C ^β
38 Leu	8.43	123.61	4.37	177.06	54.93	42.66
39 Ala	8.51	126.56	4.61		50.70	18.27
40 Pro			4.44	177.16	63.01	32.26
41 Lys	8.62	121.90		176.95	56.51	33.35
42 Lys	8.61	123.65		176.64	56.52	33.35
43 Val	8.58	124.08	4.09	176.30	62.57	33.11
44 Val	8.62	126.65	4.11	176.19	62.35	33.06
45 Lys	8.71	126.98		176.61	56.41	33.77
46 Lys	8.67	124.16		176.73	56.50	33.54
47 Lys	8.72	123.92		176.81	56.41	33.55
48 Ser	8.74	119.73	4.77		57.00	63.24
49 Pro				177.21	63.43	32.51
50 Thr	8.55	116.04	4.31	174.85	62.58	70.02
51 Val	8.54	124.07	4.15	176.43	62.46	33.21
52 Thr	8.53	119.80	4.33	174.26	62.15	70.10
53 Ala	8.59	127.93	4.36	176.99	52.77	19.55
54 Lys	8.20	126.14	4.16		57.96	33.91

C - NMR resonances of the phosphorylated linker region of Hho1p

Residue	H ^N	N	H ^α	C'	C ^α	C ^β
2 Lys				176.15	56.59	33.48
3 Lys	8.78	124.65		176.49	56.23	33.63
4 Ser	9.15	121.47			56.82	64.53
5 Pro				176.92	63.38	32.38
6 Glu	8.69	121.71		176.76	56.74	30.50
7 Val	8.52	123.06	4.24	176.26	62.45	32.91
8 Lys	8.70	126.49		176.57	56.37	33.37
9 Lys	8.66	124.01		176.80	56.34	33.50
10 Glu	8.70	122.80		176.49	56.68	30.50
11 Lys	8.61	122.34		176.40	56.67	33.24
12 Glu	8.77	123.92		176.55	56.49	30.51
13 Val	8.58	122.49	4.08	176.43	62.51	33.09
14 Ser	9.16	123.67			56.37	64.61
15 Pro			4.46	176.91	63.35	32.43
16 Lys	8.61	122.57	4.67		53.92	32.94
17 Pro				177.20	63.13	32.47
18 Lys	8.72	121.91		176.93	56.61	33.37
19 Gln	8.65	122.00	4.33	175.83	55.69	29.88
20 Ala	8.67	126.12	4.31	177.86	52.61	19.41
21 Ala	8.65	123.69	4.39	178.34	52.73	19.49
22 Thr	8.38	113.22	4.38	174.83	61.96	70.05
23 Ser	8.52	118.11	4.55	174.59	58.43	63.93
24 Val	8.44	121.70	4.10	176.46	62.27	32.99
25 Ser	8.65	120.35	4.51	174.69	58.15	63.99
26 Ala	8.81	126.83	4.35	178.88	53.36	19.28
27 Thr	8.96	115.34	4.24	175.53	63.36	71.99
28 Ala	8.69	125.90	4.34	179.47	53.86	19.08
29 Ser	8.68	115.25	4.30	176.08	60.46	63.09
30 Lys	8.31	122.52	4.29	177.50	57.30	32.81
31 Ala	8.19	123.45	4.39	178.81	53.41	18.93
32 Lys	8.33	120.08		177.43	56.99	33.00
33 Ala	8.36	124.34		178.32	53.15	19.14
34 Ala	8.39	122.40		178.58	53.07	19.25
35 Ser	8.42	114.43	4.50	175.50	58.87	63.75
36 Thr	8.33	116.16	4.36	174.81	62.48	69.75
37 Lys	8.36	123.47		176.68	56.63	33.11

Residue	H ^N	N	H ^α	C'	C ^α	C ^β
38 Leu	8.38	123.27	4.37	177.02	54.92	42.59
39 Ala	8.48	126.40	4.61		50.67	18.14
40 Pro				177.09	62.97	32.28
41 Lys	8.62	121.84		176.94	56.53	33.33
42 Lys	8.60	123.58		176.61	56.48	33.34
43 Val	8.56	123.96	4.24	176.26	62.53	33.08
44 Val	8.60	126.50	4.23	176.16	62.37	33.00
45 Lys	8.71	126.93		176.70	56.36	33.42
46 Lys	8.74	124.10		176.71	56.47	33.48
47 Lys	8.71	123.83		176.79	56.36	33.52
48 Ser	8.74	119.63	4.27		57.03	63.17
49 Pro			4.45	177.18	63.38	32.43
50 Thr	8.55	115.99	4.31	174.81	62.51	69.91
51 Val	8.54	124.03		176.40	62.39	33.09
52 Thr	8.52	119.79	4.33	174.23	62.10	69.98
53 Ala	8.59	127.93	4.30	176.96	52.74	19.45
54 Lys	8.20	126.14	4.16		57.92	33.80

Bibliography

Bibliography

- Ahmad, K., Henikoff, S., 2002. The histone variant H3.3 marks active chromatin by replication-independent nucleosome assembly. *Mol Cell* 9 (6), 1191–200.
- Alami, R., Fan, Y., Pack, S., Sonbuchner, T. M., Besse, A., Lin, Q., Greally, J. M., Skoultchi, A. I., Bouhassira, E. E., 2003. Mammalian linker-histone subtypes differentially affect gene expression *in vivo*. *Proc Natl Acad Sci U S A* 100 (10), 5920–5.
- Alexandrow, M. G., Hamlin, J. L., 2005. Chromatin decondensation in S-phase involves recruitment of Cdk2 by Cdc45 and histone H1 phosphorylation. *J Cell Biol* 168 (6), 875–86.
- Ali, T., 2001. Characterization of Hho1p, the putative *Saccharomyces cerevisiae* histone H1. Ph.D. thesis, University of Cambridge.
- Ali, T., Coles, P., Stevens, T. J., Stott, K., Thomas, J. O., 2004. Two homologous domains of similar structure but different stability in the yeast linker histone, Hho1p. *J Mol Biol* 338 (1), 139–48.
- Ali, T., Thomas, J. O., 2004. Distinct properties of the two putative "globular domains" of the yeast linker histone, Hho1p. *J Mol Biol* 337 (5), 1123–35.
- Allan, J., Hartman, P. G., Crane-Robinson, C., Aviles, F. X., 1980. The structure of histone H1 and its location in chromatin. *Nature* 288 (5792), 675–9.
- Allan, J., Mitchell, T., Harborne, N., Bohm, L., Crane-Robinson, C., 1986. Roles of H1 domains in determining higher order chromatin structure and H1 location. *J Mol Biol* 187 (4), 591–601.
- Andrew, C. D., Warwicker, J., Jones, G. R., Doig, A. J., 2002. Effect of phosphorylation on alpha-helix stability as a function of position. *Biochemistry* 41 (6), 1897–905.
- Arents, G., Burlingame, R. W., Wang, B. C., Love, W. E., Moudrianakis, E. N., 1991. The nucleosomal core histone octamer at 3.1 Å resolution: a tripartite protein assembly and a left-handed superhelix. *Proc Natl Acad Sci U S A* 88 (22), 10148–52.
- Ausio, J., Dong, F., van Holde, K. E., 1989. Use of selectively trypsinized nucleosome core particles to analyze the role of the histone "tails" in the stabilization of the nucleosome. *J Mol Biol* 206 (3), 451–63.

- Balasubramanian, B., Lowry, C. V., Zitomer, R. S., 1993. The Rox1 repressor of the *Saccharomyces cerevisiae* hypoxic genes is a specific DNA-binding protein with a high-mobility-group motif. *Mol Cell Biol* 13 (10), 6071–8.
- Balhorn, R., Chalkley, R., Granner, D., 1972. Lysine-rich histone phosphorylation. A positive correlation with cell replication. *Biochemistry* 11 (6), 1094–8.
- Baneres, J. L., Martin, A., Parello, J., 1997. The N tails of histones H3 and H4 adopt a highly structured conformation in the nucleosome. *J Mol Biol* 273 (3), 503–8.
- Barra, J. L., Rhounim, L., Rossignol, J. L., Faugeron, G., 2000. Histone H1 is dispensable for methylation-associated gene silencing in *Ascobolus immersus* and essential for long life span. *Mol Cell Biol* 20 (1), 61–9.
- Bates, D. L., Thomas, J. O., 1981. Histones H1 and H5: one or two molecules per nucleosome? *Nucleic Acids Res* 9 (22), 5883–94.
- Baxevanis, A. D., Landsman, D., 1998. Homology model building of Hho1p supports its role as a yeast histone H1 protein. *In Silico Biol* 1 (1), 5–11.
- Baxter, N. J., Williamson, M. P., 1997. Temperature dependence of ¹H chemical shifts in proteins. *J Biomol NMR* 9 (4), 359–69.
- Bednar, J., Horowitz, R. A., Grigoryev, S. A., Carruthers, L. M., Hansen, J. C., Koster, A. J., Woodcock, C. L., 1998. Nucleosomes, linker DNA, and linker histone form a unique structural motif that directs the higher-order folding and compaction of chromatin. *Proc Natl Acad Sci U S A* 95 (24), 14173–8.
- Bergink, S., Salomons, F. A., Hoogstraten, D., Groothuis, T. A., de Waard, H., Wu, J., Yuan, L., Citterio, E., Houtsmuller, A. B., Neefjes, J., Hoeijmakers, J. H., Vermeulen, W., Dantuma, N. P., 2006. DNA damage triggers nucleotide excision repair-dependent monoubiquitylation of histone H2A. *Genes Dev* 20 (10), 1343–52.
- Bernstein, B. E., Liu, C. L., Humphrey, E. L., Perlstein, E. O., Schreiber, S. L., 2004. Global nucleosome occupancy in yeast. *Genome Biol* 5 (9), R62.
- Bharath, M. M., Ramesh, S., Chandra, N. R., Rao, M. R., 2002. Identification of a 34 amino acid stretch within the C-terminus of histone H1 as the DNA-condensing domain by site-directed mutagenesis. *Biochemistry* 41 (24), 7617–27.
- Binz, T., D’Mello, N., Horgen, P. A., 1998. A comparison of DNA methylation levels in selected isolates of higher fungi. *Mycologia* 90 (5), 785–790.
- Boy de la Tour, E., Laemmli, U. K., 1988. The metaphase scaffold is helically folded: sister chromatids have predominantly opposite helical handedness. *Cell* 55 (6), 937–44.

- Bradbury, E. M., Inglis, R. J., Matthews, H. R., 1974. Control of cell division by very lysine rich histone (F1) phosphorylation. *Nature* 247 (439), 257–61.
- Brenner, C., Deplus, R., Didelot, C., Lorient, A., Viré, E., De Smet, C., Gutierrez, A., Danovi, D., Bernard, D., Boon, T., Pelicci, P. G., Amati, B., Kouzarides, T., de Launoit, Y., Di Croce, L., Fuks, F., 2005. Myc represses transcription through recruitment of DNA methyltransferase corepressor. *EMBO J* 24 (2), 336–46.
- Brown, D. T., Izard, T., Misteli, T., 2006. Mapping the interaction surface of linker histone H1(0) with the nucleosome of native chromatin *in vivo*. *Nat Struct Mol Biol* 13 (3), 250–5.
- Bryson, K., McGuffin, L. J., Marsden, R. L., Ward, J. J., Sodhi, J. S., Jones, D. T., 2005. Protein structure prediction servers at University College London. *Nucleic Acids Res* 33 (Web Server issue), W36–8.
- Bussey, H., Storms, R. K., Ahmed, A., Albermann, K., Allen, E., Ansorge, W., Araujo, R., Aparicio, A., Barrell, B., Badcock, K., Benes, V., Botstein, D., Bowman, S., Brückner, M., Carpenter, J., Cherry, J. M., Chung, E., Churcher, C., Coster, F., Davis, K., Davis, R. W., Dietrich, F. S., Delius, H., DiPaolo, T., Hani, J., 1997. The nucleotide sequence of *Saccharomyces cerevisiae* chromosome XVI. *Nature* 387 (6632 Suppl), 103–5.
- Campoy, F. J., Meehan, R. R., McKay, S., Nixon, J., Bird, A., 1995. Binding of histone H1 to DNA is indifferent to methylation at CpG sequences. *J Biol Chem* 270 (44), 26473–81.
- Carballo, M., Puigdomènech, P., Palau, J., 1983. DNA and histone H1 interact with different domains of HMG 1 and 2 proteins. *EMBO J* 2 (10), 1759–64.
- Caron, F., Thomas, J. O., 1981. Exchange of histone H1 between segments of chromatin. *J Mol Biol* 146 (4), 513–37.
- Catez, F., Yang, H., Tracey, K. J., Reeves, R., Misteli, T., Bustin, M., May 2004. Network of dynamic interactions between histone H1 and high-mobility-group proteins in chromatin. *Mol Cell Biol* 24 (10), 4321–8.
- Cato, L., Stott, K., Watson, M., Thomas, J. O., 2008. The interaction of HMGB1 and linker histones occurs through their acidic and basic tails. *J Mol Biol* 384 (5), 1262–72.
- Cedar, H., 1988. DNA methylation and gene activity. *Cell* 53 (1), 3–4.
- Celic, I., Masumoto, H., Griffith, W. P., Meluh, P., Cotter, R. J., Boeke, J. D., Verreault, A., 2006. The sirtuins Hst3 and Hst4p preserve genome integrity by controlling histone H3 lysine 56 deacetylation. *Curr Biol* 16 (13), 1280–9.
- Cerf, C., Lippens, G., Ramakrishnan, V., Muyldermans, S., Segers, A., Wyns, L., Wodak, S. J., Hallenga, K., 1994. Homo- and heteronuclear two-dimensional NMR studies of the globular domain of histone H1: full assignment, tertiary

structure, and comparison with the globular domain of histone H5. *Biochemistry* 33 (37), 11079–86.

- Certa, U., Colavito-Shepanski, M., Grunstein, M., 1984. Yeast may not contain histone H1: the only known 'histone H1-like' protein in *Saccharomyces cerevisiae* is a mitochondrial protein. *Nucleic Acids Res* 12 (21), 7975–85.
- Chadee, D. N., Taylor, W. R., Hurta, R. A., Allis, C. D., Wright, J. A., Davie, J. R., 1995. Increased phosphorylation of histone H1 in mouse fibroblasts transformed with oncogenes or constitutively active mitogen-activated protein kinase kinase. *J Biol Chem* 270 (34), 20098–105.
- Chadwick, B. P., Willard, H. F., 2001a. A novel chromatin protein, distantly related to histone H2A, is largely excluded from the inactive X chromosome. *J Cell Biol* 152 (2), 375–84.
- Chadwick, B. P., Willard, H. F., 2001b. Histone H2A variants and the inactive X chromosome: identification of a second macroH2A variant. *Hum Mol Genet* 10 (10), 1101–13.
- Chang, B., Chen, Y., Zhao, Y., Bruick, R. K., 2007. JMJD6 is a histone arginine demethylase. *Science* 318 (5849), 444–7.
- Chowdhury, D., Keogh, M. C., Ishii, H., Peterson, C. L., Buratowski, S., Lieberman, J., 2005. gamma-H2AX dephosphorylation by protein phosphatase 2A facilitates DNA double-strand break repair. *Mol Cell* 20 (5), 801–9.
- Clark, D. J., Hill, C. S., Martin, S. R., Thomas, J. O., 1988. Alpha-helix in the carboxy-terminal domains of histones H1 and H5. *EMBO J* 7 (1), 69–75.
- Clark, D. J., Thomas, J. O., 1986. Salt-dependent co-operative interaction of histone H1 with linear DNA. *J Mol Biol* 187 (4), 569–80.
- Clark, D. J., Thomas, J. O., 1988. Differences in the binding of H1 variants to DNA. Cooperativity and linker-length related distribution. *Eur J Biochem* 178 (1), 225–33.
- Collins, S. R., Miller, K. M., Maas, N. L., Roguev, A., Fillingham, J., Chu, C. S., Schuldiner, M., Gebbia, M., Recht, J., Shales, M., Ding, H., Xu, H., Han, J., Ingvarsdottir, K., Cheng, B., Andrews, B., Boone, C., Berger, S. L., Hieter, P., Zhang, Z., Brown, G. W., Ingles, C. J., Emili, A., Allis, C. D., Toczyski, D. P., Weissman, J. S., Greenblatt, J. F., Krogan, N. J., 2007. Functional dissection of protein complexes involved in yeast chromosome biology using a genetic interaction map. *Nature* 446 (7137), 806–10.
- Compton, J. L., Bellard, M., Chambon, P., 1976. Biochemical evidence of variability in the DNA repeat length in the chromatin of higher eukaryotes. *Proc Natl Acad Sci U S A* 73 (12), 4382–6.

- Contreras, A., Hale, T. K., Stenoien, D. L., Rosen, J. M., Mancini, M. A., Herrera, R. E., 2003. The dynamic mobility of histone H1 is regulated by cyclin/CDK phosphorylation. *Mol Cell Biol* 23 (23), 8626–36.
- Cubizolles, F., Martino, F., Perrod, S., Gasser, S. M., 2006. A homotrimer-heterotrimer switch in Sir2 structure differentiates rDNA and telomeric silencing. *Mol Cell* 21 (6), 825–36.
- Cui, F., Zhurkin, V. B., 2009. Distinctive sequence patterns in metazoan and yeast nucleosomes: implications for linker histone binding to AT-rich and methylated DNA. *Nucleic Acids Res* 37 (9), 2818–29.
- Daujat, S., Zeissler, U., Waldmann, T., Happel, N., Schneider, R., 2005. HP1 binds specifically to Lys26-methylated histone H1.4, whereas simultaneous Ser27 phosphorylation blocks HP1 binding. *J Biol Chem* 280 (45), 38090–5.
- Davie, J. R., Saunders, C. A., Walsh, J. M., Weber, S. C., 1981. Histone modifications in the yeast *S. Cerevisiae*. *Nucleic Acids Res* 9 (13), 3205–16.
- De, S., Brown, D. T., Lu, Z. H., Leno, G. H., Wellman, S. E., Sittman, D. B., 2002. Histone H1 variants differentially inhibit DNA replication through an affinity for chromatin mediated by their carboxyl-terminal domains. *Gene* 292 (1-2), 173–81.
- De Lucia, F., Faraone-Mennella, M. R., D’Erme, M., Quesada, P., Caiafa, P., Farina, B., 1994. Histone-induced condensation of rat testis chromatin: testis-specific H1t versus somatic H1 variants. *Biochem Biophys Res Commun* 198 (1), 32–9.
- De Napoles, M., Mermoud, J. E., Wakao, R., Tang, Y. A., Endoh, M., Appanah, R., Nesterova, T. B., Silva, J., Otte, A. P., Vidal, M., Koseki, H., Brockdorff, N., 2004. Polycomb group proteins Ring1A/B link ubiquitylation of histone H2A to heritable gene silencing and X inactivation. *Dev Cell* 7 (5), 663–76.
- Deterding, L. J., Bungler, M. K., Banks, G. C., Tomer, K. B., Archer, T. K., 2008. Global changes in and characterization of specific sites of phosphorylation in mouse and human histone H1 isoforms upon CDK inhibitor treatment using mass spectrometry. *J Proteome Res* 7 (6), 2368–79.
- Diffley, J. F., Stillman, B., 1991. A close relative of the nuclear, chromosomal high-mobility group protein HMG1 in yeast mitochondria. *Proc Natl Acad Sci U S A* 88 (17), 7864–8.
- Dilworth, D. J., Tackett, A. J., Rogers, R. S., Yi, E. C., Christmas, R. H., Smith, J. J., Siegel, A. F., Chait, B. T., Wozniak, R. W., Aitchison, J. D., 2005. The mobile nucleoporin Nup2p and chromatin-bound Prp20p function in endogenous NPC-mediated transcriptional control. *J Cell Biol* 171 (6), 955–65.

- Dion, M. F., Kaplan, T., Kim, M., Buratowski, S., Friedman, N., Rando, O. J., 2007. Dynamics of replication-independent histone turnover in budding yeast. *Science* 315 (5817), 1405–8.
- Dolinski, K. J., Heitman, J., 1999. Hmo1p, a high mobility group 1/2 homolog, genetically and physically interacts with the yeast FKBP12 prolyl isomerase. *Genetics* 151 (3), 935–44.
- Dorigo, B., Schalch, T., Bystricky, K., Richmond, T. J., 2003. Chromatin fiber folding: requirement for the histone H4 N-terminal tail. *J Mol Biol* 327 (1), 85–96.
- Dorigo, B., Schalch, T., Kulangara, A., Duda, S., Schroeder, R. R., Richmond, T. J., 2004. Nucleosome arrays reveal the two-start organization of the chromatin fiber. *Science* 306 (5701), 1571–3.
- Downs, J. A., Kosmidou, E., Morgan, A., Jackson, S. P., 2003. Suppression of homologous recombination by the *Saccharomyces cerevisiae* linker histone. *Mol Cell* 11 (6), 1685–92.
- Errington, N., Doig, A. J., 2005. A phosphoserine-lysine salt bridge within an alpha-helical peptide, the strongest alpha-helix side-chain interaction measured to date. *Biochemistry* 44 (20), 7553–8.
- Escher, D., Schaffner, W., 1997. Gene activation at a distance and telomeric silencing are not affected by yeast histone H1. *Mol Gen Genet* 256 (4), 456–61.
- Fan, J. Y., Gordon, E., Luger, K., Hansen, J. C., Tremethick, D. J., 2002. The essential histone variant H2A.Z regulates the equilibrium between different chromatin conformational states. *Nat Struct Biol* 9 (3), 172–6.
- Fan, Y., Nikitina, T., Morin-Kensicki, E. M., Zhao, J., Magnuson, T. R., Woodcock, C. L., Skoultchi, A. I., 2003. H1 linker histones are essential for mouse development and affect nucleosome spacing *in vivo*. *Mol Cell Biol* 23 (13), 4559–72.
- Fan, Y., Nikitina, T., Zhao, J., Fleury, T. J., Bhattacharyya, R., Bouhassira, E. E., Stein, A., Woodcock, C. L., Skoultchi, A. I., 2005. Histone H1 depletion in mammals alters global chromatin structure but causes specific changes in gene regulation. *Cell* 123 (7), 1199–212.
- Fan, Y., Sirotkin, A., Russell, R. G., Ayala, J., Skoultchi, A. I., 2001. Individual somatic H1 subtypes are dispensable for mouse development even in mice lacking the H1(0) replacement subtype. *Mol Cell Biol* 21 (23), 7933–43.
- Farrow, N. A., Muhandiram, R., Singer, A. U., Pascal, S. M., Kay, C. M., Gish, G., Shoelson, S. E., Pawson, T., Forman-Kay, J. D., Kay, L. E., 1994. Backbone dynamics of a free and phosphopeptide-complexed Src homology 2 domain studied by ¹⁵N NMR relaxation. *Biochemistry* 33 (19), 5984–6003.
- Field, L. M., Lyko, F., Mandrioli, M., Prantera, G., 2004. DNA methylation in insects. *Insect Mol Biol* 13 (2), 109–15.

- Finch, J. T., Klug, A., 1976. Solenoidal model for superstructure in chromatin. *Proc Natl Acad Sci U S A* 73 (6), 1897–901.
- Finch, J. T., Lutter, L. C., Rhodes, D., Brown, R. S., Rushton, B., Levitt, M., Klug, A., 1977. Structure of nucleosome core particles of chromatin. *Nature* 269 (5623), 29–36.
- Formosa, T., Eriksson, P., Wittmeyer, J., Ginn, J., Yu, Y., Stillman, D. J., 2001. Spt16-Pob3 and the HMG protein Nhp6 combine to form the nucleosome-binding factor SPN. *EMBO J* 20 (13), 3506–17.
- Franklin, S. G., Zweidler, A., 1977. Non-allelic variants of histones 2a, 2b and 3 in mammals. *Nature* 266 (5599), 273–5.
- Freidkin, I., Katcoff, D. J., 2001. Specific distribution of the *Saccharomyces cerevisiae* linker histone homolog HHO1p in the chromatin. *Nucleic Acids Res* 29 (19), 4043–51.
- Fuks, F., 2005. DNA methylation and histone modifications: teaming up to silence genes. *Curr Opin Genet Dev* 15 (5), 490–5.
- Furukawa, Y., Ikuta, N., Omata, S., Yamauchi, T., Isobe, T., Ichimura, T., 1993. Demonstration of the phosphorylation-dependent interaction of tryptophan hydroxylase with the 14-3-3 protein. *Biochem Biophys Res Commun* 194 (1), 144–9.
- Gadal, O., Labarre, S., Boschiero, C., Thuriaux, P., 2002. Hmo1, an HMG-box protein, belongs to the yeast ribosomal DNA transcription system. *EMBO J* 21 (20), 5498–507.
- Garcia, B. A., Busby, S. A., Barber, C. M., Shabanowitz, J., Allis, C. D., Hunt, D. F., 2004. Characterization of phosphorylation sites on histone H1 isoforms by tandem mass spectrometry. *J Proteome Res* 3 (6), 1219–27.
- Garcia, B. A., Hake, S. B., Diaz, R. L., Kauer, M., Morris, S. A., Recht, J., Shabanowitz, J., Mishra, N., Strahl, B. D., Allis, C. D., Hunt, D. F., 2007. Organismal differences in post-translational modifications in histones H3 and H4. *J Biol Chem* 282 (10), 7641–55.
- Ghaemmaghami, S., Huh, W. K., Bower, K., Howson, R. W., Belle, A., Dephoure, N., O’Shea, E. K., Weissman, J. S., 2003. Global analysis of protein expression in yeast. *Nature* 425 (6959), 737–41.
- Goffeau, A., Barrell, B. G., Bussey, H., Davis, R. W., Dujon, B., Feldmann, H., Galibert, F., Hoheisel, J. D., Jacq, C., Johnston, M., Louis, E. J., Mewes, H. W., Murakami, Y., Philippsen, P., Tettelin, H., Oliver, S. G., 1996. Life with 6000 genes. *Science* 274 (5287), 546, 563–7.
- Goldknopf, I. L., Busch, H., 1977. Isopeptide linkage between nonhistone and histone 2A polypeptides of chromosomal conjugate-protein A24. *Proc Natl Acad Sci U S A* 74 (3), 864–8.

- Gottlieb, S., Esposito, R. E., 1989. A new role for a yeast transcriptional silencer gene, SIR2, in regulation of recombination in ribosomal DNA. *Cell* 56 (5), 771–6.
- Goytisolo, F. A., Gerchman, S. E., Yu, X., Rees, C., Graziano, V., Ramakrishnan, V., Thomas, J. O., 1996. Identification of two DNA-binding sites on the globular domain of histone H5. *EMBO J* 15 (13), 3421–9.
- Green, G. R., Lee, H. J., Poccia, D. L., 1993. Phosphorylation weakens DNA binding by peptides containing multiple "SPKK" sequences. *J Biol Chem* 268 (15), 11247–55.
- Guillemette, B., Bataille, A. R., Gevry, N., Adam, M., Blanchette, M., Robert, F., Gaudreau, L., 2005. Variant histone H2A.Z is globally localized to the promoters of inactive yeast genes and regulates nucleosome positioning. *PLoS Biol* 3 (12), e384.
- Gurley, L. R., D'Anna, J. A., Barham, S. S., Deaven, L. L., Tobey, R. A., 1978. Histone phosphorylation and chromatin structure during mitosis in Chinese hamster cells. *Eur J Biochem* 84 (1), 1–15.
- Gurley, L. R., Valdez, J. G., Buchanan, J. S., 1995. Characterization of the mitotic specific phosphorylation site of histone H1. Absence of a consensus sequence for the p34cdc2/cyclin B kinase. *J Biol Chem* 270 (46), 27653–60.
- Han, J., Zhou, H., Li, Z., Xu, R. M., Zhang, Z., 2007. Acetylation of lysine 56 of histone H3 catalyzed by RTT109 and regulated by ASF1 is required for replisome integrity. *J Biol Chem* 282 (39), 28587–96.
- Happel, N., Doenecke, D., 2009. Histone H1 and its isoforms: contribution to chromatin structure and function. *Gene* 431 (1-2), 1–12.
- Harvey, A. C., Downs, J. A., 2004. What functions do linker histones provide? *Mol Microbiol* 53 (3), 771–5.
- Hellauer, K., Sirard, E., Turcotte, B., 2001. Decreased expression of specific genes in yeast cells lacking histone H1. *J Biol Chem* 276 (17), 13587–92.
- Hendrickson, F. M., Cole, R. D., 1994. Selectivity in the interaction of various DNA sequences with H1 histone. *Biochemistry* 33 (10), 2997–3006.
- Henzel, M. J., Lever, M. A., Crawford, E., Th'ng, J. P., 2004. The C-terminal domain is the primary determinant of histone H1 binding to chromatin *in vivo*. *J Biol Chem* 279 (19), 20028–34.
- Herrera, J. E., West, K. L., Schiltz, R. L., Nakatani, Y., Bustin, M., 2000. Histone H1 is a specific repressor of core histone acetylation in chromatin. *Mol Cell Biol* 20 (2), 523–9.

- Hewish, D. R., Burgoyne, L. A., 1973. Chromatin sub-structure. The digestion of chromatin DNA at regularly spaced sites by a nuclear deoxyribonuclease. *Biochem Biophys Res Commun* 52 (2), 504–10.
- Hizume, K., Yoshimura, S. H., Takeyasu, K., 2005. Linker histone H1 *per se* can induce three-dimensional folding of chromatin fiber. *Biochemistry* 44 (39), 12978–89.
- Hoffmann, R., Reichert, I., Wachs, W. O., Zeppezauer, M., Kalbitzer, H. R., 1994. ^1H and ^{31}P NMR spectroscopy of phosphorylated model peptides. *Int J Pept Protein Res* 44 (3), 193–8.
- Hohmann, P., Tobey, R. A., Gurley, L. R., 1976. Phosphorylation of distinct regions of fl histone. Relationship to the cell cycle. *J Biol Chem* 251 (12), 3685–92.
- Holliday, R., 1994. Epigenetics: an overview. *Dev Genet* 15 (6), 453–7.
- Holt, L. J., Tuch, B. B., Villen, J., Johnson, A. D., Gygi, S. P., Morgan, D. O., 2009. Global analysis of Cdk1 substrate phosphorylation sites provides insights into evolution. *Science* 325 (5948), 1682–6.
- Horn, P. J., Carruthers, L. M., Logie, C., Hill, D. A., Solomon, M. J., Wade, P. A., Imbalzano, A. N., Hansen, J. C., Peterson, C. L., 2002. Phosphorylation of linker histones regulates ATP-dependent chromatin remodeling enzymes. *Nat Struct Biol* 9 (4), 263–7.
- Huang, J., Brito, I. L., Villen, J., Gygi, S. P., Amon, A., Moazed, D., 2006. Inhibition of homologous recombination by a cohesin-associated clamp complex recruited to the rDNA recombination enhancer. *Genes Dev* 20 (20), 2887–901.
- Huang, J., Moazed, D., 2003. Association of the RENT complex with nontranscribed and coding regions of rDNA and a regional requirement for the replication fork block protein Fob1 in rDNA silencing. *Genes Dev* 17 (17), 2162–76.
- Huynh, V. A., Robinson, P. J., Rhodes, D., 2005. A method for the *in vitro* reconstitution of a defined "30 nm" chromatin fibre containing stoichiometric amounts of the linker histone. *J Mol Biol* 345 (5), 957–68.
- Hymes, J., Fleischhauer, K., Wolf, B., 1995. Biotinylation of histones by human serum biotinidase: assessment of biotinyl-transferase activity in sera from normal individuals and children with biotinidase deficiency. *Biochem Mol Med* 56 (1), 76–83.
- Imai, S., Armstrong, C. M., Kaeberlein, M., Guarente, L., 2000. Transcriptional silencing and longevity protein Sir2 is an NAD-dependent histone deacetylase. *Nature* 403 (6771), 795–800.
- Izaurrealde, E., Kas, E., Laemmli, U. K., 1989. Highly preferential nucleation of histone H1 assembly on scaffold-associated regions. *J Mol Biol* 210 (3), 573–85.

- Jacobs, S. A., Taverna, S. D., Zhang, Y., Briggs, S. D., Li, J., Eisenberg, J. C., Allis, C. D., Khorasanizadeh, S., 2001. Specificity of the HP1 chromo domain for the methylated N-terminus of histone H3. *EMBO J* 20 (18), 5232–41.
- Jedrusik, M. A., Schulze, E., 2007. Linker histone HIS-24 (H1.1) cytoplasmic retention promotes germ line development and influences histone H3 methylation in *Caenorhabditis elegans*. *Mol Cell Biol* 27 (6), 2229–39.
- Jenuwein, T., Allis, C. D., 2001. Translating the histone code. *Science* 293 (5532), 1074–80.
- Jiang, L., Smith, J. N., Anderson, S. L., Ma, P., Mizzen, C. A., Kelleher, N. L., 2007a. Global assessment of combinatorial post-translational modification of core histones in yeast using contemporary mass spectrometry. LYS4 trimethylation correlates with degree of acetylation on the same H3 tail. *J Biol Chem* 282 (38), 27923–34.
- Jiang, T., Zhou, X., Taghizadeh, K., Dong, M., Dedon, P. C., 2007b. N-formylation of lysine in histone proteins as a secondary modification arising from oxidative DNA damage. *Proc Natl Acad Sci U S A* 104 (1), 60–5.
- Jones, D. T., 1999. Protein secondary structure prediction based on position-specific scoring matrices. *J Mol Biol* 292 (2), 195–202.
- Jones, P. L., Veenstra, G. J., Wade, P. A., Vermaak, D., Kass, S. U., Landsberger, N., Strouboulis, J., Wolffe, A. P., 1998. Methylated DNA and MeCP2 recruit histone deacetylase to repress transcription. *Nat Genet* 19 (2), 187–91.
- Juan, L. J., Utley, R. T., Adams, C. C., Vettese-Dadey, M., Workman, J. L., 1994. Differential repression of transcription factor binding by histone H1 is regulated by the core histone amino termini. *EMBO J* 13 (24), 6031–40.
- Juan, L. J., Utley, R. T., Vignali, M., Bohm, L., Workman, J. L., 1997. H1-mediated repression of transcription factor binding to a stably positioned nucleosome. *J Biol Chem* 272 (6), 3635–40.
- Kaeberlein, M., McVey, M., Guarente, L., 1999. The SIR2/3/4 complex and SIR2 alone promote longevity in *Saccharomyces cerevisiae* by two different mechanisms. *Genes Dev* 13 (19), 2570–80.
- Kalakonda, N., Fischle, W., Boccuni, P., Gurvich, N., Hoya-Arias, R., Zhao, X., Miyata, Y., Macgrogan, D., Zhang, J., Sims, J. K., Rice, J. C., Nimer, S. D., 2008. Histone H4 lysine 20 monomethylation promotes transcriptional repression by L3MBTL1. *Oncogene* 27 (31), 4293–304.
- Kamakaka, R. T., Biggins, S., 2005. Histone variants: deviants? *Genes Dev* 19 (3), 295–310.
- Kamakaka, R. T., Thomas, J. O., 1990. Chromatin structure of transcriptionally competent and repressed genes. *EMBO J* 9 (12), 3997–4006.

- Kawasaki, H., Taira, K., 2004. Induction of DNA methylation and gene silencing by short interfering RNAs in human cells. *Nature* 431 (7005), 211–7.
- Khochbin, S., 2001. Histone H1 diversity: bridging regulatory signals to linker histone function. *Gene* 271 (1), 1–12.
- Kim, J., Daniel, J., Espejo, A., Lake, A., Krishna, M., Xia, L., Zhang, Y., Bedford, M. T., 2006. Tudor, MBT and chromo domains gauge the degree of lysine methylation. *EMBO Rep* 7 (4), 397–403.
- Kim, S., Paik, W. K., 1965. Studies on the origin of epsilon-N-methyl-L-lysine in protein. *J Biol Chem* 240 (12), 4629–34.
- Kolodrubetz, D., Burgum, A., 1990. Duplicated NHP6 genes of *Saccharomyces cerevisiae* encode proteins homologous to bovine high mobility group protein 1. *J Biol Chem* 265 (6), 3234–9.
- Kourmouli, N., Jeppesen, P., Mahadevhaiah, S., Burgoyne, P., Wu, R., Gilbert, D. M., Bongiorno, S., Prantera, G., Fanti, L., Pimpinelli, S., Shi, W., Fundele, R., Singh, P. B., 2004. Heterochromatin and tri-methylated lysine 20 of histone H4 in animals. *J Cell Sci* 117 (Pt 12), 2491–501.
- Kouzarides, T., 2007. Chromatin modifications and their function. *Cell* 128 (4), 693–705.
- Krishnakumar, R., Gamble, M. J., Frizzell, K. M., Berrocal, J. G., Kininis, M., Kraus, W. L., 2008. Reciprocal binding of PARP-1 and histone H1 at promoters specifies transcriptional outcomes. *Science* 319 (5864), 819–21.
- Krogan, N. J., Cagney, G., Yu, H., Zhong, G., Guo, X., Ignatchenko, A., Li, J., Pu, S., Datta, N., Tikuisis, A. P., Punna, T., Peregrin-Alvarez, J. M., Shales, M., Zhang, X., Davey, M., Robinson, M. D., Paccanaro, A., Bray, J. E., Sheung, A., Beattie, B., Richards, D. P., Canadian, V., Lalev, A., Mena, F., Wong, P., Starostine, A., Canete, M. M., Vlasblom, J., Wu, S., Orsi, C., Collins, S. R., Chandran, S., Haw, R., Rilstone, J. J., Gandi, K., Thompson, N. J., Musso, G., St Onge, P., Ghanny, S., Lam, M. H., Butland, G., Altaf-Ul, A. M., Kanaya, S., Shilatifard, A., O’Shea, E., Weissman, J. S., Ingles, C. J., Hughes, T. R., Parkinson, J., Gerstein, M., Wodak, S. J., Emili, A., Greenblatt, J. F., 2006. Global landscape of protein complexes in the yeast *Saccharomyces cerevisiae*. *Nature* 440 (7084), 637–43.
- Kumar, N. M., Walker, I. O., 1980. The binding of histones H1 and H5 to chromatin in chicken erythrocyte nuclei. *Nucleic Acids Res* 8 (16), 3535–51.
- Laemmli, U. K., Kas, E., Poljak, L., Adachi, Y., 1992. Scaffold-associated regions: cis-acting determinants of chromatin structural loops and functional domains. *Curr Opin Genet Dev* 2 (2), 275–85.
- Lambert, J. P., Mitchell, L., Rudner, A., Baetz, K., Figeys, D., 2009. A novel proteomics approach for the discovery of chromatin-associated protein networks. *Mol Cell Proteomics* 8 (4), 870–82.

- Landsman, D., 1996. Histone H1 in *Saccharomyces cerevisiae*: a double mystery solved? Trends Biochem Sci 21 (8), 287–8.
- Lee, C. K., Shibata, Y., Rao, B., Strahl, B. D., Lieb, J. D., 2004. Evidence for nucleosome depletion at active regulatory regions genome-wide. Nat Genet 36 (8), 900–5.
- Lever, M. A., Th'ng, J. P., Sun, X., Hendzel, M. J., 2000. Rapid exchange of histone H1.1 on chromatin in living human cells. Nature 408 (6814), 873–6.
- Levine, A., Yeivin, A., Ben-Asher, E., Aloni, Y., Razin, A., 1993. Histone H1-mediated inhibition of transcription initiation of methylated templates in vitro. J Biol Chem 268 (29), 21754–9.
- Levy, A., Eyal, M., Hershkovits, G., Salmon-Divon, M., Klutstein, M., Katcoff, D. J., 2008. Yeast linker histone Hho1p is required for efficient RNA polymerase I processivity and transcriptional silencing at the ribosomal DNA. Proc Natl Acad Sci U S A 105 (33), 11703–8.
- Li, B., Pattenden, S. G., Lee, D., Gutierrez, J., Chen, J., Seidel, C., Gerton, J., Workman, J. L., 2005. Preferential occupancy of histone variant H2AZ at inactive promoters influences local histone modifications and chromatin remodeling. Proc Natl Acad Sci U S A 102 (51), 18385–90.
- Li, C., Mueller, J. E., Elflin, M., Bryk, M., 2008. Linker histone H1 represses recombination at the ribosomal DNA locus in the budding yeast *Saccharomyces cerevisiae*. Mol Microbiol 67 (4), 906–19.
- Li, X., Gerber, S. A., Rudner, A. D., Beausoleil, S. A., Haas, W., Villen, J., Elias, J. E., Gygi, S. P., 2007. Large-scale phosphorylation analysis of alpha-factor-arrested *Saccharomyces cerevisiae*. J Proteome Res 6 (3), 1190–7.
- Liebich, H. M., Gesele, E., Wirth, C., Woll, J., Jobst, K., Lakatos, A., 1993. Non-enzymatic glycation of histones. Biol Mass Spectrom 22 (2), 121–3.
- Lindner, H., Sarg, B., Hoertnagl, B., Helliger, W., 1998. The microheterogeneity of the mammalian H1(0) histone. Evidence for an age-dependent deamidation. J Biol Chem 273 (21), 13324–30.
- Liu, C. L., Kaplan, T., Kim, M., Buratowski, S., Schreiber, S. L., Friedman, N., Rando, O. J., 2005. Single-nucleosome mapping of histone modifications in *S. cerevisiae*. PLoS Biol 3 (10), e328.
- Liu, D., Wang, C., Li, J., Wang, Z., Xu, B., Wei, Z., Lin, Z., Qin, J., Cao, E., Bai, C., 2001. Visualization of reconstituted solenoid chromatin structure by tapping mode atomic force microscopy. Surf. Interface Anal. 32, 20–26.
- Lowary, P. T., Widom, J., 1989. Higher-order structure of *Saccharomyces cerevisiae* chromatin. Proc Natl Acad Sci U S A 86 (21), 8266–70.

- Lowary, P. T., Widom, J., 1998. New DNA sequence rules for high affinity binding to histone octamer and sequence-directed nucleosome positioning. *J Mol Biol* 276 (1), 19–42.
- Lu, J., Kobayashi, R., Brill, S. J., 1996. Characterization of a high mobility group 1/2 homolog in yeast. *J Biol Chem* 271 (52), 33678–85.
- Lu, X., Hamkalo, B., Parseghian, M. H., Hansen, J. C., 2009. Chromatin condensing functions of the linker histone C-terminal domain are mediated by specific amino acid composition and intrinsic protein disorder. *Biochemistry* 48 (1), 164–72.
- Lu, X., Hansen, J. C., 2004. Identification of specific functional subdomains within the linker histone H1⁰ C-terminal domain. *J Biol Chem* 279 (10), 8701–7.
- Luger, K., Mader, A. W., Richmond, R. K., Sargent, D. F., Richmond, T. J., 1997. Crystal structure of the nucleosome core particle at 2.8 Å resolution. *Nature* 389 (6648), 251–60.
- Lyko, F., Ramsahoye, B. H., Jaenisch, R., 2000. DNA methylation in *Drosophila melanogaster*. *Nature* 408 (6812), 538–40.
- Maresca, T. J., Freedman, B. S., Heald, R., 2005. Histone H1 is essential for mitotic chromosome architecture and segregation in *Xenopus laevis* egg extracts. *J Cell Biol* 169 (6), 859–69.
- Mavrich, T. N., Ioshikhes, I. P., Venters, B. J., Jiang, C., Tomsho, L. P., Qi, J., Schuster, S. C., Albert, I., Pugh, B. F., 2008. A barrier nucleosome model for statistical positioning of nucleosomes throughout the yeast genome. *Genome Res* 18 (7), 1073–83.
- McArthur, M., Thomas, J. O., 1996. A preference of histone H1 for methylated DNA. *EMBO J* 15 (7), 1705–14.
- Meersseman, G., Pennings, S., Bradbury, E. M., 1991. Chromatosome positioning on assembled long chromatin. Linker histones affect nucleosome placement on 5 S rDNA. *J Mol Biol* 220 (1), 89–100.
- Meneghini, M. D., Wu, M., Madhani, H. D., 2003. Conserved histone variant H2A.Z protects euchromatin from the ectopic spread of silent heterochromatin. *Cell* 112 (5), 725–36.
- Merz, K., Hondele, M., Goetze, H., Gmelch, K., Stoeckl, U., Griesenbeck, J., 2008. Actively transcribed rRNA genes in *S. cerevisiae* are organized in a specialized chromatin associated with the high-mobility group protein Hmo1 and are largely devoid of histone molecules. *Genes Dev* 22 (9), 1190–204.
- Misteli, T., Gunjan, A., Hock, R., Bustin, M., Brown, D. T., 2000. Dynamic binding of histone H1 to chromatin in living cells. *Nature* 408 (6814), 877–81.

- Moll, R., Wintersberger, E., 1976. Synthesis of yeast histones in the cell cycle. *Proc Natl Acad Sci U S A* 73 (6), 1863–7.
- Moore, S. C., Jason, L., Ausio, J., 2002. The elusive structural role of ubiquitinated histones. *Biochem Cell Biol* 80 (3), 311–9.
- Morrison, A. J., Highland, J., Krogan, N. J., Arbel-Eden, A., Greenblatt, J. F., Haber, J. E., Shen, X., 2004. INO80 and gamma-H2AX interaction links ATP-dependent chromatin remodeling to DNA damage repair. *Cell* 119 (6), 767–75.
- Murray, K., 1964. The Occurrence of Epsilon-N-Methyl Lysine in Histones. *Biochemistry* 3, 10–5.
- Nacheva, G. A., Guschin, D. Y., Preobrazhenskaya, O. V., Karpov, V. L., Ebralidse, K. K., Mirzabekov, A. D., 1989. Change in the pattern of histone binding to DNA upon transcriptional activation. *Cell* 58 (1), 27–36.
- Nan, X., Ng, H. H., Johnson, C. A., Laherty, C. D., Turner, B. M., Eisenman, R. N., Bird, A., 1998. Transcriptional repression by the methyl-CpG-binding protein MeCP2 involves a histone deacetylase complex. *Nature* 393 (6683), 386–9.
- Neelin, J. M., Callahan, P. X., Lamb, D. C., Murray, K., 1964. The Histones of Chicken Erythrocyte Nuclei. *Can J Biochem Physiol* 42, 1743–52.
- Neidhardt, F. C., Bloch, P. L., Smith, D. F., 1974. Culture medium for enterobacteria. *J Bacteriol* 119 (3), 736–47.
- Nelson, P. P., Albright, S. C., Wiseman, J. M., Garrard, W. T., 1979. Reassociation of histone H1 with nucleosomes. *J Biol Chem* 254 (22), 11751–60.
- Ng, H. H., Feng, Q., Wang, H., Erdjument-Bromage, H., Tempst, P., Zhang, Y., Struhl, K., 2002. Lysine methylation within the globular domain of histone H3 by Dot1 is important for telomeric silencing and Sir protein association. *Genes Dev* 16 (12), 1518–27.
- Nightingale, K., Wolffe, A. P., 1995. Methylation at CpG sequences does not influence histone H1 binding to a nucleosome including a *Xenopus borealis* 5 S rRNA gene. *J Biol Chem* 270 (9), 4197–200.
- Nishioka, K., Rice, J. C., Sarma, K., Erdjument-Bromage, H., Werner, J., Wang, Y., Chuikov, S., Valenzuela, P., Tempst, P., Steward, R., Lis, J. T., Allis, C. D., Reinberg, D., 2002. PR-Set7 is a nucleosome-specific methyltransferase that modifies lysine 20 of histone H4 and is associated with silent chromatin. *Mol Cell* 9 (6), 1201–13.
- Okano, M., Bell, D. W., Haber, D. A., Li, E., 1999. DNA methyltransferases Dnmt3a and Dnmt3b are essential for *de novo* methylation and mammalian development. *Cell* 99 (3), 247–57.

- Ono, K., Kusano, O., Shimotakahara, S., Shimizu, M., Yamazaki, T., Shindo, H., 2003. The linker histone homolog Hho1p from *Saccharomyces cerevisiae* represents a winged helix-turn-helix fold as determined by NMR spectroscopy. *Nucleic Acids Res* 31 (24), 7199–207.
- Orrego, M., Ponte, I., Roque, A., Buschati, N., Mora, X., Suau, P., 2007. Differential affinity of mammalian histone H1 somatic subtypes for DNA and chromatin. *BMC Biol* 5, 22.
- Osmotherly, L., 2006. The yeast linker histone homologue, Hho1p: unstructured regions and further characterisation of domain structure. Master's thesis, University of Cambridge.
- Ottaviani, D., Lever, E., Takousis, P., Sheer, D., 2008. Anchoring the genome. *Genome Biol* 9 (1), 201.
- Palmer, D. K., O'Day, K., Trong, H. L., Charbonneau, H., Margolis, R. L., 1991. Purification of the centromere-specific protein CENP-A and demonstration that it is a distinctive histone. *Proc Natl Acad Sci U S A* 88 (9), 3734–8.
- Panchal, S. C., Bhavesh, N. S., Hosur, R. V., 2001. Improved 3D triple resonance experiments, HNN and HN(C)N, for HN and ¹⁵N sequential correlations in (¹³C, ¹⁵N) labeled proteins: application to unfolded proteins. *J Biomol NMR* 20 (2), 135–47.
- Pang, C. N., Gasteiger, E., Wilkins, M. R., 2010. Identification of arginine- and lysine-methylation in the proteome of *Saccharomyces cerevisiae* and its functional implications. *BMC Genomics* 11, 92.
- Pannetier, M., Julien, E., Schotta, G., Tardat, M., Sardet, C., Jenuwein, T., Feil, R., 2008. PR-SET7 and SUV4-20H regulate H4 lysine-20 methylation at imprinting control regions in the mouse. *EMBO Rep* 9 (10), 998–1005.
- Patterton, H. G., Landel, C. C., Landsman, D., Peterson, C. L., Simpson, R. T., 1998. The biochemical and phenotypic characterization of Hho1p, the putative linker histone H1 of *Saccharomyces cerevisiae*. *J Biol Chem* 273 (13), 7268–76.
- Paull, T. T., Johnson, R. C., 1995. DNA looping by *Saccharomyces cerevisiae* high mobility group proteins NHP6A/B. Consequences for nucleoprotein complex assembly and chromatin condensation. *J Biol Chem* 270 (15), 8744–54.
- Paulson, J. R., Mesner, P. W., Delrow, J. J., Mahmoud, N. N., Ciesielski, W. A., 1992. Rapid analysis of mitotic histone H1 phosphorylation by cationic disc electrophoresis at neutral pH in minigels. *Anal Biochem* 203 (2), 227–34.
- Peng, K., Vucetic, S., Radivojac, P., Brown, C. J., Dunker, A. K., Obradovic, Z., 2005. Optimizing long intrinsic disorder predictors with protein evolutionary information. *J Bioinform Comput Biol* 3 (1), 35–60.

- Pennings, S., Meersseman, G., Bradbury, E. M., 1994. Linker histones H1 and H5 prevent the mobility of positioned nucleosomes. *Proc Natl Acad Sci U S A* 22 (91), 10275–9.
- Perry, C. A., Annunziato, A. T., 1991. Histone acetylation reduces H1-mediated nucleosome interactions during chromatin assembly. *Exp Cell Res* 196 (2), 337–45.
- Pham, A. D., Sauer, F., 2000. Ubiquitin-activating/conjugating activity of TAFII250, a mediator of activation of gene expression in *Drosophila*. *Science* 289 (5488), 2357–60.
- Philo, J. S., 2006. Improved methods for fitting sedimentation coefficient distributions derived by time-derivative techniques. *Anal Biochem* 354 (2), 238–46.
- Plath, K., Fang, J., Mlynarczyk-Evans, S. K., Cao, R., Worringer, K. A., Wang, H., de la Cruz, C. C., Otte, A. P., Panning, B., Zhang, Y., 2003. Role of histone H3 lysine 27 methylation in X inactivation. *Science* 300 (5616), 131–5.
- Poirier, G. G., de Murcia, G., Jongstra-Bilen, J., Niedergang, C., Mandel, P., 1982. Poly(ADP-ribosyl)ation of polynucleosomes causes relaxation of chromatin structure. *Proc Natl Acad Sci U S A* 79 (11), 3423–7.
- Puig, S., Matallana, E., Perez-Ortin, J. E., 1999. Stochastic nucleosome positioning in a yeast chromatin region is not dependent on histone H1. *Curr Microbiol* 39 (3), 168–72.
- Radivojac, P., Vacic, V., Haynes, C., Cocklin, R. R., Mohan, A., Heyen, J. W., Goebel, M. G., Iakoucheva, L. M., 2010. Identification, analysis, and prediction of protein ubiquitination sites. *Proteins* 78 (2), 365–80.
- Ramakrishnan, V., 1997. Histone structure and the organization of the nucleosome. *Annu Rev Biophys Biomol Struct* 26, 83–112.
- Ramakrishnan, V., Finch, J. T., Graziano, V., Lee, P. L., Sweet, R. M., 1993. Crystal structure of globular domain of histone H5 and its implications for nucleosome binding. *Nature* 362 (6417), 219–23.
- Ramon, A., Muro-Pastor, M. I., Scazzocchio, C., Gonzalez, R., 2000. Deletion of the unique gene encoding a typical histone H1 has no apparent phenotype in *Aspergillus nidulans*. *Mol Microbiol* 35 (1), 223–33.
- Ray-Gallet, D., Gerard, A., Polo, S., Almouzni, G., 2005. Variations on the topic of the "histone code". *Medecine sciences : M/S* 21 (4), 384–389.
- Renz, M., Day, L. A., 1976. Transition from noncooperative to cooperative and selective binding of histone H1 to DNA. *Biochemistry* 15 (15), 3220–8.
- Richmond, T. J., Davey, C. A., 2003. The structure of DNA in the nucleosome core. *Nature* 423 (6936), 145–50.

- Ridsdale, J. A., Hendzel, M. J., Delcuve, G. P., Davie, J. R., 1990. Histone acetylation alters the capacity of the H1 histones to condense transcriptionally active/competent chromatin. *J Biol Chem* 265 (9), 5150–6.
- Robinson, P. J., An, W., Routh, A., Martino, F., Chapman, L., Roeder, R. G., Rhodes, D., 2008. 30 nm chromatin fibre decompaction requires both H4-K16 acetylation and linker histone eviction. *J Mol Biol* 381 (4), 816–25.
- Robinson, P. J., Fairall, L., Huynh, V. A., Rhodes, D., 2006. EM measurements define the dimensions of the "30-nm" chromatin fiber: evidence for a compact, interdigitated structure. *Proc Natl Acad Sci U S A* 103 (17), 6506–11.
- Roque, A., Iloro, I., Ponte, I., Arrondo, J. L., Suau, P., 2005. DNA-induced secondary structure of the carboxyl-terminal domain of histone H1. *J Biol Chem* 280 (37), 32141–7.
- Roque, A., Ponte, I., Arrondo, J. L., Suau, P., 2008. Phosphorylation of the carboxy-terminal domain of histone H1: effects on secondary structure and DNA condensation. *Nucleic Acids Res* 36 (14), 4719–26.
- Roth, A. F., Wan, J., Bailey, A. O., Sun, B., Kuchar, J. A., Green, W. N., Phinney, B. S., Yates, J. R., Davis, N. G., 2006. Global analysis of protein palmitoylation in yeast. *Cell* 125 (5), 1003–13.
- Roth, S. Y., Allis, C. D., 1992. Chromatin condensation: does histone H1 dephosphorylation play a role? *Trends Biochem Sci* 17 (3), 93–8.
- Routh, A., Sandin, S., Rhodes, D., 2008. Nucleosome repeat length and linker histone stoichiometry determine chromatin fiber structure. *Proc Natl Acad Sci U S A* 105 (26), 8872–7.
- Sambrook, J., Fritsch, E. F., Maniatis, T., 1989. *Molecular cloning - a laboratory manual*. Cold Spring Harbor Laboratory Press.
- Sanderson, A., Stott, K., Stevens, T. J., Thomas, J. O., 2005. Engineering the structural stability and functional properties of the GI domain into the intrinsically unfolded GII domain of the yeast linker histone Hho1p. *J Mol Biol* 349 (3), 608–20.
- Santisteban, M. S., Arents, G., Moudrianakis, E. N., Smith, M. M., 1997. Histone octamer function in vivo: mutations in the dimer-tetramer interfaces disrupt both gene activation and repression. *EMBO J* 16 (9), 2493–506.
- Sarg, B., Helliger, W., Talasz, H., Forg, B., Lindner, H. H., 2006. Histone H1 phosphorylation occurs site-specifically during interphase and mitosis: identification of a novel phosphorylation site on histone H1. *J Biol Chem* 281 (10), 6573–80.
- Satchwell, S. C., Drew, H. R., Travers, A. A., 1986. Sequence periodicities in chicken nucleosome core DNA. *J Mol Biol* 191 (4), 659–75.

- Schäfer, G., McEvoy, C. R., Patterton, H. G., 2008. The *Saccharomyces cerevisiae* linker histone Hho1p is essential for chromatin compaction in stationary phase and is displaced by transcription. *Proc Natl Acad Sci U S A* 105 (39), 14838–43.
- Schäfer, G., Smith, E. M., Patterton, H. G., 2005. The *Saccharomyces cerevisiae* linker histone Hho1p, with two globular domains, can simultaneously bind to two four-way junction DNA molecules. *Biochemistry* 44 (50), 16766–75.
- Schalch, T., Duda, S., Sargent, D. F., Richmond, T. J., 2005. X-ray structure of a tetranucleosome and its implications for the chromatin fibre. *Nature* 436 (7047), 138–41.
- Schlissel, M. S., Brown, D. D., 1984. The transcriptional regulation of *Xenopus* 5s RNA genes in chromatin: the roles of active stable transcription complexes and histone H1. *Cell* 37 (3), 903–13.
- Schneider, J., Bajwa, P., Johnson, F. C., Bhaumik, S. R., Shilatifard, A., 2006. Rtt109 is required for proper H3K56 acetylation: a chromatin mark associated with the elongating RNA polymerase II. *J Biol Chem* 281 (49), 37270–4.
- Schultz, D. C., Ayyanathan, K., Negorev, D., Maul, G. G., Rauscher, 3rd, F. J., 2002. SETDB1: a novel KAP-1-associated histone H3, lysine 9-specific methyltransferase that contributes to HP1-mediated silencing of euchromatic genes by KRAB zinc-finger proteins. *Genes Dev* 16 (8), 919–32.
- Schwarzinger, S., Kroon, G. J., Foss, T. R., Chung, J., Wright, P. E., Dyson, H. J., 2001. Sequence-dependent correction of random coil NMR chemical shifts. *J Am Chem Soc* 123 (13), 2970–8.
- Segal, E., Fondufe-Mittendorf, Y., Chen, L., Thastrom, A., Field, Y., Moore, I. K., Wang, J. P., Widom, J., 2006. A genomic code for nucleosome positioning. *Nature* 442 (7104), 772–8.
- Shen, X., Gorovsky, M. A., 1996. Linker histone H1 regulates specific gene expression but not global transcription *in vivo*. *Cell* 86 (3), 475–83.
- Shen, X., Ranallo, R., Choi, E., Wu, C., 2003. Involvement of actin-related proteins in ATP-dependent chromatin remodeling. *Mol Cell* 12 (1), 147–55.
- Shi, X., Hong, T., Walter, K. L., Ewalt, M., Michishita, E., Hung, T., Carney, D., Peña, P., Lan, F., Kaadige, M. R., Lacoste, N., Cayrou, C., Davrazou, F., Saha, A., Cairns, B. R., Ayer, D. E., Kutateladze, T. G., Shi, Y., Côté, J., Chua, K. F., Gozani, O., 2006. ING2 PHD domain links histone H3 lysine 4 methylation to active gene repression. *Nature* 442 (7098), 96–9.
- Shooter, K. V., Goodwin, G. H., Johns, E. W., 1974. Interactions of a purified non-histone chromosomal protein with DNA and histone. *Eur J Biochem* 47 (2), 263–70.

- Simpson, R. T., 1978. Structure of the chromatosome, a chromatin particle containing 160 base pairs of DNA and all the histones. *Biochemistry* 17 (25), 5524–31.
- Sinz, A., 2003. Chemical cross-linking and mass spectrometry for mapping three-dimensional structures of proteins and protein complexes. *J Mass Spectrom* 38 (12), 1225–37.
- Sivolob, A., Prunell, A., 2003. Linker histone-dependent organization and dynamics of nucleosome entry/exit DNAs. *J Mol Biol* 331 (5), 1025–40.
- Snijders, A. P., Pongdam, S., Lambert, S. J., Wood, C. M., Baldwin, J. P., Dickman, M. J., 2008. Characterization of post-translational modifications of the linker histones H1 and H5 from chicken erythrocytes using mass spectrometry. *J Proteome Res* 7 (10), 4326–35.
- Sommer, 1978. Yeast chromatin: search for histone H1. *Mol Gen Genet* 161 (3), 323–31.
- Songyang, Z., Blechner, S., Hoagland, N., Hoekstra, M. E., Piwnica-Worms, H., Cantley, L. C., 1994. Use of an oriented peptide library to determine the optimal substrates of protein kinases. *Curr Biol* 4 (11), 973–82.
- Spadafora, C., Bellard, M., Compton, J. L., Chambon, P., 1976. The DNA repeat lengths in chromatins from sea urchin sperm and gastrule cells are markedly different. *FEBS Lett* 69 (1), 281–5.
- Spellman, P. T., Sherlock, G., Zhang, M. Q., Iyer, V. R., Anders, K., Eisen, M. B., Brown, P. O., Botstein, D., Futcher, B., 1998. Comprehensive identification of cell cycle-regulated genes of the yeast *Saccharomyces cerevisiae* by microarray hybridization. *Mol Biol Cell* 9 (12), 3273–97.
- Spera, S., Bax, A., 1991. Empirical Correlation between Protein Backbone Conformation and C^α and C^β ^{13}C Nuclear magnetic Resonance Chemical Shifts. *J Am Chem Soc* 113, 5490–5492.
- Srebrevna, L., Zlatanova, J., Miloshev, G., Tsanev, R., 1987. Immunological evidence for the existence of H1-like histone in yeast. *Eur J Biochem* 165 (2), 449–54.
- Stafford, W. F., 1992. Boundary analysis in sedimentation transport experiments: a procedure for obtaining sedimentation coefficient distributions using the time derivative of the concentration profile. *Anal Biochem* 203 (2), 295–301.
- Staynov, D. Z., 2008. The controversial 30 nm chromatin fibre. *Bioessays* 30 (10), 1003–9.
- Staynov, D. Z., Crane-Robinson, C., 1988. Footprinting of linker histones H5 and H1 on the nucleosome. *EMBO J* 7 (12), 3685–91.

- Stevenson-Lindert, L. M., Fowler, P., Lew, J., 2003. Substrate specificity of CDK2-cyclin A. What is optimal? *J Biol Chem* 278 (51), 50956–60.
- Strahl, B. D., Allis, C. D., 2000. The language of covalent histone modifications. *Nature* 403 (6765), 41–5.
- Strickland, W. N., Strickland, M., Brandt, W. F., Von Holt, C., Lehmann, A., Wittmann-Liebold, B., 1980. The primary structure of histone H1 from sperm of the sea urchin *Parechinus angulosus*. 2. Sequence of the C-terminal CNBr peptide and the entire primary structure. *Eur J Biochem* 104 (2), 567–78.
- Suzuki, M., 1989. SPKK, a new nucleic acid-binding unit of protein found in histone. *EMBO J* 8 (3), 797–804.
- Szerlong, H., Saha, A., Cairns, B. R., 2003. The nuclear actin-related proteins Arp7 and Arp9: a dimeric module that cooperates with architectural proteins for chromatin remodeling. *EMBO J* 22 (12), 3175–87.
- Szwarcwort-Cohen, M., Kasulin-Boneh, Z., Sagee, S., Kassir, Y., 2009. Human Cdk2 is a functional homolog of budding yeast Ime2, the meiosis-specific Cdk-like kinase. *Cell Cycle* 8 (4), 647–54.
- Talasz, H., Helliger, W., Puschendorf, B., Lindner, H., 1996. *In vivo* phosphorylation of histone H1 variants during the cell cycle. *Biochemistry* 35 (6), 1761–7.
- Tanny, J. C., Dowd, G. J., Huang, J., Hilz, H., Moazed, D., 1999. An enzymatic activity in the yeast Sir2 protein that is essential for gene silencing. *Cell* 99 (7), 735–45.
- Tarassov, K., Messier, V., Landry, C. R., Radinovic, S., Serna Molina, M. M., Shames, I., Malitskaya, Y., Vogel, J., Bussey, H., Michnick, S. W., 2008. An *in vivo* map of the yeast protein interactome. *Science* 320 (5882), 1465–70.
- Thastrom, A., Lowary, P. T., Widlund, H. R., Cao, H., Kubista, M., Widom, J., 1999. Sequence motifs and free energies of selected natural and non-natural nucleosome positioning DNA sequences. *J Mol Biol* 288 (2), 213–29.
- Th'ng, J. P., Guo, X. W., Swank, R. A., Crissman, H. A., Bradbury, E. M., 1994. Inhibition of histone phosphorylation by staurosporine leads to chromosome decondensation. *J Biol Chem* 269 (13), 9568–73.
- Th'ng, J. P., Sung, R., Ye, M., Hendzel, M. J., 2005. H1 family histones in the nucleus. Control of binding and localization by the C-terminal domain. *J Biol Chem* 280 (30), 27809–14.
- Thoma, F., Koller, T., Klug, A., 1979. Involvement of histone H1 in the organization of the nucleosome and of the salt-dependent superstructures of chromatin. *J Cell Biol* 83 (2 Pt 1), 403–27.
- Thomas, J. O., 1984. The higher order structure of chromatin and histone H1. *J Cell Sci Suppl* 1, 1–20.

- Thomas, J. O., 1989. Chemical cross-linking of histones. *Methods Enzymol* 170, 549–71.
- Thomas, J. O., 1998. Isolation and fractionation of chromatin and linker histones. In: Gould, H. J. (Ed.), *Chromatin. A practical approach*. Oxford University Press, pp. 1–33.
- Thomas, J. O., Furber, V., 1976. Yeast chromatin structure. *FEBS Lett* 66 (2), 274–80.
- Thomas, J. O., Kornberg, R. D., 1975. An octamer of histones in chromatin and free in solution. *Proc Natl Acad Sci U S A* 72 (7), 2626–30.
- Thomas, J. O., Kornberg, R. D., 1978. The study of histone–histone associations by chemical cross-linking. *Methods Cell Biol* 18, 429–40.
- Thomas, J. O., Rees, C., 1983. Exchange of histones H1 and H5 between chromatin fragments. A preference of H5 for higher-order structures. *Eur J Biochem* 134 (1), 109–15.
- Thomas, J. O., Thompson, R. J., 1977. Variation in chromatin structure in two cell types from the same tissue: a short DNA repeat length in cerebral cortex neurons. *Cell* 10 (4), 633–40.
- Thorne, A. W., Sautiere, P., Briand, G., Crane-Robinson, C., 1987. The structure of ubiquitinated histone H2B. *EMBO J* 6 (4), 1005–10.
- Tong, A. H., Lesage, G., Bader, G. D., Ding, H., Xu, H., Xin, X., Young, J., Berriz, G. F., Brost, R. L., Chang, M., Chen, Y., Cheng, X., Chua, G., Friesen, H., Goldberg, D. S., Haynes, J., Humphries, C., He, G., Hussein, S., Ke, L., Krogan, N., Li, Z., Levinson, J. N., Lu, H., Menard, P., Munyana, C., Parsons, A. B., Ryan, O., Tonikian, R., Roberts, T., Sdicu, A. M., Shapiro, J., Sheikh, B., Suter, B., Wong, S. L., Zhang, L. V., Zhu, H., Burd, C. G., Munro, S., Sander, C., Rine, J., Greenblatt, J., Peter, M., Bretscher, A., Bell, G., Roth, F. P., Brown, G. W., Andrews, B., Bussey, H., Boone, C., 2004. Global mapping of the yeast genetic interaction network. *Science* 303 (5659), 808–13.
- Tong, A. H. Y., Boone, C., 2006. Synthetic genetic array analysis in *Saccharomyces cerevisiae*. *Methods Mol Biol* 313, 171–92.
- Travers, A. A., 1987. DNA bending and nucleosome positioning. *Trends Biochem Sci* 12, 108–112.
- Tsai, C. D., Ma, B., Kumar, S., Wolfson, H., Nussinov, R., 2001a. Protein folding: binding of conformationally fluctuating building blocks via population selection. *Crit Rev Biochem Mol Biol* 36 (5), 399–433.
- Tsai, C. J., Ma, B., Sham, Y. Y., Kumar, S., Nussinov, R., 2001b. Structured disorder and conformational selection. *Proteins* 44 (4), 418–27.

- Tse, C., Sera, T., Wolffe, A. P., Hansen, J. C., 1998. Disruption of higher-order folding by core histone acetylation dramatically enhances transcription of nucleosomal arrays by RNA polymerase III. *Mol Cell Biol* 18 (8), 4629–38.
- Turner, B. M., Birley, A. J., Lavender, J., 1992. Histone H4 isoforms acetylated at specific lysine residues define individual chromosomes and chromatin domains in *Drosophila polytene* nuclei. *Cell* 69 (2), 375–84.
- Ushinsky, S. C., Bussey, H., Ahmed, A. A., Wang, Y., Friesen, J., Williams, B. A., Storms, R. K., 1997. Histone H1 in *Saccharomyces cerevisiae*. *Yeast* 13 (2), 151–61.
- Vakoc, C. R., Mandat, S. A., Olenchock, B. A., Blobel, G. A., 2005. Histone H3 lysine 9 methylation and HP1gamma are associated with transcription elongation through mammalian chromatin. *Mol Cell* 19 (3), 381–91.
- van Holde, K., 1989. *Chromatin*. Springer-Verlag, New York.
- van Leeuwen, F., Gafken, P. R., Gottschling, D. E., 2002. Dot1p modulates silencing in yeast by methylation of the nucleosome core. *Cell* 109 (6), 745–56.
- Vaquero, A., Scher, M., Lee, D., Erdjument-Bromage, H., Tempst, P., Reinberg, D., 2004. Human SirT1 interacts with histone H1 and promotes formation of facultative heterochromatin. *Mol Cell* 16 (1), 93–105.
- Varga-Weisz, P., Zlatanova, J., Leuba, S. H., Schroth, G. P., van Holde, K., 1994. Binding of histones H1 and H5 and their globular domains to four-way junction DNA. *Proc Natl Acad Sci U S A* 91 (9), 3525–9.
- Veron, M., Zou, Y., Yu, Q., Bi, X., Selmi, A., Gilson, E., Defossez, P. A., 2006. Histone H1 of *Saccharomyces cerevisiae* inhibits transcriptional silencing. *Genetics* 173 (2), 579–87.
- Villar-Garea, A., Imhof, A., 2008. Fine mapping of posttranslational modifications of the linker histone H1 from *Drosophila melanogaster*. *PLoS One* 3 (2), e1553.
- Virstedt, J., Berge, T., Henderson, R. M., Waring, M. J., Travers, A. A., 2004. The influence of DNA stiffness upon nucleosome formation. *J Struct Biol* 148 (1), 66–85.
- Vranken, W. F., Boucher, W., Stevens, T. J., Fogh, R. H., Pajon, A., Llinas, M., Ulrich, E. L., Markley, J. L., Ionides, J., Laue, E. D., 2005. The CCPN data model for NMR spectroscopy: development of a software pipeline. *Proteins* 59 (4), 687–96.
- Ward, I. M., Chen, J., 2001. Histone H2AX is phosphorylated in an ATR-dependent manner in response to replicational stress. *J Biol Chem* 276 (51), 47759–62.

- Waterborg, J. H., 2000. Steady-state levels of histone acetylation in *Saccharomyces cerevisiae*. *J Biol Chem* 275 (17), 13007–11.
- Watt, F., Molloy, P. L., 1988. Cytosine methylation prevents binding to DNA of a HeLa cell transcription factor required for optimal expression of the adenovirus major late promoter. *Genes Dev* 2 (9), 1136–43.
- Webb, M., Thomas, J. O., 1999. Structure-specific binding of the two tandem HMG boxes of HMG1 to four-way junction DNA is mediated by the A domain. *J Mol Biol* 294 (2), 373–87.
- Weber, S., Isenberg, I., 1980. High mobility group proteins of *Saccharomyces cerevisiae*. *Biochemistry* 19 (10), 2236–40.
- Weintraub, H., 1984. Histone-H1-dependent chromatin superstructures and the suppression of gene activity. *Cell* 38 (1), 17–27.
- Wells, D., Brown, D., 1991. Histone and histone gene compilation and alignment update. *Nucleic Acids Res* 19 Suppl, 2173–88.
- Wells, D., McBride, C., 1989. A comprehensive compilation and alignment of histones and histone genes. *Nucleic Acids Res* 17 Suppl, r311–46.
- White, C. L., Suto, R. K., Luger, K., 2001. Structure of the yeast nucleosome core particle reveals fundamental changes in internucleosome interactions. *EMBO J* 20 (18), 5207–18.
- Wierzbicki, A. T., Jerzmanowski, A., 2005. Suppression of histone H1 genes in *Arabidopsis* results in heritable developmental defects and stochastic changes in DNA methylation. *Genetics* 169 (2), 997–1008.
- Wilmes, G. M., Bergkessel, M., Bandyopadhyay, S., Shales, M., Braberg, H., Cagney, G., Collins, S. R., Whitworth, G. B., Kress, T. L., Weissman, J. S., Ideker, T., Guthrie, C., Krogan, N. J., 2008. A genetic interaction map of RNA-processing factors reveals links between Sem1/Dss1-containing complexes and mRNA export and splicing. *Mol Cell* 32 (5), 735–46.
- Winston, E., Allis, C. D., 1999. The bromodomain: a chromatin-targeting module? *Nat Struct Biol* 6 (7), 601–4.
- Wintersberger, U., Smith, P., Letnansky, K., 1973. Yeast chromatin. Preparation from isolated nuclei, histone composition and transcription capacity. *Eur J Biochem* 33 (1), 123–30.
- Wirth, M., Paap, F., Fischle, W., Wenzel, D., Agafonov, D. E., Samatov, T. R., Wisniewski, J. R., Jedrusik-Bode, M., 2009. HIS-24 linker histone and SIR-2.1 deacetylase induce H3K27me3 in the *Caenorhabditis elegans* germ line. *Mol Cell Biol* 29 (13), 3700–9.

- Wishart, D. S., Sykes, B. D., Richards, F. M., 1991. Relationship between nuclear magnetic resonance chemical shift and protein secondary structure. *J Mol Biol* 222 (2), 311–33.
- Wisniewski, J. R., Zougman, A., Kruger, S., Mann, M., 2007. Mass spectrometric mapping of linker histone H1 variants reveals multiple acetylations, methylations, and phosphorylation as well as differences between cell culture and tissue. *Mol Cell Proteomics* 6 (1), 72–87.
- Wohlschlegel, J. A., Johnson, E. S., Reed, S. I., Yates, J. R., 2004. Global analysis of protein sumoylation in *Saccharomyces cerevisiae*. *J Biol Chem* 279 (44), 45662–8.
- Wondrak, G. T., Cervantes-Laurean, D., Jacobson, E. L., Jacobson, M. K., 2000. Histone carbonylation *in vivo* and *in vitro*. *Biochem J* 351 Pt 3, 769–77.
- Woodcock, C. L., Frado, L. L., Rattner, J. B., 1984. The higher-order structure of chromatin: evidence for a helical ribbon arrangement. *J Cell Biol* 99 (1 Pt 1), 42–52.
- Woodcock, C. L., Skoultchi, A. I., Fan, Y., 2006. Role of linker histone in chromatin structure and function: H1 stoichiometry and nucleosome repeat length. *Chromosome Res* 14 (1), 17–25.
- Worcel, A., Strogatz, S., Riley, D., 1981. Structure of chromatin and the linking number of DNA. *Proc Natl Acad Sci U S A* 78 (3), 1461–5.
- Wright, P. E., Dyson, H. J., 2009. Linking folding and binding. *Curr Opin Struct Biol* 19 (1), 31–8.
- Wu, C., Bassett, A., Travers, A., 2007. A variable topology for the 30-nm chromatin fibre. *EMBO Rep* 8 (12), 1129–34.
- Wu, R. S., Tsai, S., Bonner, W. M., 1982. Patterns of histone variant synthesis can distinguish G0 from G1 cells. *Cell* 31 (2 Pt 1), 367–74.
- Xue, X., Lehming, N., 2008. Nhp6p and Med3p regulate gene expression by controlling the local subunit composition of RNA polymerase II. *J Mol Biol* 379 (2), 212–30.
- Yaneva, J., Leuba, S. H., van Holde, K., Zlatanova, J., 1997. The major chromatin protein histone H1 binds preferentially to *cis*-platinum-damaged DNA. *Proc Natl Acad Sci U S A* 94 (25), 13448–51.
- Yao, J., Lowary, P. T., Widom, J., 1991. Linker DNA bending induced by the core histones of chromatin. *Biochemistry* 30 (34), 8408–14.
- Yasuda, H., Matsumoto, Y., Mita, S., Marunouchi, T., Yamada, M., 1981. A mouse temperature-sensitive mutant defective in H1 histone phosphorylation is defective in deoxyribonucleic acid synthesis and chromosome condensation. *Biochemistry* 20 (15), 4414–9.

- Yu, Q., Kuzmiak, H., Zou, Y., Olsen, L., Defossez, P. A., Bi, X., 2009. *Saccharomyces cerevisiae* linker histone Hho1p functionally interacts with core histone H4 and negatively regulates the establishment of transcriptionally silent chromatin. *J Biol Chem* 284 (2), 740–50.
- Zalensky, A. O., Siino, J. S., Gineitis, A. A., Zalenskaya, I. A., Tomilin, N. V., Yau, P., Bradbury, E. M., 2002. Human testis/sperm-specific histone H2B (hTSH2B). Molecular cloning and characterization. *J Biol Chem* 277 (45), 43474–80.
- Zanton, S. J., Pugh, B. F., 2006. Full and partial genome-wide assembly and disassembly of the yeast transcription machinery in response to heat shock. *Genes Dev* 20 (16), 2250–65.
- Zardo, G., D'Erme, M., Reale, A., Strom, R., Perilli, M., Caiafa, P., 1997. Does poly(ADP)-ribosylation regulate the DNA methylation pattern? *Biochemistry* 36 (26), 7937–43.
- Zhou, Y. B., Gerchman, S. E., Ramakrishnan, V., Travers, A., Muyldermans, S., 1998. Position and orientation of the globular domain of linker histone H5 on the nucleosome. *Nature* 395 (6700), 402–5.
- Zhu, B., Zheng, Y., Pham, A. D., Mandal, S. S., Erdjument-Bromage, H., Tempst, P., Reinberg, D., 2005. Monoubiquitination of human histone H2B: the factors involved and their roles in HOX gene regulation. *Mol Cell* 20 (4), 601–11.
- Zlatanova, J., Caiafa, P., Van Holde, K., 2000. Linker histone binding and displacement: versatile mechanism for transcriptional regulation. *FASEB J* 14 (12), 1697–704.
- Zuiderweg, E. R. P., 2002. Mapping protein-protein interactions in solution by NMR spectroscopy. *Biochemistry* 41 (1), 1–7.